HOT EXTRUSION OF ALUMINIUM POWDER

A THESIS

submitted in fulfilment of the requirements for the award of the degree of

DOCTOR OF PHILOSOPHY

in

METALLURGICAL ENGINEERING

By

ASHOK KUMAR

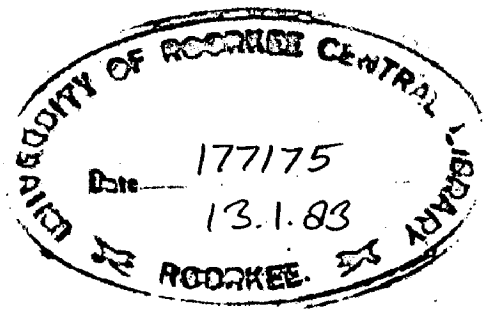

DEPARTMENT OF METALLURGICAL ENGINEERING
UNIVERSITY OF ROORKEE
ROORKEE-247 672
INDIA

February, 1981

CANDIDATE'S DECLARATION

I hereby certify that the work which is being presented in the thesis entitled, 'HOT EXTRUSION OF ALUMINIUM POWDER' in fulfilment of the requirement for the award of the Degree of Doctor of Philosophy, submitted in the Department of Metallurgical Engineering of University of Roorkee, is an authentic record of my own work carried out during the period from December, 1976 to February, 1981 under the supervision of Dr. M.L. Mehta, Professor in Metallurgical Engineering and Dr. P.C. Jain, Reader in Civil Engineering.

The matter embodied in this thesis has not been submitted by me for the award of any other degree.

Ashokumar
(ASHOK KUMAR)

This is to certify that the above statement made by the candidate is correct to the best of our knowledge.

(P.C. JAIN)
Reader in Civil Engg.

M.L. Mehta
(M.L. MEHTA)
Professor in Metallurgical Engg.

UNIVERSITY OF ROORKEE
ROORKEE (U.P.)-247 672,
INDIA.

Dated :
February 26 ,1981.

A C K N O W L E D G E M E N T S

The author expresses his deep sense of gratitude to Dr. M.L. Mehta, Professor in Metallurgical Engineering and Dr. P.C. Jain, Reader in Civil Engineering, University of Roorkee, Roorkee, for their inspiring guidance, lasting encouragement and whole hearted co-operation at all stages of the work. Their painstaking efforts and immense care in going through the manuscript and suggestions for its improvement are gratefully acknowledged.

The author is grateful to Prof. M.N. Saxena, Prof. M.L. Kapoor, Head, Metallurgical Engineering Department and Prof. R.J. Garde, Head, Civil Engineering Department, for providing various facilities throughout the duration of this work.

Dr. P.S. Mishra and Dr. A.K. Patwardhan, Readers, Metallurgical Engineering Department, have taken personal and keen interest in the work which encouraged the author from time to time. The author gratefully acknowledges their constructive criticism and valuable suggestions for the improvement of the various aspects of the present work.

Sincere thanks are due to Dr. P.N. Godbole, Reader in Civil Engineering and Dr. S. Dalela, Reader in Mechanical and Industrial Engineering, for their help during the initial stages.

Special thanks are due to

- Department of Science and Technology, Government of India, for financing this project.
- University Grants Commission, Government of India, for providing fellowship in the initial stages of the work.
- Sri Subhash Pundir and Sri Alok Sinha, BHEL, Hardwar, for their help in fabrication of the dies.
- My friends, who have extended their help in proof reading and bringing out the final get up of the thesis.
- Miss Jyoti Lata Pandey, for her co-operation and help during the research.
- Sri K.S. Pandey and Sri S.S. Singh, for their useful discussions.
- Staff of Regional Computer Centre, Chandigarh, for their help and generosity in permitting the use of its Computer facilities.
- S/Sri S.P. Kush, S.K. Seth, R.M. Mangal, S.B.Sharma and S.N. Kaushik, for their assistance during the experimental work.
- Sri M.C. Vaish, for preparing the drawings nicely Sri V.P. Kaushish, for typing the manuscript.

ASHOK KUMAR

S Y N O P S I S

Extrusion of metal powders is a well established forming process and its potential especially for shaping brittle powders into useful products was realised in the very early stages when filaments of electric bulbs were successfully manufactured. The application of this technique to softer metal powders like iron, copper and aluminium is a recent innovation. Although the experimental technique for producing extruded products from powder is well developed, theoretical analysis of the process involved received little attention. The earliest attempt in this direction was initiated as late as 1970 when some well established theories of metal forming were applied to the extrusion of aluminium powder and its alloys. Application of the slip line field theory and upper bound analysis could predict the load required for extrusion which was lower than that required for the extrusion of cast billet into final product of the same geometry. It was emphasised that unlike the extrusion of a cast billet, powder billet during extrusion must necessarily be subjected to massive shear zones along slip lines in order that a strong and coherent product was obtained. Based on this reasoning the use of square edge dies with relatively higher reduction ratios ($R > 10:1$) was favoured. Experimentation was confined mainly to a temperature of $300^{\circ}C$ and the theoretical analysis employed had its own limitations because of simplified assumptions

made . So also, a systematic analysis of the microstructural changes that occurred during the extrusion process was lacking. Under the above mentioned experimental and theoretical constraints, the following major conclusions were arrived at :

i) Densification preceeds the actual extrusion process.

ii) Redundant work is mainly responsible for welding, fragmentation, rewelding and eventually sintering of individual powder particle to yield a coherent mass.

iii) Homogeneous work of deformation merely contributes to shape change and does not control either the coherency of the product or its strength.

iv) Wedge shaped dies are unsuitable for obtaining (a) coherent mass and (b) proper surface finish.

v) Attainment of coherent product was not possible at reduction ratios less than 10:1.

The proposed theory was deficient in predicting the condition under which a coherent mass (extruded product) could be obtained. Similarly fundamental concepts on the mode of deformation pattern and metal flow were not fully developed, as the theory propounded failed to provide basic data on pressure distribution, velocity vectors, effective strain rate and such other parameters within the mass being extruded.

The present investigation is aimed at providing comprehensive information on the above aspects. This has been achieved by utilizing analytical approach (velocity-pressure formulation) based on the finite element method (FEM). A

modified yield criterion for porous products has been employed since the density of a porous product continuously changes during extrusion. Based on this approach, it has been possible to obtain precise information on velocity, pressure and effective strain rate distribution inside a billet while being extruded.

Extrusion studies have been carried out on aluminium powders at low ($R < 10:1$) as well as high reduction ratios ($R > 10:1$) through square and wedge shaped dies over a temperature range from 300 to 500°C. The relationship between extrusion pressure and extrusion parameters (reduction ratio and temperature) was found to be linear. The experimental results have been discussed in relation to theoretical deductions obtained by FEM. While studying the effect of temperature on extrusion, it was noticed that around 400°C there is a change in the mode of deformation. This has been duly supported by microstructural investigations. The important findings of the present investigation are :

i) An estimation of velocity, pressure and effective strain rate distribution within a powder preform while undergoing extrusion.

ii) Nature of the pressure and effective strain rate contours as a basis of predicting whether or not a coherent mass would be produced.

iii) Homogeneous work of deformation and not the redundant work as the sole factor contributing to the formation of strong and coherent mass.

iv) Successful production of coherent extruded product through wedge shaped dies at both low and high reduction ratios and also through square dies even at low reduction ratios.

v) Product obtained through wedge shaped dies being at least 10-20 % more stronger than those obtained through square dies.

vi) Existence of dead metal zone boundary parallel to the die axis at low reduction ratios and its gradual shifting to the die corners as reduction ratio is increased.

vii) Establishment of a correlation between bulk parameters (namely velocity, pressure and effective strain rate contours) and the microstructural features as influenced by extrusion parameters.

viii) Conditions leading to the formation of substructure and its role in controlling the extrusion pressure and the final tensile properties of the extruded product are discussed.

C O N T E N T S

NOTATIONS

A_i	Area of the powder preform (mm^2)
A_o	Area of the extruded product (mm^2)
CZ	Constraint free zone
D	Diameter of powder preform (mm)
DMZ	Dead metal zone
EPC	Extrusion pressure contour (analytical)
EZ	Elastic zone
H	Height of powder preform (mm)
HZ	Hydrostatic zone
J_1, J_2	Invariants of stress tensor
J_2', J_3'	Invariants of deviatoric stress tensor
k	Yield stress in shear (N/mm^2)
ΔL	Difference between peak and steady state load (ton)
NE	Number of elements
PZ	Plastic zone
p	Extrusion pressure
R	Reduction ratio (Area of the powder preform/Area of extruded product)
Rc	Rockwell hardness number
r, θ, z	Cylindrical co-ordinates
S_{ij}	Component of stress deviator where i refers to plane and j refers to direction
T	Extrusion temperature (^oC)
Tm	Melting temperature (^oC)
UTS	Ultimate tensile strength (N/mm^2)

u,v	Component of velocity in x and y directions respectively (mm/sec)
u_i	Velocity of the ram (mm/sec)
u_o	Velocity of the extruded product (mm/sec)
$\underline{u}/p$	Velocity pressure formulation
x,y,z	Cartesian coordinates
Y	Yield stress in tension (N/mm^2)
YS	Yield stress (N/mm^2)

Greek Symbols

α	Coefficient of friction
γ_{12}	Shear strain
$\dot{\gamma}_{12}$	Shear strain rate
$\varepsilon_1,\varepsilon_2,\varepsilon_3$	Principal normal strains
$\dot{\varepsilon}_1,\dot{\varepsilon}_2,\dot{\varepsilon}_3$	Strain rates
ε_{ij}	Component of strain invariants
$\bar{\varepsilon}$	Effective strain
$\dot{\bar{\varepsilon}}$	Effective strain rate
λ	Constant of proportionality
μ	Coefficient of viscosity ($N s/mm^2$)
$\bar{\mu}$	Pseudo-viscosity coefficient for Bingham plastic fluids ($N s/mm^2$)
ν	Poisson's ratio
ρ	Percentage theoretical density
$\sigma_1,\sigma_2,\sigma_3$	Principal normal stress
σ_m	Mean pressure or first stress invariant
$\bar{\sigma}$	Effective stress

τ	Shear stress (N/mm^2)
τ_y	Yield shear stress for Bingham plastic fluids (N/mm^2)

Vectors and Matrices

$\{\ \}$	Denote column and row matrix
$[\ ]$	Denote rectangular matrix
$\{a\}$, $\underline{a}$	Vector of unknown nodal parameters
$\{F\}$, $\underline{F}$	Vector containing body forces per unit volume
$[K]$, $\underline{K}$	Stiffness matrix
$[N]$, $\underline{N}$	Shape function matrix
$\bar{\underline{t}}$	Vector containing tractions
$\{\varepsilon\}$	Vector containing strains
$\{\dot{\varepsilon}\}$	Vector containing strain rates
$\{\sigma\}$, $\underline{\sigma}$	Vector containing stress.

LIST OF TABLES

LIST OF FIGURES

C H A P T E R - I

INTRODUCTION

Among the many processes for converting metal powders into useful solid products, the hot extrusion process is relatively new. It offers simultaneous densification and large reduction in a single operation. Alloys having wide freezing range are very prone to segregation in castings. This leads to problems in hot working and results in poor yield. However, this problem can be overcome by adopting the powder extrusion path. Significant advantage of metal powder extrusion process is that sintering is eliminated which follows cold compaction in conventional powder metallurgy. While in sintering of aluminium base products the oxide film surrounding powder particles obstructs the diffusion process and adversely affects the densification. This difficulty may be eliminated to a large extent by hot extrusion where oxide film is effectively broken under heavy plastic deformation, thereby accelerating sintering during hot extrusion.

Although some data on hot extrusion of aluminium powder exist, many questions regarding the mechanism of densification and the effects of extrusion parameters on the nature of the final product remain unprobed.

In the present investigation extrusion studies have been carried out on aluminium powder at low (R=1.3:1 to 7:1) as well as high reduction ratios (R=10:1 to 80:1) through

square and wedge shaped dies over a temperature range, 300 to 500°C. The relationship between extrusion pressure and extrusion parameters was established. Analytical extrusion pressures were calculated based on plastic/visco-plastic metal flow conforming to non-Newtonian fluid behaviour. An analytical approach namely velocity pressure formulation based on the finite element method (FEM) has been used to calculate the velocity vectors, pressure and effective strain rate distribution inside a billet while being extruded. A modified yield criterion for porous compacts has been employed since the density of a porous compact continuously changes during extrusion. The experimental results have been discussed in relation to analytical deductions obtained by FEM.

While studying the effect of temperature on extrusion, it was noticed that around 400°C there is a change in the mode of deformation. This has been duly supported by micro-structural investigations. Macrostructural studies of the longitudinal section of the extruded product were also carried out to examine the defects in the product and shape of dead metal zone (DMZ) boundary with respect to reduction ratios and temperatures.

1.1 LAYOUT OF THE THESIS

The thesis has been divided into eight chapters :

The Chapter II deals with literature review. The extrusion process has been described with respect to

extrusion parameters, nature of the process and densification mechanism. Analytical methods have also been described to calculate the extrusion pressure and other parameters.

The Chapter III deals in detail with the general formulation of the problem with regard to the experimental approach to be adopted and analytical techniques to be pursued.

The experimental procedures have been described in Chapter IV.

In Chapter V computer program, parametric studies and modification in yield criterion have been given.

Chapter VI deals with experimental results which are discussed with respect to coherency of the extruded product and shape of dead metal zone. Further, the micro- and macrostructural investigations carried out on longitudinal and transverse sections and their correlation with the analytical plots have also been high lighted.

Some aspects such as existance of DMZ and the role of redundant work needing critical analysis have been put forth in Chapter VII.

Chapter VIII deals with the main findings of the present investigation.

C H A P T E R - II

LITERATURE REVIEW

2.1 INTRODUCTION

Powder extrusion studies have been carried out on a number of materials namely aluminium and its alloys, tin-bronzes, nickel and its alloys, chromium and chromium-base composite materials, uranium, thorium, zirconium, sponge iron and steel powder. However, in the last decade studies on extrusion of powders both with regard to the influence of process variables and the application of theoretical models for predicting extrusion pressure have been mostly confined to aluminium and aluminium based systems.

2.2 EXTRUSION THROUGH CYLINDRICAL SQUARE EDGE DIE

2.2.1 Aluminium and its Alloys

Sheppard and Chare [1] carried out hot extrusion of atomised aluminium powder [2] mainly at 300°C at reduction ratios from 5:1 to 50:1 at a ram speed 5-7 mm/sec, and reported that the pressure required for extruding a powder billet was less than that for a cast billet of the same composition. Sheppard and co-workers [3-6] also extruded a number of aluminium base alloy powders viz. Al-5%Fe, Al-3.6%Mn-0.95% Al_2O_3, Al-2.4%Fe-1.01% Al_2O_3 in the temperature range

---

Compositions are in weight percent.

250 to 450°C, Al-1.9%Al_2O_3, Al-3.59%Mn and Al-7%Mg-2%Zn in the temperature range from 250 to 550°C at a ram speed varying from 0.5 to 150 mm/sec employing reduction ratio from 5:1 to 50:1. They reported that the powder billet attained 100% of the theoretical density before extrusion started. Sheppard and McShane [7] extruded the Al-0.5%Mg-0.5%Si alloy powder through reduction ratio from 5:1 to 180:1 in the temperature range from 250°C to 540°C. Hansen [8,9] carried out extrusion of aluminium base powder alloy by blending the aluminium powder with fine oxide powders. The blended powders were mainly extruded at 500°C after hot pressing through reduction ratio 15:1. The aim of the investigation was simply to examine the properties of the extruded products.

2.2.2 Other Non-Ferrous Alloy Powder

Sheppard and Greasley [10] reported the experimental results of extrusion of tin-bronzes, single phase and two phase ally powder for reduction ratios 10:1 to 180:1 in the temperature range from 450 to 850°C. Gregory and Goetzel [11] conducted experiments on extrusion of 80/20 nickel-chromium alloy powder either with titanium carbide or alumina and thoria. The cold compacts were sintered at 2000°F (1093°C) and 2280°F (1250°C) and then extruded at the same temperatures at which they were sintered. The strength at 1500°C and 1800°C was considerably higher in comparison to that of as cast

state. Bhattacharya [14] produced close end tube by backward cold extrusion of copper powder. Before extrusion the powder billet was either sintered or compacted followed by annealing at low temperature. Chromium and Chromium-niobium sintered composite materials [15] were extruded at 1200°C employing a reduction ratio of 10:1. The rod after extrusion was sintered in hydrogen atmosphere and it was observed that the structure of the extruded product remained unchanged before and after sintering. The density of the sintered product was found to decrease with higher sintering temperature due to rapid diffusion of niobium into Chromium matrix.

2.2.3 Iron and Steel Powder

Dunkley and Causton [16,17] carried out hot extrusion of tool steel and high speed steel powders with R from 10:1 to 30:1 at a ram speed, 10-20 x 10^3 mm/sec in the temperature range from 1000-1200°C. They reported that for reduction ratio 13:1, no difference in extrusion pressure for cast and powder billets was observed. Vollmer and Jones [18] extruded cold pressed billets of sponge iron powder into bars and tubes at two different temperatures, 1000°C and 1150°C at a ram speed of 10 to 25 mm/sec. The density of the product extruded at 1150°C was higher than 99.5% of the theoretical density. Oxide type inclusions were found on the fractured surfaces of tensile sample, which have an undesirable influence on the properties of extruded product. Thompson et al [19] produced

short tubes on an industrial scale from sintered sponge iron powder billets by cold extrusion. They concluded that fully dense tubes could be obtained by extruding the billet (80% of theoretical density) at 85% reduction (R = 3.0:1).

2.3 EXTRUSION THROUGH CYLINDRICAL WEDGE SHAPED DIE

Gregory [20] has suggested that the 'gelling' and die 'pickup' during powder extrusion could be eliminated by using wedge shaped dies. Chare and Sheppard [1] using wedge shaped dies extruded commercially pure aluminium powder and reported that acceptable surface finish could not be achieved and that the threshold extrusion ratio at which coherent mass was produced for square dies was raised considerably. They have suggested that in square edge dies the massive shear zones were formed and redundant work played an essential and important role in building the coherent mass by welding, breaking and rewelding of powder particles.

Singh and Davies [21] performed 'backward' and 'forward' cold extrusion of different grades of sintered sponge iron powders through cylindrical wedge shaped dies with 120 degree entry angle and reduction ratios lower than 5:1 at slow and high speeds. They found that extrusion pressure was higher at higher speeds than at lower speeds. This difference was more marked during backward extrusion. In forward extrusion, there was a limiting reduction ratio

2:1, below which coherent mass was not possible. Negm and Davies [22] carried out forward and backward extrusion of sintered sponge iron powder compacts of initial density which was 87% of theoretical value at reduction ratios from 2:1 to 7:1 in the temperature range, 880 to 1030°C at low and high speeds. They reported that extrusion pressure was lowered with decrease in extrusion speed and with an increase in the initial density. They found that the density of the extruded product increased with the speed of extrusion and initial density. The density of the product also increased with the reduction ratio for the same initial density both in the forward and backward extrusions.

Loewensteen [23] has converted the loose powder of uranium, thorium, zirconium and other rare-earth metal powders into rods by extruding in the temperature range, 800 - 900°C and reported that nearly 100 % of the theoretical density of the extruded product was achieved. In these materials effect of reduction ratio has not been reported.

2.4 EXTRUSION PARAMETERS

2.4.1 Extrusion Pressure

For pure aluminium powder [1] it was shown that the pressure required to produce solid metal from powder was considerably less than that required for cast billet. The extrusion pressure may be enumerated by considering

- the compact strength at each velocity discontinuities due to shear. On the basis of upper bound analysis it was shown for copper, nickel [13] and aluminium-base alloys powders [3-7] that the pressure required for extrusion of powder billet was lower than that for the cast billet. Similar observations were reported experimentally for nickel and aluminium-base alloys. For the alloys having low stacking fault energy [10], in which dynamic recrystallisation was the predominant softening process, the difference in pressure for extrusion of powder and cast billet was small. This was attributed to varying the rheological properties throughout the quasi-static zone. This was concluded on the basis of the observation that yield stress was different at different locations in the partially extruded billet [10]. Chare et al [4] calculated extrusion pressure for cast aluminium alloys using a minimised upper bound analysis and showed that over a wide range of temperature and reduction ratios, the pressure required for powder extrusion was less than half of that required for cast billet and that the pressure required for extrusion of Al-Zn-Mg alloy powder was 27 % less than that for the corresponding cast alloy.

Sheppard and Greasley [10] used the initial maximum pressure, obtained from load-displacement diagrams as the pressure for extruding tin-bronze alloy powder because they found excessive temperature drop while extruding, which led to a considerable increase in pressure at the

end of the extrusion stroke. Dunkley and Causton [16] used the steady state load as extrusion pressure.

2.4.1.1 Effect of Reduction Ratio On Extrusion Pressure

Chare et al [1] reported that for aluminium and its alloy in powder form, the extrusion process was much less dependent on reduction ratio as compared to that for cast material. However, the linear relationship was observed between $\ell n R$ ($R > 10:1$) and extrusion pressure (p) as in case of cast material. This could be expressed in the following form :

$$p = A + B \ell n R$$

where p - Extrusion pressure

R - reduction ratio

A and B are constants.

The values of constants A and B depended upon reduction ratios and were different for cast and powder materials. However, at low reduction ratios ($R < 10$) this relationship did not hold good for the powder extrusion. Dunkley and Causton [15,16] confirmed the above relationship to be true for the powder extrusion of tool and high speed steel at high reduction ratios.

2.4.1.2 Effect of Temperature On Extrusion Pressure

Chare and Sheppard [3-7] observed that the initial billet temperature had the same effect on extrusion pressure independent of the state of the material. They

found a linear relationship between extrusion pressure and log of initial billet temperature for aluminium powder [1] and aluminium-base alloy powder of the form:

$$p = a - b \log T$$

where a and b are constants. The values of a and b were different for pure aluminium powder and aluminium base alloys. As the billet temperature increased the extrusion pressure decreased.

2.4.1.3 Effect of Strain Rate On Extrusion Pressure

Chandra and Jonas [24,25] conducted extrusion of strain rate senstive material through square edge dies at reduction ratios from 40:1 to 160:1 and showed that the extrusion pressure was strong function of strain rate senstivity of the flow stress of the material.

Experiments on extrusion of pure aluminium powder by Sheppard and Chare [1] showed that ram speed had little effect on extrusion pressure and mechanical properties of the extruded product. They reported for Al-Fe alloy powder that the extrusion process was less strain rate senstive as compared with that of the cast alloy. Sheppard [6] further investigated the effect of strain rate on extrusion pressure using the Al-Mn-Al_2O_3 powder alloy and showed that powder extrusion process was essentially not strain rate senstive as shown in Fig. 2.1. He proposed, 'This was due to that the process was dependent upon the strength of weld necks and local

for the extrusion of aluminium base alloy powders [3-9].

It was observed for pure aluminium [2] and nickel rich alloy powders [13] that the extrusion pressure varied with the particle shape. The extrusion pressure was the highest for pure flake type of powder and lowest for purely spherical shape powders.

2.4.2 Reduction Ratio And Coherency of the Extruded Product

Sheppard and Chare [1,6] reported that in case of powder extrusion process there was a transient reduction ratio (R = 10:1) below which full material properties could not be developed and coherent mass could not, therefore, be achieved. They stated on the basis of the upper-bound analysis that the reduction ratio should be a function of deformation zone and for lower reduction ratios (R < 10:1) the shear zones would be smaller with fewer velocity discontinuities resulting in incoherent product. The relationship

$$p = A + B \ln R$$

valid for high reduction ratios would not hold good at low reduction ratios (R < 10:1) due to negative slope in the p vs.ln R curve. For extrusion of tool steel and high speed steel powders, Dunkley and Causton [16] reported that the coherent product was not expected below a transition reduction ratio lying between 5:1 and 10:1. As the reduction ratio was reduced from 10:1 to 5:1 the slope

diffusion rates rather than on finally deve. oped flow stress'. The strain rate was calculated according to method proposed by Felthan [26] where the strain rate was estimated by calculating the time required to fill the quasi-static deformation zone and also the total strain occurring in that time.

In the extrusion of Al-Mg-Si alloy powder [7] through reduction ratio 80:1 at 500°C, a peak in the load-displacement curve was observed at high strain rates (13 mm/sec) while no peak was observed at low strain rate (4mm/sec) as evident from Fig. 2.2. To explain this, it was proposed that at high strain rates an excess of dislocations was generated immediately after the compaction zone before the onset of dynamic softening processes (e.g. recovery) where as at low strain rates the rate of dislocation production was never large enough to overcome the dynamic softening process.

2.4.1.4 Effect Of Particle Size And Shape On Extrusion Pressure

For pure aluminium powder it was shown [1,2] that the pressure required for extruding the small particles was much higher than for larger particles. In case of smaller particles, larger surface area would result in greater number of welds and more work would be required to shear these weld necks during the 'powder properties' phase of extrusion. Similar observations were reported

of p vs. log R line changed and dropped away towards the origin. They suggested that a 'knee' should exist in the curve between extrusion pressure and reduction ratio between R = 5:1 and R = 9:1 as shown in Fig. 2.3 and the relationship between pressure and reduction ratio for low reduction ratio might be

$$p = K_1 \log R$$

They also suggested that the minimum value of R for the production of a sound product was very senstive to minor variations in heating, lubrication and speed but sound product could not be expected below reduction ratio 10:1. Singh and Davies [21] reported that for the extrusion of sintered sponge iron powder billet this transition reduction ratio was lowered to 2:1.

2.5 NATURE OF EXTRUSION PROCESS

For aluminium-base alloys [5] the extrusion process was thermally activated and the activation energies for hot deformation of these powder alloys were close to the value for self diffusion in aluminium [5]. It was suggested that the climb of edge dislocations or the motion of jogged screw dislocations must be the rate controlling mechanism for deformation of powders because a three dimensional net work was found in microstructure which showed that growth of these networks during recovery must be due to climb of edge dislocations and migration of 'jogs' with dislocations such

that rate of recovery depended on the self diffusion coefficient.

2.6 MECHANICAL PROPERTIES OF THE EXTRUDED PRODUCT

2.6.1 Effect of Reduction Ratio

For pure aluminium powder [1] reduction ratio had little effect on hardness, elongation and proof stress. However, aluminium powder extruded below a reduction ratio of 10:1 could not achieve its maximum properties as the material extruded at a reduction ratio 5:1 was found to be extremely brittle. A similar effect was also observed for other aluminium base alloy powders [3-9].

2.6.2 Effect of Particle Size

For pure aluminium [1,2] and aluminium based alloys [3-6] a linear relationship exists between proof stress and the square root of particle diameter which could be quantified by Petch equation. As the particle diameter decreased, the proof stress of the extruded product at room temperature as well as 400°C increased while percentage elongation decreased. Further, although the aluminium base alloy powders [3-9] also behaved the same way, the mechanical properties were found to be much less dependent upon particle size in comparison to the pure aluminium powder. The mechanical properties of the extruded product were much more dependent upon the microstructure and shape of the particles than on particle

size. A product extruded from flaky powder gave better overall mechanical properties than a product made from spherical powders. This is because the bridges formed on compacting the powder were difficult to break. The mechanical properties of aluminium base alloy products, extruded from powder, were compared with those extruded from cast alloys [6] and it was found that both high and low temperature tensile properties were far superior in the case of the powder products. Ductility of the extruded powder product was lower but much higher than what is obtained in conventional powder metallurgy parts.

Mechanical properties of tin-bronze single phase and two phase alloy powder products [18] were found to vary throughout the length of the product, being higher at rear end than at the front end. The difference in properties was perhaps due to a steady decrease in temperature of the billet throughout the press stroke. It was reported that diameter of the original preform had no significant effect on the grain size of the extruded product for single phase alloys because deformation occurred by dynamic recrystallization followed by metadynamic and static recrystallization while in two phase alloys final grain size of product was dependent on original particle size because only dynamic recrystallisation was the predominant mechanism.

2.6.3 Extrusion Temperature

The mechanical properties varied with the initial billet temperature as reported for pure aluminium [1,2] and aluminium base alloy powders [3-6]. As the extrusion temperature increases, the room temperature proof stress falls considerably, while that at 400°C remains unaffected. This was explained by stating that subgrain strengthening was not effective. It was further reported that the elongation obtained was controlled by initial billet temperature and increases considerably as the extrusion temperature rises. Hansen [7,8] also observed this trend in aluminium-base powder alloys. The elongation at room temperature and at 400°C improved as the temperature increased.

2.7 ROLE OF REDUNDANT WORK

In many metal forming processes like wire drawing, forging and extrusion, the load needed to affect the desired change is seriously underestimated, the error being due to appreciable internal distortion of the work piece, beyond that strictly needed for shape change caused by shearing action which consumes energy. This energy does not contribute directly to the formation of the final product. The additional work thus expended is known as the redundant work [27].

The reason for the underestimation of working loads during extrusion is that the total work done (WT) is

regarded as a sum of three components; work done for homogeneous deformation (WH) which represents the least possible work required for shape change, work done due to die wall friction (WF) and redundant work (WR) which does not contribute directly to the shape change. In the case of powder extrusion the redundant work is used for internal distortion of the powder particles [5].

Thus $WT = WH + WF + WR$

but these are not entirely separable, because the flow constraint will be influenced by the friction at the die surface, so WR will depend upon friction. In the relation

$$p = A + B \log R$$

the logarithmic term represents the contribution of work for homogeneous deformation while the first term represents the contribution towards redundant work [28].

Sheppard and Greasley [9] reported that the ratio B/A generally represents the proportion of useful work to redundant work. This ratio for the extrusion of cast billet is approximately 2[10] while in the case of the powder extrusion the B/A ratio for single phase alloy is 0.95 (average) and for the two phase alloy 0.32 (average) i.e. there is a greater redundant work of the total energy required for deformation during extrusion of powder. This higher proportion of redundant work is used to build a coherent mass.

2.8 DENSIFICATION DURING POWDER EXTRUSION PROCESS

Sheppard and Charc [3] proposed a mechanism based on upper bound analysis suggesting how a coherent mass may be built up from a powder mass during the extrusion process. According to them the deformation during extrusion process occurs in a quasi-static zone (Fig.2.4) which may be further divided into two emerging regions; powder properties and the final properties at exit end of zone. The densification process was investigated for Al-7%Mg-2%Zn alloy powder by examining the development of microstructure throughout the quasi-static deformation zone by taking sections from the partially extruded billet at four different positions.

Microstructure at the rear end of the billet corresponding to area ABE (Fig.2.4) showed tightly packed particles showing little overall deformation but the material had attained the theoretical density and had just commenced its transverse of the quasi-static deformation zone. Yield strength of the material in this zone was very low which showed poor cohesion between particles and little resistance to shear. After passing through this initial band of velocity discontinuity along line AB (Fig. 2.4) caused by shear, the microstructure near the mid point of the line OA showed some elongation in the particles and at this stage most of redundant work appeared to contribute towards elongation rather than towards cohesion of particles. This

means that the part of the extrusion energy was utilised towards the deformation of individual particles but interfaces remained incoherent, which contributed little towards an increase in the yield strength.

The microstructure in the dead metal zone corresponding to area OAD (Fig.2.4) and of the product at the last discontinuity along line OC showed that welding between particles takes place due to continuous interaction between particles and velocity discontinuities along the line OC contributing towards elongation of particles.

The building of a coherent mass from powder particle was due to breaking and welding caused by shearing action along the line AB until the shear strength of inter particle bond assumed the properties of the final material due to velocity discontinuities caused by massive shearing process along line OC (Fig.2.4).

Sheppard and Greasely [10,29] also examined the densification during powder extrusion of tin-bronze alloy powders by observing the microstructural changes in the partially extruded billet of 8T (Cu-8.2%Sn-0.2%P) single phase alloy and that of a 8T 15P(Cu-7.4%Sn-1.5%P) two phase alloy. They reported that the flow pattern of powder extrusion showed a 45° dead metal zone. The compressive stresses were not sufficient to consolidate the powder in dead metal zone for single phase alloy.

Macrographs showed that particle structure was retained in the dead metal zone and also in a region of about 2 mm at the rear face of the billet due to little shear at ram/billet interface. At the billet edge (in contact with container there was a thin surface film in which the powder structure was destroyed due to shear which is always present at this surface during extrusion. However, a subcutaneous layer about 1 mm thick existed in which the powder structure was retained. In the case of two phase alloys, the microstructure along the entire billet surface (in contact with container retained the powder structure well into the deformation zone because regions of intense shear existed within the billet and localised velocity discontinuity existed at the entery of the deformation zone.

It was proposed that the densification mechanism is also dependent on stacking fault energy of the material; and quite different from that occurring in high stacking fault energy alloys involving the major process as one of the dynamic recovery as evident from fibrous structure and sub-grain formation observed in hot worked aluminium and its alloy [10].

The microstructure of Al-5%Mg-5%Si alloy powder [7] was examined and it was reported that the product exhibited a fibrous cold worked structure. The original powder particles got elongated in the direction of metal flow and the elongation was dependent on the extrusion

ratio. The cold worked microstructure was produced even when extrusion was performed above the recrystallization temperature of the alloy. The microstructure of the transverse section only showed equiaxed grains. It was also shown by thermal activation evidence that dynamic recovery was the dominant mechanism.

2.9 ANALYTICAL METHODS FOR DETERMINATION OF EXTRUSION PRESSURE

Conventional analytical methods for prediction of extrusion pressure are slip line field theory and upper bond technique based on the flow of metal through a die. These methods are strictly applicable under plane strain conditions [30] and it can be stated that :

$$dw = k.u.ds \qquad .. (2.1)$$

where

k = shear yield stress

u = magnitude of velocity discontinuity

s = length of velocity discontinuity

w = work done.

Applying this to the specific case of plane strain extrusion of a homogeneous material as shown in Fig. 2.4, we get

$$p.\ \frac{(a+b)}{2}\ .\ 1 = k\ (AB.\overline{23} + BC.\overline{24} + BO\ \overline{34} + CO\ \overline{45} + AO\ \overline{13}) \qquad .. (2.2)$$

Sheppard [6] applied this equation to non-homogeneous powder compacts by taking different values of yield stress in different shear zones. Thus, for plane strain extrusion of powder compact the equation (2.2) becomes :

$$p.\left(\frac{a+b}{2}\right).1 = k_1(Ab.\overline{23} + BC.\overline{24}) + k_2.\overline{AO}.\overline{13}+k_3.\overline{BO}.\overline{34} + k_4.OC.\overline{45} \quad .. (2.3)$$

here k_1 presents the resistance to shear of the powder compact which is virtually zero and k_4 represents the resistance to shear of the final product which would be the same or greater than that of conventionally processed products. The remaining shear terms depend upon the average shear strength of material in the corresponding rigid quasi-static triangle. This method is also applicable to the axisymmetric problems of extrusion. Alexander [31] proposed a kinematically admissible velocity field for axisymmetric extrusion by determining the velocity components from the geometry of the stream lines. Subsequently others [32,33] also obtained hodographs for upper bound analysis as obtained by Alexander. A graphical method was developed by Adie and Alexander [34] to obtain kinematically admissible velocity field using single, double or triple triangular arrangements of velocity discontinuities. Thomson [35] showed that in the case of axisymmetric extrusion the material flow was similar to that of plane strain for identical configuration and the magnitude of the velocity during axisymmetric

extrusion is the square of the velocity during plane strain extrusion. Sheppard and McShane [36] have used the upper bound technique to calculate the extrusion pressure for axisymmetric extrusion of powder compacts and they considered the surface area of the velocity discontinuities and squared the magnitude of the velocities. Hence, the modified equation for axisymmetric extrusion for upper bound solution (Fig.2.4) is given as:

$$p.(a+b)^2.1 = k_{AB}.A_{AB}\,(\overline{23})^2 + k_{BC}.A_{BC}.(\overline{25})^2 + k_{BO}.A_{BO}(\overline{34})^2 + k_{OC}.A_{DC}(\overline{45})^2 + k_{AC}.A_{AC}(\overline{13})^2 \qquad .. (2.4)$$

Based on this equation the extrusion pressure was calculated in three different ways and compared with experimentally determined values for reduction ratios from 10:1 to 80:1. In the first case the plane strain solution was minimised by using Equation (2.3), where as in the second case more velocity discontinuities as obtained from the observed physical field, were incorporated. In third case a modified equation applicable to an axisymmetric case as given by the Equation (2.4) was minimised. This comparison revealed that the first method is not valid while the second and third methods predict the extrusion pressures close to the experimentally determined value only in a very narrow reduction ratio range (25:1 to 40:1) as shown in Fig.2.5. McShane et al.[28] further modified their theory by incorporating

strains and strain rate by considering an expression of the form $\bar{\sigma} = K\varepsilon'^{m}\ \dot{\bar{\varepsilon}}^{n}$ where K', m and n are constants and used this relation to predict the extrusion pressure for aluminium alloy in the range of reduction ratios from 10:1 to 180:1. The constants were determined by minimising the function using penalty function approach. The mean effective strain rate was determined by using the equation

$$\dot{\bar{\varepsilon}} = \left[\frac{2}{3} \left(\dot{\varepsilon}_{\theta}^{2} + \dot{\varepsilon}_{r}^{2} + \frac{1}{2} \dot{\varepsilon}_{r\theta}^{2} \right) \right]^{1/2} \qquad .. (2.5)$$

which is a function of r and θ only. The strains were calculated from slip line field.

This theory is applicable for strains up to 2.3. When the strains are in excess of 2.3, the flow stress is no longer strain senstive since the compact has become 100 percent dense. These authors claim that using the above penalty function optimization, excellent correlation between theory and experimental work was obtained. This type of curve fitting, will,in fact be needed for every experimental observation either for cast billet or powder billet. It seems that the comparison of the experimental and the theoretical results have been achieved by using some sort of curve fitting technique.

The pressure was also calculated for the extrusion of cast billet by upper bound analysis for wedge shaped dies [37].

2.10 OTHER ANALYTICAL METHODS FOR DETERMINATION OF EXTRUSION PRESSURE USING FINITE ELEMENT METHOD

Slip line field theory has been used extensively, out of the various approximate methods available to predict the loads and deformation in various metal forming processes. Although it has been used for both plane strain and axisymmetric conditions but have several limitations [38-41]:

(i) The elastic strains are neglected. It assumes the material as rigid perfectly plastic (without strain hardening and temperature effect).

(ii) The internal forces are neglected and the problem is treated as quasi-static.

(iii) It is applicable to only simple boundaries - straight boundaries with friction or without friction.

In recent years the above difficulties have been over come by finite element method (FEM) which has been successfully extended to various non-linear fields, in particular to the large deformation and plasticity problems. More recently these metal forming problems have been analysed as non-Newtonian fluid flow problems where solid has been taken as flowing like a viscous fluid with variable viscosity. The above analysis has been briefly reviewed in the following section.

2.10.1 Elasto-Plastic Analysis Using FEM

Zienkiewicz and Nayak [42,43] have shown that the elasto-plastic analysis using FEM gives useful and comparable results for the various metal forming processes, namely extrusion. They considered various types of material non-linearities, i.e. ideally plastic, strain hardening etc. as well as different situations like plane stress/strain and axisymmetric cases.

These methods are useful in the context of small geometrical changes, but when these changes are quite large, to the extent that elastic deformation is negligible, then these methods are either not applicable or are quite expensive as far as the computations are concerned.

2.10.2 Penalty Function Approach

Penalty function approach are used to modify variational principles used in the finite element analysis to enforce constraint. The problem of viscous incompressible flow can be treated as a problem of constrained minimisation of functional. Zienkiewicz and Godbole[44,45] have used this approach for plastic flow of metals and metal forming problems especially for extrustion. It does not involve a pressure field, the unknowns are less than the velocity pressure formulation, resulting in decreased computational cost. The solutions can be made closer to the solution of Navier-Stokes equation by the

adjustment of a parameter (Poisson's ratio ν -0.5). Its application to some hot metal forming problems has been recently reported [46] which also include the calculation of mean stress in addition to deviatoric stresses.

In spite of the above merits, the method suffers from an draw back; that the value of ν or λ is quite important, and its value which is problem dependent, has to be very carefully chosen.

2.10.3 Stream Function Approach

Stream function approach has been used for the viscous incompressible flow of Newtonian and non-Newtonian fluids. Goon et al[47] originally suggested this procedure and obtained some solutions using mapping techniques. Godbole [48] used this procedure for the viscous incompressible flow of non-Newtonian fluids and extended for plastic/viscoplastic flow. He has shown that plastic/viscoplastic flows are analogous to the flow of non-Newtonian fluids.

2.10.4 Velocity-Pressure Formulation

To overcome the draw back of penalty function approach a new formulation; velocity pressure-involving velocities and pressures, was chosen for solving viscous incompressible non-Newtonian flow problems. Zienkiewicz and Jain [49] have successfully used the velocity pressure

formulation for various metal forming problems. Virtual work principle has been used to formulate the problem, with velocities and pressures as unknowns. This has been extended with certain modifications for the present study and the details are available in the subsequent chapters.

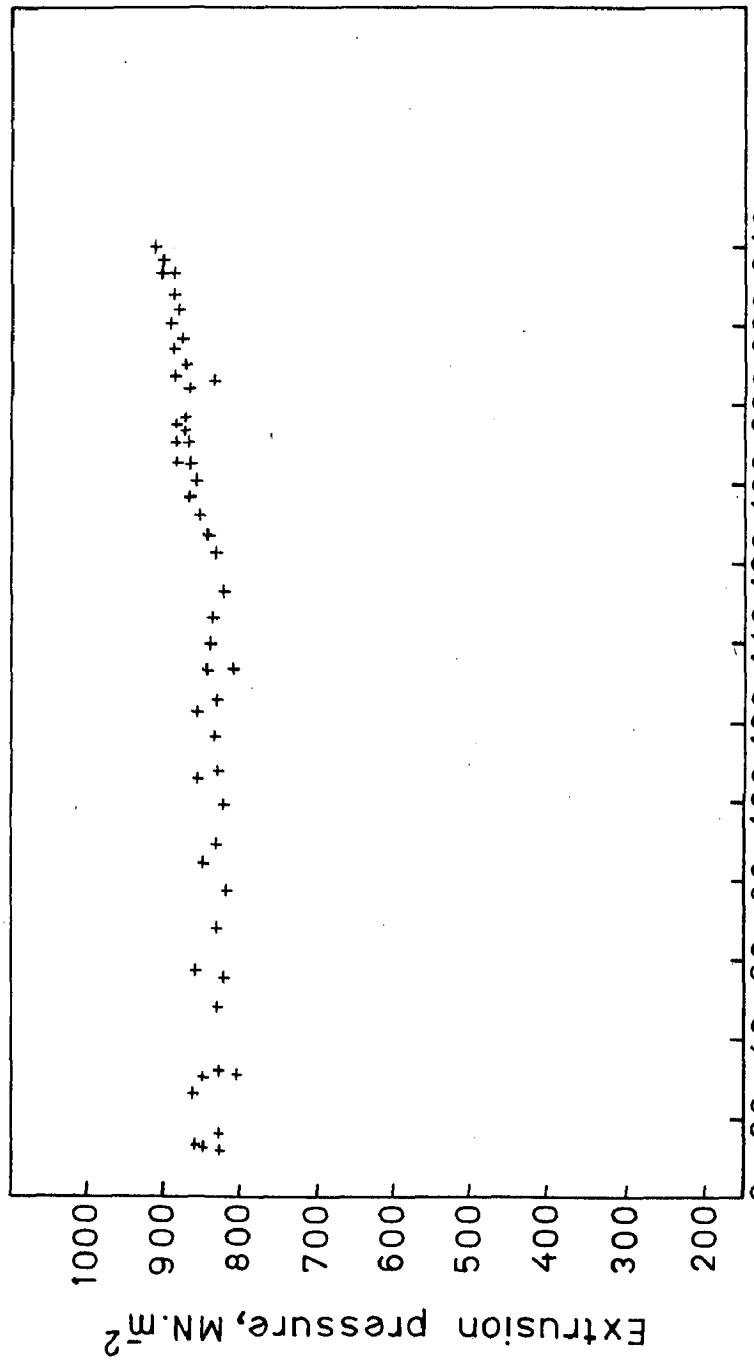

FIG.2.1 THE EFFECT OF STRAIN-RATE UPON EXTRUSION PRESSURE.[67]

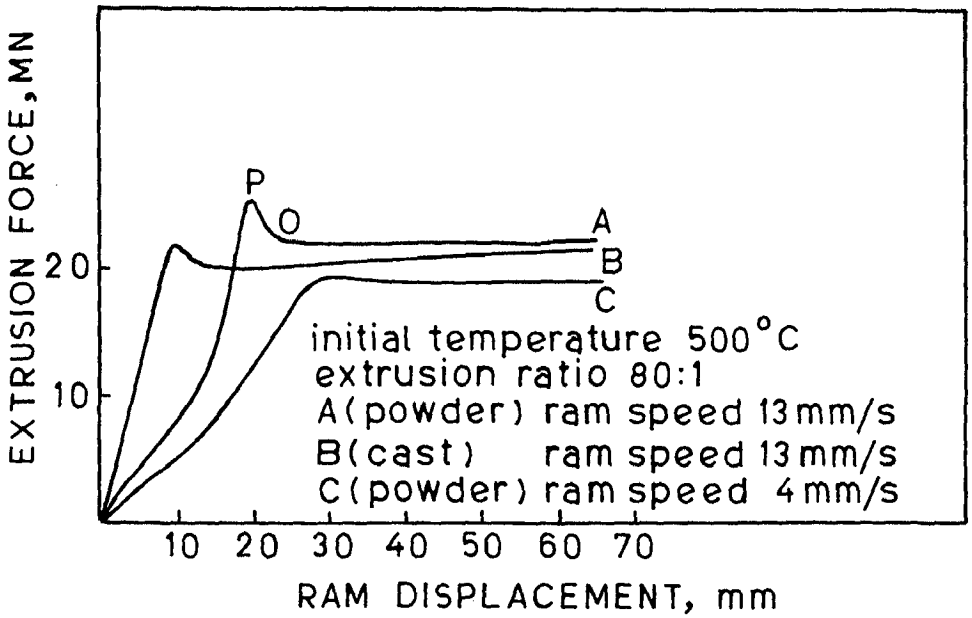

FIG.2.2 LOAD-DISPLACEMENT DIAGRAM.[7]

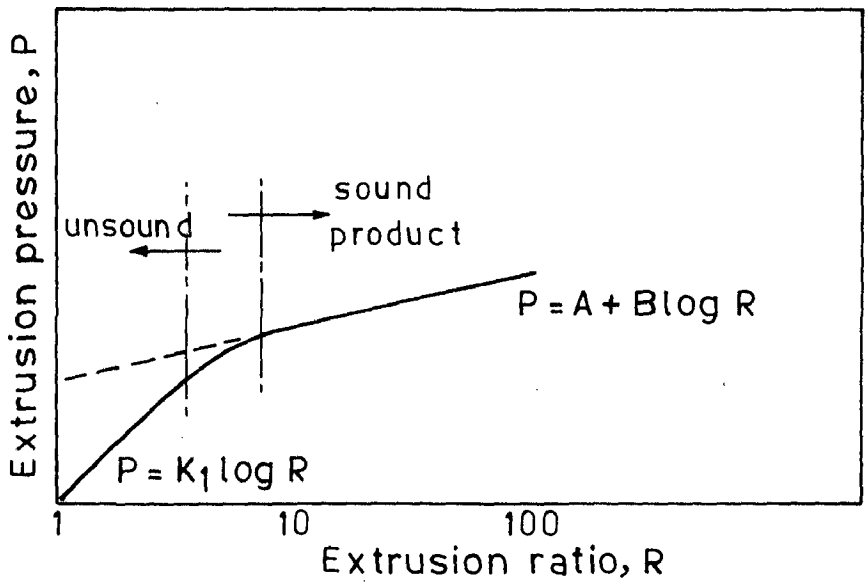

FIG.2.3 PROBABLE REAL PRESSURE/log EXTRUSION RATIO RELATION FOR POWDER BILLET EXTRUSION.[16]

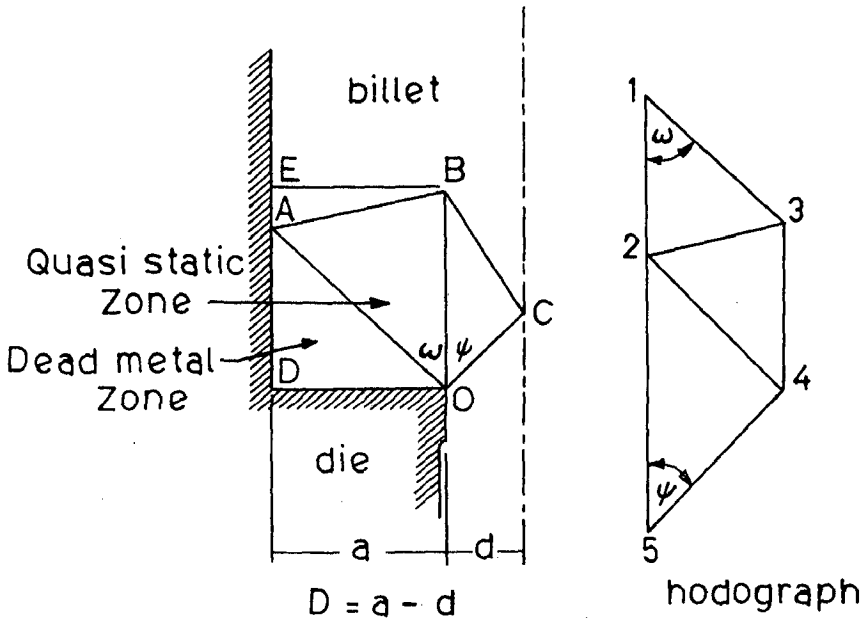

FIG.2.4 UPPER BOUND SOLUTION FOR PLAIN-STRAIN EXTRUSION.[6]

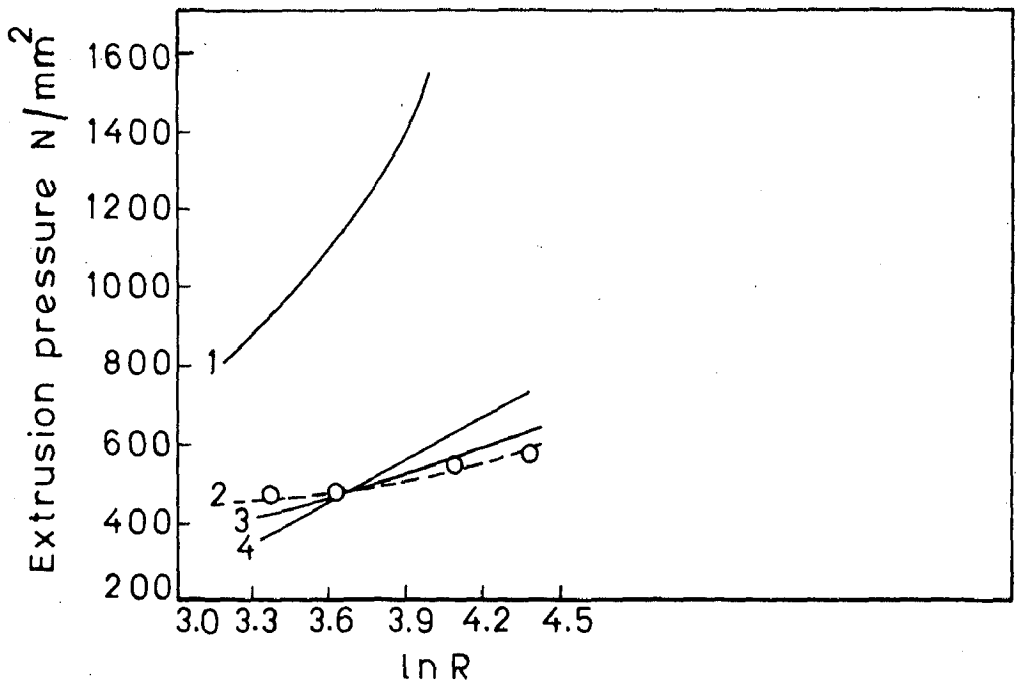

FIG.2.5 COMPARISON OF EXPERIMENTAL AND THEORETICAL RESULTS.[36] (1=Minimized; 2=Experimental; 3=Observed physical field; 4=Minimised axisymmetry)

C H A P T E R - III

FORMULATION OF THE PROBLEM

3.1 INTRODUCTION

A critical analysis of the literature reveals that there have been mainly two approaches to understand the process of extrusion of aluminium powder through square edge dies :

i) The experimental approach involving (a) an examination of the effect of extrusion parameters on the extrusion pressure and quality of the product, and (b) the microstructural changes during the process.

ii) Analytical approach based on upper bound solution to predict the extrusion pressure assuming that intensive shear zones are formed in the billet being extruded.

It has been further suggested that redundant work is an important parameter for achieving coherency. In order to maximise redundant work square edge dies with high reduction ratios ($R > 10:1$) were mainly employed for powder extrusion due to existence of massive shear zones. It was argued that coherent mass can not be obtained at low reduction ratios ($R < 10:1$) due to the formation of shorter massive shear zones (and hence lesser redundant work) which is insufficient to yield coherent extruded product. On the basis of this reasoning the possibility of employing wedge shaped dies for powder extrusion was not favoured. However, it is felt that role of homogeneous work of deformation with

regard to coherency of the product should be properly examined.

Effect of temperature on the coherency of the product has not been considered so far. However, it was anticipated that this, being an important parameter in controlling densification, would definitely influence coherency. It is also expected that structural changes before and after the extrusion of aluminium powder by way of metallographic examination would provide concise information on the mechanism of densification/bonding between the individual particles and their subsequent deformation - an area which is still unexplained.

It is, therefore, proposed to investigate the problem from both the angles i.e. experimental as well as analytical approach, using square and wedge shaped dies for various reduction ratios (low, less than 10:1, and high reduction ratio) and at different temperatures, 300 to 500°C. Analytical approach using finite element method with velocity pressure formulation has been adopted.

3.2 EXPERIMENTAL APPROACH

In view of the above it was approached to investigate the following :

i) Extrusion through square dies at low ($R < 10:1$) and high reduction ratios ($R > 10:1$) in the temperature range from 300 to 500°C.

ii) Extrusion through wedge shaped dies with semicone angle of 45° at low and high reduction ratios (R=1.6:1 to 80:1) in the same temperature range as in case of square die.

iii) The effect of extrusion temperature and reduction ratios on coherency of the product.

iv) To establish a relation between extrusion pressure and extrusion parameters (reduction ratio and temperature).

v) To critically analyse the role of redundant work, work for homogeneous deformation and frictional effect in the extrusion process.

vi) To investigate density changes of the mass being extruded.

vii) To compare the quality of the extruded product in square dies and wedge shaped dies by way of tensile properties measurements and detailed macroscopic examination of the cross-sections and the surface.

viii) To investigate in detail the microstructural changes that occur in the billet and its subsequent emergence as an extruded product.

3.3 ANALYTICAL APPROACH

Metal forming problems have been analysed using slip line approach and subsequently upper bound technique. Both these techniques involved some inherent assumptions as indicated in section 2.10. Finite element method was then used for these non-Newtonian flow problems and various approaches viz. elasto-plastic analysis, penalty function approach, stream line approach and velocity pressure formulation have been used for cast billet. The velocity pressure formulation was employed by Jain [50] to analyse number of problems in static and quasi-static situations involving free surface problems with large surface deformations and with

changing contact boundaries. This formulation is also capable of considering strain hardening and friction effects.

In the present investigation it is proposed to analyse the problem of extrusion of aluminium powder by using velocity pressure formulation which gives us :

i) Flow of metal in the form of velocity vectors at different sections of the billet and die.

ii) The variation of pressure inside the billet.

iii) The effective strain rate can be directly obtained inside the billet.

It is also proposed to establish a correlation between the experimental and analytical studies.

3.4 VELOCITY-PRESSURE FORMULATION

Although the details of the formulation are now well established but for the sake of completeness these are briefly reproduced in the following section indicating the modification incorporated for the present investigation wherever necessary.

3.4.1 Finite Element Method (FEM)

FEM is a technique in which a continuum with infinite degree of freedom is approximated by an assemblage of sub-regions (elements), each of which has a simple geometry (triangle, rectangle, prism etc.). The number of unknowns are finite and each element interconnects with its neighbours through the element nodes which usually (but not always) lie on the element boundaries. Thus, any

continuum must first be divided into finite number of elements.

Briefly, the analysis of a continuum by finite element method has three basic steps :

i) Idealization, in which the continuum is divided into an assemblege of discrete elements.

ii) Evaluation of element characteristics such as stiffness, stress, mass matrices etc.

iii) Assembly and solution of the simultaneous equations, calculation of stresses etc.

Idealization is not usually a difficult problem. However, the most important step is the determination of element characteristics. Most of the literature on the finite element deals with this aspect. Attempt is always made to produce an element which is well behaved, converges faster and whose properties can be generated cheaply.

The third step, namely the assembly and solution of equations is more or less standardized for linear problems. For non-linear problems the solution usually proceeds iteratively. The complete details of this method are available elsewhere [51,52].

3.4.2 Non-Newtonian Fluids

All those fluids for which the flow curve (shear stress τ Vs shear strain $\dot{\gamma}$) is not linear through the origin at a given temperature and pressure are said to be non-Newtonian i.e. those which have the variable viscosity. The behaviour of time-independent Bingham fluids (Fig. 3.1) can

be represented by,

$$\tau = \tau_y + \bar{\mu}\,\dot{\gamma}^n \qquad ..(3.1)$$

where the values of τ_y and $\bar{\mu}$ and n are as shown in Fig. 3.1 for different types of time-independent non-Newtonian fluids. The apparent viscosity can be expressed as :

$$\mu = \frac{\tau_y}{\dot{\gamma}} + \bar{\mu}\,\dot{\gamma}^{n-1} \qquad ..(3.2)$$

It will be shown later that the behaviour of plastic/visco-plastic fluids can be represented in a similar manner as that of Bingham fluids.

3.4.3 Plastic/Viscoplastic Flow

Because of the great growth of interest over the past few years in metal forming and particularly extrusion, attempts have been made by various researchers [42-50] to set up a theoretical frame work within which a rational appreciation of the various features of the process could be given. Since a mathematical model can never reproduce the physical process which takes place, it is necessary to make various idealizations to bring it into the frame work of mathematical analysis. Clearly, these different analysis can give very good first approximation to the loads required to perform operations and provide indication of the manner in which the material deforms.

For mechanical forming processes like extrusion, identation, forming, rolling, etc. the following assumptions are usually made :

i) The elastic strains are negligible when compared to large rate-dependent plastic strains; thus, the concept of rigid plastic behaviour is well applicable here i.e. the material does not deform till the yield stress is reached, but as soon as yield stress is reached, the material flows like a fluid.

ii) Material is incompressible (no volumetric changes occur). " This assumption holds good for square shaped dies when the material attains nearly 100 % density of the theoretical value before the extrusion starts. In case of wedge shaped dies a proper account of compressibility/compaction has been taken. The details are available in Chapter 5.3."

iii) The flow is highly viscous and can be treated as quasi-static.

iv) For such creeping flows, convective terms in Navier-Stokes equations lose significance. On the other hand, friction and strain-hardening play an important part in such plastic flow problems.

It has been established that starting from the general form of viscoplastic model, and using some yield criterion (usually Von-Mises), viscosity can be shown to be dependent upon strain rates and the yield properties for a plastic/viscoplastic material, and such dependence resembles that of the Bingham type non-Newtonian fluids. Thus, the metal-forming problems (rigid plastic materials) can be treated as non-Newtonian fluid flow cases.

3.4.4 Viscous Incompressible Flow Formulation Using Virtual Work Principle

3.4.4.1 Virtual Work Principle

The virtual work principle is simply an alternative statement of the equilibrium conditions. It states," In a system for which internal forces (stresses) and external applied forces are in equilibrium, the application of any (virtual) system of displacement and corresponding internal strains compatible with it, results in equality of external and internal work".

In the case of fluids, this is also applicable if we replace displacements by velocities and strains by strain rates, and the equilibrium of a specified mass by an arbitrary surface can be considered at an instant of time.

Thus, we can write :

$$\int_{\Omega} \delta \dot{\underline{\varepsilon}}^T \underline{\sigma} \, d\Omega - \int_{\Omega} \delta \underline{u}^T \underline{F} \, d\Omega - \int_{\Gamma_t} \delta \underline{u}^T \bar{\underline{t}} \, d\Gamma = 0 \quad ..(3.3)$$

where $\delta\underline{u}$ and $\delta\dot{\underline{\varepsilon}}$ are virtual velocity and strain rates changes for any flow domain Ω in which tractions $\bar{\underline{t}}$ are specified on boundary Γ_t and where $\delta\underline{u}$ is zero on boundary Γ_u where velocities are given.

3.4.4.2 Discretization with Velocity and Pressure Fields

Describing the velocity and pressure fields by trial functions as :

$$\underline{u} = \sum N_i^u \, a_i^u = \underline{N}_i^u \, \underline{a}^u$$

$$\underline{p} = \sum N_i^p \, a_i^p = \underline{N}^p \, \underline{a}^p \qquad ..(3.4)$$

in which $\underline{N}^u$ and $\underline{N}^p$ are appropriate shape functions, defined element by element. It will be observed from the nature of integrals involved that we require C^c continuity for the velocity field, but discontinuous function can be used to describe the pressure field.

For axisymmetric case as in the present study the velocities and pressure have the trial shape functions as :

$$\underline{u} = \begin{Bmatrix} v_z \\ v_r \end{Bmatrix} = \underline{N}^u \, \underline{a}^u \qquad ..(3.5)$$

$$\underline{p} = \underline{N}^p \, \underline{a}^p$$

For cases of slow steady state viscous flow using the above shape functions and virtual work principle Equation (3.3), we get a simple set of equations which can be written as :

$$\begin{bmatrix} \underline{K}^u & \underline{K}^p \\ \underline{K}^{p^T} & 0 \end{bmatrix} \begin{Bmatrix} \underline{a}^u \\ \underline{a}^p \end{Bmatrix} + \begin{Bmatrix} \underline{F}^u \\ 0 \end{Bmatrix} = 0 \qquad .,(3.6)$$

$$\underline{K} \, \underline{a} + \underline{F} = 0 \qquad ..(3.7)$$

where $\underline{K}$ is the stiffness matrix.

The matrix $\underline{K}$ is dependent on the stress level, or alternatively on the level of strain rates. Thus,

$$\underline{K} = \underline{K} (\underline{\sigma}) = \underline{K} (\dot{\underline{\varepsilon}}) = \underline{K} (\underline{a}) \qquad ..(3.8)$$

The variables associated with K^{th} node are :

$$a_K = \begin{Bmatrix} v_z^K \\ v_r^K \\ p^K \end{Bmatrix} \qquad ..(3.9)$$

Using a cylindrical coordinate system (Fig. 3.2) in case of laminar flow the components of submatrix $a_{k\ell}$ is explicitly given by :

$$a_{k\ell} = \sum_{e=1}^{NE} \int\int_{A^e} \begin{bmatrix} a_1 & a_2 & a_3 \\ a_4 & a_5 & a_6 \\ a_7 & a_8 & a_9 \end{bmatrix} dA^e \qquad ..(3.10)$$

where

$$a_1 = \mu \left[2 \frac{\partial N_i^u}{\partial z} \cdot \frac{\partial N_j^u}{\partial z} + \frac{\partial N_i^u}{\partial r} \cdot \frac{\partial N_j^u}{\partial r} \right]$$

$$a_2 = \mu \left[\frac{\partial N_i^u}{\partial r} \cdot \frac{\partial N_j^u}{\partial z} \right]$$

$$a_3 = N_j^p \frac{\partial N_i^u}{\partial z}$$

$$a_4 = \mu \left[\frac{\partial N_i^u}{\partial z} \cdot \frac{\partial N_j^u}{\partial r} \right]$$

$$a_5 = \mu \left[2 \frac{\partial N_i^u}{\partial r} \cdot \frac{\partial N_j^u}{\partial r} + \frac{2 N_i^u N_j^u}{r^2} + \frac{\partial N_i^u}{\partial z} \cdot \frac{\partial N_j^u}{\partial z} \right]$$

$$a_6 = N_j^p \left[\frac{\partial N_i^u}{\partial r} + \frac{N_i^u}{r} \right]$$

$$a_7 = N_i^p \cdot \frac{\partial N_j^u}{\partial z}$$

$$a_8 = N_i^p \left[\frac{\partial N_i^u}{\partial r} + \frac{N_i^u}{r} \right]$$

$$a_9 = 0 \ .$$

3.4.5 Plastic/Viscoplastic Flow as Non-Newtonian Flow

If elastic deformation is negligible, a very general description of behaviour of most of the materials can be given in terms of viscoplasticity. A particular form of this can be written following Perzyna [53] who defines the strain rate $\dot{\varepsilon}_{ij}$ as :

$$\dot{\varepsilon}_{ij} = \gamma < \varphi(F) > \frac{\partial Q}{\partial \sigma_{ij}} \qquad ..(3.11)$$

where $F = F (\sigma_{ij} , T, \varepsilon_{ij})$ is the description of yield surface and $Q = Q (\sigma_{ij}, T, \varepsilon_{ij})$ is the definition of a plastic potential.

Here, $< \varphi(F) > = 0$ if $F < 0$

and $< \varphi(F) > = \varphi(F)$ if $F \geq 0$ ..(3.12)

(T = extrusion temperature, φ = a suitable functional form)

The most common description of viscoplastic flow of metals (and any other materials) follows the assumption that both the yield and plastic potential surfaces are identical, and that these depend only on the second stress invariant, i.e. :

$$F = Q = \sqrt{3}\sqrt{J_2} - Y \qquad ..(3.13)$$

where

$$J_2 = \frac{1}{2} S_{ij} S_{ij}$$

Y = uniaxial yield stress.

In general, γ itself is dependent on the temperature, T, and the accumulated effective strain, $\bar{\varepsilon}$. The strain rate second invariant is defined as :

$$\dot{\bar{\varepsilon}}^2 = 2\,\dot{\varepsilon}_{ij}\,\dot{\varepsilon}_{ij} \qquad ..(3.14)$$

From Equation (3.13), the Equation (3.11) of general flow can be written as :

$$\dot{\varepsilon}_{ij} = \gamma < \varphi(\sqrt{3}\sqrt{J_2} - \gamma) > \frac{\sqrt{3}}{2\sqrt{J_2}}\, S_{ij} \qquad ..(3.15)$$

Clearly the strain rates are such that

$$\dot{\varepsilon}_{ij} = 0$$

i.e. the material flows without the volume change, and in the equivalent elastic model it has to assume incompressible behaviour. In such an equivalent model, one can compare the Equation (3.15) to an elastic shear deformation given by

$$\dot{\varepsilon}_{ij} = \frac{1}{2\mu}\, S_{ij} \qquad ..(3.16)$$

in which μ is shear modulus. Indeed, the shear modulus and viscosity play an identical part in viscous and elastic behaviour. Thus, viscosity is identified by :

$$\frac{1}{2\mu} = \frac{\gamma\sqrt{3}}{2\sqrt{J_2}} < \varphi\,(\,\sqrt{3}\sqrt{J_2} - Y\,) > \qquad ..(3.17)$$

and this is a function of the stress level.

An equivalent equation in terms of the strain rate, from Equations (3.13) and (3.16), can be written as :

$$J_2 = 2\mu^2\,\dot{\varepsilon}_{ij}\,\varepsilon_{ij} = \mu^2\,\dot{\bar{\varepsilon}}^2 \qquad ..(3.18)$$

Here, from expression (3.17) and (3.18) one gets

$$\dot{\bar{\varepsilon}} = \gamma \sqrt{3} < \varphi (\sqrt{3} \mu \dot{\bar{\varepsilon}}^2 - \gamma) > \quad ..(3.19)$$

from which μ can be found for any strain rate function.

For an exponential type law Equation (3.15) takes the form :

$$\dot{\varepsilon}_{ij} = \gamma < (\sqrt{3} \sqrt{J_2} - \gamma)^n > \frac{\sqrt{3}}{2\sqrt{J_2}} S_{ij} \quad ..(3.20)$$

and μ can be evaluated explicitly from Equation (3.19) as :

$$\mu = \frac{\gamma + [\frac{\dot{\bar{\varepsilon}}}{\gamma \sqrt{3}}]^{1/n}}{\sqrt{3} \dot{\bar{\varepsilon}}} \quad ..(3.21)$$

Equations (3.20) and (3.21) are of great generality. Ideally plastic material with a fixed yield point, is simply obtained by taking $\gamma = \infty$ which gives

$$\mu = [\frac{Y}{\sqrt{3} \dot{\bar{\varepsilon}}}] \quad ..(3.22)$$

The form of Equation (3.21) is identical to Equation (3.2) for non-Newtonian fluids. It is, thus, clearly observed that the plastic/viscoplastic flow is a special case of non-Newtonian fluid (Bingham fluid) and, by using Equation (3.22), rigid plastic material can be analysed as non-Newtonian fluid.

3.4.6 Some Important Aspects of Metal Forming Process

3.4.6.1 Frictional Effect

If the boundary of the container is rough and friction is present, the extrusion pressure increases with the

length of the section between the ram and die. For this reason the solutions are less general than those for the frictionless case. The effects of boundary friction were introduced by inserting a narrow layer of elements between the boundary of the container wall and the die with billet, and assigning different values to the friction coefficient. The effect of friction was considered by varying the yield properties of boundary layer elements, depending upon the mean pressure existing in those elements. The pressure dependence of yield strength presents a useful device for dealing with friction conditions. The relation

$$k = \frac{Y}{\sqrt{3}} = \alpha \sigma_m \qquad ..(3.23)$$

α = friction coefficient

σ_m = pressure or first stress invariant

gives a good approximation to purely frictional behaviour.

3.4.6.2 Strain Hardening Effect

The true characteristics of most materials show considerable strain hardening, and the assumption of ideal plasticity may not be correct for such materials. In a transient situation, it is not difficult to include such strain hardening in the calculations. As at such stage of the deformation the strain rates are known, the total strain, and in particular the total (scaler) effective second strain invariant, can be evaluated, and the yield strength can then appropriately be updated.

3.4.6.3 Singularity Effects

When dealing with rough boundaries and also at the exit from the die, exact boundary conditions can only be effectively dealt with by making the mesh singular at these points. These have been studied with respect to axisymmetric problems of square and wedge shaped dies.

3.4.6.4 Sequence of Operation

We start from a prescribed initial value of viscosity in the first iteration and solve for Newtonian velocities, using Equation (3.6) knowing the velocities, the strain rates ($\dot{\varepsilon}_{ij}$), and hence the effective strain rate [$\dot{\bar{\varepsilon}} = \sqrt{2\ \dot{\varepsilon}_{ij}\ \dot{\varepsilon}_{ij}}$] can be obtained. Then using Equation (3.21), a new value of viscosity is obtained which modifies the [K] matrix accordingly.

Iteration of the type :

$$\{ a^{n+1} \} = - [K^{n}]^{-1} \{ F \} \qquad ..(3.24)$$

are then performed to get the results of desired accuracy. The effect of convective terms (if needed) can also be included simultaneously in these subsequent iterations.

3.4.6.5 Convergence Criterion.

In the iterative procedure, it is necessary to ensure that the desired accuracy has been obtained, and then the iterations can be terminated. Since we are mainly interested in velocities, the following criterion was set:

$$|U_{new} - U_{old}| < \text{some absolute value}$$

where U_{new} is the current velocity and

U_{old} is the velocity obtained in previous iteration.

The absolute value is ordinarily set as 1 percent of average axial velocity in the domain. Usually 6 to 8 iterations were sufficient to get this accuracy.

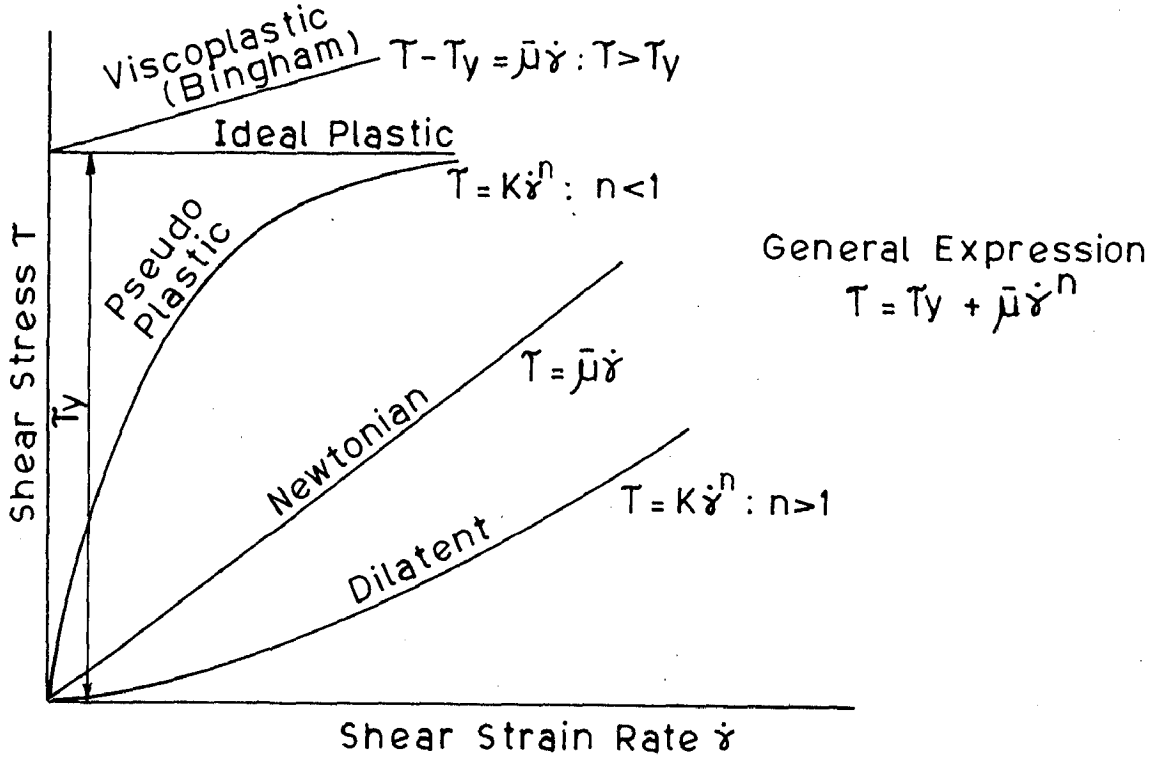

FIG.3.1 FLOW CURVES FOR VARIOUS TYPES OF TIME-INDEPENDENT NON-NEWTONIAN FLUIDS.

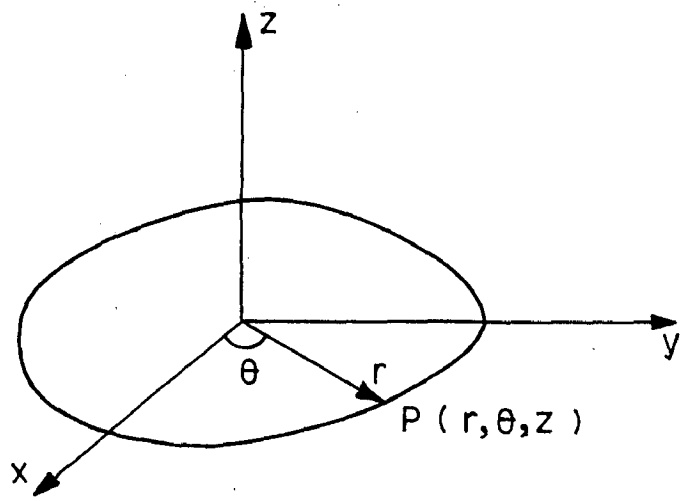

FIG.3.2 CYLINDRICAL CO-ORDINATE SYSTEM.

CHAPTER - IV

EXPERIMENTAL PROCEDURE

4.1 INTRODUCTION

In this chapter experimental procedure for hot extrusion of aluminium powder has been described. Experiments on cylindrical powder compacts were conducted to establish a yield criterion at high temperatures. Yield stress of the billet being extruded was also determined at the extrusion temperatures.

4.2 ALUMINIUM POWDER AND ITS CHARACTERISTICS

4.2.1 Particle Size Distribution

Atomised aluminium powder, 99.5% pure supplied by M/s Metal Powder Company, Madurai, India, was used in the present study. The particle size distribution determined by sieve analysis is given in Table 4.1.

TABLE - 4.1

PARTICLE SIZE DISTRIBUTION OF POWDER

S.No.	Size in Microns	Weight % of powder
1	+ 147	6.3
2	+ 74	17.5
3	+ 45	30.7
4	- 45	45.5

4.2.2 Particle Shape

Shape of the powder particles was examined by Stereo Microscope and Scanning Electron Microscope. It was observed that aluminium powder was of flake type.

4.2.3 Apparent Density and Flow Rate

Apparent density and flow rate of the powder were determined according to ASTM standard Nos.B417-64 and B213-48 [55].

Flow rate of the powder was very poor and no flow data could be recorded by Hall Flowmeter. The apparent density of the powder was found to be 1 gm/c.c.

4.2.4 Chemical Analysis

The chemical analysis of the powder was carried out to determine the insolubles. It was found to have 0.32% insolubles.

4.3 EXPERIMENTAL SET-UP

In the present investigation direct extrusion process has been employed. The experimental set-up consists of extrusion assembly as shown in Fig. 4.1.

4.3.1 Extrusion Assembly

It consists of two parts (i) the preform container and (ii) extrusion die. Both the parts were fabricated from hot die steel having the chemical composition 5% Cr,

0.35%C , 1.0% V and 1.5% Mo. It was hardened and tempered to hardness, Rc-55. The internal surface finish of the preform container, die surface and ram was of the order of one micron. Toolings were manufactured as per our drawing (Figs. 4.2(a),(b) and (c)) by B.H.E.L., Hardwar.

4.3.2 Powder Preform Preparation

Cold preform of aluminium powder, was prepared by compacting aluminium powder in a cylindrical die of 27 mm diameter to 85% theoretical density. The height of the compact varied from 40 to 50 mm. The single action hydraulic press, 20T capacity was employed. The die was lubricated by zinc stearate. Powder was dry compacted.

4.4 EXTRUSION

Colloidal graphite powder solution in acetone was applied as lubricant to the wall of the container and die surface before it was heated to the extrusion temperature. Two thermocouples were used.

The thermocouple touching the outer surface of the die was connected to temperature controller and the other thermocouple was introduced inside the container. When the extrusion temperature reached, the temperature indicated by the first thermocouple was set on the controller and then powder preform and the ram was introduced. Sufficient time was allowed before starting the extrusion to ensure that the powder preform attained the

extrusion temperature. The extrusion was carried out mainly at three different temperatures namely, 300, 400 and 500°C. Square edge dies having low reduction ratios, 1.3:1, 1.6:1, 2.1:1, 2.6:1, 3.2:1 and high reduction ratios, 10:1, 20:1, 30:1, 40:1 and 80:1 were employed. Wedge shaped dies with 45° semicone angle having low reduction ratios, 1.6:1, 2.0:1, 3.5:1, 7:1 and high reduction ratios, 12:1, 30:1, 45:1 and 80:1 were used. Extrusion tests were carried out on 20 and 40 tons Universal Testing Machine at a ram speed 1 mm/sec and the load ram displacement diagrams were recorded on a strip chart recorder.

4.5 DETERMINATION OF YIELD CRITERION

The density of the extruded product and the billet being extruded was not found to be 100% of theoretical value at low reduction ratios ($R < 10:1$) both in square and wedge dies. Hence, a yield criterion for porous compacts was established to take into account the variation in density at different temperatures.

Cold compacted cylindrical aluminium powder preforms, having 85% of the theoretical density and $H/D < 1$ were compressed at different temperatures viz. 300, 400, 450 and 500°C. The technique of incremental straining was used. Loading and unloading the preform during compression test was gradually performed. For heating the specimen upto required temperature, the specimen was kept in a cylindrical

furnace of 100 mm diameter and 125 mm height. A thermocouple was inserted inside the furnace to control the temperature. The specimen temperature was measured by another thermocouple. Graphite powder (-300 mesh) was used as a lubricant at the interfaces and it was smeared after each increment of strain. This provided minimum and uniform interface frictional condition and barreling was negligible leading to axisymmetric deformation. After each known incremental loading the specimen was cooled in air to room temperature, the height and diameter were measured at different places to get average of these. These data were used to calculate the density, transverse strain, axial strain and axial stress for all the values of incremental strains.

4.6 DETERMINATION OF YIELD STRESS OF BILLET BEING EXTRUDED

In order to determine the yield stress of the billet being extruded the extrusion tests at all reduction ratios (through square die) were stopped at maximum load and the tensile specimens were prepared from longitudinal direction of the unextruded billet and the yield stress of these samples were determined at the same temperature at which they were extruded. The test was carried out at a strain rate of 1.6 mm/min using a motorised Monsanto Tensometer, Type 'W'. A high temperature furnace was fabricated using a band heater of 2000 watts, 15 cm long and 5 cm diameter.

A copper tube of 2 mm internal diameter was brazed on the outer surface of mild steel furnace shell to cool the outer surface. The tensile specimen was positioned in the middle of the furnace and two thermocouples touching shoulders of the tensile specimen were used to ensure that the sample remained at uniform temperature. The tensile tests were carried out and load - extension curves were recorded on strip chart recorder. The 0.2% proof stress/yield stress determined from the load-extension curves are given in Table 4.2 for different reduction ratios in the case of square dies. These values were also used for wedge shaped dies. They were used for analytical study to calculate the pressure and effective strain rate. Table 4.2 shows that the yield stress value increased with increase of reduction ratio. However, tensile specimen could not be prepared from the billet being extruded at 300°C due to brittleness.

4.7 DENSITY MEASUREMENTS

The density measurements [56] as per IS: 4841-1968 of the extruded product and the unextruded billet under steady state condition were carried out.

4.7.1 Test Procedure

The density of the extruded product and the product being extruded were measured by Archimedes principle. To measure the weight of the specimen, stanton electronic

semimicro balance having senstivity of 1 x 10^{-5} gm was used. Porous specimens were dipped in paraffin wax to prevent the water from entering the pores. Before weighing the specimen the excess paraffin wax was removed from the outer surface of the specimen.

TABLE - 4.2

YIELD STRESS OF BILLET BEING EXTRUDED FOR SQUARE EDGE DIES

S.No.	Reduction Ratio	0.2% Proof Stress (N/mm^2)	
		500°C	400°C
1.	1.3:1	25.0	36.0
2.	1.6:1	25.3	36.3
3.	2.1:1	26.0	36.8
4.	2.6:1	26.7	37.4
5.	3.2:1	27.5	38.0
6.	10:1	28.5	42.2
7.	20:1	31.2	46.3
8.	30:1	32.4	50.6
9.	40:1	33.7	52.8
10.	80:1	36.0	57.0

4.8 MEASUREMENT OF TENSILE PROPERTIES

Tensile tests on the product extruded through square dies for reduction ratios, 1.3:1 to 10:1, and wedge dies for 1.6:1 to 12:1, at temperatures 300 to 500°C, were

carried out at room temperature. The tests were performed on motorised Monsanto Tensometer, Type 'W' at a strain rate of 1.6 mm/min.

4.9 METALLOGRAPHIC STUDIES

The longitudinal and transverse section of the extruded products were electropolished and etched using 'Elypovist' Electropolisher. The electrolyte used was a mixture of nitric acid (65 %) 300 ml and methyl alcohol 700 ml. The polishing time varied from 25 to 40 sec and the voltage across the electrodes was maintained at 24 volts. Whereas the etching time varied from 3 to 5 sec and the voltage across the electrodes was maintained at 12 volts. The microstructure of polished and etched specimens were examined by Metavert Incident Light Microscope, Model No. 2GA.

Macrostructural studies were also carried out to identify the dead metal zone boundary and extrusion defects.

The Scanning Electron Microscope (SEM) studies of the fractured surface of the tensile specimen tested at room temperature were also carried out for reduction ratios, 1,3:1, 3.2:1 and 10:1 at 500^{o}C in case of square dies.

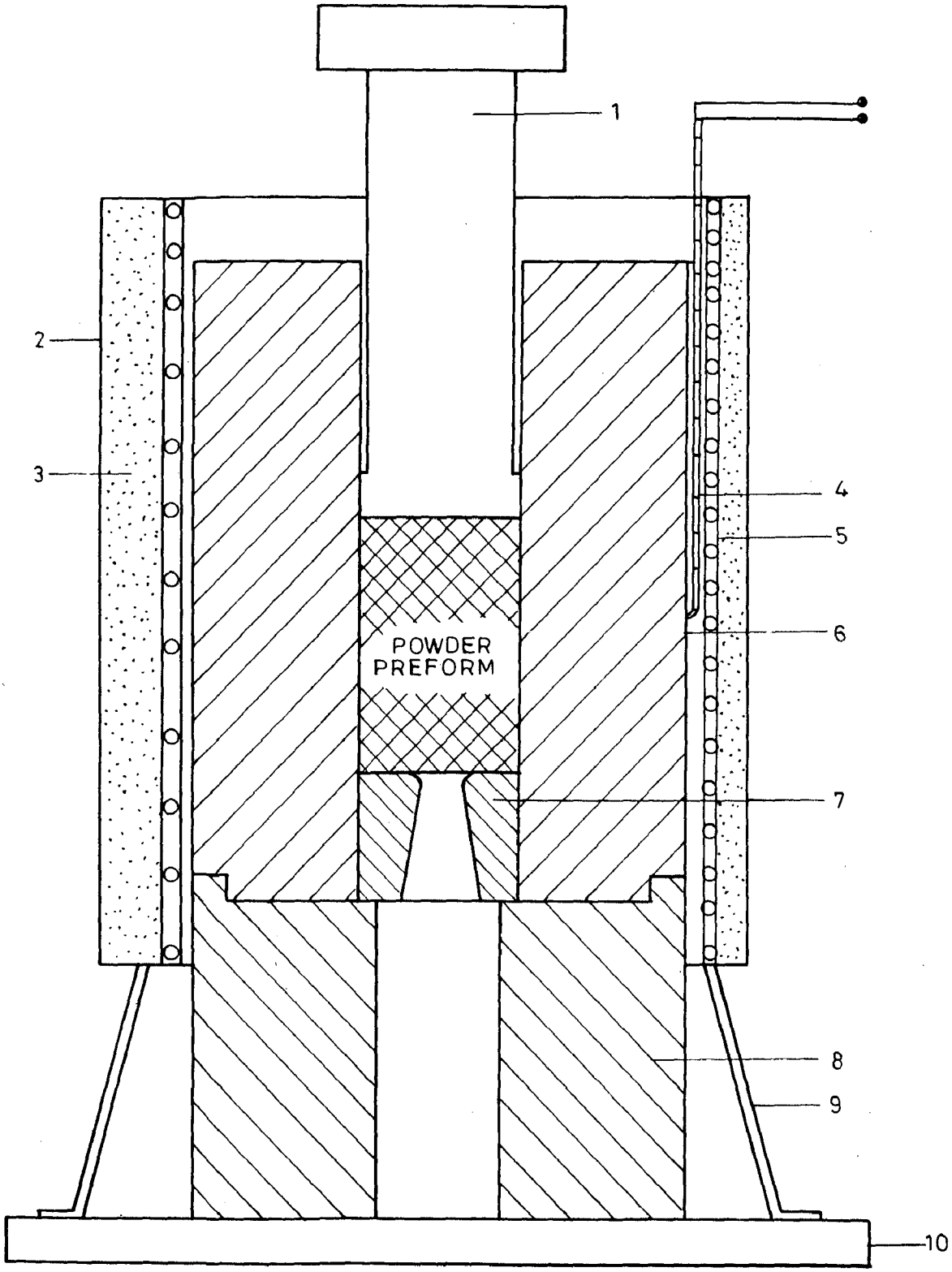

1 RAM
2 OUTER SHELL OF FURNACE
3 ASBESTES POWDER
4 THERMOCOUPLE
5 BAND HEATER
6 PREFORM CONTAINER
7 DIE
8 DUMMY BLOCK
9 HEATER STAND
10 BOTTOM PLATEN

FIG.4.1— EXTRUSION ASSEMBLY (SCHEMATIC SECTION)

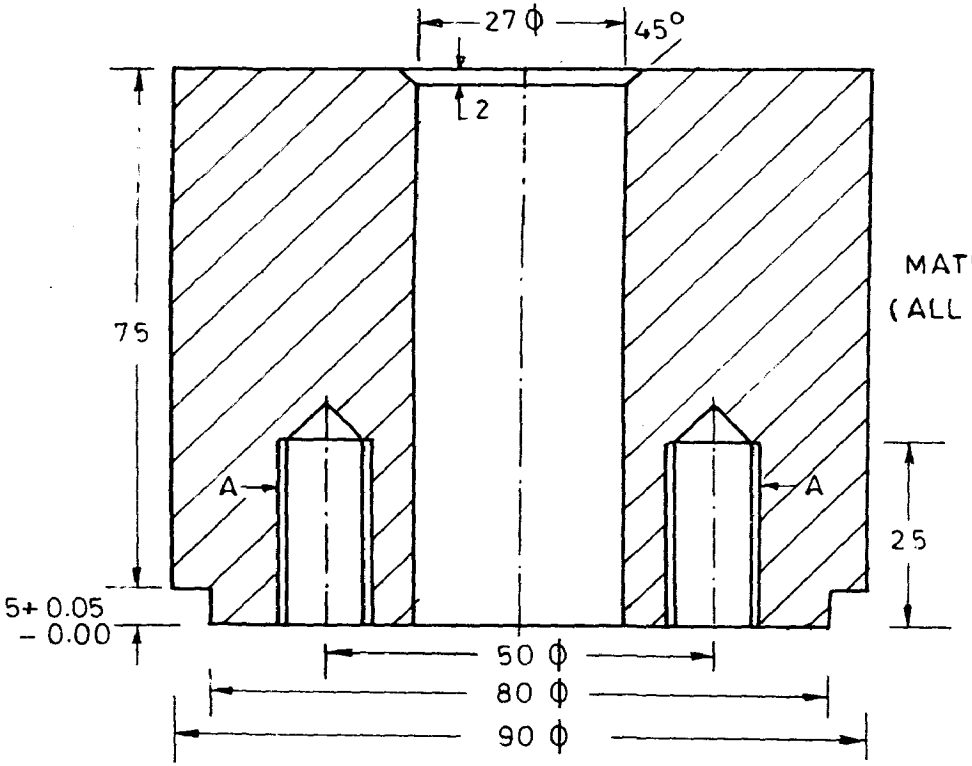

A = 4 NOS. M x 12 TAPPED HOLES AT 90 pcd EQUISPACED AND 25 DEEP EQUIAXIAL

FIG.4.2 (a)-PREFORM CONTAINER

MATERIAL- HOT DIE STEEL
(ALL DIMENSIONS IN mm)

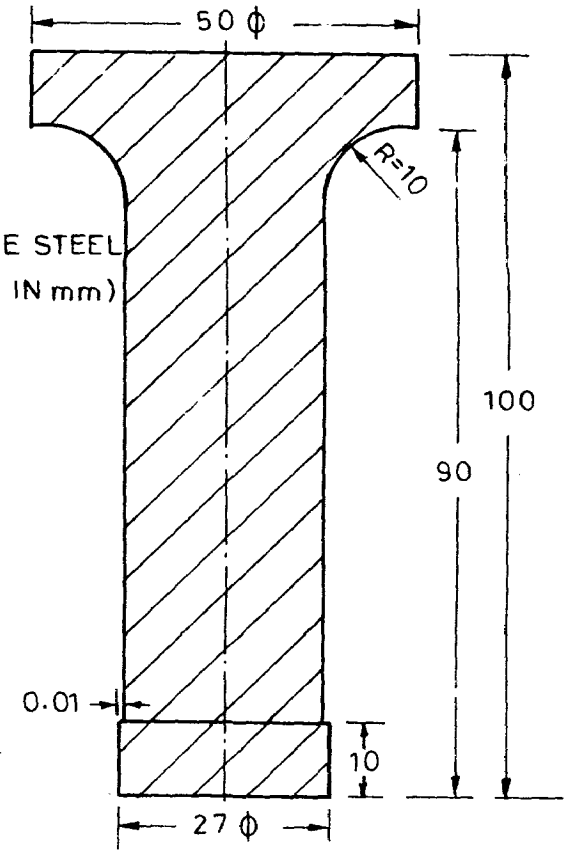

FIG.4.2 (b)-RAM

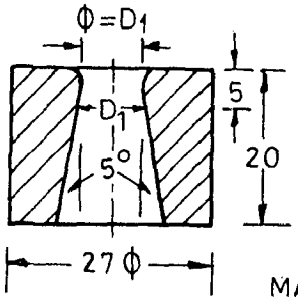

D_1	D_1
8.5	23.0
5.8	21.5
4.8	20.0
4.2	18.8
3.0	15.0

MATERIAL - HOT DIE STEEL

(ALL DIMENSIONS ARE IN mm)

INSERTS USED FOR SQUARE EDGE DIE

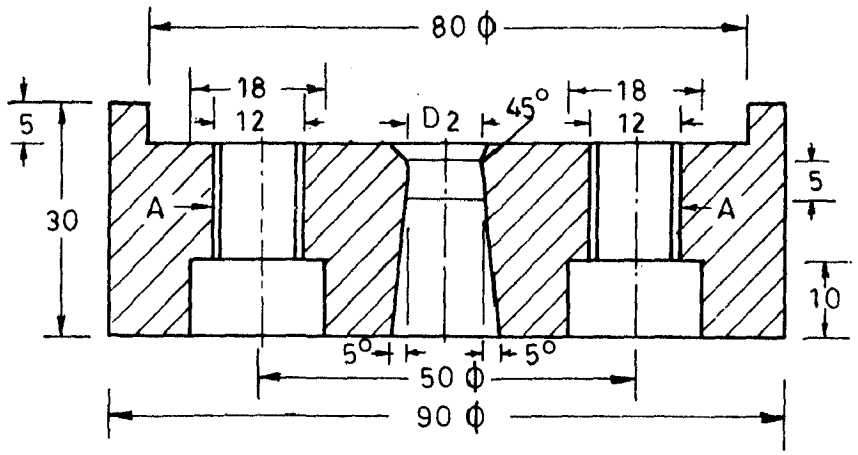

A = 4 NOS. HOLES FOR M×12 ALLEN SCREWS AT 90 pcd EQUISPACED AND EQUIAXIAL

D_2	D_2
21.5	7.0
20.0	5.0
14.3	4.0
10·2	3.0

MATERIAL-HOT DIE STEEL

(ALL DIMENSIONS ARE IN mm)

WEDGE SHAPED DIE

FIG.4.2(c)-DIES

C H A P T E R - V

ANALYTICAL WORK

5.1 INTRODUCTION

In this chapter computer programming using velocity . pressure formulation (u/p), parameteric study and modification in analytical formulation are described. The results of this study have been used to analyse the actual extrusion problem in subsequent chapters.

5.2 COMPUTER PROGRAM

The velocity pressure (u/p) formulation has been used by which the pressures as well as velocities can be obtained. Using this formulation a computer program has been developed for axisymmetric case to solve the two dimensional steady state viscous incompressible and compressible flow problems (plastic/viscoplastic flow problems as non-Newtonian fluids) using Navier-Stokes equations [57] as the basic equations. The program has been executed on a DEC 2050 system. The compressibility effect has been considered by taking into account the density of the billet being extruded and the extruded product by modifying the yield criterion as discussed in section 5.4. The computer program incorporated 8 noded isoparametric parabolic element with three degrees of freedom (u,v,p) at corner nodes and two degrees of freedom (u,v) at middle nodes as shown in Fig. 5.1

It uses an unsymmetric frontal equation solver [58] using the Gaussian elimination method. The basic variables

used are the velocities and pressure while temperature effect was considered by taking the value of yield stress of the billet being extruded at the extrusion temperature. Parabolic shape function is used for the velocity field and linear shape function for the pressure. This has been reported [57] to give better results. 3 x 3 Gauss-Legendre quadrature rule is used for integration.

The boundary conditions are in the form of free tractions or velocities or both and the iterations are done for the variable viscosity. The effects of boundary friction were introduced by inserting a narrow layer of elements near the die surface (for square and wedge dies) and by assigning the different values to the friction coefficient.

The velocities (u,v) and pressure at each node and effective strain rate at all the nine Gauss points are calculated as shown in block diagrams, Fig.5.2, with friction coefficient 0.05 for low reduction ratio ($R < 10:1$) and 0.10 for high reduction ratios ($R > 10:1$) in both the cases (for square and wedge shaped dies). Velocities, pressures and effective strain rates were also calculated without friction ($\alpha=0$) for square dies at low reduction ratios. It seems that the effect of friction is more in case of low reduction ratios ($R < 10:1$) than high reduction ratios($R > 10:1$) for square dies. Hence, for analytical study, $\alpha = 0$ was used for low reduction ratios(1.3:1to 3.2:1). The actual value of friction coefficient would depend upon the lubricant used. The total pressure at the ram boundary was summed up and was considered as the analytical extrusion pressure. The effect of friction coefficient on extrusion pressure per unit yield stress was

studied for square dies at low and high reduction ratios.

5.3 PARAMETRIC STUDIES

The following parameters have been studied in order to improve the accuracy of the results :

i) Effect of configuration adopted for extrusion
ii) Effect of different shapes of element
iii) Effect of iteration
iv) Effect of mesh size
v) Frictional effect.

5.3.1 Configuration Adopted for Extrusion

To ascertain the static stage of extrusion two analyses were made assuming frictionless conditions. First, a stage of extrusion when the billet just starts extruding (Fig. 5.3) and another stage of extrusion when some length of billet had extruded (20 elements mesh as shown in Fig.5.4) were considered for reduction ratio, 3.2:1. In the first case, the velocities at the outlet nodes are not constant as shown in Fig. 5.3(b), while in the other case the velocities at the outlet nodes are constant as shown in Fig. 5.4(b). The latter represents the steady state of extrusion and also satisfies the condition of continuity. In both the cases the extrusion pressure per unit yield stress (p/Y) was obtained and is given in Table 5.1. This shows that as the billet length decreases p/Y value is almost same in case of frictionless condition. Therefore, this configuration has been used for further analysis.

TABLE - 5.1

EFFECT OF BILLET CONFIGURATION

Sl. No.	Billet length	p/Y
1.	25 mm	4.055
2.	12 mm	4.056

5.3.2 Effect of Different Shapes of Element

A 24 element problem has been analysed by taking the elements in the direction of metal flow for reduction ratio, 3.2:1 assuming frictionless condition and a stage of steady state. The shape of the elements and the boundary conditions are shown in Fig.5.5(a). The pressure and velocities at all nodes were obtained after convergence. These velocities are shown in Fig. 5.5(b). The p/Y value is compared with the p/Y value obtained for 20 rectangular elements mesh and is given in Table 5.2. Results reveal that there is not much difference in the p/Y values.

TABLE - 5.2

EFFECT OF DIFFERENT SHAPES OF ELEMENT

Sl. No.	p/Y value of rectangular element mesh	p/Y value for modified element mesh
1.	4.05	3.90

Therefore, either of these can be used. Hence, for simplicity rectangular element has been used for square dies and modified mesh has been used for wedge dies.

5.3.3 Effect of Iteration

For the problem as shown in Fig. 5.3(a) the p/Y values were obtained upto 15th iteration and results are given in Table 5.3.

TABLE - 5.3

EFFECT OF ITERATIONS ON p/Y VALUE

No. of Iteration	p/Y value
1	2.080
2	4.220
3	4.150
4	4.100
5	4.080
6	4.070
7	4.060
8	4.055
9	4.052
10	4.045
11	4.045
12	4.042
13	4.040
14	4.040
15	4.040

It is evident that the difference in p/Y values after 8th iteration is very small i.e. negligible. Hence, in further analyses for other problems the velocity, pressure and effective strain rate were obtained in 8th iteration.

5.3.4 Effect of Mesh Size

The result of 20 elements mesh problem for R, 3.2:1 (Fig. 5.4) is compared with 44 elements configuration as shown in Fig. 5.6, the boundary conditions remaining the same. The p/Y value for 8, 20 and 44 elements mesh problems are shown in Fig. 5.7. The result shows that by increasing the number of elements from 20 to 44 the p/Y value changes by 7.4 %. Therefore, for further work finer mesh has been used.

5.3.5 Frictional Behaviour

For a given configuration, the effect of boundary friction was introduced by inserting a narrow layer of elements between the boundary and the billet and assigning different values to the friction coefficient.

When dealing with rough boundaries and also at the exit from the die (point A and B respectively in Fig. 5.8), exact boundary conditions (by retaining only one node at these points) can only be effectively dealt with, by making the mesh singular at these points. It was noticed that singularity at the exit tip improves the general behaviour and a better presentation of flow pattern was achieved. Therefore, for further analyses singularity effect was considered.

The convergence study was also conducted by incorporating friction elements near the die surface. The 27 rectangular element and 48 rectangular element problems with friction coefficient, 0.05, were analysed for R, 3.2:1, and a stage of steady state, as shown in Figs. 5.9 and 5.10 respectively. The extrusion pressure per unit yield stress was obtained in 8th iteration. The p/Y value of these mesh solutions are shown in Fig. 5.11, indicating that as the number of element increases the p/Y value decreases and compared well with experimental values discussed in Chapter VI.

On the basis of these parametric studies the other problems of different reduction ratios were analysed by taking rectangular elements (for square die), finer mesh and a stage of steady state extrusion. In case of rough boundaries singularity effect was considered. Results were obtained after 8 iterations.

5.3.6 Effect of Friction for Various Reduction Ratios

The effect of different values of friction coefficient on p/Y values were determined and shown in Fig. 5.12 for square dies at different reduction ratios. Results show that the value of p/Y increases sharply upto the friction coefficient value of 0.10 and then increases slowly upto the value of 0.2 and then becomes almost constant upto the value of 0.5. It may be noted that the effect of friction coefficient on low reduction ratios is higher than that on high reduction ratios.

5.4 COMPARISON OF STEADY STATE EXPERIMENTAL EXTRUSION PRESSURE WITH ANALYTICAL VALUES (BY UPPER BOUND TECHNIQUE AND FEM)

The analytical extrusion pressure was calculated by upper bound technique as determined by Sheppard et al.[36] using a modified Equation (2.4) for axisymmetric condition.

Figure 5.13 shows a simple deformation field and hodograph (velocity field) for reduction ratio, 3.2:1. From this Fig. analytical extrusion pressures, calculated at 400 and 500°C using yield stress value at the same temperatures and those by FEM, were compared with the experimental values. The results are given in Table 5.4.

TABLE - 5.4

COMPARISON BETWEEN EXPERIMENTAL AND ANALYTICAL VALUES

R	Temperature °C	Extrusion Pressure(N/mm^2)		
		Experimental Value	By Upper Bound Solution	By FEM $\alpha = 0.05$
3.2:1	500	110	92.7	108.9
3.2:1	400	152.8	128.1	150.5

Results show that the experimental values are very close to analytical values determined by FEM as the difference is only about 1% while the difference is about 16% in the case of upper bound analysis. Thus, FEM is more precise for such metal forming problems than upper bound analysis. Hence, in further study for other reduction ratios extrusion pressures were determined only by FEM.

5.5 YIELD CRITERION

It is reported for aluminium powder extrusion [1] that in square dies with high reduction ratios (R > 10:1), densification was very nearly complete before extrusion started. However, experimental observations, described in the latter chapters, revealed that in wedge shaped dies for all reduction ratios and square dies at low reduction ratios (R < 10:1) the situation was different, as the extrusion started before full densification was achieved. In steady state extrusion the density of the product and the billet being extruded was not found to be 100% of theoretical density. A variation in density was found mainly at low reduction ratios (R <10:1) in both square and wedge shaped dies. A change in analytical approach was, therefore, necessary and modifications made in analytical formulation by using yield criterion for porous compacts, have been discussed.

5.5.1 Yield Criterion for Porous Compacts

As density of the extruded product and billet being extruded was observed to be less than theoretical value, therefore a yield criterion for porous compact has been evolved at high temperatures.

In a fully dense material, yielding is a function only of the second invariant of the stress deviator, J_2'

$$f = (3 J_2')^{1/2} \qquad ..(5.1)$$

In porous powder preform, a hydrostatic stress does cause yielding. Therefore, the yield criterion for these

materials must be a function of hydrostatic stress as well as the deviatoric stress.

$$f = f(J_1 , J_2) \qquad ..(5.2)$$

where

$$J_1 = \sigma_1 + \sigma_2 + \sigma_3$$

represents the hydrostatic stress and is the first invariant of stress tensor. J_1 can be related to J_2' and J_2, the second invariant of stress. Hence, we can write :

$$J_1 = [\, 3(J_2 - J_2') \,]^{1/2} \qquad ..(5.3)$$

Therefore, yield function will be

$$f = f(J_2 , J_2') \qquad ..(5.4)$$

It was proposed by Khun [59] that yielding for sintered porous iron powder preforms may be expressed as :

$$y = [\, 3 J_2' - (1-2\nu) J_2 \,]^{1/2} \qquad ..(5.5)$$

where

ν = Poisson's ratio

J_2' = Second invariant of stress deviator,

$$= \frac{1}{6} [(\sigma_1 - \sigma_2)^2 + (\sigma_2 - \sigma_3)^2 + (\sigma_3 - \sigma_1)]^2$$

where, σ_1, σ_2 and σ_3 are principal stresses

J_2 = Second invariant of stress tensor

$$= -(\sigma_1 \sigma_2 + \sigma_2 \sigma_3 + \sigma_3 \sigma_1).$$

The density and the ν after each incremental load were calculated from the dimensional changes of the test samples. Figure 5.14 shows the variation of ν with density and the relationship is linear. It may be noted that the ν is a

function of density of the material only, and not the temperature. In other words the ν is same at a given density regardless of the test temperatures and can be determined using Fig. 5.14. On extrapolating the curve to 100 % density the ν comes out to be 0.5 , which therefore, justifies using the yield criterion for porous compacts given by Equation (5.5), in the present study.

5.5.2 Modification in Analytical Formulation

If elastic deformation is negligible, a very general description of behaviour of most materials can be given in terms of viscoplasticity. A particular form of this can be written following Perzyna [53] who defines the strain rate, $\dot{\varepsilon}_{ij}$:

$$\dot{\varepsilon}_{ij} = \gamma \langle \varphi(F) \rangle \frac{\partial Q}{\partial \sigma_{ij}} \qquad ..(5.6)$$

where $F = F (\sigma_{ij} , T, \varepsilon_{ij})$ is the description of a yield surface and $Q = Q(\sigma_{ij} , T, \varepsilon_{ij})$ is the description of a plastic potential.

Here, $\langle \varphi(F) \rangle = 0$ if $F < 0$

$$\langle \varphi(F) \rangle \equiv \varphi (F) \text{ if } F \geq 0 \qquad ..(5.7)$$

(T = extrusion temperature, φ = a suitable functional form)

Using Equation (5.5) :

$$F = Q = [3 J_2' - (1-2\nu) J_2]^{1/2} - y \qquad ..(5.8)$$

$$J_2' = \frac{1}{2} S_{ij} S_{ij} = \frac{1}{2} (S_{11}^2 + S_{22}^2 + S_{33}^2) \qquad ..(5.9)$$

$$J_2 = -(S_{11}\,S_{22} + S_{22}\,S_{33} + S_{33}\,S_{11}) \qquad ..(5.10)$$

y = uniaxial yield stress of fully dense material.

In general, y itself is dependent on extrusion temperature, T, and the accumulated effective strain, $\bar{\varepsilon}$. The effective strain rate second invariant is defined as :

$$\dot{\bar{\varepsilon}}^2 = \frac{1}{2}\,\dot{\varepsilon}_{ij}\,\dot{\varepsilon}_{ij} \qquad ..(5.11)$$

The effective strain rate will be :

$$\dot{\bar{\varepsilon}}^2 = \frac{2}{3}\left[\,\dot{\varepsilon}_{11}^2 + \dot{\varepsilon}_{22}^2 + \frac{1}{2}\,\gamma_{12}^2\,\right] \qquad ..(5.12)$$

for two dimensional axisymmetric flow.

From Equations(5.6) and (5.8) we get an equation of modified viscosity as below proceeding similarly as explained in section 3.4.5

$$\mu = \frac{\left[\,y^2 + (1 - 2\nu)\,J_2\,\right]^{1/2}}{\sqrt{3}\,\dot{\bar{\varepsilon}}} \qquad ..(5.13)$$

J_2 in terms of strain rate can be written as :

$$J_2 = -(\dot{\varepsilon}_{11}\,\dot{\varepsilon}_{22} + \dot{\varepsilon}_{22}\,\dot{\varepsilon}_{33} + \dot{\varepsilon}_{33}\,\dot{\varepsilon}_{11} - \frac{1}{4}\,\gamma_{12}^2) \qquad ..(5.14)$$

By substituting the value of J_2 in Equation (5.13) we get the final equation :

$$\mu = \frac{1}{\sqrt{3}}\,\frac{\left[y^2-(1-2\nu)(\dot{\varepsilon}_{11}\,\dot{\varepsilon}_{22}+\dot{\varepsilon}_{22}\dot{\varepsilon}_{33}+\dot{\varepsilon}_{33}\dot{\varepsilon}_{11}-\frac{1}{4}\,\gamma_{12}^2)\,\right]^{1/2}}{\dot{\bar{\varepsilon}}} \qquad ..(5.15)$$

For the porous compact, the value of poisson's ratio depend upon the density of the porous compact. And for fully dense material $\nu = 0.5$ and this gives

$$\mu = \frac{y}{\sqrt{3}\,\dot{\bar{\varepsilon}}} \quad . \qquad ..(5.16)$$

This is the same equation which we get for the fully dense material.

This modified equation given by (5.15) has been used for square and wedge shaped dies for low reduction ratios ($R < 10:1$) where the complete densification was not observed before extrusion. The ν was determined for various densities observed in the experiment using Fig. 5.14.

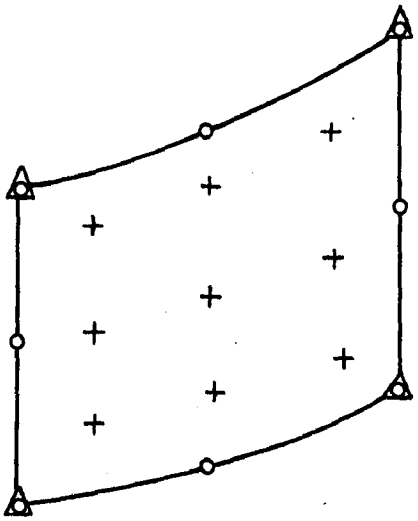

$\underline{u}/p$ (3x3 Gauss Rule)

o Velocities as nodal parameter

Δ Pressure as nodal parameter

FIG.5.1 TWO DIMENSIONAL ISOPARAMETRIC PARABOLIC ELEMENTS.

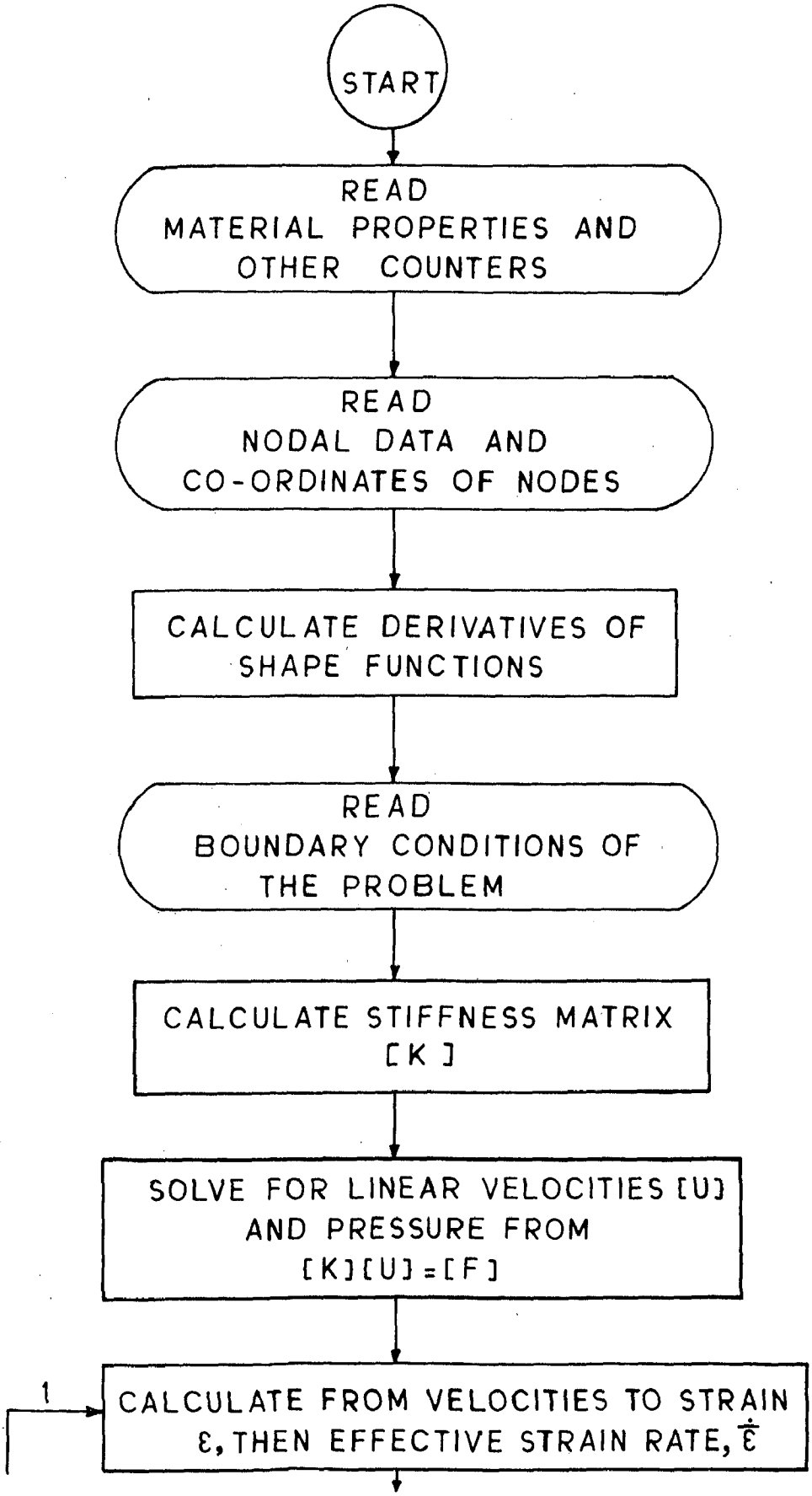

FIG.5.2(a) FLOW CHART OF COMPUTER PROGRAM.

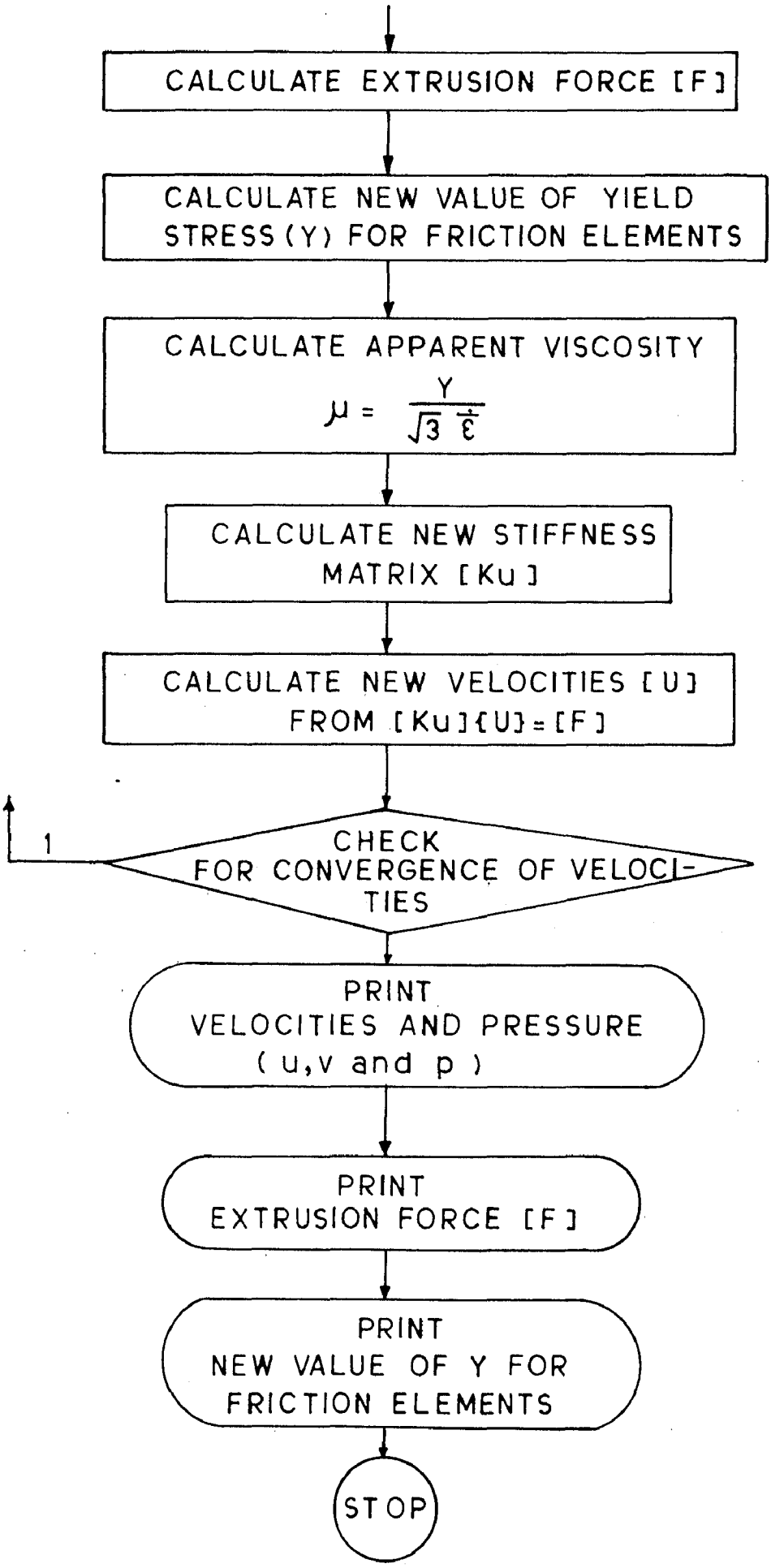

FIG. 5.2(b) FLOW CHART OF COMPUTER PROGRAM.

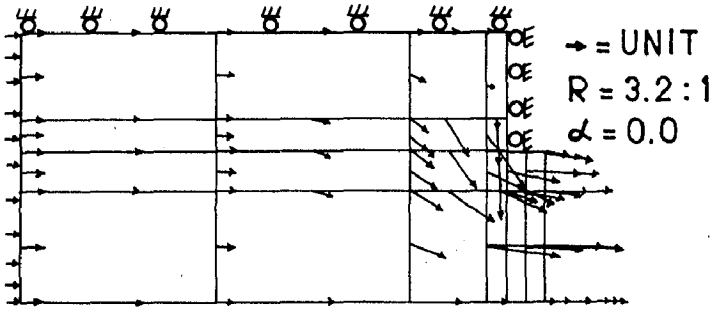

(b) Velocity vectors (20 elements. mesh)

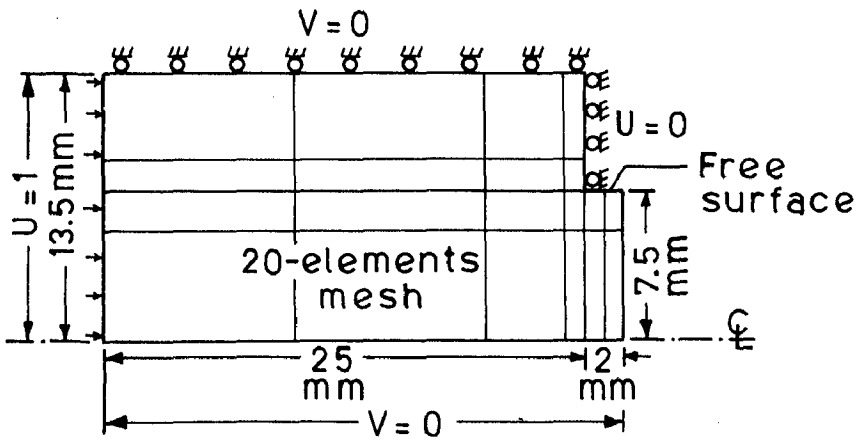

(a) Mesh and Boundary condition.

FIG. 5.3 EXTRUSION JUST STARTED.

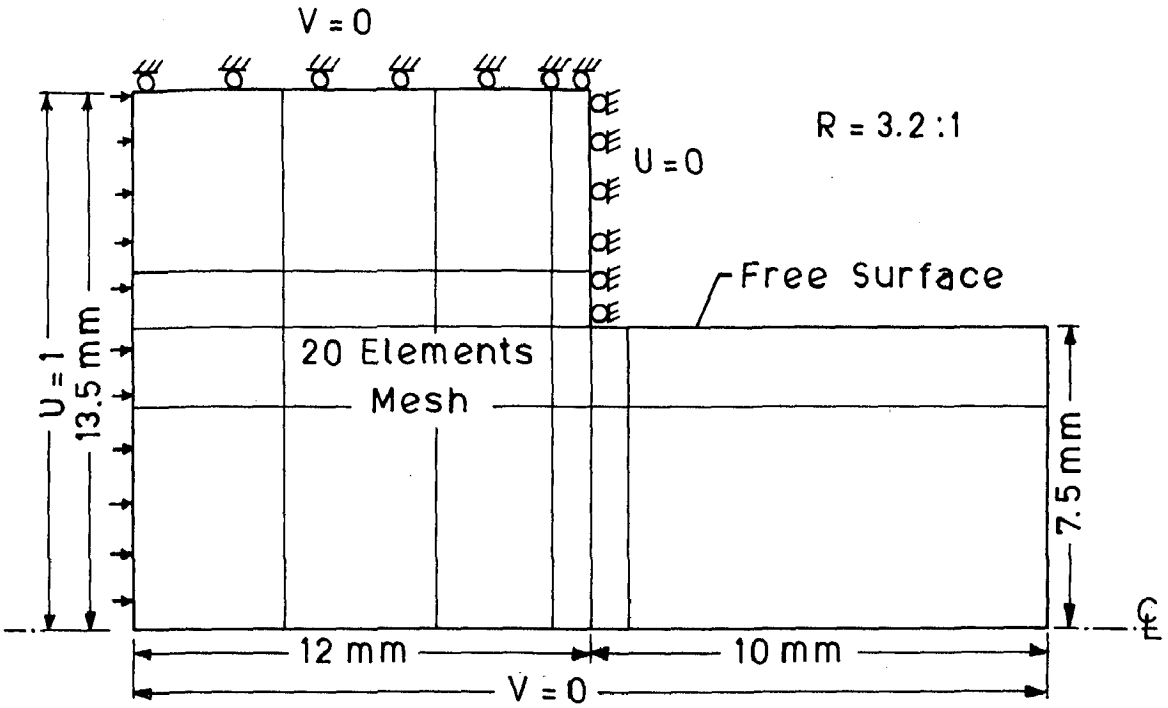

(a) Mesh and Boundary conditions.

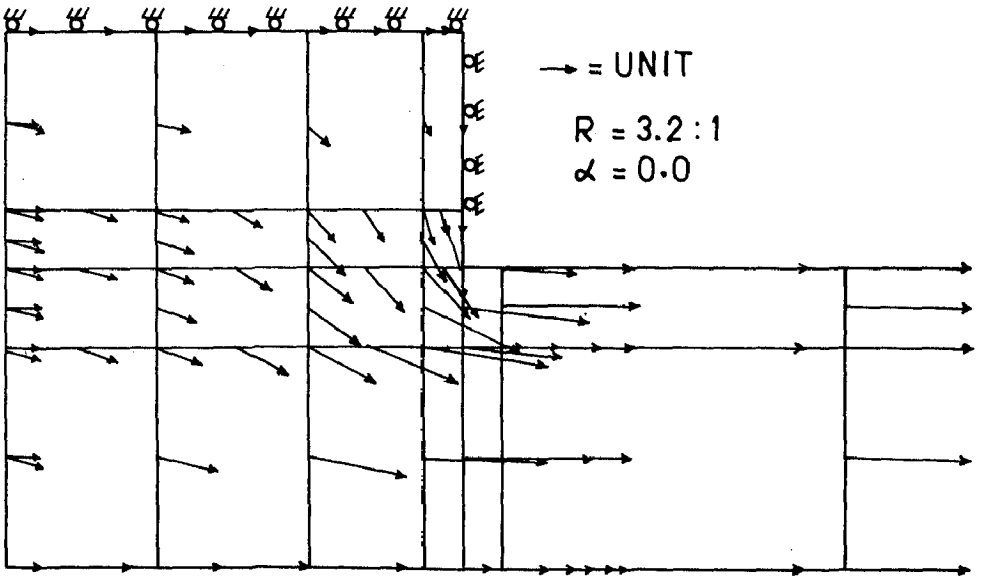

(b) Velocity vectors (20 elements mesh)

FIG.5.4 STEADY STATE EXTRUSION WITH 20 ELEMENTS MESH.

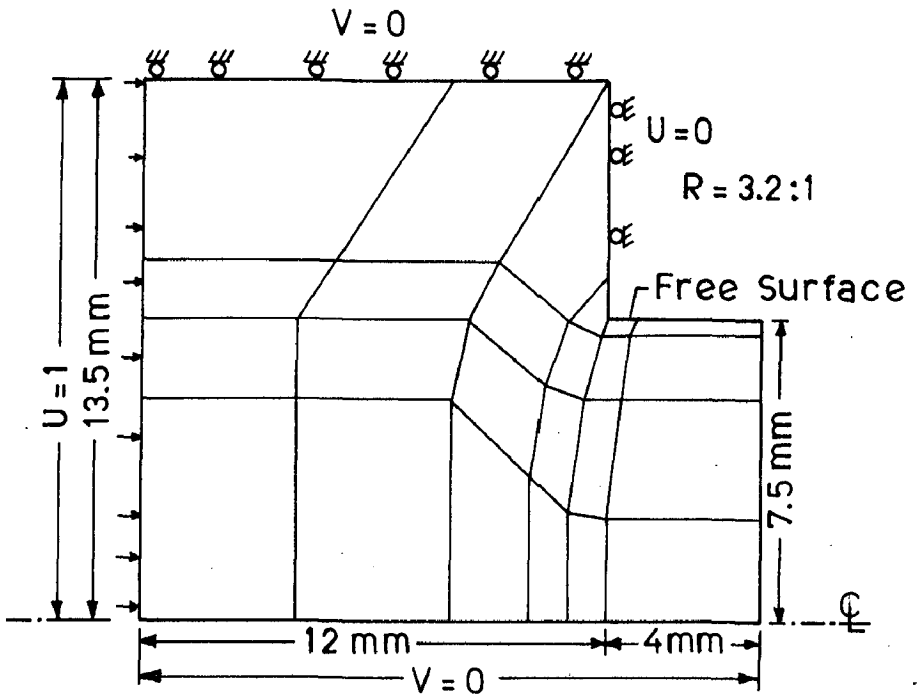

(a) Mesh and Boundary conditions.

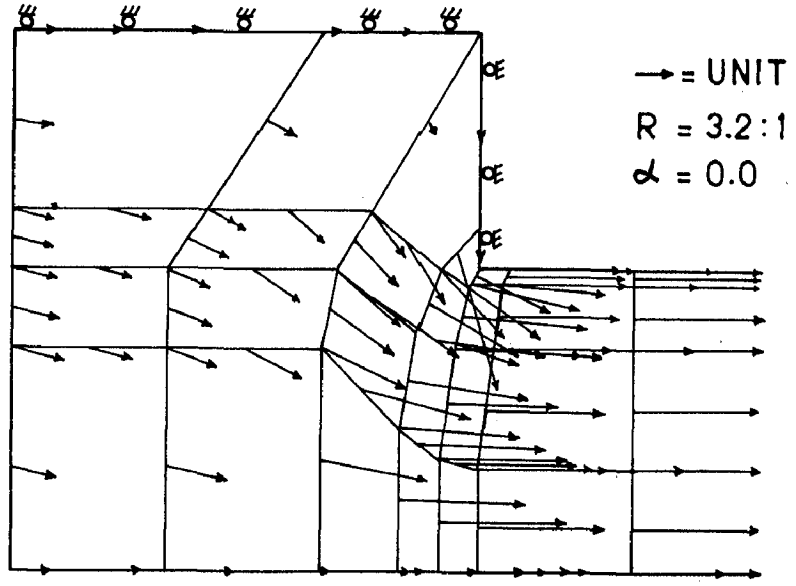

(b) Velocity vectors of modified mesh

FIG.5.5 STEADY STATE EXTRUSION WITH MODIFIED MESH.

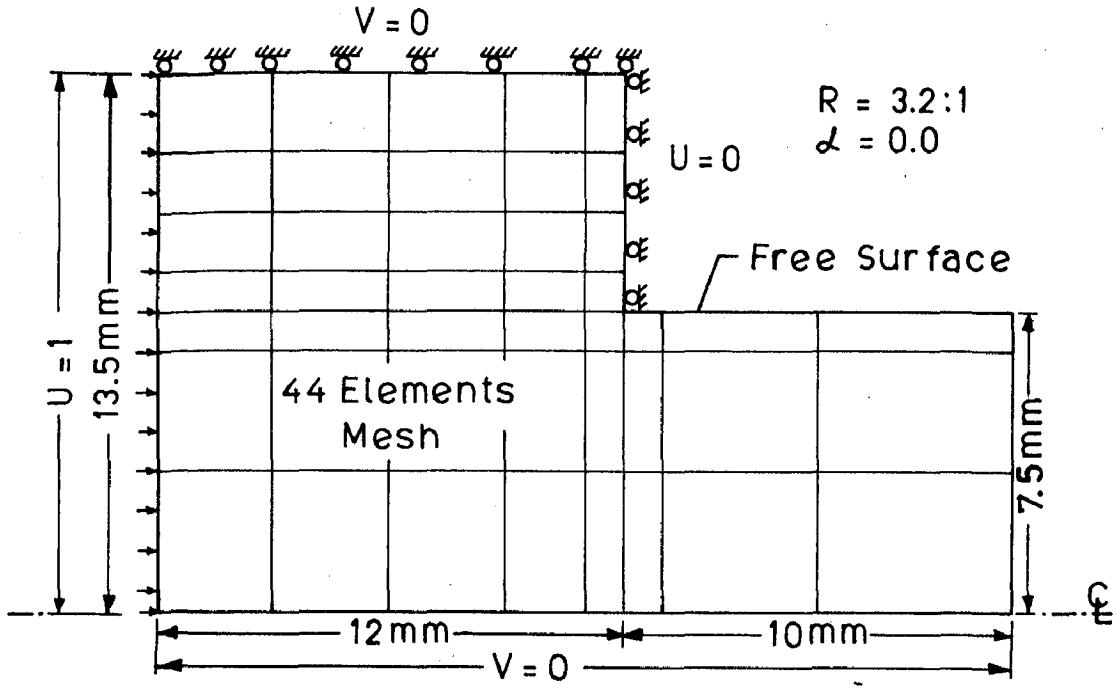

(a) Mesh and Boundary conditions.

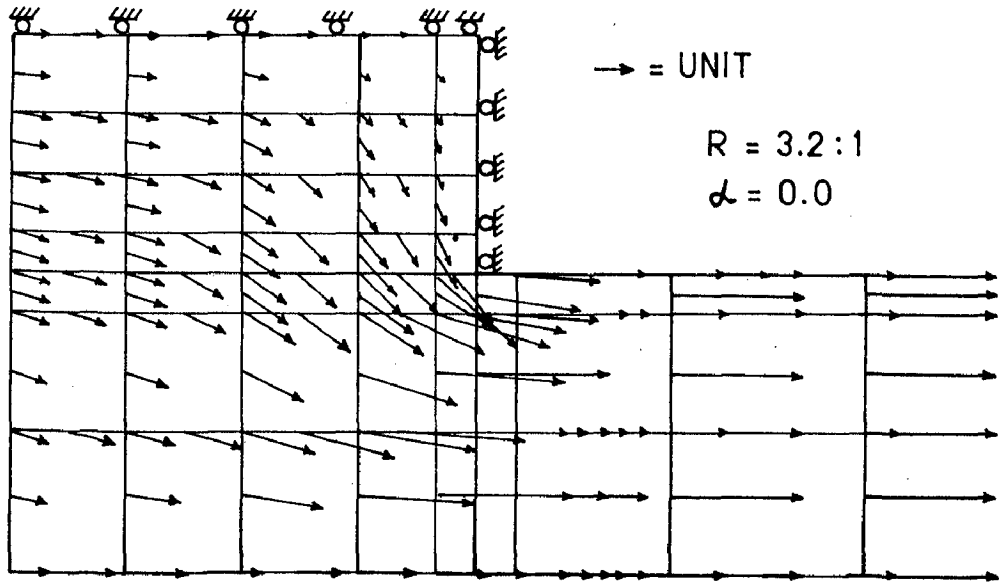

(b) Velocity vectors (44 elements mesh)

FIG.5.6 STEADY STATE EXTRUSION WITH 44 ELEMENTS MESH.

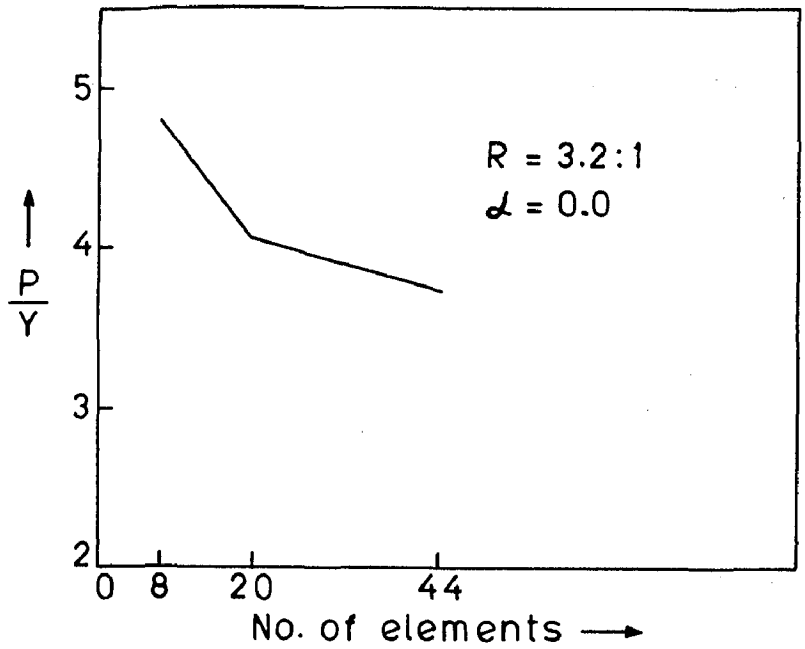

FIG.5.7 EFFECT OF MESH SIZE.

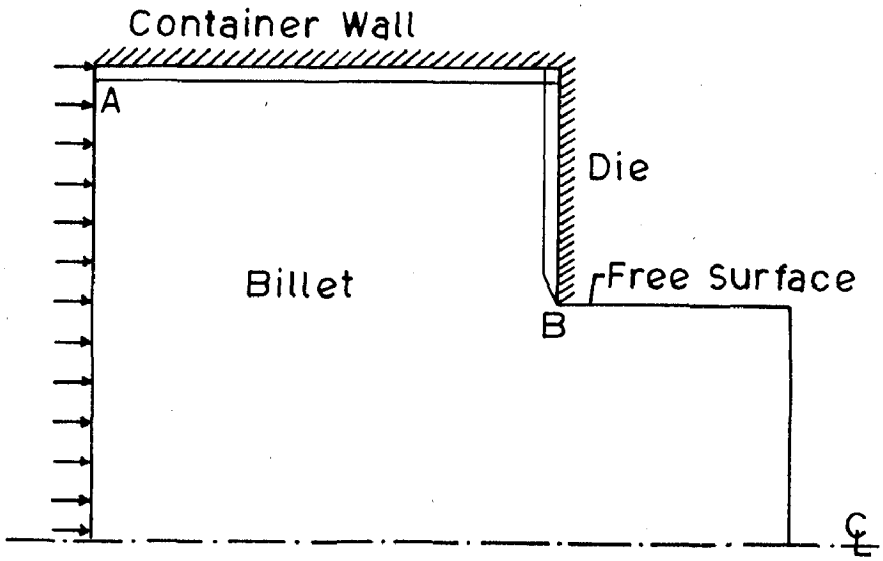

FIG.5.8 STEADY STATE EXTRUSION
(Singularity Effect)

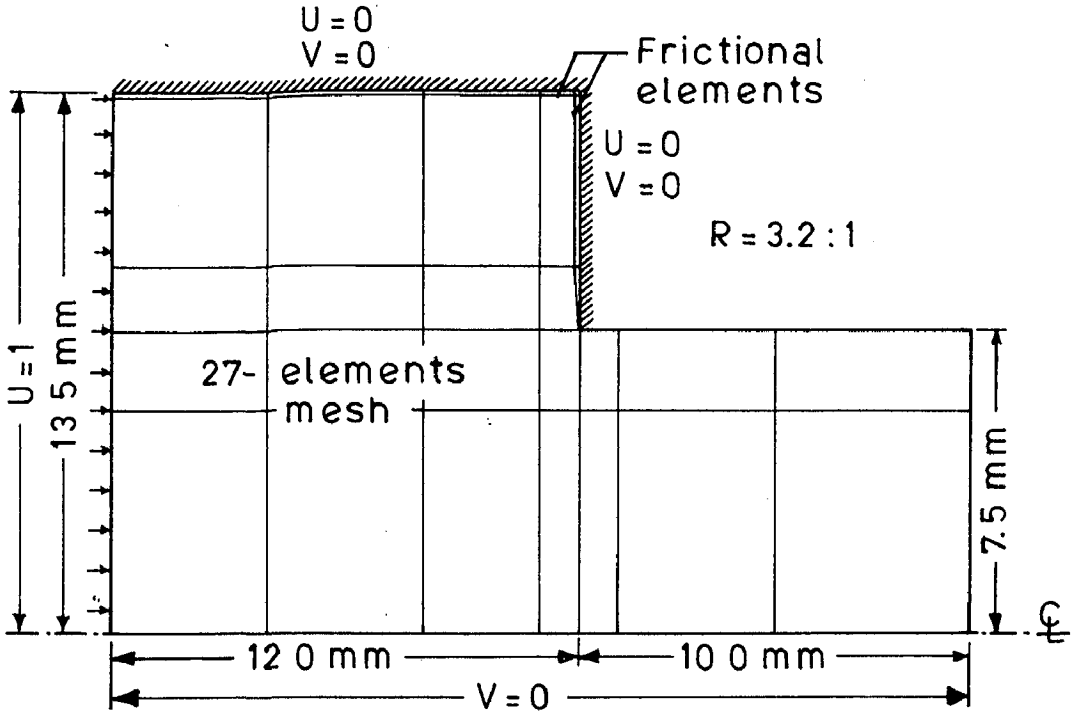

(a) Mesh and Boundary conditions.

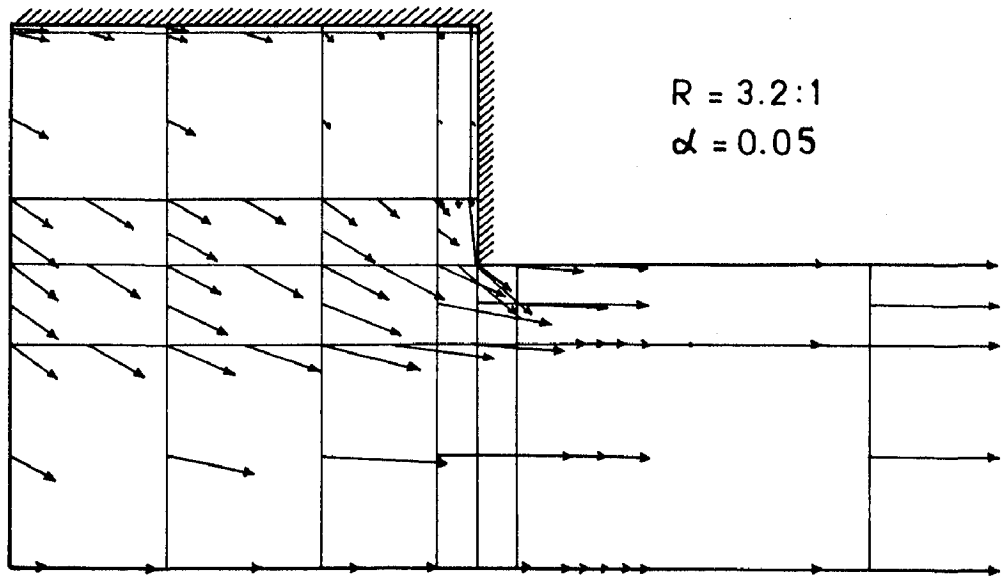

(b) Velocity vectors (27 elements mesh)

FIG. 5.9 STEADY STATE EXTRUSION WITH FRICTIONAL ELEMENTS.

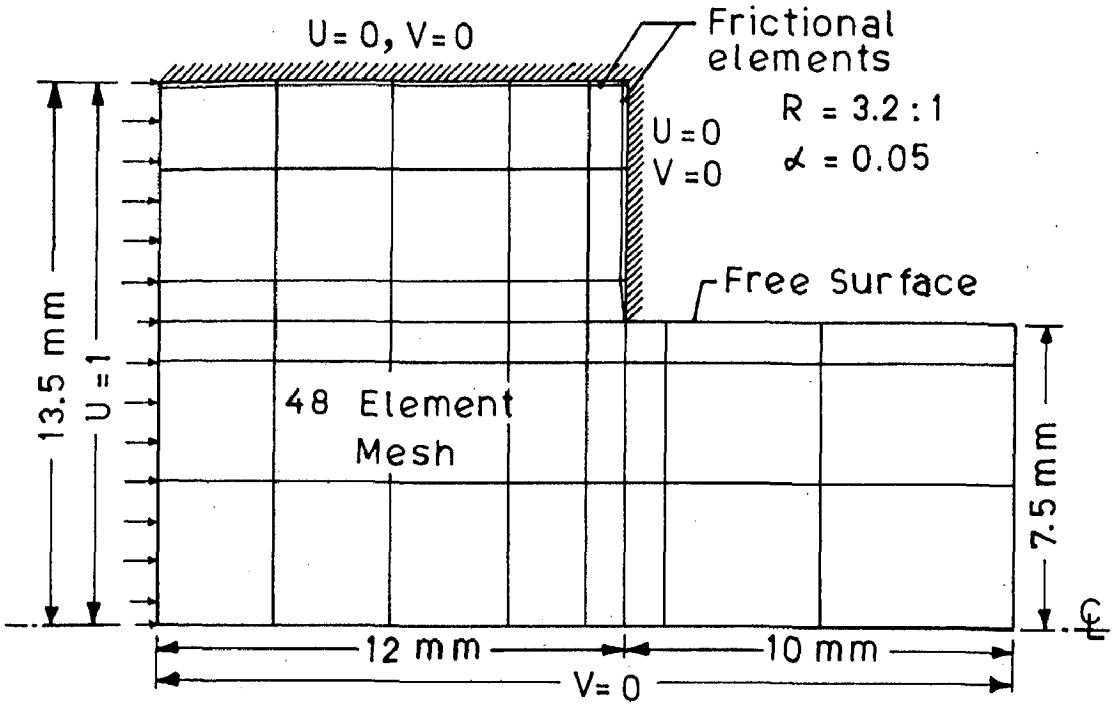

(a) Mesh and Boundary conditions.

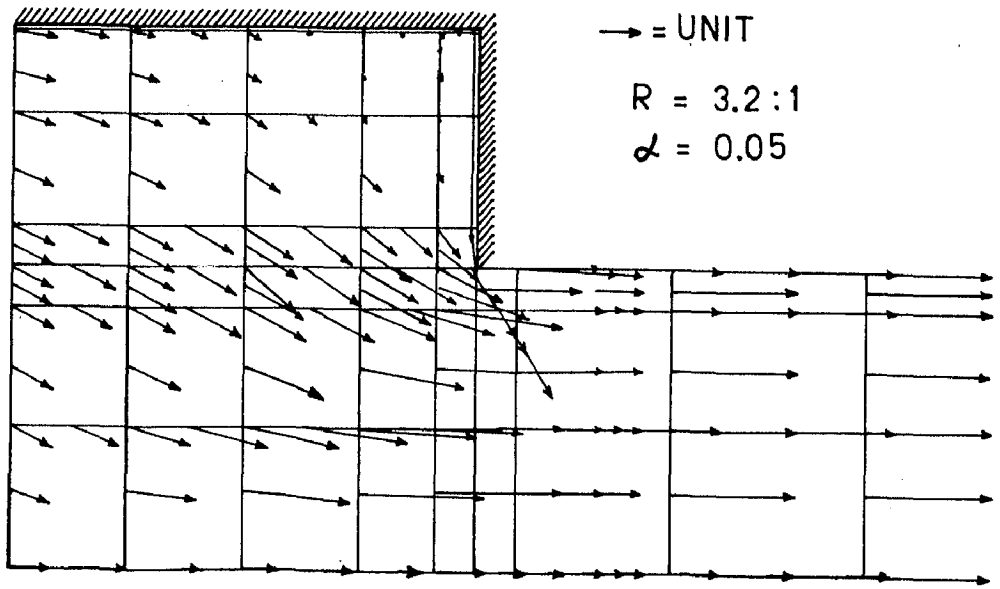

(b) Velocity vectors. (48 elements mesh)

FIG. 5.10 STEADY STATE EXTRUSION WITH FRICTIONAL ELEMENTS.

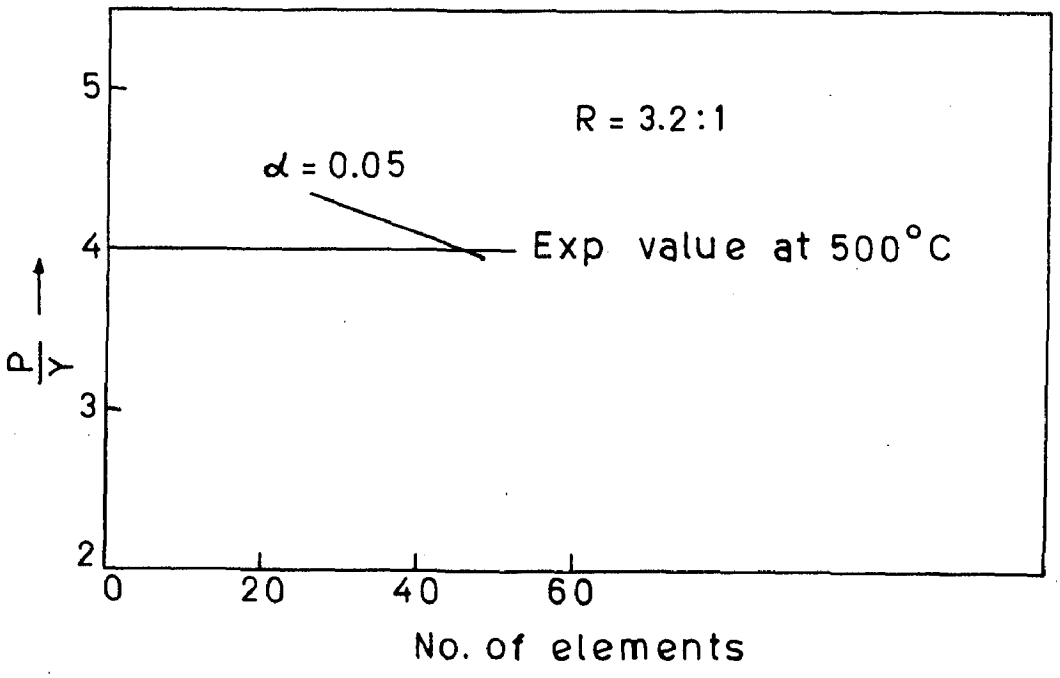

FIG.5.11 EFFECT OF MESH ELEMENTS (WITH FRICTION) ON P/Y VALUE.

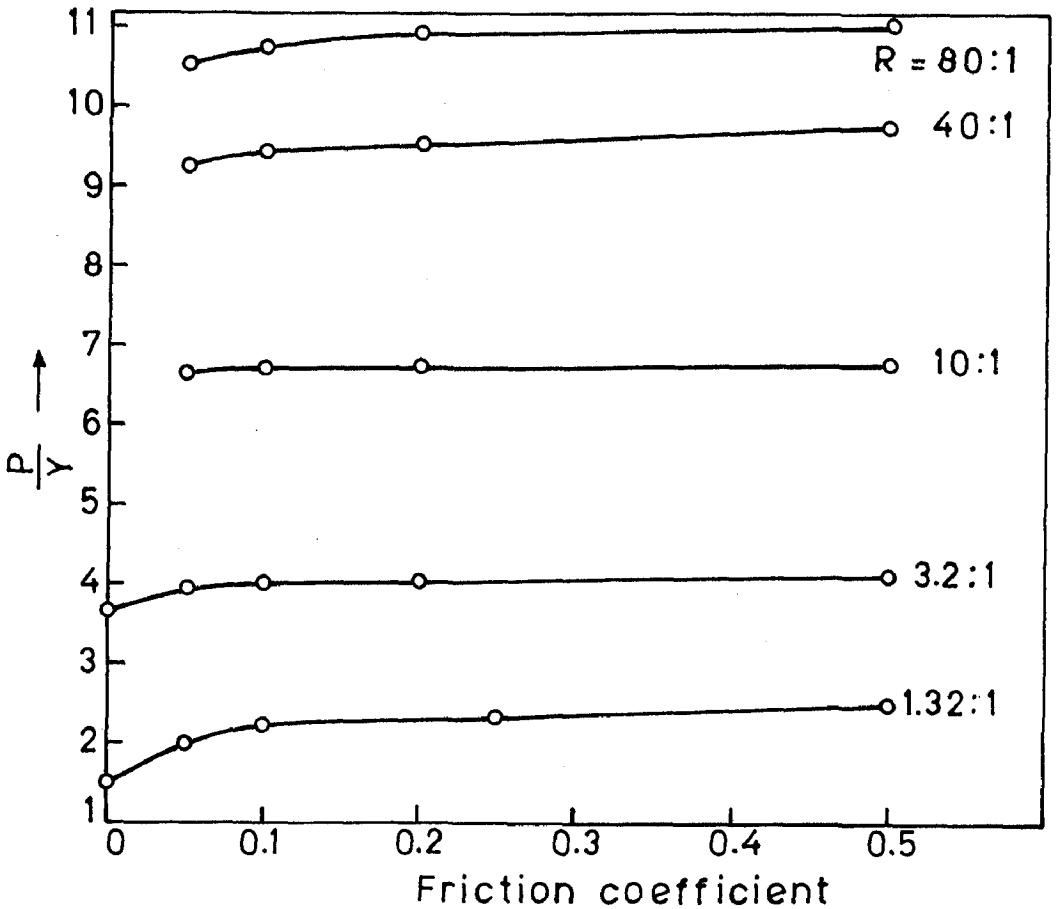

FIG.5.12 EFFECT OF FRICTION COEFFICIENT ON EXTRUSION PRESSURE PER UNIT YIELD STRESS.

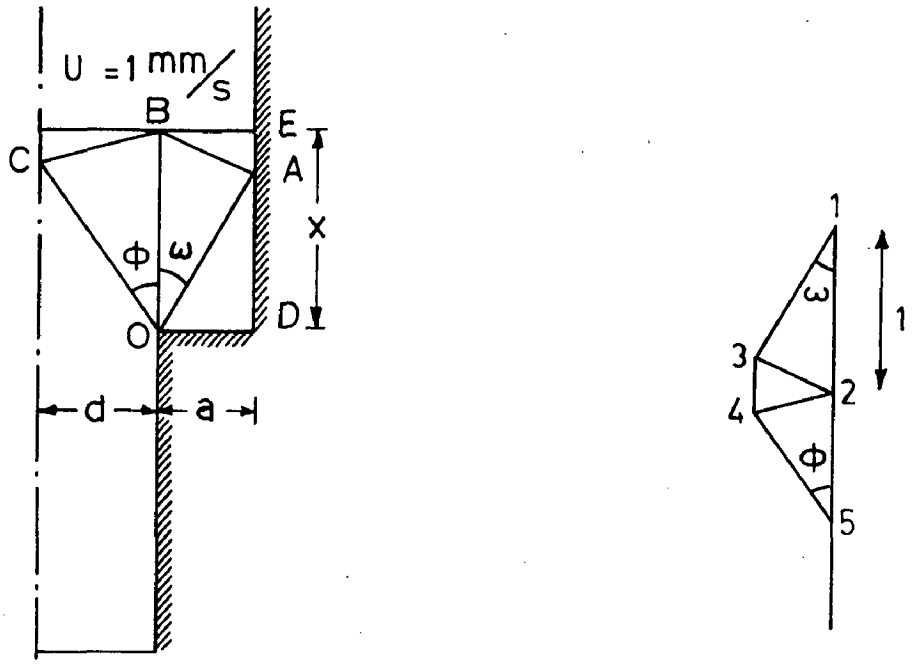

(a) Deformation field

(b) Hodograph velocity field

FIG.5.13 UPPER BOUND SOLUTION FOR R = 3:2:1

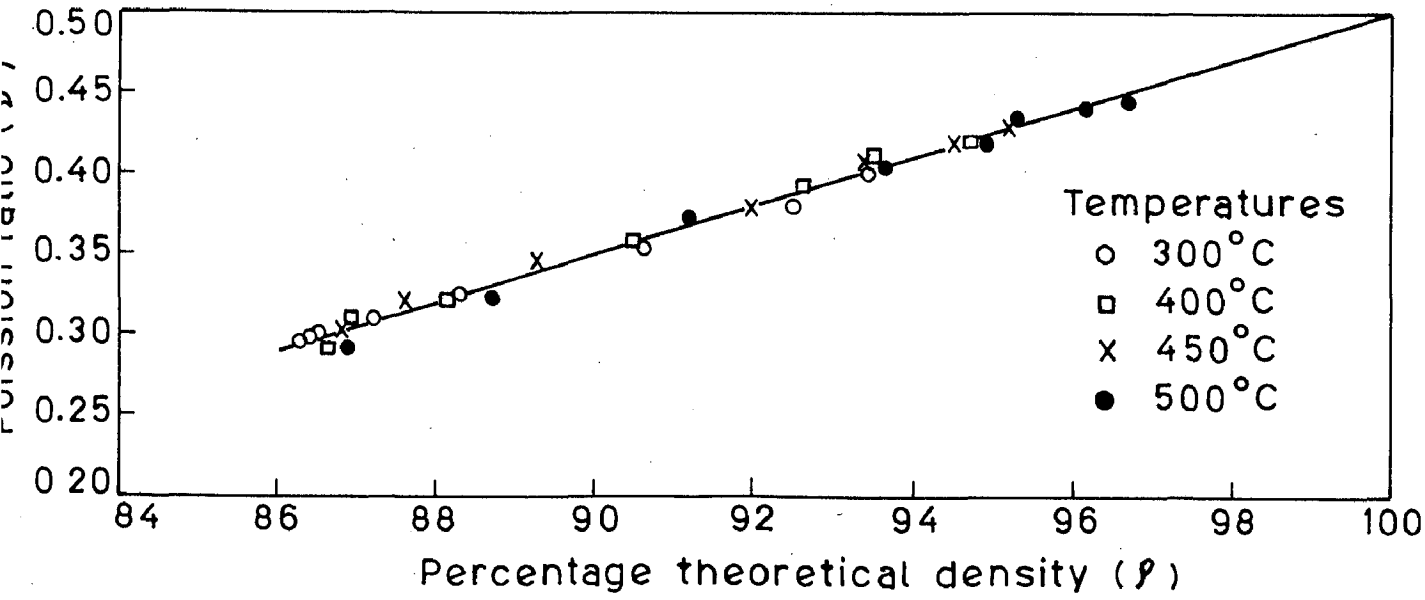

FIG.5.14 VARIATION OF POISSION RATIO WITH DENSITY.

CHAPTER - VI

RESULTS AND DISCUSSION

6.1 INTRODUCTION

In the present chapter experimental and analytical studies, carried out by extruding the aluminium powder through square and wedge shaped dies under axisymmetric condition having reduction ratios, 1.3:1 to 80:1, are discussed. The effect of extrusion parameters (reduction ratio and extrusion temperature) on the extrusion pressure were investigated. The load-ram displacement diagrams, density measurements and tensile properties of the extruded products were determined. Analytical steady state extrusion pressure (using FEM) was calculated by taking into account the friction for all reduction ratios and under frictionless condition for low reduction ratios only for square dies. The modified yield criterion for porous material is incorporated in the analytical approach to take into consideration the density variation in the billet being extruded. The analytical extrusion pressures were compared with the experimental steady state extrusion pressures. The analysis also provided the velocity vectors, average pressure contours and average effective strain rate contours which are discussed with respect to coherency/deformation of the extruded product and the shape of dead metal zone (DMZ). On the basis of analytical

extrusion pressure contour (EPC line*), a model has been proposed for the coherency criteria of the products.

Microstructural studies have been carried out in detail during billets journey from the container and dies opening both through square and wedge shaped dies for various reduction ratios in the temperature range 300 to 500°C. These microstructures also provide a good opportunity to link the extrusion parameters, analytical results and the final tensile properties of the extruded product.

Macrostructural studies of the longitudinal section of billet being extruded were carried out both in square and wedge shaped dies to identify the extrusion defects, if any and to propose the reasons for these defects. These studies were also made for square dies to see the effect of reduction ratios on DMZ boundary.

6.2 EXTRUSION THROUGH CYLINDRICAL SQUARE EDGE DIES

6.2.1 Low Reduction Ratios (R < 10:1)

The experimental results obtained from the extrusion through square edge dies with low reduction ratios, 1.3:1, 1.6:1, 2.1:1, 2.6:1 and 3.2:1 at different temperatures, 300, 400 and 500°C are discussed with respect to coherency of the extruded product with the help of extrusion parameters and analytical results.

---

* EPC line refers to that contour in the billet being extruded whose value is equal to the analytical extrusion pressure .

6.2.1.1 Load-Ram Displacement Diagrams

A typical load-ram displacement diagrams at 500°C for different reduction ratios (1.3 to 3.2:1) are shown in Fig. 6.1 which also includes diagram for cast billet for comparison purpose. The extrusion pressure required to extrude the cast billet is more than that required for powder compact, this confirms the earlier findings[1]. The curves can be divided into two regions. The initial portion of the curves corresponding to cast and powder billets exhibit distinct differences. In the case of powder billet it corresponds to the compaction zone because extrusion does not start, although the ram displacement continues. Whereas, in the case of cast billet this portion of the curve remains very steep. It is, therefore, evident that cast billet does not extrude till the required pressure is attained. In order to ascertain densification of powder billet (R=3.2:1) at the start of extrusion, the extrusion pressure was released as soon as the maximum pressure reached. It was observed that the material at this pressure has just started extruding and the density of the billet approached the theoretical value (99.98 %).

Load-ram displacement diagrams corresponding to other extrusion temperatures, 300 and 400°C were similar.

6.2.1.2 Extrusion Pressure

Extrusion pressure(p) was plotted against logarithmic of reduction ratio(R) as shown in Fig.6.2. The relationship

between p and log R was found to be linear and can be expressed as :

$$p = A + B \log R \qquad N/mm^2$$

where A and B are constants whose values were determined from Fig. 6.2 and are given in Table 6.1. These results do not confirm the suggestion put forward by Dunkley and Causton[16] and Sheppard[6] that at low reduction ratios the curve should pass through origin.

TABLE - 6.1

VALUES OF CONSTANTS A AND B AT DIFFERENT EXTRUSION TEMPERATURES

S.No.	Temperature ^oC	Value of A	Value of B
1	300	34.0	405.3
2	400	26.2	256.9
3	450	24.9	209.2
4	500	13.3	193.6

When extrusion pressure (p) was plotted against logarithmic of extrusion temperature (T) for different reduction ratios (1.3:1 to 3.2:1) linear behaviour as shown in Fig. 6.3 was observed and can be expressed as :

$$p = a - b \log T \qquad N/mm^2$$

Table 6.2 gives the values of constant a and b at different reduction ratios.

TABLE - 6.2

VALUES OF CONSTANTS a AND b AT DIFFERENT REDUCTION RATIOS

S.No.	R	a	b
1	1.3:1	575.0	200.7
2	1.6:1	939.8	329.4
3	2.1:1	1248.4	436.0
4	2.6:1	1290.7	442.4
5	3.2:1	1881.3	664.3

A change in the slope of the curve was observed at 400°C corresponding to reduction ratios 2.1:1, 2.6:1 and 3.2:1. To ascertain the existence of this change in slope at 400°C more temperatures, 350, 425, 475 and 530°C were investigated for R, 3.2:1, as shown in Fig. 6.3 and the value of constants a and b are given in Table 6.3.

TABLE - 6.3

VALUES OF CONSTANTS a AND b AT DIFFERENT REDUCTION RATIOS AFTER SLOPE CHANGE

S.No.	R	a	b
1	2.1:1	1000.5	343.5
2	2.6:1	963.3	321.5
3	3.2:1	745.9	225.4

It may be noted from Tables 6.2 and 6.3 that at a higher extrusion temperature namely above 400°C, there is a lowering of slope, suggesting a change in the flow behaviour of the material.

6.2.1.3 Density Measurements

The densities of the extruded product and the unextruded billet in steady state condition are given in Table 6.4. For a given reduction ratio, the density of the extruded product increases with temperature. At the lowest reduction ratio, 1.3:1 the density is 98.69% at 300°C, which increased to 98.82% of theoretical density at 500°C, where as at reduction ratio, 3.2:1, the density of the extruded product varied from 99.68% to 100% of theoretical density. The difference between the densities of the extruded product and the billet being extruded are extremely small indicating hardly any densification during extrusion.

TABLE - 6.4

DENSITY OF THE EXTRUDED PRODUCT AND THE BILLET BEING EXTRUDED

S. No.	T°C \ R	% Theoretical Density of Extruded Product					% Theoretical density of Billet being extruded R = 3.2:1
		1.3:1	1.6:1	2.1:1	2.6:1	3.2:1	
1	300	98.69	98.78	99.89	98.93	99.68	99.58
2	400	98.97	99.13	99.34	99.87	99.97	99.73
3	450	99.63	99.81	99.44	99.85	99.97	99.85
4	500	99.82	99.92	99.96	99.98	100.00	99.94

6.2.1.4 Tensile Properties of Extruded Product

Results are given in Table 6.5. At a given extrusion temperature the tensile properties improved with increase in reduction ratio. It may be noted that extruded product was found to be incoherent in the case of two reduction ratios 1.3:1 and 1.6:1 at 300 and 400°C but coherent mass was obtained at reduction ratios 2.1:1 at 300°C. However, coherent product was obtained above 400°C for all reduction ratios. At higher extrusion temperature, 500°C there is substantial drop in room temperature tensile strength and consequently large increase in ductility.

6.2.1.5 Comparison Between Analytical and Experimental Extrusion Pressures

Analytical extrusion pressures were obtained at 400 and 500°C for low reduction ratios by taking the actual length of the billet being extruded (H = 12 mm) which remained in the container after achieving the steady state condition of extrusion and taking the density equal to theoretical density. A fine mesh as shown in Figs. 6.5(a), 6.7(a) and 6.9(a) for reduction ratios, 1.3:1, 2.1:1 and 3.2:1 respectively, was used with friction coefficient, 0.05 for reduction ratios, 1.3:1 to 3.2:1. These analytical values are compared with experimental values in Table 6.6. There is a close agreement between these values for all reduction ratios except in case of reduction ratios, 1.3:1 and 1.6:1. The extrusion pressures were also obtained with frictionless conditions for all reduction ratios using fine mesh (44 elements) and are given in Table 6.6.

TABLE - 6.5

TENSILE PROPERTIES OF EXTRUDED PRODUCT AT ROOM TEMPERATURE

(a) FOR LOW REDUCTION RATIOS (R < 10:1)

S. No.	T / R	300°C			400°C			500°C		
		UTS N/mm^2	YS N/mm^2	Elongation %	UTS N/mm^2	YS N/mm^2	Elongation %	UTS N/mm^2	YS N/mm^2	Elongation %
1	1.3:1	Incoherent Product						39.0	35.0	2.0
2	1.6:1	Incoherent Product						53.0	41.0	6.2
3	2.1:1	114.0	80.0	8.0	93.0	71.2	11.3	70.5	52.5	14.0
4	2.6:1	122.2	85.3	14.8	105.6	76.3	16.5	98.0	64.0	19.3
5	3.2:1	132.0	101.4	17.5	116.0	88.0	21.3	103.0	75.2	27.7

(b) FOR HIGH REDUCTION RATIOS (R> 10:1)

6	10:1	156.2	133.4	22.6	128.5	102.0	28.4	115.3	93.0	36.6
7	30:1							138.5	117.0	42.0
8	40:1							137.0	113.0	37.0
9	80:1							127.0	102.0	33.0

TABLE - 6.6

COMPARISON OF EXPERIMENTAL WITH ANALYTICAL EXTRUSION PRESSURES(SQUARE EDGE DIES)

Reduction Ratio	Extrusion Pressure (N/mm^2)					
	$T = 500^oC$			$T = 400^oC$		
	Experimental Values	By FEM		Experimental Values	By FEM	
		$\alpha=0.0$	$\alpha=0.05$		$\alpha=0.0$	$\alpha=0.05$
1.3:1	38.5	38.57	51.2	55.4	55.5	71.3
1.6:1	54.6	51.8	63.5	81.8	74.3	88.6
2.1:1	75.7	70.0	76.9	110.0	99.2	109.0
2.6:1	89.8	85.4	92.5	128.5	119.6	129.6
3.2:1	105.6	100.9	108.9	149.6	139.0	150.5

It is clear from the Table 6.6 that for reduction ratio 1.3:1, the analytical extrusion pressure with frictionless condition is nearer to the experimental value, which suggests that the friction is very small in this case. For reduction ratio 1.6:1 and above a suitable value of coefficient of friction ranging between zero and 0.05 should be used. Employing modified yield criterion for porous compacts the analytical extrusion pressures were also determined for reduction ratios, 1.3:1 and 1.6:1 at 500^oC by taking the variation in the density of the extruded product and the billet being extruded, observed experimentally and friction coefficient 0.05. Results are given in Table 6.7.

TABLE - 6.7

EFFECT OF DENSITY ON ANALYTICAL EXTRUSION PRESSURE

Reduction Ratio	Extrusion Temperature ^{o}C (α)	% Theoretical density of unextruded product	% Theoretical density of extruded product	Analytical Extrusion Pressure (N/mm^2)	
				ρ = 100 %	Varying density
1.3:1	500	0.05	99.42	99.82	51.2	50.5
1.6:1	500	0.05	99.65	99.92	63.5	62.7

It may be noted that analytical pressures considering variable density are marginally smaller than those taking 100 % theoretical density. This difference is only of the order of 2 %. Therefore, analytical extrusion pressures have been calculated by considering the material fully dense in square edge dies.

6.2.1.6 Velocity Vectors

Figures 6.4(b), 6.6(b) and 6.8(b) show the velocity vectors (arrows indicate the direction and their magnitudes) as obtained by FEM for reduction ratios, 1.3:1, 2.1:1 and 3.2:1 respectively, assuming friction coefficient equal to 0.05. The velocity vectors depict the flow of metal at different sections of the die. The ratio of velocity at outlet and the velocity at inlet gives the continuity requirement,

i.e. $u_i A_i = u_o A_o$

or $$\frac{u_o}{u_i} = \frac{A_i}{A_o} = \text{Reduction Ratio} .$$

Figures 6.9(a) and 6.10(a) show the resultant velocity along the die axis (line 1-1), the line passing through the point of discontinuity of the die (line 2-2) and near the die wall (line 3-3) for reduction ratios, 1.3:1 and 3.2:1 respectively. It may be noted that velocity along the die axis is maximum (which becomes equal to the velocity of extruded product near the die exit). The velocity along the container wall remains lowest and approaches to zero value even before reaching square edge of the die. The velocity along the plane passing through the point of discontinuity increases slowly upto point of discontinuity and after the die exit the velocity increases sharply and attains the velocity of the extruded product.

The velocity distribution perpendicular to the direction of metal flow along the planes $1'-1'$ to $4'-4'$ is also plotted and is shown in Figs. 6.9(b) and 6.10(b). The velocity along the exit plane is constant upto the point of discontinuity from the die axis and then becomes zero at the nodes of the square edge of the die. The velocity along the other planes decreases as moving away from die axis and then becomes zero at the container surface.

In Figures 6.4(b), 6.6(b) and 6.8(a) the region in which the velocities are small may be termed as DMZ. It is expected that the material is static in the DMZ and the same is observed by plotting the velocity vectors, except that in

this zone, with frictional conditions, there is a movement of material in the direction opposite to the direction of extrusion as the velocity vectors are opposite to the direction of metal flow. The magnitude of these velocities are,however,very small. The velocity vectors at the exit are indeed parallel to the die surface and their magnitude is equal to the velocity of the extruded product satisfying the condition of continuity. But in case of 1.3:1 and 1.6:1 at 400°C continuity condition was not satisfied while at other reduction ratios the continuity requirement was satisfied at 400 and 500°C. This may be due to the fact that at 400°C for reduction ratios, 1.3:1 and 1.6:1 coherent mass was not achieved experimentally.

6.2.1.7 Average Pressure Contours

Figures 6.4(c), 6.5(a),6.6(c)and 6.7(a) show the average pressure contours at 400°C for reduction ratios, 1.3:1 to 2.6:1 and Figs. 6.4(e), 6.5(c) and 6.8(c) at 500°C for reduction ratios, 1.3:1, 1.6:1 and 3.2:1 respectively inside the billet being extruded in steady state condition with α, 0.05.

All pressure contours meet in the narrow region of the point of discontinuity, in other words there is a very sharp variation of pressure in this region. These pressure contours indicate that in the region near the DMZ where there is a poor flow of material the pressure build up, even more than the analytical extrusion pressure, is present. This is more so in case of lowest reduction ratio, 1.3:1 where the continuity condition is not satisfied at 400°C.

Experimentally also this reduction ratio has yielded incoherent product at 400°C and below 400°C. However, on account of good flow conditions the pressure drops and maximum drop of pressure is along the die axis. There is also an indication from these pressure contours that the pressure persists even beyond the die exit. It may be noticed that in Figs. 6.4(c), 6.4(e), 6.5(a), 6.5(c), 6.6(c), 6.7(a) and 6.8(c) the shaded region (PZ) between the pressure contour corresponding to the extrusion pressure (EPC line, shown by bold line) and the pressure contour which correspond to the yield stress of the material being extruded represents the plastic zone where extensive flow of material occurs. The shaded region (HZ) above the EPC line shows region of hydrostatic forces where material movement is very little. The shaded region (EZ) below the pressure contour line which indicate yield stress of the material is the region of elastic zone which represents material flow under low pressure (below yield strength of the material). The shaded region (CZ), below the pressure contour line of 0.0 value is the region where strains are getting relieved and material flows under constraint free condition.

It was also observed from these pressure contours that pressure much greater than the actual extrusion pressure are developed in the DMZ. The position of the DMZ appears to shift in the direction opposite to the direction of metal flow and the DMZ no more remains at an angle of 45° from the point of discontinuity as considered in earlier theories of plastic flow such as slip line and upper bound[30].

According to average pressure contours, it may be stated that the hydrostatic region (which is equivalent to DMZ) where the material is subjected to compressive forces of much higher magnitude than the extrusion pressure, extends along the direction opposite to the metal flow as well as perpendicular to the metal flow in case of lower reduction ratios. This is particularly more predominant in those cases where the product was found to be incoherent. The same region compresses towards the corner of the extrusion container in case of relatively higher reduction ratios, much more than what was predicted earlier as 45° angle from the point of discontinuity.

It may be seen from Fig. 6.11 that position of EPC line can easily predict the possibility of coherency in a particular case. For instance, it was observed that the position of the pressure contour corresponding to the value of analytical extrusion pressure (EPC) has great bearing on the prospect of getting coherent product. If the EPC is above the horizontal line in the extrusion container as shown in Fig. 6.11, the product has been invariably coherent. If the EPC line falls on the horizontal line, it happens to be a limiting case of coherency. However, if EPC line drops below horizontal line the product is always incoherent. This observation is true for all reduction ratios and temperatures investigated. In case of reduction ratios, 1.3:1 and 1.6:1 at 400°C, the EPC line falls below the horizontal line (Figs.6.4(a) and 6.5(a)) and experimentally also at these reduction ratios incoherent mass was obtained. In case

of reduction ratio, 2.1:1 at 400°C (Fig. 6.6(c)) and 1.3:1, 1.6:1 at 500°C (Figs. 6.4(e) and 6.5(c)) the EPC line remains almost horizontal and at these reduction ratios and temperatures coherent mass was obtained experimentally.

6.2.1.8 Effective Strain Rate Contours

Figures 6.4(d), 6.5(b), 6.6(d) and 6.7(b) show the average effective strain rate contours at 400°C for reduction ratios, 1.3:1 to 2.6:1 and Figs. 6.5(f), 6.6(d) and 6.9(d) at 500°C for reduction ratios, 1.3:1, 1.6:1 and 3.2:1 respectively. These effective strain rate contours have been plotted assuming zero elastic strains and steady state extrusion. As in the case of pressure contours, the highest effective strain rates are concentrated around the point of discontinuity (maximum of unit 2.0 for reduction ratio 3.2:1 and unit 1.0 for reduction ratio 1.3:1). By considering a strain rate contour of unit 0.2 in above figures, the contour is in a very narrow region of point of discontinuity for reduction ratios, 1.3:1 and 1.6:1 and the extensive plastic deformation occur only in this narrow region of point of discontinuity. This is likely to develop zones of differential plastic deformation (predominently by shear mechanism) of the material in the container resulting in development of defects such as cracks in these reduction ratios, and incoherent product must be obtained at 400°C and lower temperatures. Experimentally also incoherent product was obtained upto 400°C for these reduction ratios. In the cases of reduction ratios, 2.1:1, 2.6:1, at 400°C and 3.2:1

at 500°C the effective strain rate contour of unit 0.2 (Figs. 6.6(d), 6.7(b) and 6.8(d)) extends upto the centre of the die. This shows that there is an extensive plastic deformation even upto the centre of the die, i.e. die axis, resulting in coherent mass. This is also confirmed by the experiment that the extruded product no more remains incoherent for these reduction ratios. It may be noticed that as the reduction ratio increases the magnitude of contour along the die axis also increased. This shows that as the reduction ratio increases there is more extensive plastic deformation upto die axis and we get more coherent mass. The maximum effective strain rate contour along the die axis for reduction ratio, 3.2:1 corresponds to 0.4 unit. The pressure contour plot and the effective strain rate contour plot, therefore, in general, exhibit parallelism in regard to material flow and deformation during extrusion.

6.2.2 High Reduction Ratios (R > 10:1)

In the present section experimental studies carried out for high reduction ratios, 10:1, 20:1, 30:1, 40:1 and 80:1 at different temperatures, 300, 400 and 500°C are discussed with regard to the effect of extrusion parameters on extrusion pressure. Results are discussed with respect to the shape of DMZ and coherency of the products.

6.2.2.1 Load-Ram Displacement Diagrams

Load-ram displacement diagrams at 500°C for different reduction ratios (10:1 to 80:1) are shown in Fig. 6.12. Like

at low reduction ratios the curve can be divided into two regions (i) the compaction zone (ii) extrusion zone. In case of high reduction ratios the extrusion starts well before attaining the maximum load. For example, in case of reduction ratio, 10:1 and 400°C some experiments were stopped at 16 ton load (maximum load being 17.8 tons) and it was found that about 3 cm length had already extruded. At this point the density was also measured and it was found that the density of the unextruded product and the extruded product was not 100 % as reported by Sheppard [1]. When the experiments were stopped at maximum load, 17.8 tons, the density of both were found to be 100 %. This situation also continues in steady state condition. The similar behaviour is observed for all other reduction ratios and temperatures investigated. This observation suggests that pressure required to initiate extrusion is lower than the steady state extrusion pressure required to continue extrusion. Load peak was not sharp.

6.2.2.2 Density Measurements

The density of the extruded product and the billet being extruded during steady state condition were measured for all the reduction ratios at all the temperatures. Density was found to be 100 % of the theoretical value. The density of the extruded product and billet being extruded were also measured at 16 ton load where the extrusion has just started as given in Table 6.8.

TABLE - 6.8

DENSITY AT 16 TONS LOAD

R	T °C	% theoretical density of billet being extruded	% theoretical density of extruded product
10:1	400	99.5	99.6

6.2.2.3 Extrusion Pressure

The relationship between p and log R is linear as shown in Fig. 6.2 and can be expressed by the relation :

$$p = A + B \log R \quad N/mm^2$$

where A and B are constants whose values are given in Table 6.9.

TABLE - 6.9

VALUES OF CONSTANTS A AND B AT DIFFERENT TEMPERATURES

Temperature °C	A	B
300	29.6	394.8
400	15.5	306.4
500	6.6	190.8

The relationship between p and log R for higher reduction ratios is same as reported by Sheppard [1] for aluminium powder (Fig. 6.2). The difference is in values of A and B. The slope of the curve is higher than that observed in case of low reduction ratios at the same

temperature. The slope of the curve at 300°C is more steep than that at 500°C. When p was plotted against log T, a linear relationship was obtained as shown in Fig. 6.3 and can be expressed as

$$p = a - b \log T$$

where a and b are constant. The relationship is same as that reported by Sheppard [1] for aluminium powder. The difference is only in the values of a and b.

There is a change in slope at 400°C similar to the one reported in case of low reduction ratios.

6.2.2.4 Tensile Properties

Tensile properties of the product extruded through reduction ratios, 10:1 to 80:1 at 500°C were measured only at room temperature and are given in Table 6.5(b). The table shows that the tensile properties increased with reduction ratios from 10:1 to 30:1 and after that the tensile properties became constant.

6.2.2.5 Comparison Between Analytical and Experimental Extrusion Pressure

Analytical extrusion pressure were obtained at 400 and 500°C for all the reduction ratios, 10:1 to 80:1, by taking the actual length (H = 12 mm) and density (100% of theoretical) of the billet being extruded which remain in the container after achieving the steady state condition. A fine mesh (52 elements) was used with friction coefficient,

0.10. These analytical pressures were compared with the experimental steady state extrusion pressures and are given in Table 6.10. Analytical pressures for 300°C were not obtained due to lack of yield stress data.

Results show that the experimental values are in close agreement with the analytical values. The difference in both values varies from 2 to 3 % in most of the cases.

TABLE - 6.10

COMPARISON BETWEEN EXPERIMENTAL AND ANALYTICAL EXTRUSION PRESSURES

S. No.	Reduction Ratios	Extrusion Pressure (N/mm^2)			
		500°C		400°C	
		Experimental Value	By FEM α=0.10	Experimental Value	By FEM α=0.10
1.	10:1	195.6	191.0	305.0	282.8
2.	20:1	244.5	253.3	387.7	375.9
3.	30:1	279.5	287.4	454.1	448.8
4.	40:1	310.8	318.8	490.8	499.5
5.	80:1	365.0	382.8	585.1	604.8

6.2.2.6 Velocity Vectors

Figures 6.13(b) to 6.15(b) show the velocity vectors for reduction ratios, 10:1, 40:1 and 80:1 respectively at 500°C with friction coefficient, 0.10. In the above figures the region in which the velocities are small may be termed as DMZ. It may be noted that DMZ is not at an angle of 45° to the die axis and its position and angle varies with the

reduction ratio. It is expected that the material is static in DMZ and the same is observed by plotting the velocity vectors except that in this zone there is a movement of material in the direction opposite to the direction of metal flow as the velocity vectors are opposite to the direction of metal flow. The magnitudes of these velocities are however very small as shown in Figs. 6.13(b), 6.14(b) and 6.15(b), near the point of discontinuity. The velocity vectors at the exit are parallel to the die axis as expected and their magnitudes are equal to the respective velocities of the extruded product.

The magnitude of resultant velocities plotted against the distance in X-direction from the ram for reduction ratios, 10:1 and 40:1 at 500^{o}C are shown in Figs. 6.16(a) and 6.17(a). The figures show the velocity profiles along the line 1-1 corresponding to the die axis, line 2-2 corresponds to the plane passing through the point of discontinuity and line 3-3 along the container wall. The velocities along die axis are maximum which becomes equal to the velocity of the extruded product near the die exit. The velocity near the container wall remains lowest and approaches to zero value even before reaching the square edge of the die. The velocity along the plane passing through the point of discontinuity increases slowly upto the point of discontinuity and after the die exit the velocity increases sharply and attains the velocity of the extruded product.

The magnitude of the resultant velocity along the different planes perpendicular to the die axis as marked

in Figs. 6.13(a) and 6.14(a) for reduction ratios, 10:1 and 40:1 at 500°C are plotted in Figs. 6.16(b) and 6.17(b). The velocity along the die exit plane is constant upto the point of discontinuity from the die axis and then becomes zero at the nodes on the square edge of the die. The velocity along the other planes continuously decreases and approaches to zero before reaching the container surface.

6.2.2.7 Average Pressure Contours

Figures 6.13(c), 6.14(c) and 6.15(c) show the average pressure contours in the billet being extruded at 500°C for reduction ratios, 10:1, 40:1 and 80:1. It may be seen that most of the pressure contours start from the die axis and terminates along the square edge of the die. This obviously means that there is a sharp variation of pressure inside the container and that the flow of material is very extensive all along the billet being extruded. In these plots it may also be noticed that EPC line which divides hydrostatic (HZ) and plastic zone (PZ) gets confined to the top left hand corner of the container. Thus, the hydrostatic zone is limited to a very small area of the container. It may also be noticed from these pressure contours that the DMZ shrinks toward the die corner as the reduction ratio increases. The shaded region between the EPC line and the pressure contour corresponding to yield stress of the material being extruded represents the plastic zone where extensive flow of material occurs. The other shaded regions are elastic zone (EZ) and constraint free zone (CZ) respectively as

shown in Figs. 6.13(c), 6.14(c) and 6.15(c). As the reduction ratio increases the area of plastic zone i.e. the area of extensive flow of material increases.

6.2.2.8 Average Effective Strain Rate Contours

Figures 6.13(d) to 6.15(d) show the average effective strain rate contours at 500^{o}C for reduction ratios, 10:1, 40:1 and 80:1 respectively. These effective strain rate contours have been plotted assuming zero elastic strains and steady state extrusion. The highest effective strain rates are concentrated around the point of discontinuity (maximum being of unit 7.9 for reduction ratios,10:1 and 90 for 80:1). The strain rates are very low in the corner of the die indicating the presence of DMZ. Considering the strain rate contour of unit 0.5, it exists in a very wide region inside the billet being extruded while in low reduction ratio, the same contour exists in a very narrow region around the point of discontinuity i.e. from the square edge of the die to the die axis. Due to this wide range the extensive plastic deformation occur upto the die axis resulting in coherent mass. As the reduction ratio decreases the strain rate contour of same unit gets confined in the narrow region.

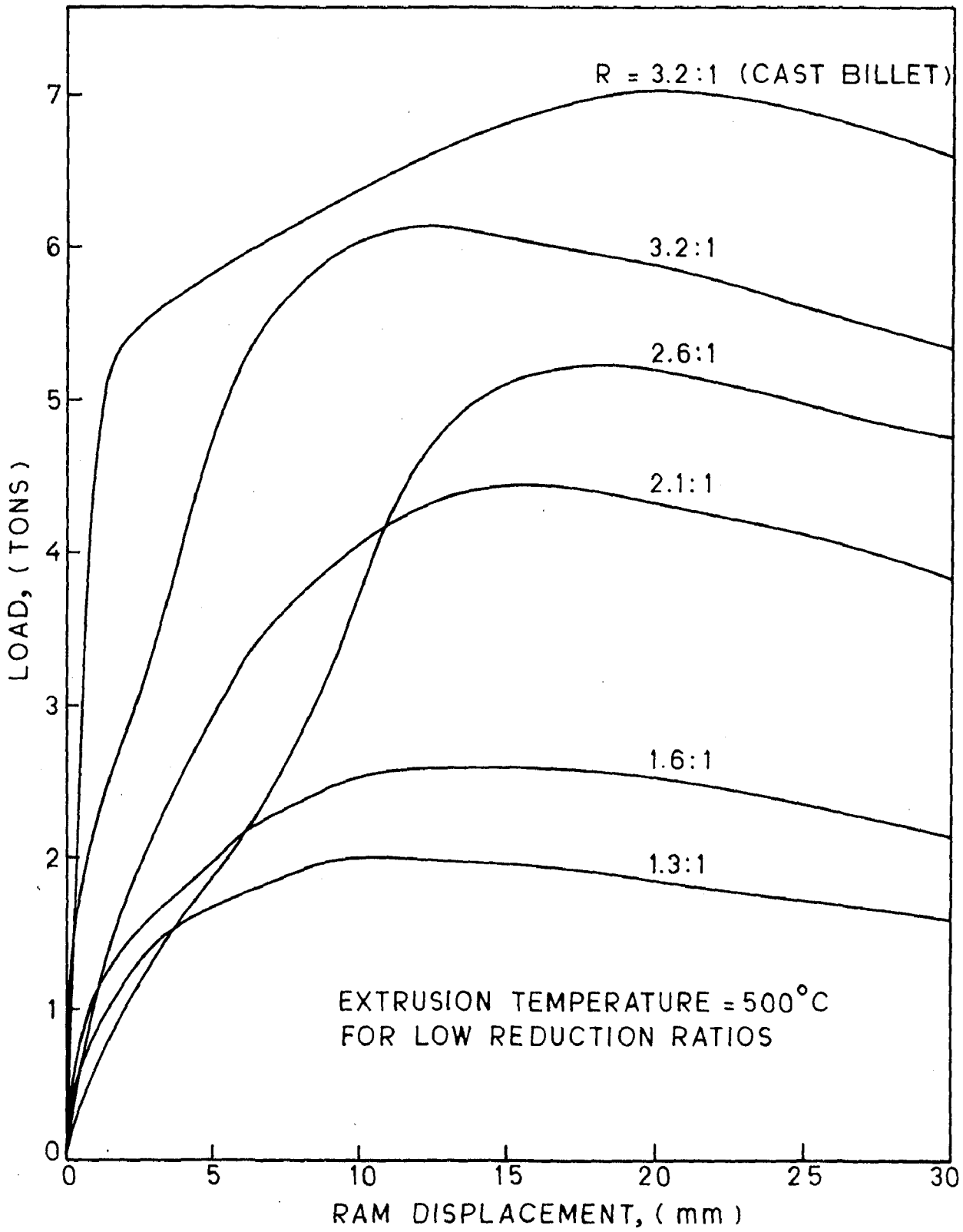

FIG. 6.1 LOAD RAM DISPLACEMENT DIAGRAMS.

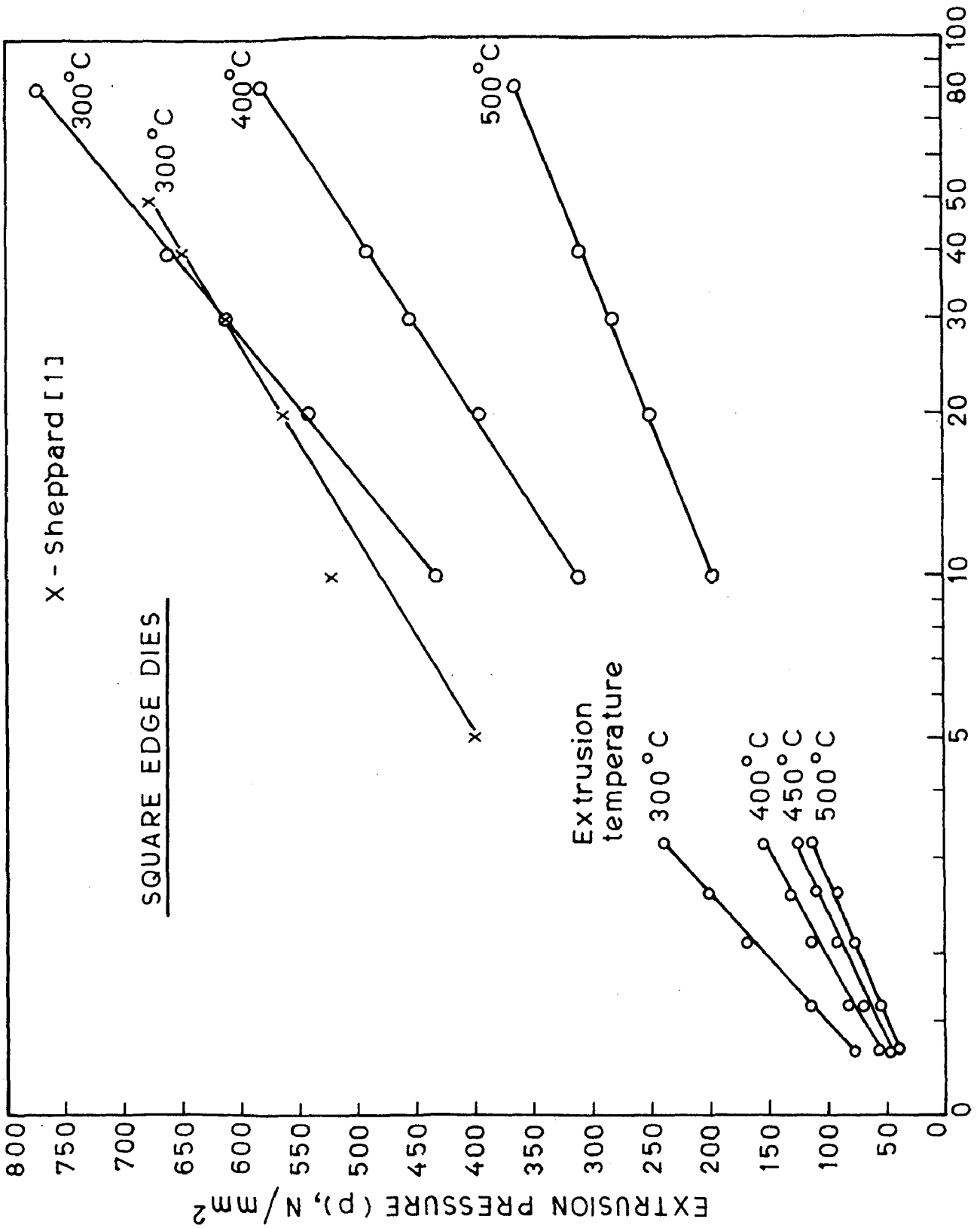

FIG.6.2 EFFECT OF REDUCTION RATIO ON EXTRUSION PRESSURE.

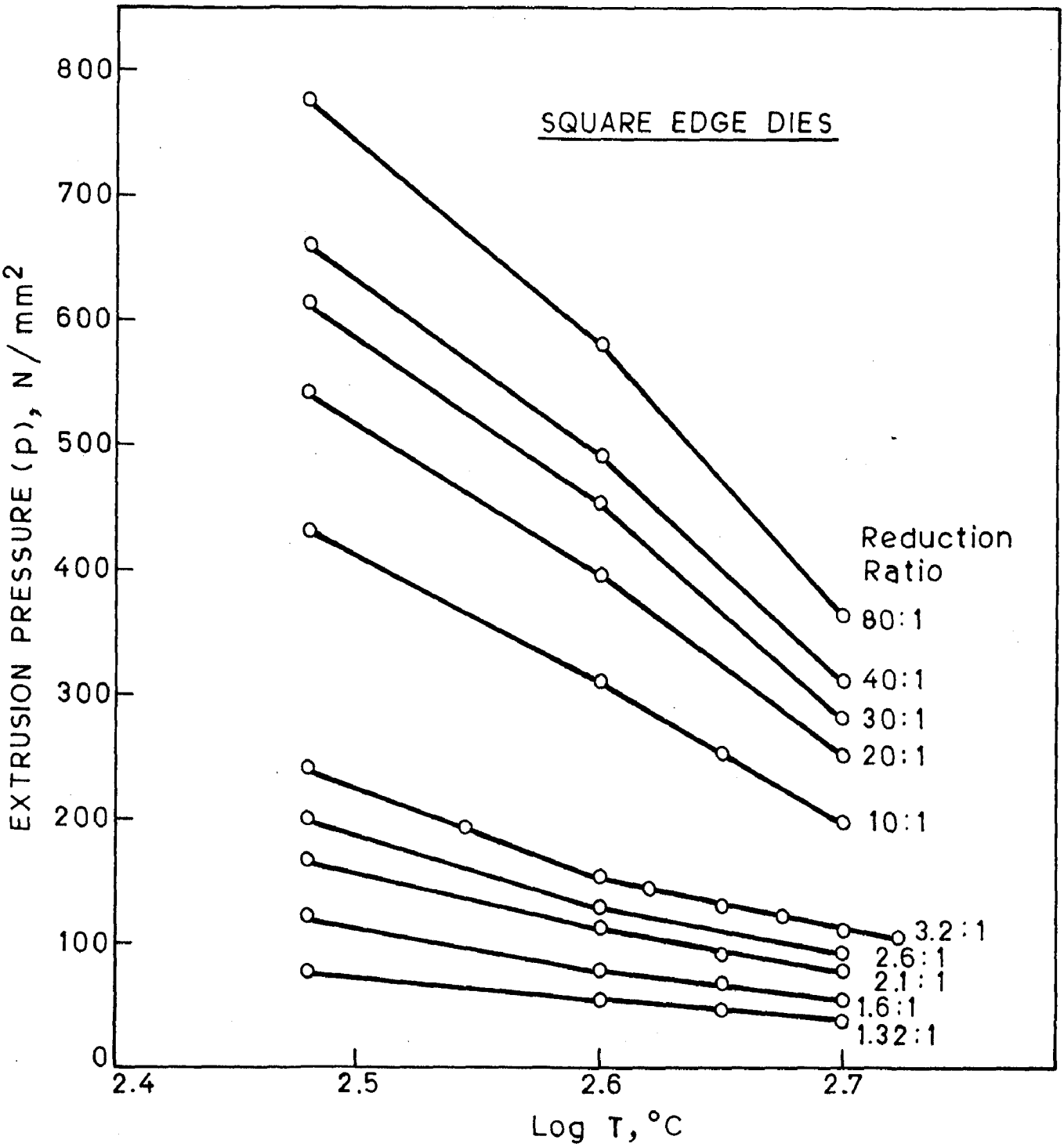

FIG.6.3 EFFECT OF EXTRUSION TEMPERATURE ON EXTRUSION PRESSURE.

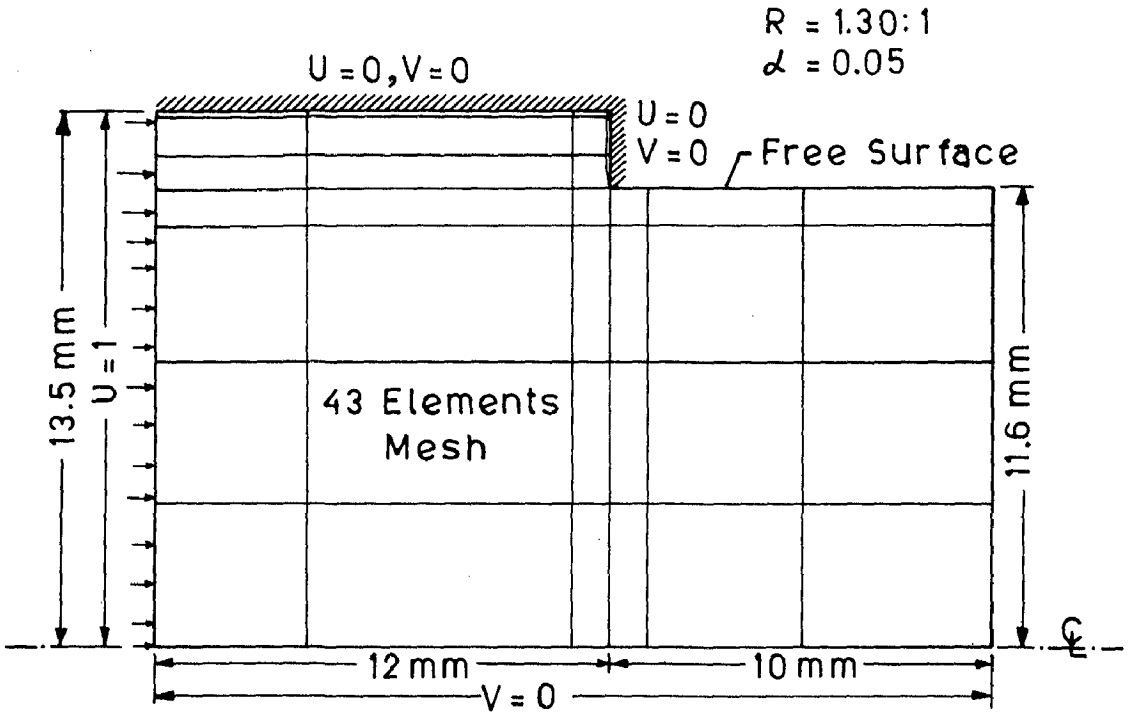

FIG.6.4 (a) MESH WITH BOUNDARY CONDITIONS.

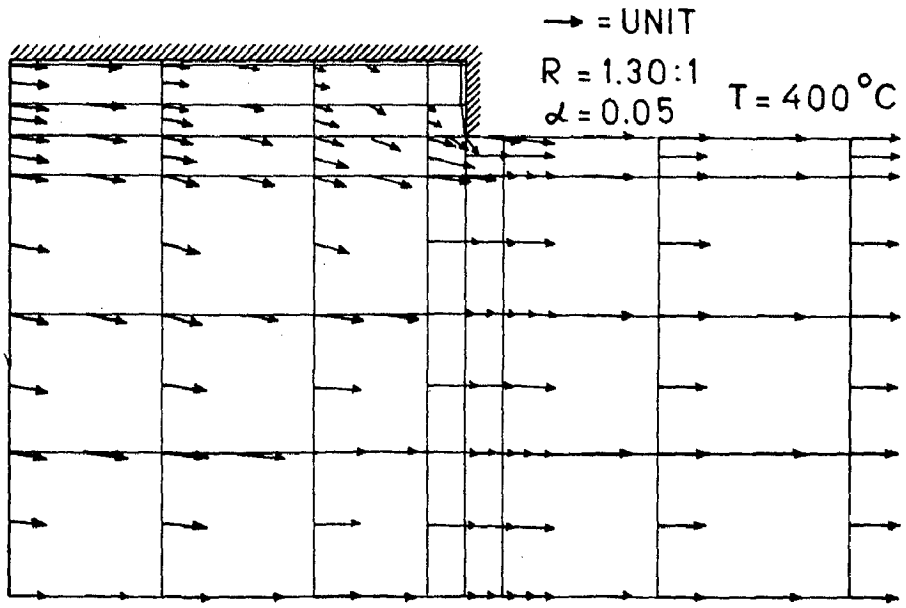

FIG.6.4 (b) VELOCITY VECTORS.(43 elements mesh)

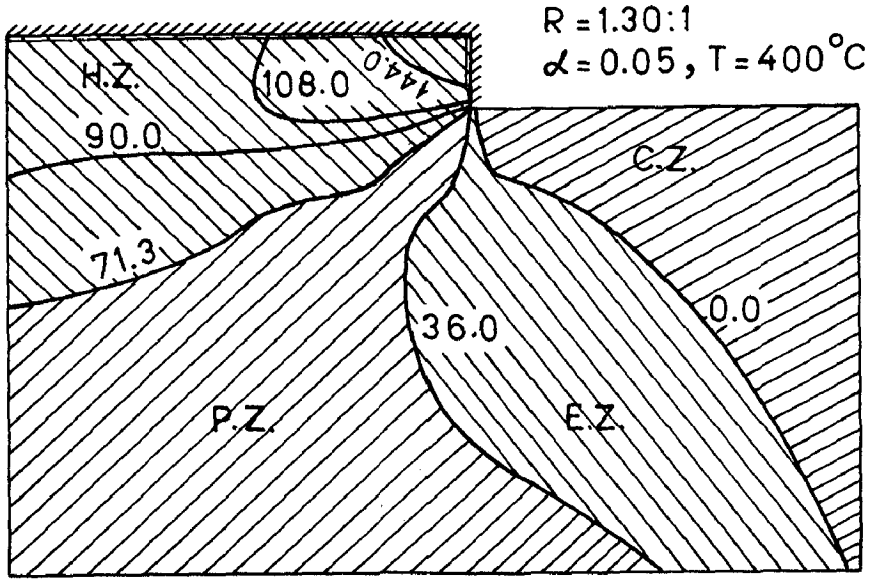

FIG. 6.4 (c) AVERAGE PRESSURE CONTOURS.
(43 elements mesh)

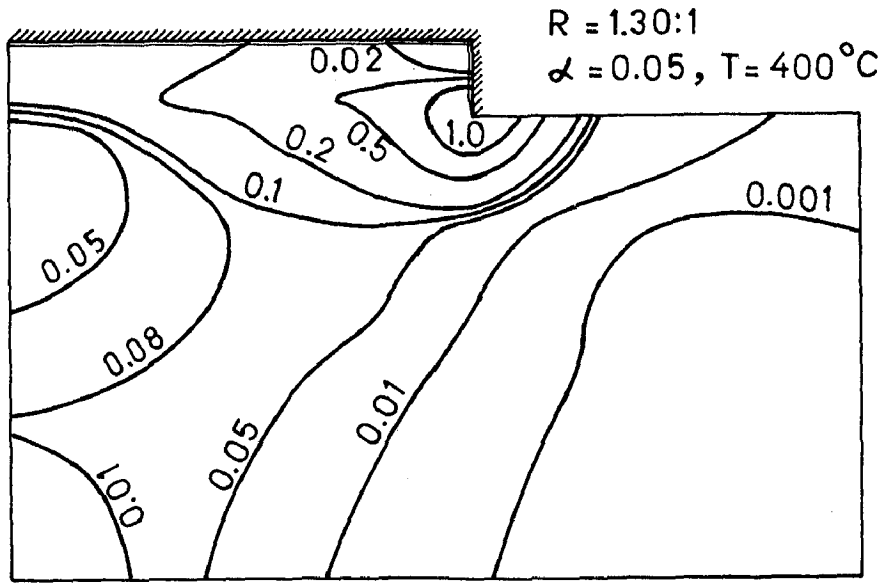

FIG. 6.4 (d) AVERAGE EFFECTIVE STRAIN RATE CONTOURS. (43 elements mesh)

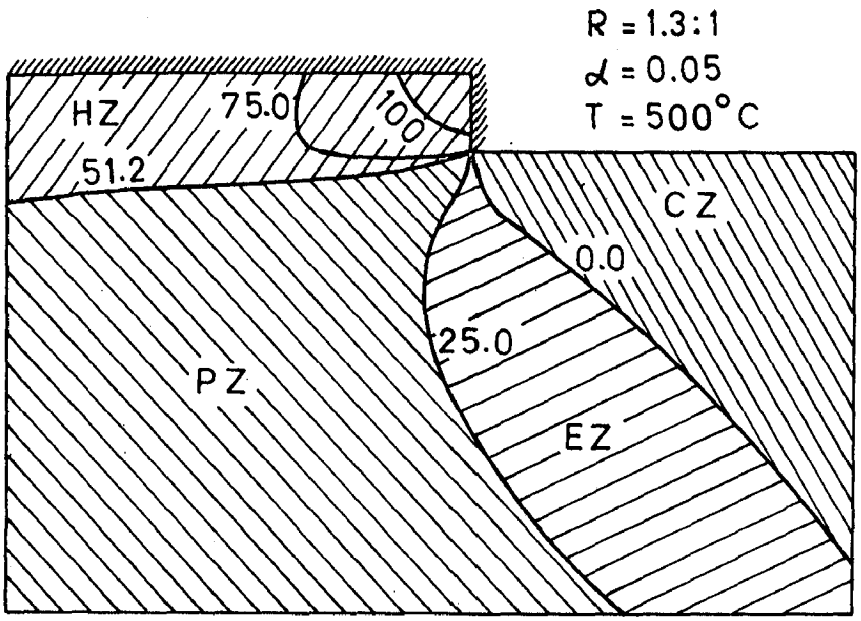

FIG. 6.4 (e) AVERAGE PRESSURE CONTOURS.
(43 elements mesh)

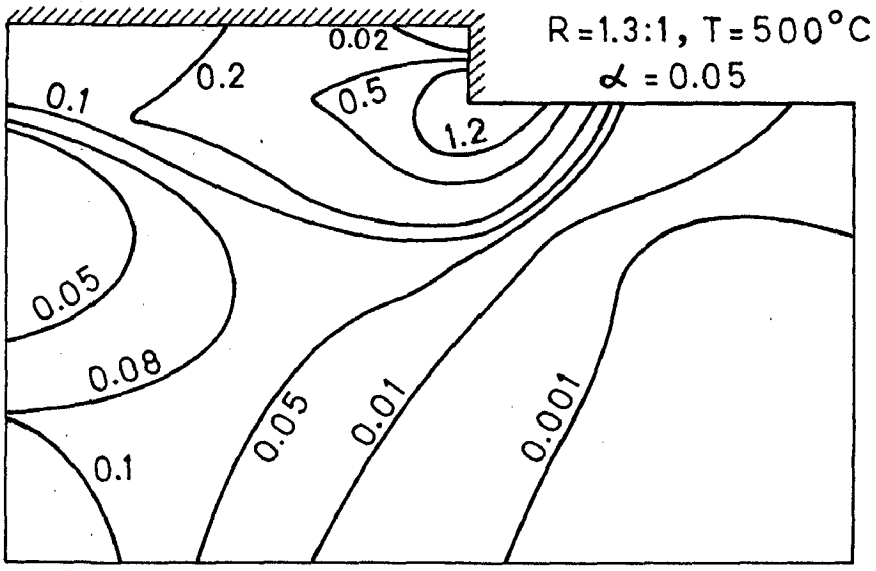

FIG. 6.4 (f) AVERAGE EFFECTIVE STRAIN RATE CONTOURS. (43 elements mesh)

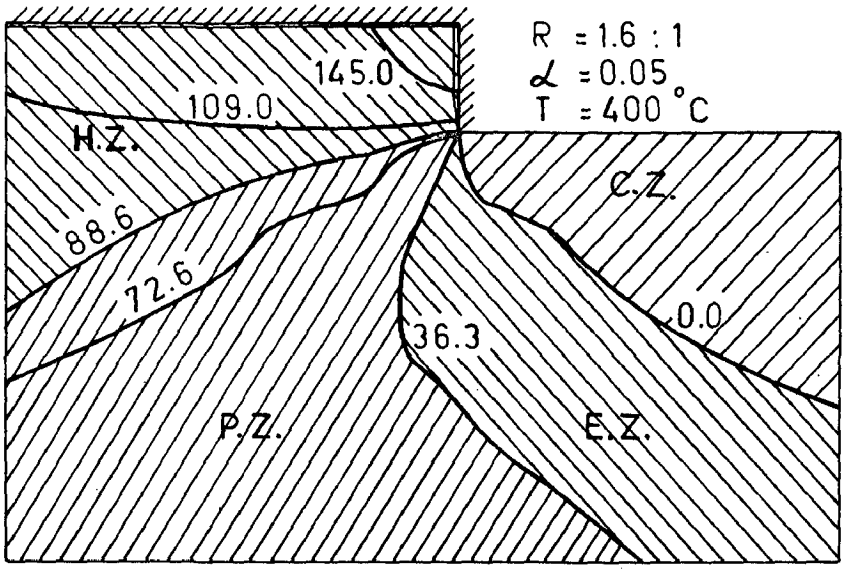

FIG. 6.5 (a) AVERAGE PRESSURE CONTOURS.
(43 elements mesh)

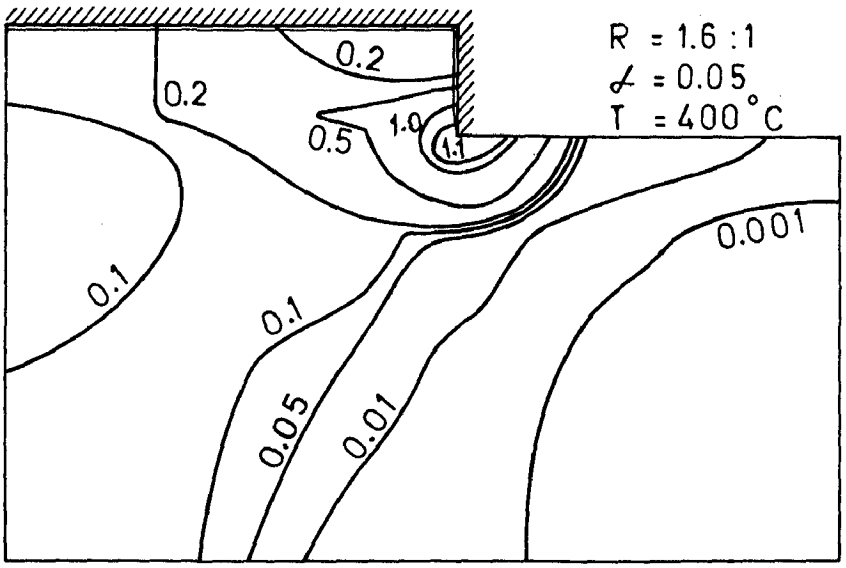

FIG 6.5 (b) AVERAGE EFFECTIVE STRAIN RATE
CONTOURS. (43 elements mesh)

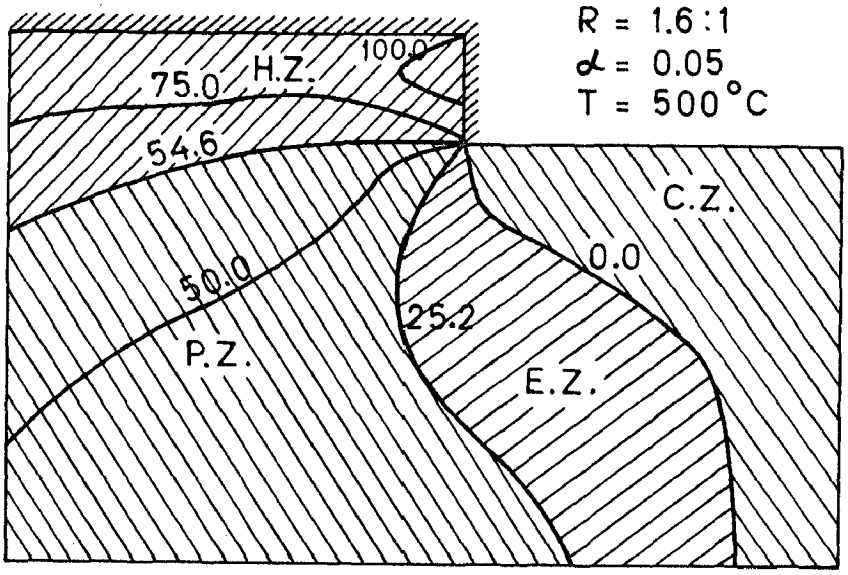

FIG. 6.5 (c) AVERAGE PRESSURE CONTOURS.
(48 elements mesh)

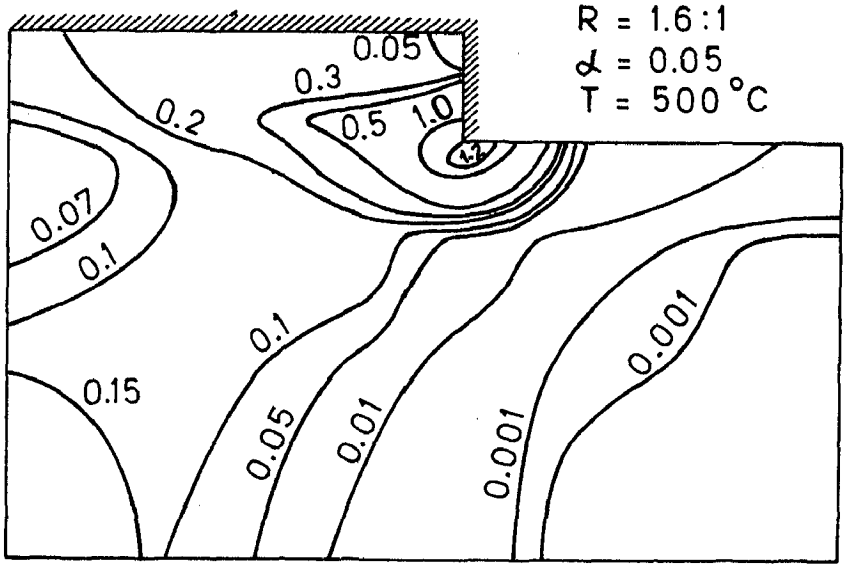

FIG. 6.5 (d) AVERAGE EFFECTIVE STRAIN RATE
CONTOURS. (48 elements mesh)

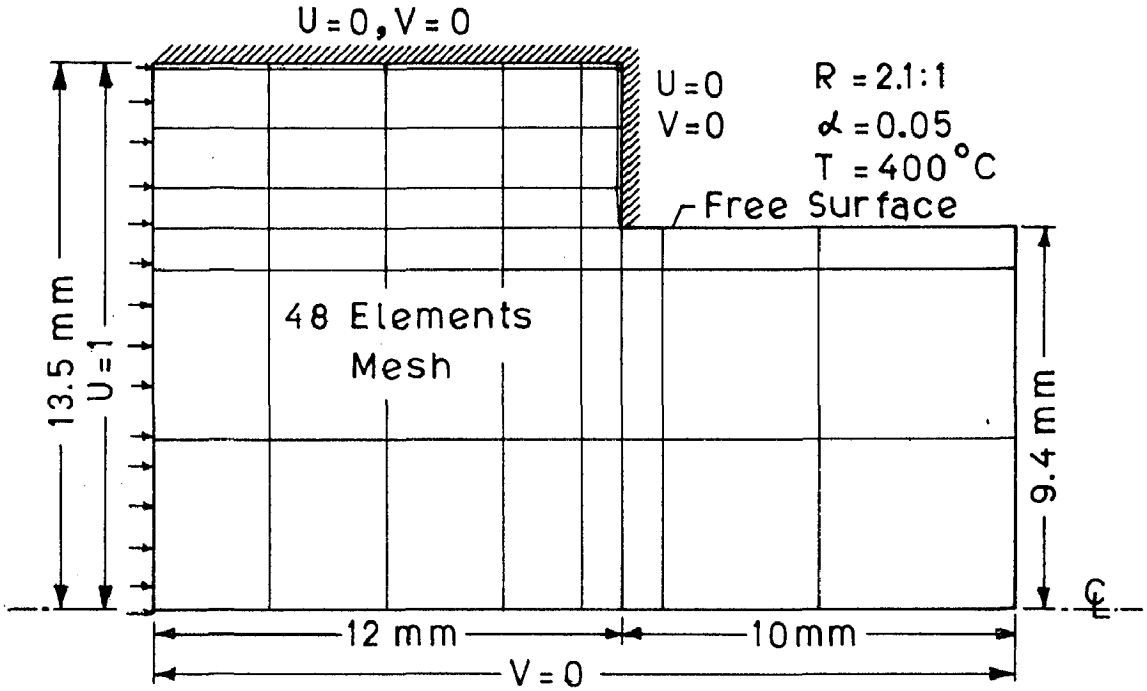

FIG. 6.6 (a) MESH WITH BOUNDARY CONDITIONS.

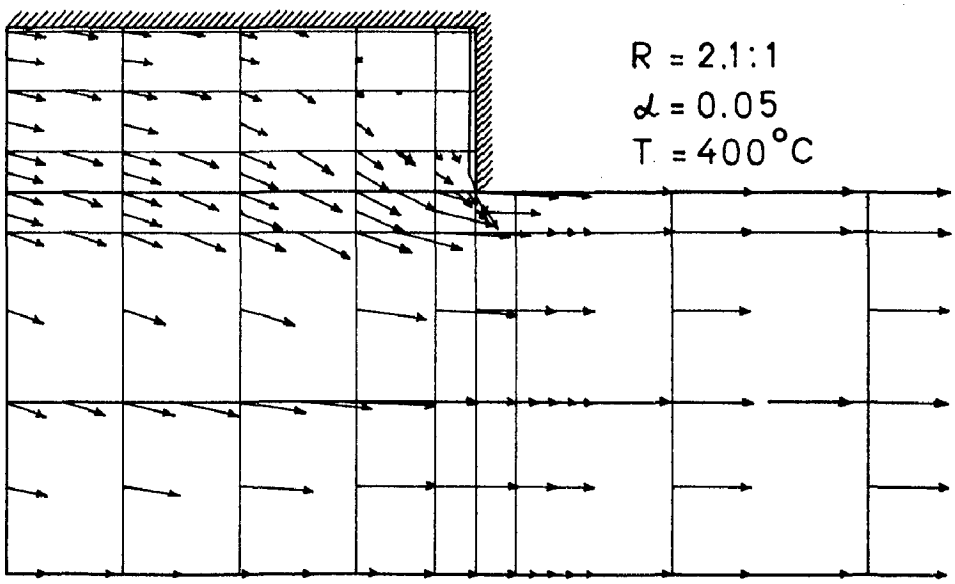

FIG. 6.6 (b) VELOCITY VECTORS. (48 elements mesh)

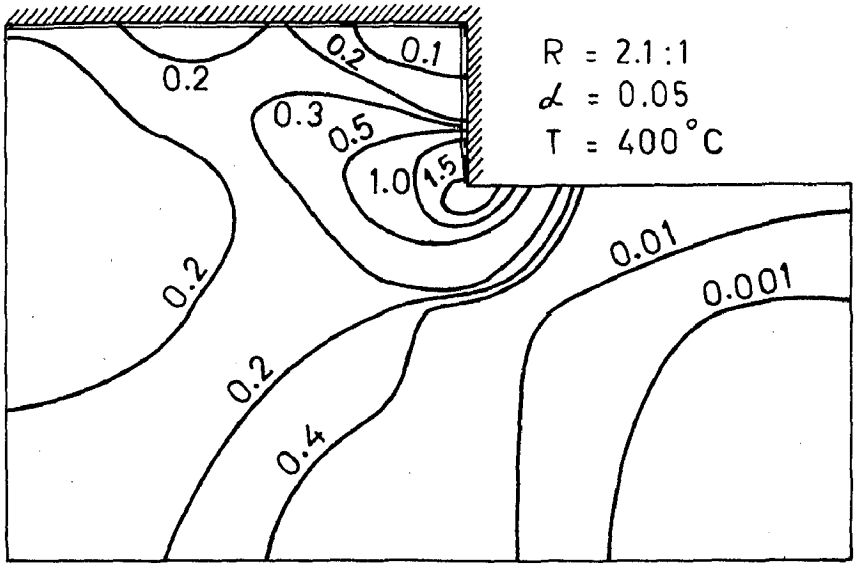

FIG. 6.6 (d) AVERAGE EFFECTIVE STRAIN RATE CONTOURS. (48 elements mesh)

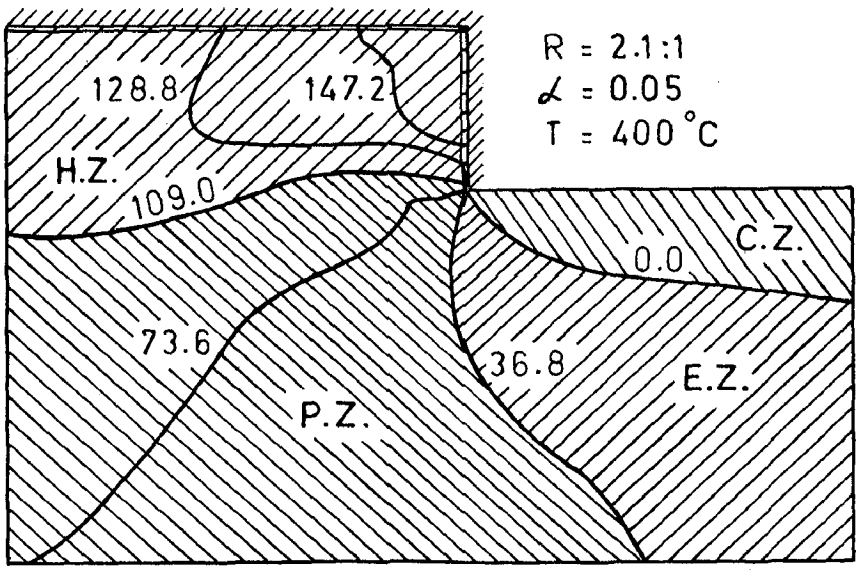

FIG. 6.6 (c) AVERAGE PRESSURE CONTOURS. (48 elements mesh)

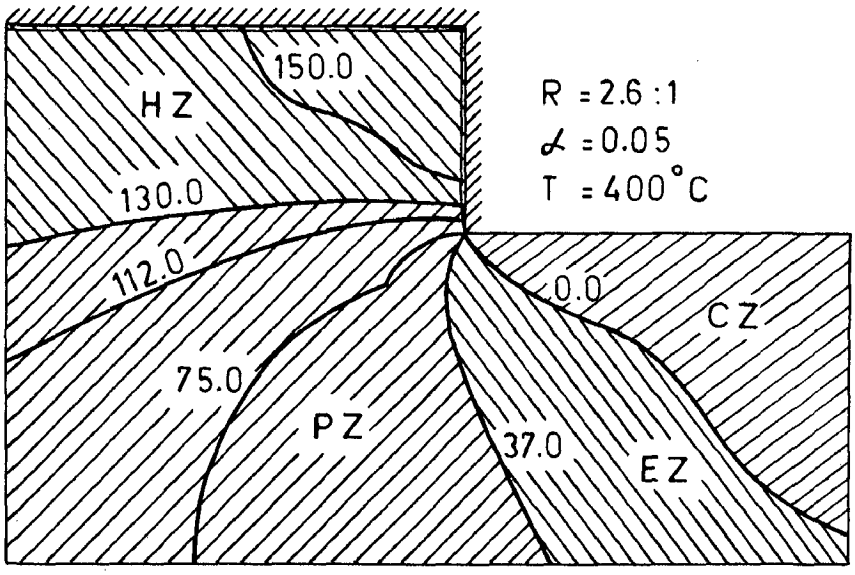

FIG. 6.7 (a) AVERAGE PRESSURE CONTOURS. (48 elements mesh)

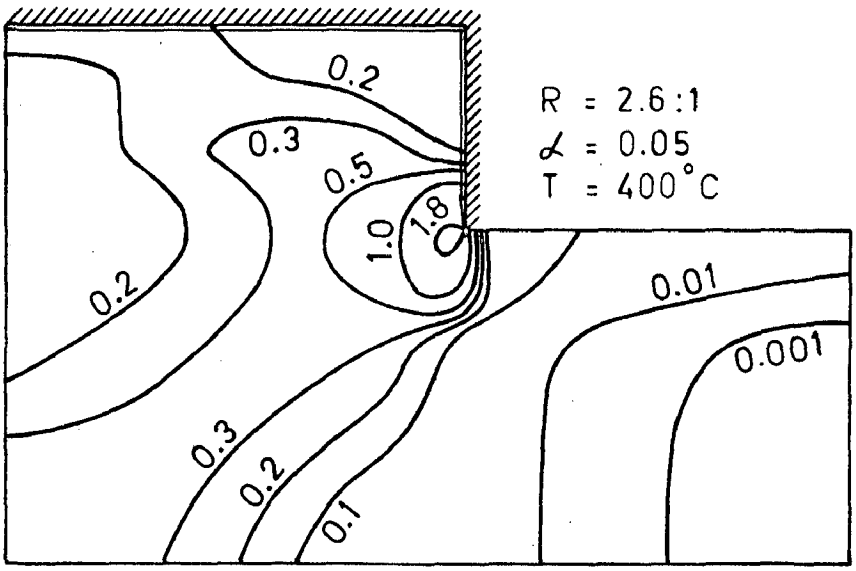

FIG. 6.7 (b) AVERAGE EFFECTIVE STRAIN RATE CONTOURS. (48 elements mesh)

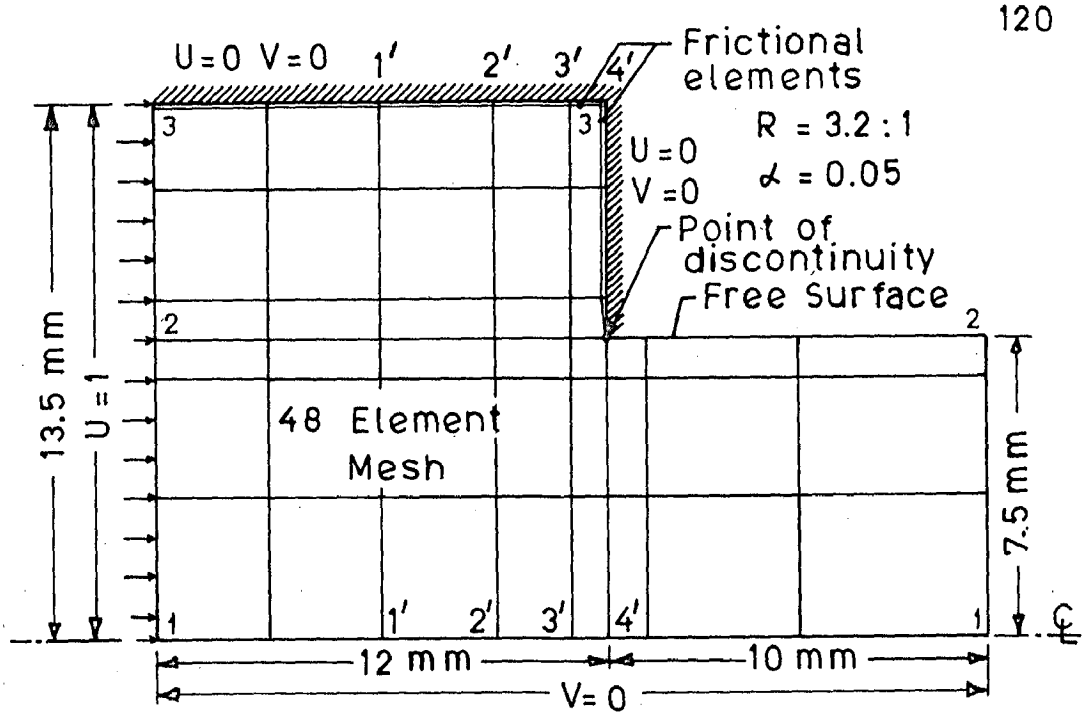

FIG. 6.8 (a) MESH AND BOUNDARY CONDITIONS.

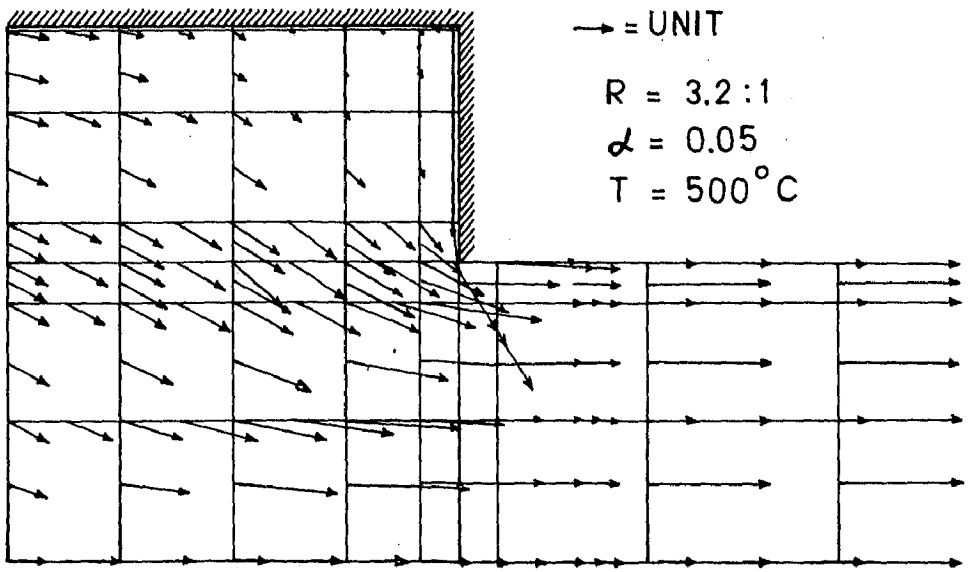

FIG. 6.8 (b) VELOCITY VECTORS. (48 elements mesh)

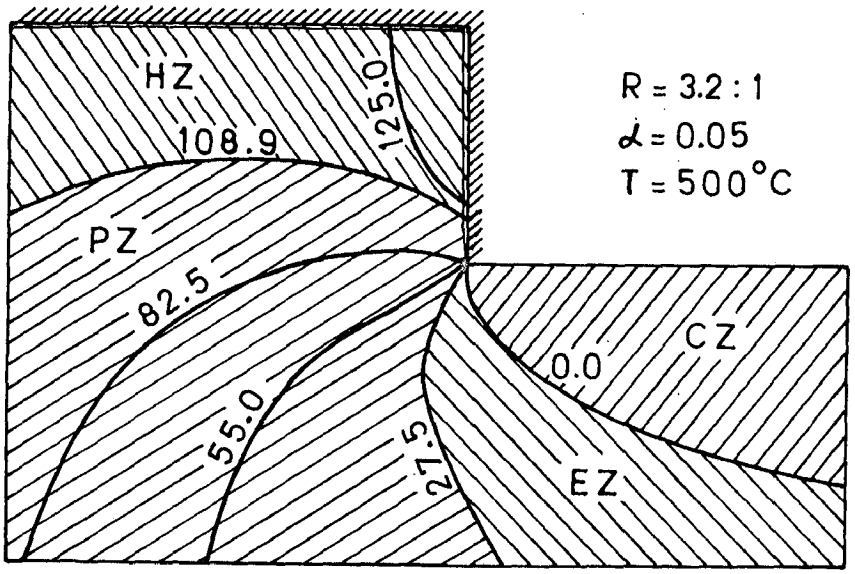

FIG. 6.8 (c) PRESSURE CONTOURS. (48 elements mesh)

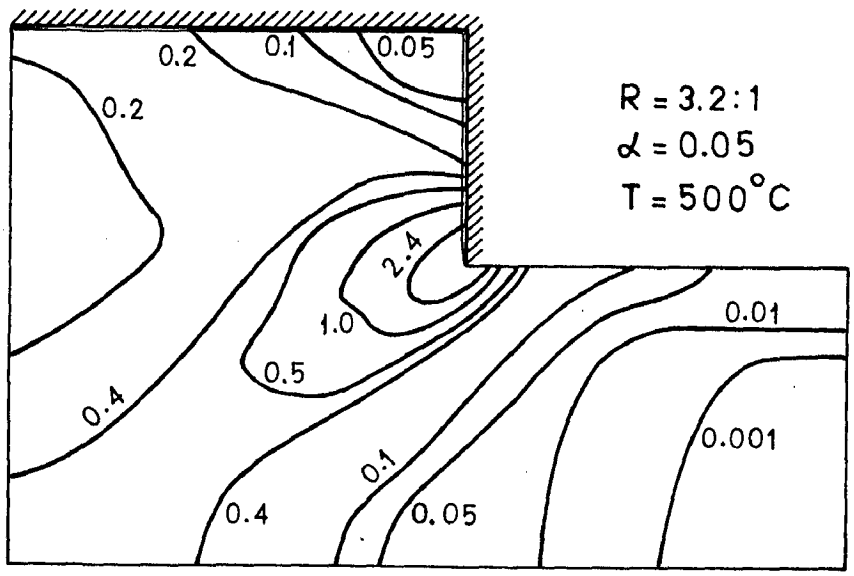

FIG.6.8(d) AVERAGE EFFECTIVE STRAIN RATE CONTOURS. (48 elements mesh)

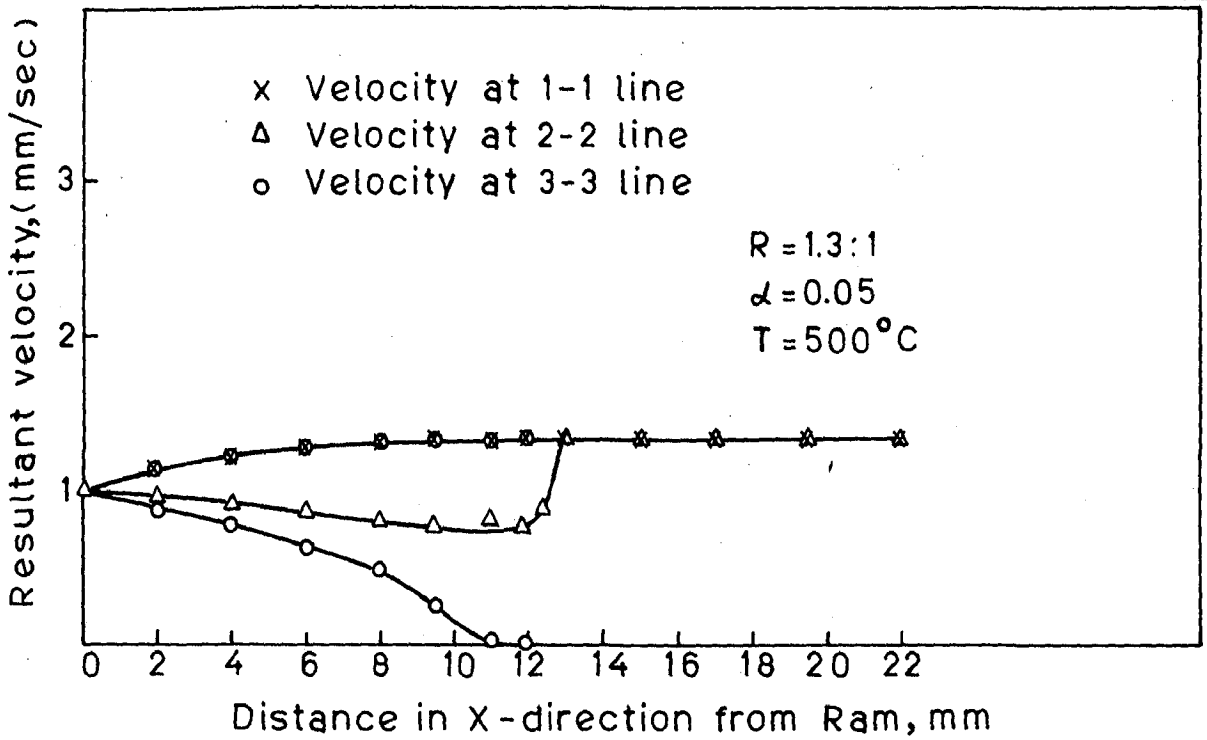

FIG.6.9 (a) VELOCITY PROFILES PARALLEL TO DIE AXIS.

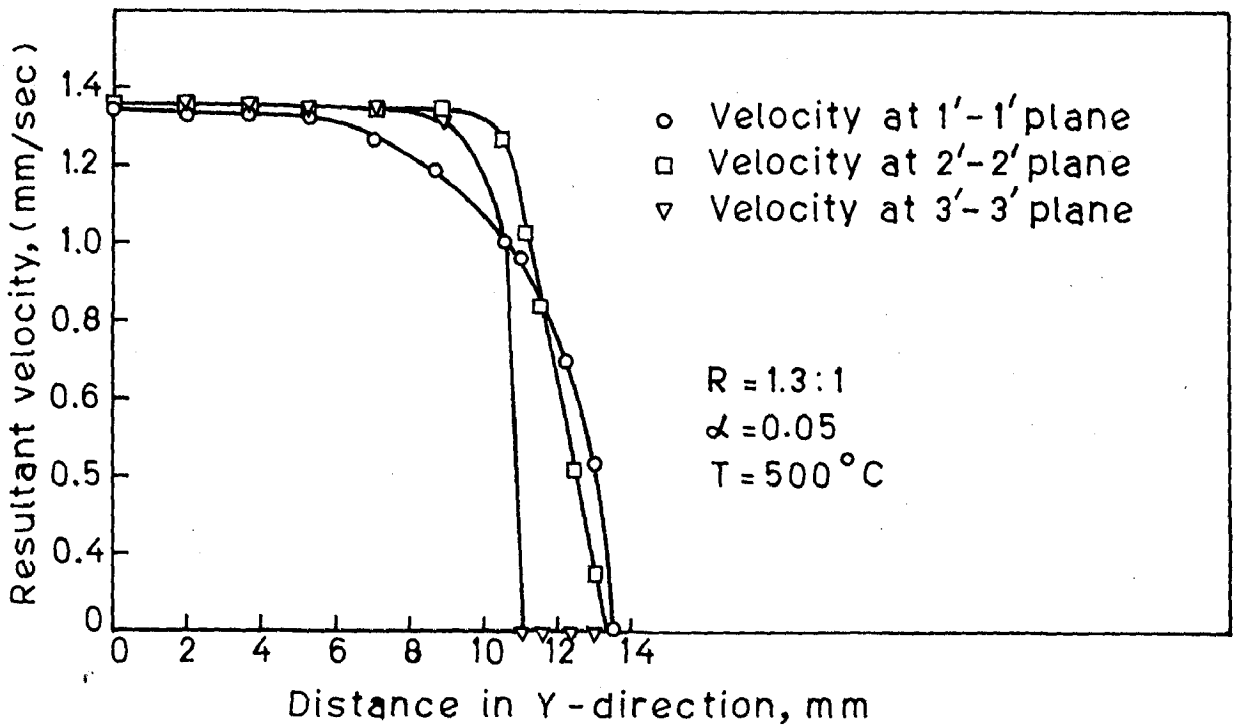

FIG.6.9 (b) VELOCITY PROFILES PERPENDICULAR TO DIE AXIS.

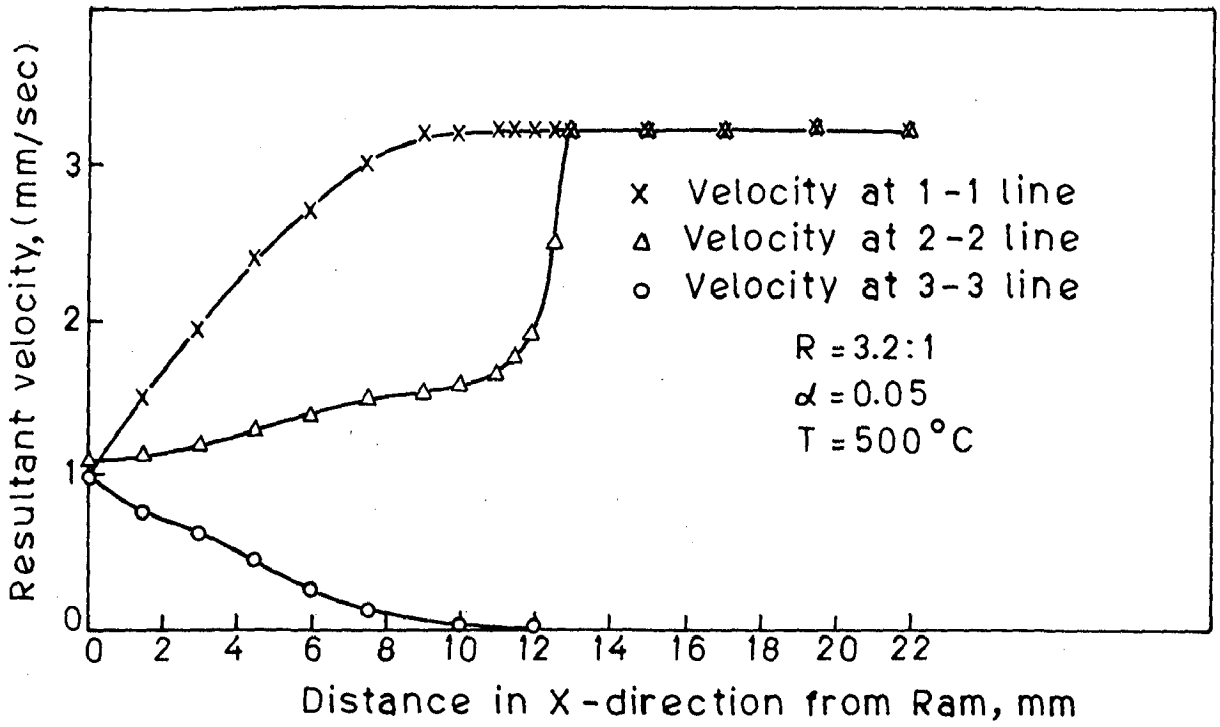

FIG. 6.10(a) VELOCITY PROFILES PARALLEL TO DIE AXIS.

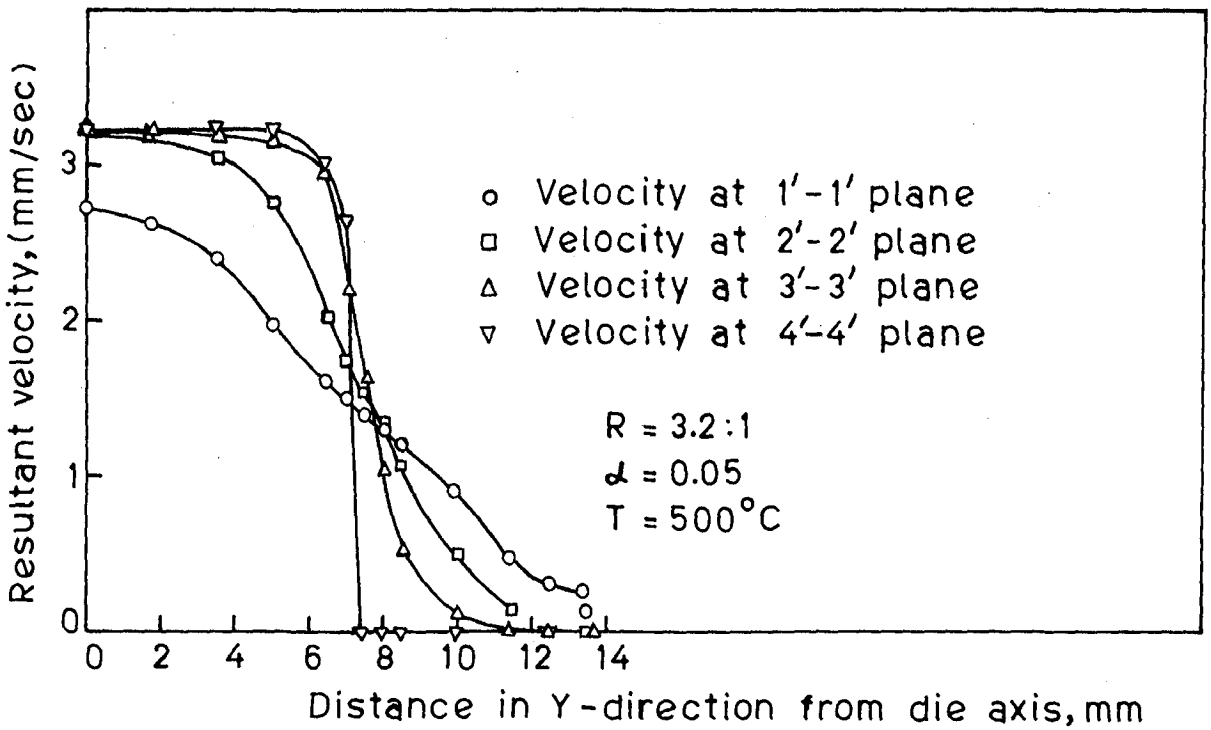

FIG. 6.10 (b) VELOCITY PROFILES PERPENDICULAR TO DIE AXIS.

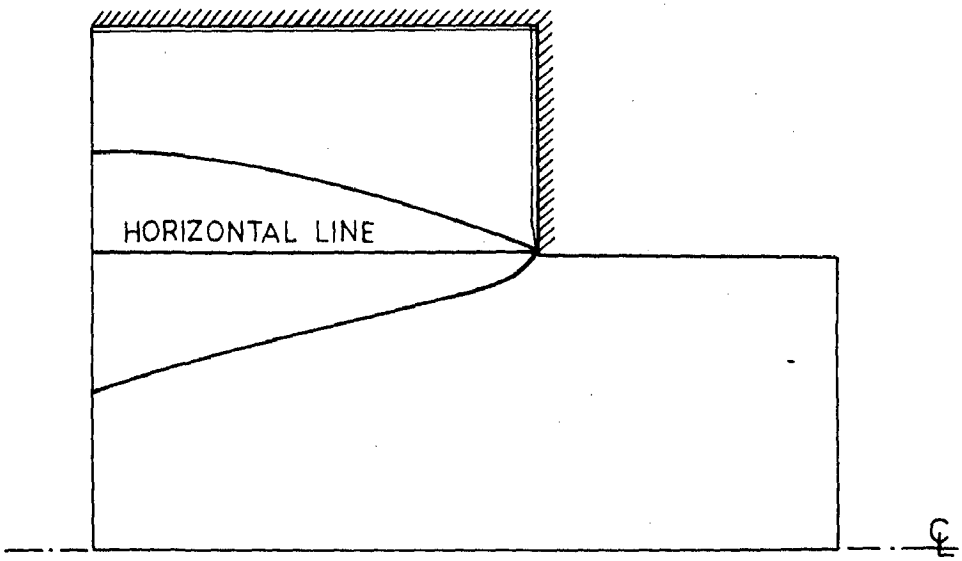

FIG. 6.11 POSSIBLE POSITIONS OF ACTUAL EXTRUSION PRESSURE CONTOUR IN THE CONTAINER.

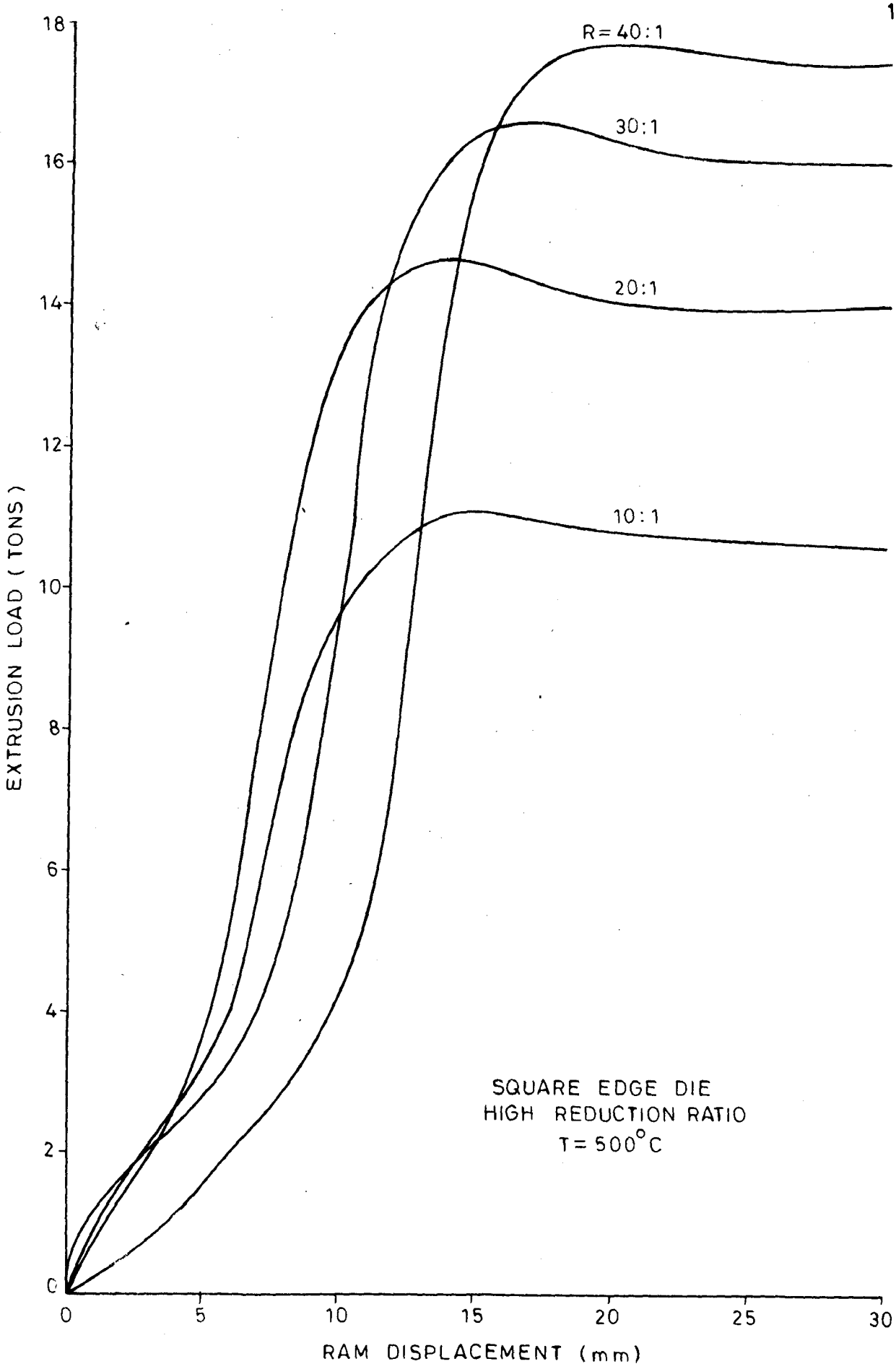

FIG. 6.12–LOAD RAM DISPLACEMENT DIAGRAMS

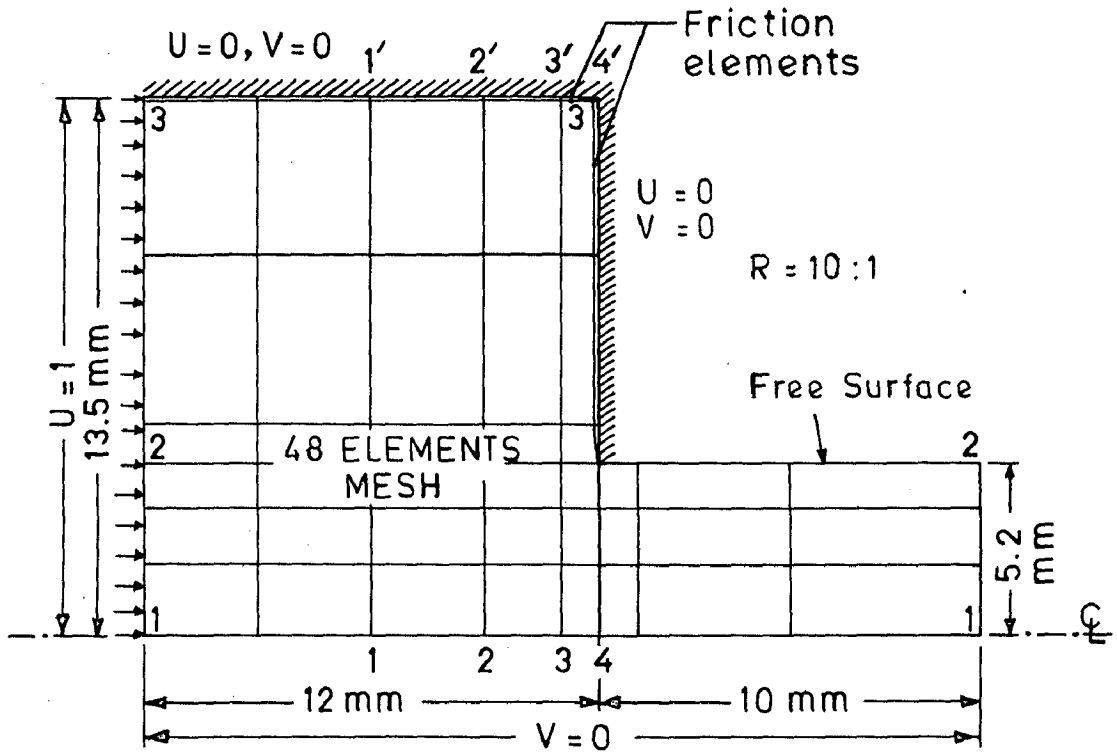

FIG. 6.13 (a) MESH AND BOUNDARY CONDITIONS.

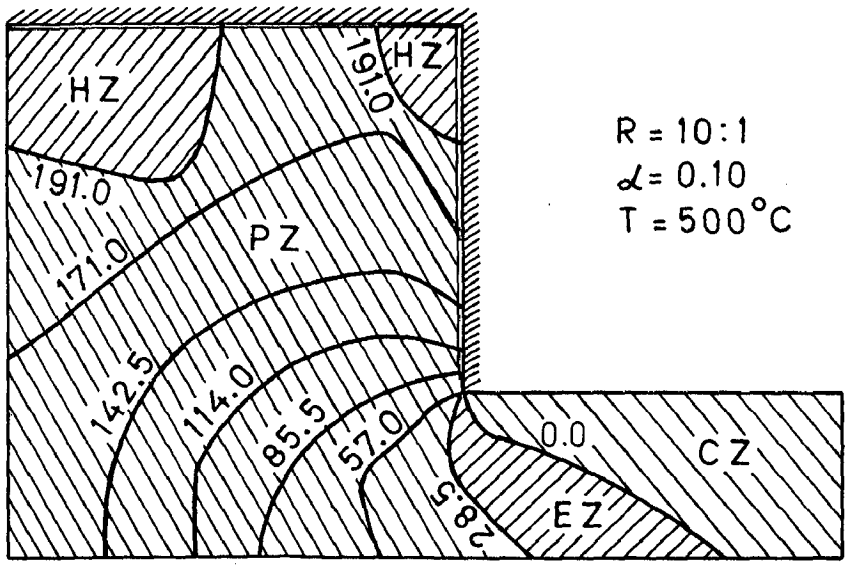

FIG. 6.13 (c) AVERAGE PRESSURE CONTOURS.
(48 elements mesh)

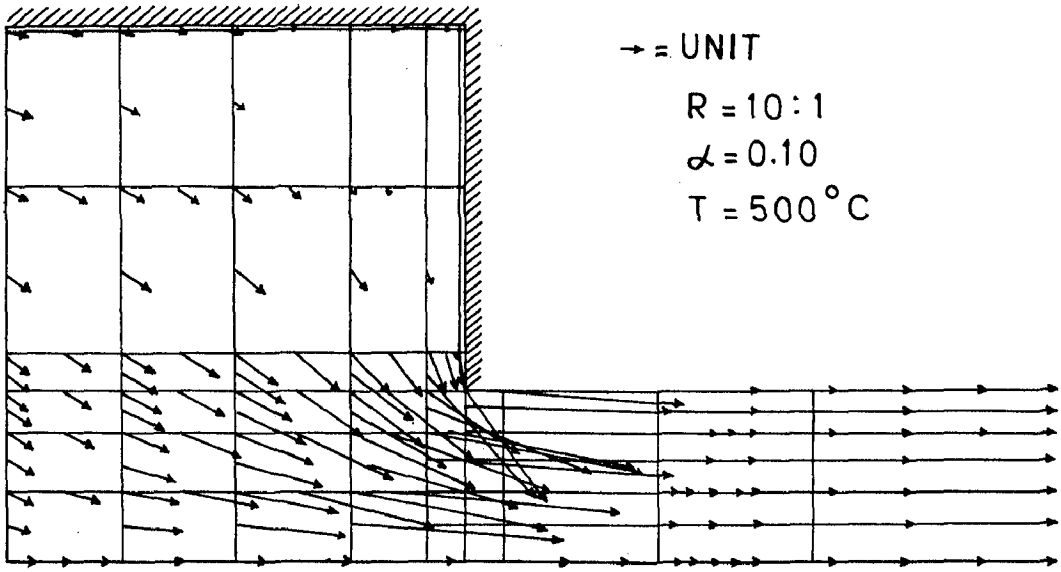

FIG. 6.13 (b) VELOCITY VECTORS. (48 elements mesh)

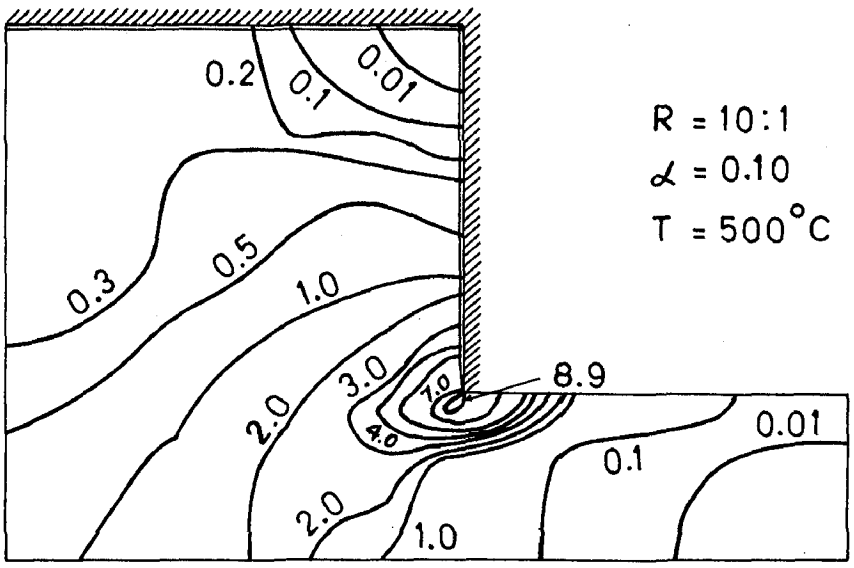

FIG. 6.13 (d) AVERAGE EFFECTIVE STRAIN RATE CONTOURS. (48 elements mesh)

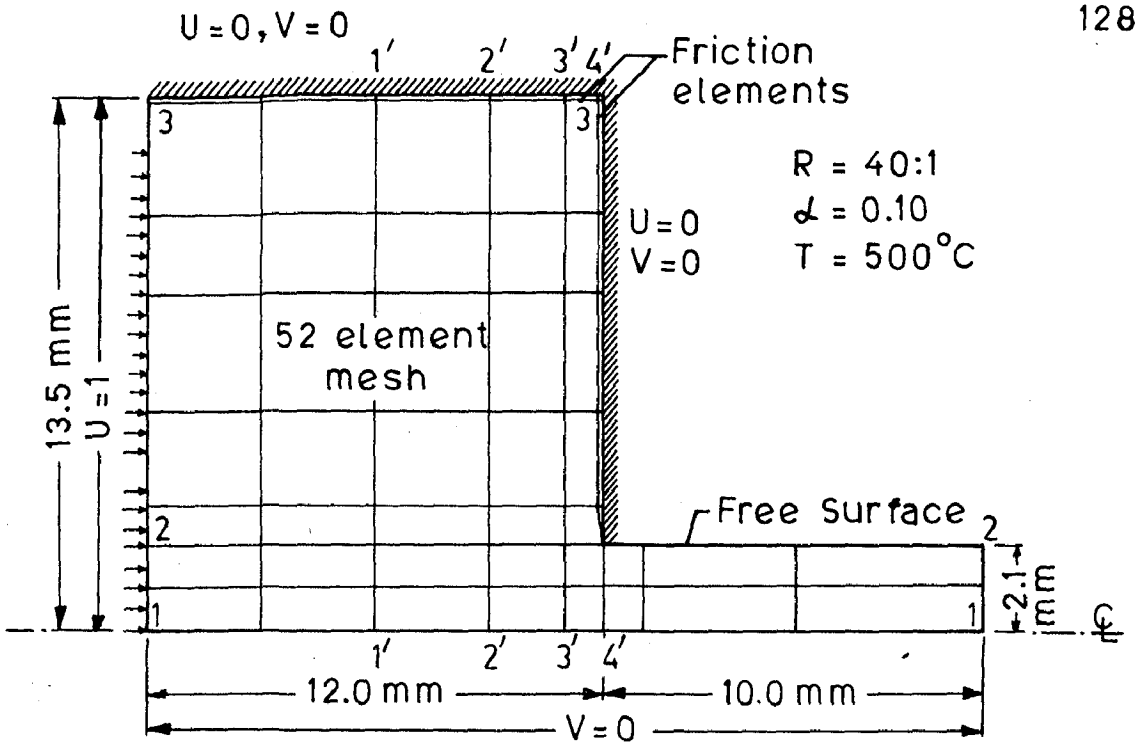

FIG.6.14(a) MESH AND BOUNDARY CONDITIONS.

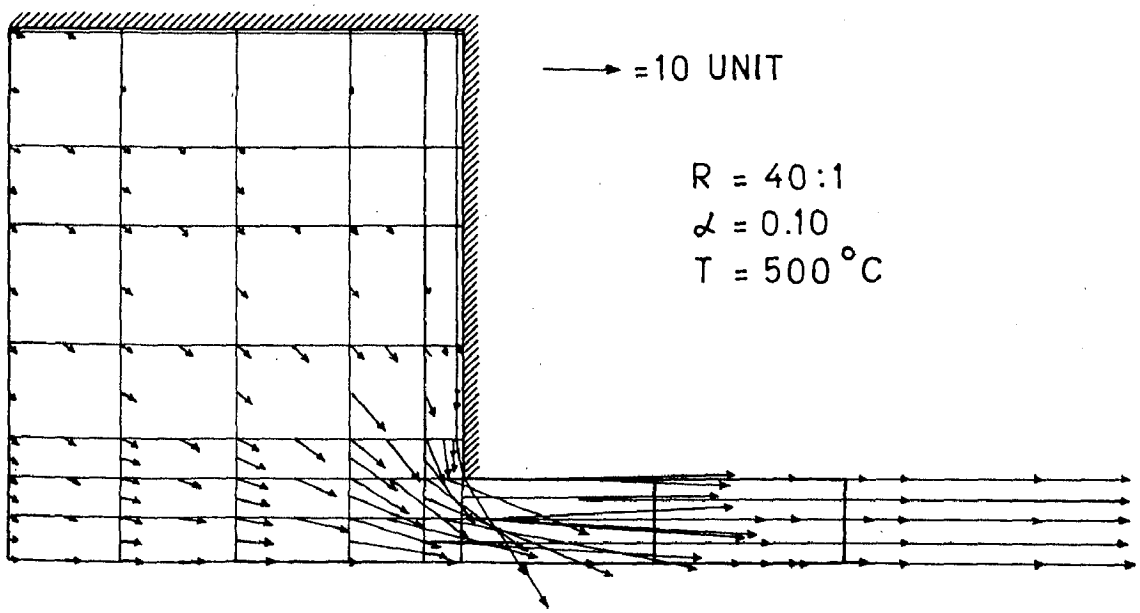

FIG.6.14(b) VELOCITY VECTORS.(52 elements mesh)

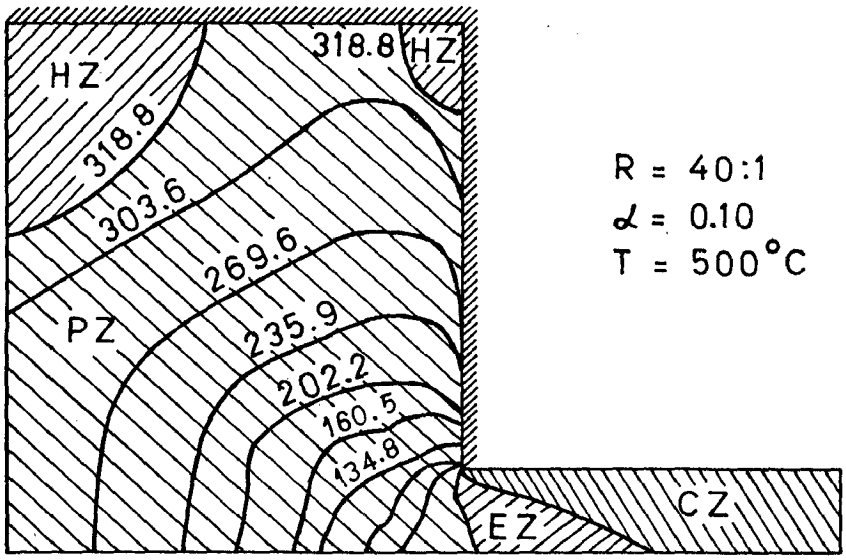

FIG.6.14(c) AVERAGE PRESSURE CONTOURS. (52 elements mesh)

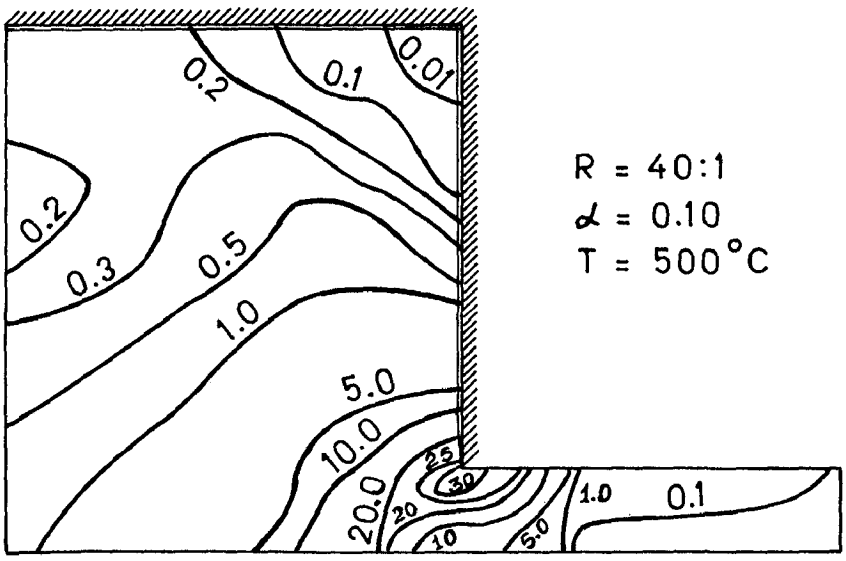

FIG.6.14(d) AVERAGE EFFECTIVE STRAIN RATE CONTOURS.(52 elements mesh)

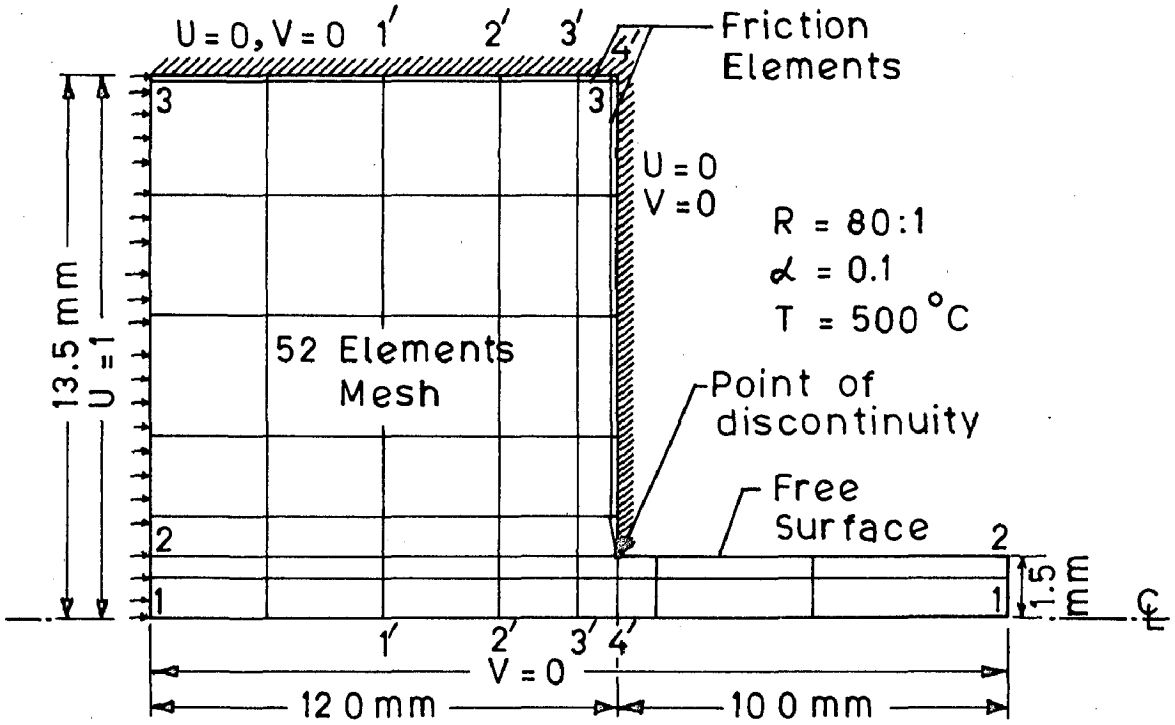

FIG. 6.15 (a) MESH AND BOUNDARY CONDITIONS.

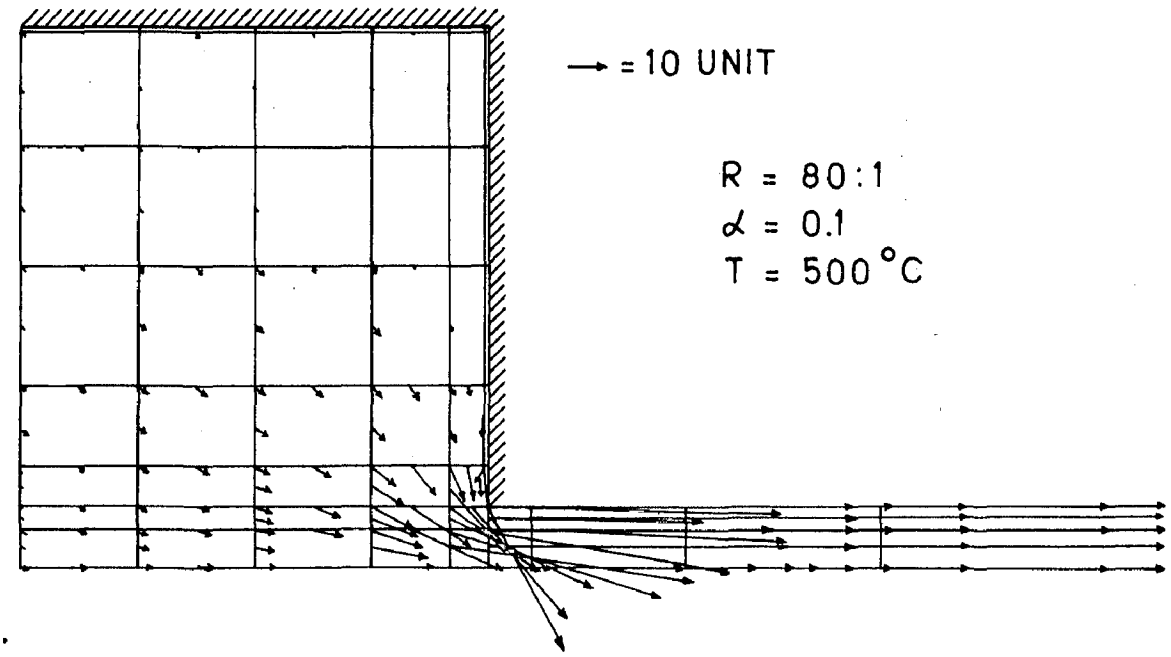

FIG. 6.15 (b) VELOCITY VECTORS. (52 elements mesh)

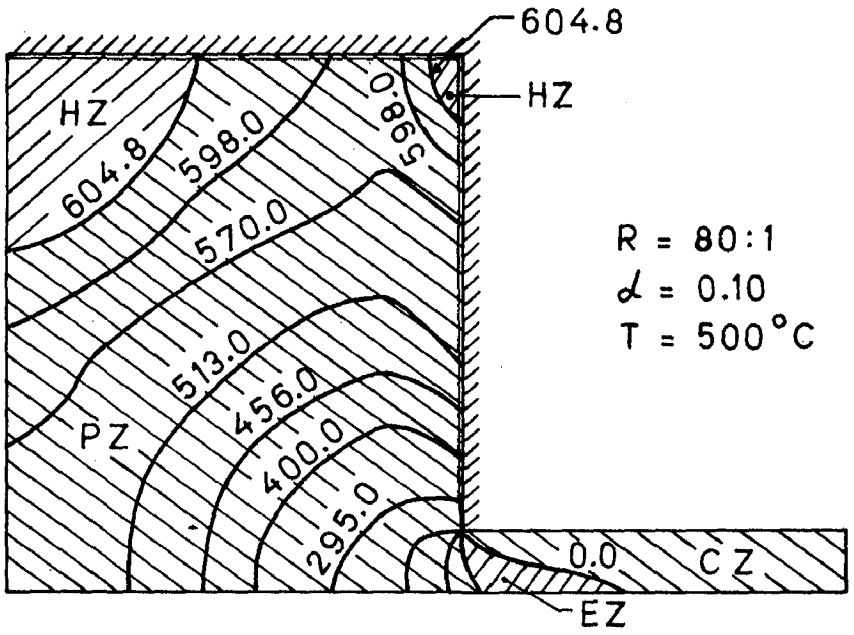

FIG.6.15 (c) AVERAGE PRESSURE CONTOURS.
(52 elements mesh)

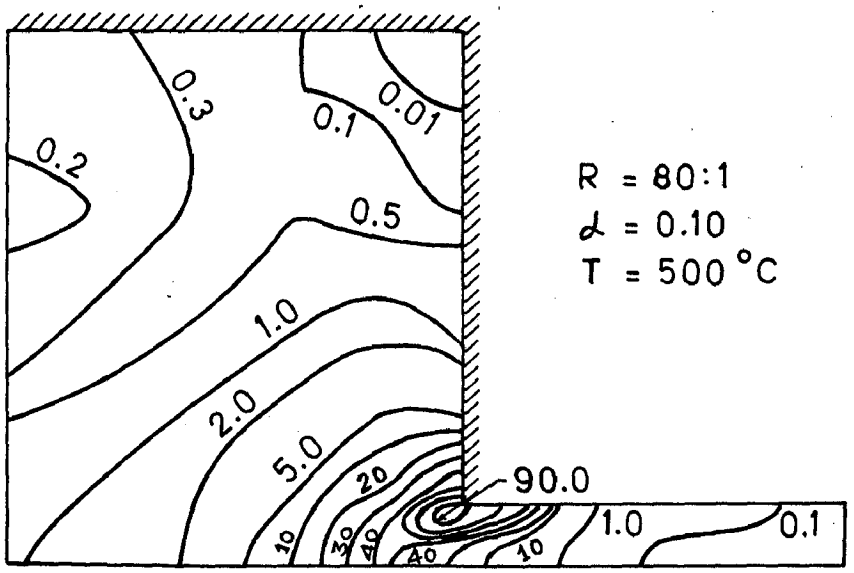

FIG.6.15 (d) AVERAGE EFFECTIVE STRAIN RATE
CONTOURS. (52 elements mesh)

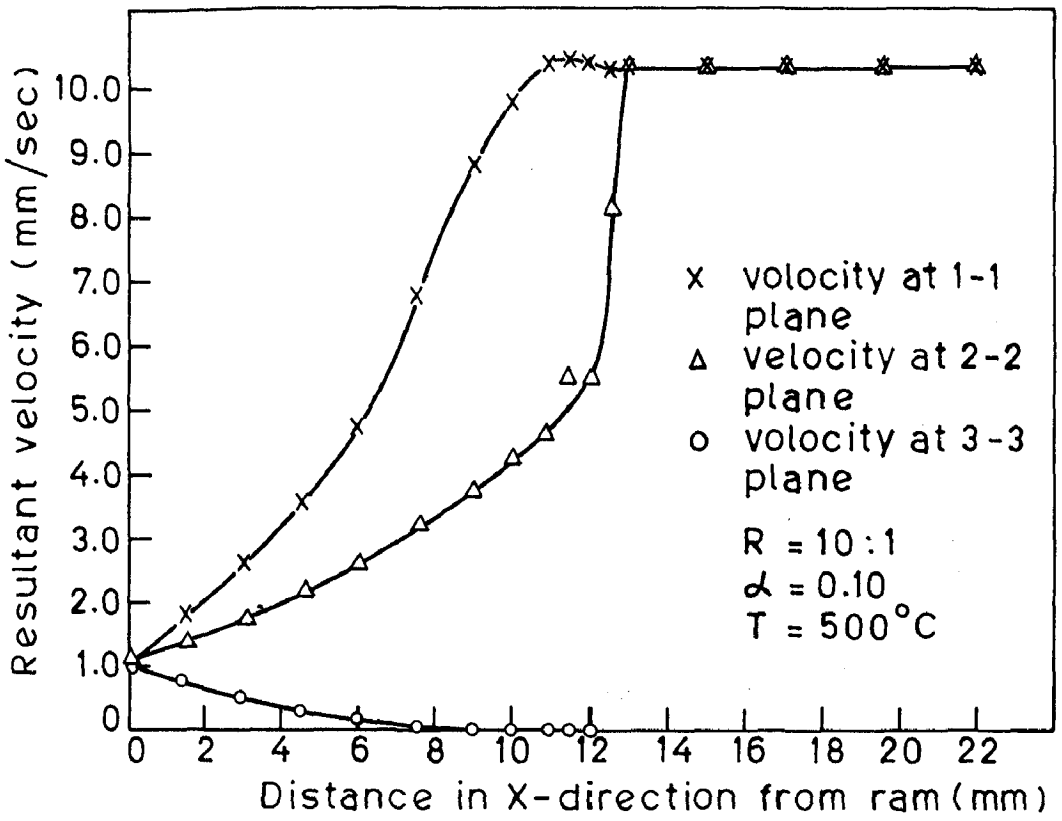

FIG. 6.16 (a) VELOCITY PROFILES PARALLEL TO DIE AXIS.

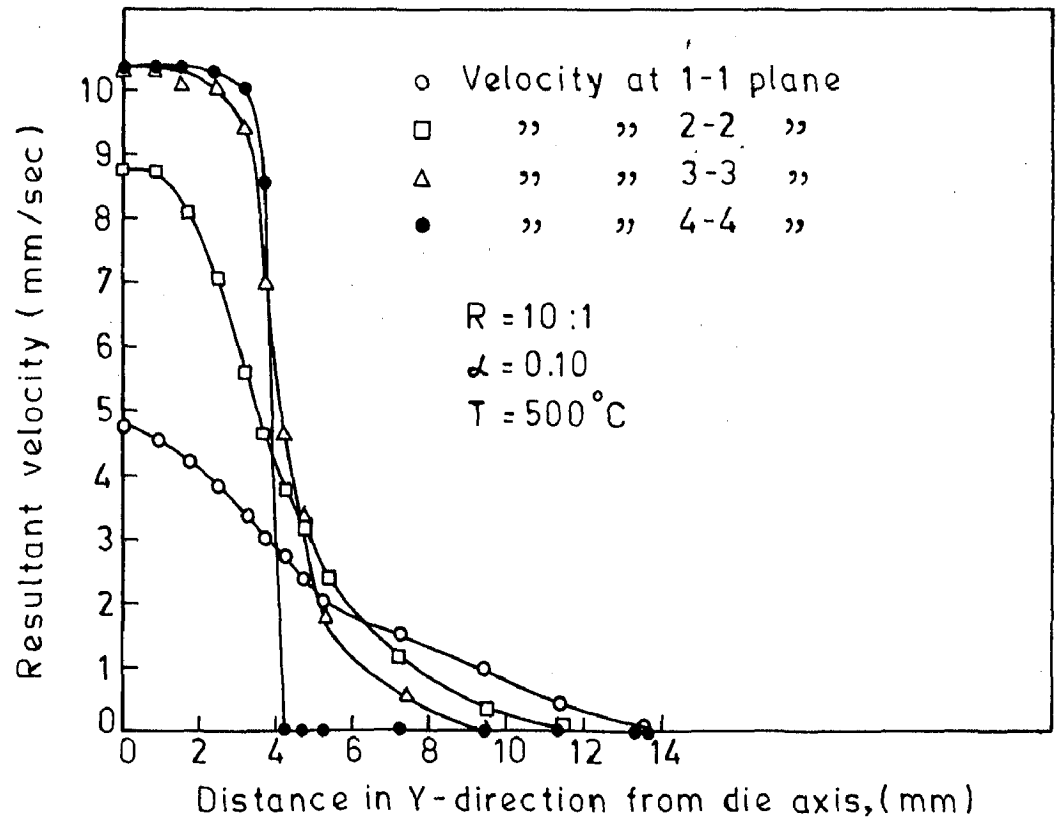

FIG. 6.16 (b) VELOCITY PROFILES PERPENDICULAR TO DIE AXIS.

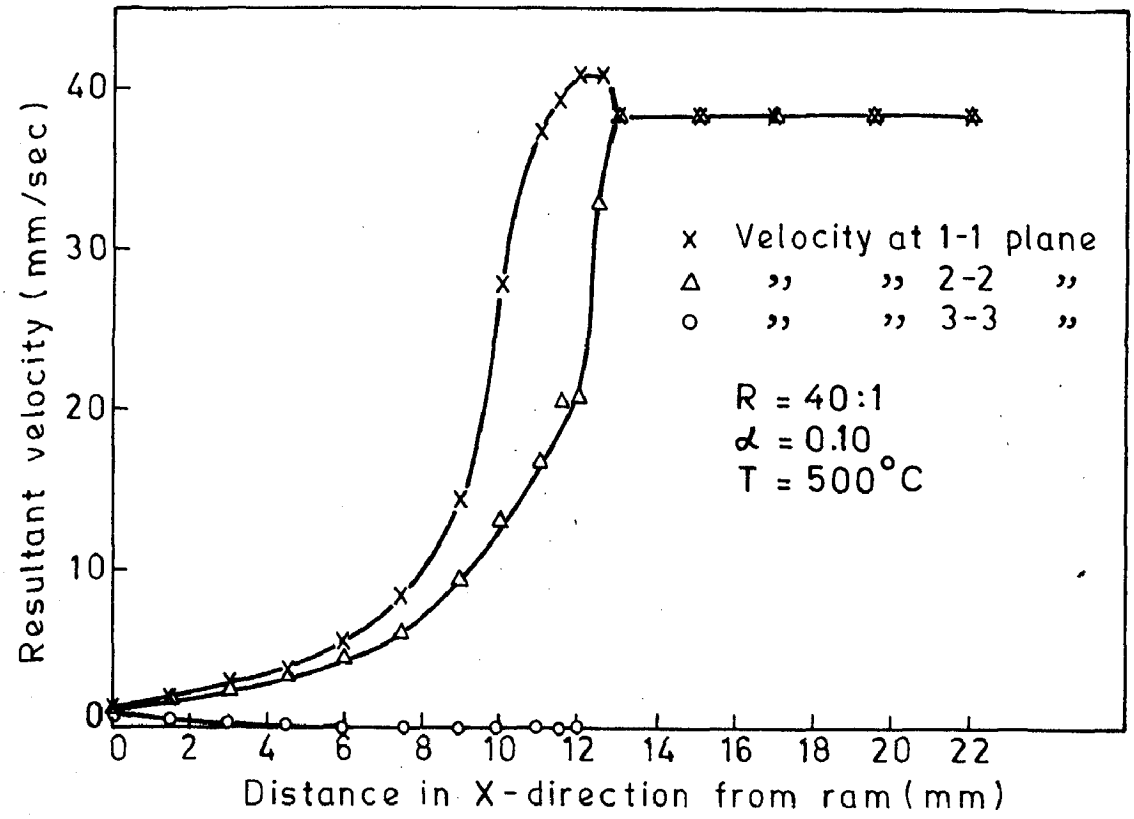

FIG. 6.17 (a) VELOCITY PROFILES PARALLEL TO DIE AXIS.

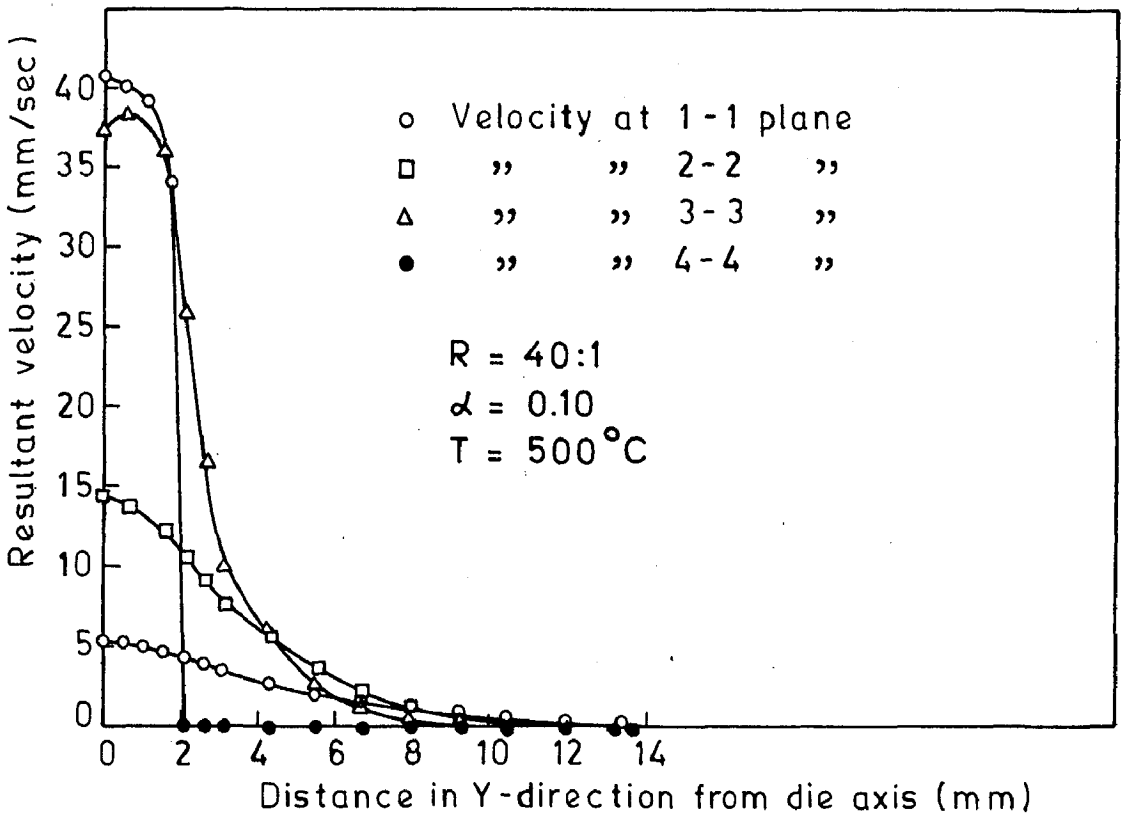

FIG. 6.17 (b) VELOCITY PROFILES PERPENDICULAR TO DIE AXIS.

6.3 EXTRUSION THROUGH CYLINDRICAL WEDGE SHAPED DIE UNDER AXISYMMETRIC CONDITION

Very little work has been reported on powder extrusion through wedge shaped dies. Sheppard et al [3] attempted extrusion of aluminium powder through wedge dies and reported that the surface finish of the extruded product was not acceptable and the threshold extrusion ratio at which coherent mass was produced increased considerably. They attributed this behaviour due to the absence of DMZ and massive shear zones in wedge shaped dies, which was considered to be responsible for building up the coherent mass. Jain [50], using FEM, concluded that extrusion pressure for cast billet is lower in wedge die as compared with that in a square die. The lower extrusion pressure, in wedge dies, might be due to the elimination of DMZ and the deformation being more homogeneous because there is no sudden reduction in area.

The basis for choosing 45° semicone angle for wedge die in the present investigation is to eliminate DMZ because several workers have reported that in square die the DMZ is oriented at 45° with respect to die axis. The present work revealed that in square dies densification was very nearly complete before extrusion started. The situation is different in wedge die, where the extrusion started well before full densification was achieved. The yield criterion modified for porous compact was, therefore, used to consider the varying density in the extruded product, conical portion and the billet being extruded. The experimental investigations were carried out to determine the extrusion pressure

under axisymmetric condition.

In contrast to the conclusion by other workers, it has been possible to achieve a coherent mass with good surface finish in extrusion through wedge die even at lowest reduction ratio 1.6:1 at 400 and 500°C and this has been justified by analytical observations.

6.3.1 Load-Ram Displacement Diagrams

Load rises initially and reaches maximum value and then falls to a constant value. The extrusion starts well before maxima is reached. This pattern is common for all the extrusion temperatures and reduction ratios investigated. Load-ram displacement curves at 500°C for different reduction ratios are given in Figs. 6.18(a and b). However, it may be noted that the initial portion of the curve, for high reduction ratios, the ram displacement observed was more and then the curve practically becomes parallel to load axis suggesting very little compaction with increasing load. The portion of the curve, before peak load is reached, may be called as compaction zone. After this, a maxima in load is attained and ram displacement commences again showing that the extrusion has started. Immediately after maxima, steady state condition is obtained when load becomes practically constant and ram displacement continues. This portion of the curve is the extrusion zone. The extrusion was observed to have started even before the peak load is reached, revealing that the load required to initiate extrusion is lower than the maxima observed in the curve,

for example, in the case of reduction ratio 45:1 at 500°C the peak load observed was 23 tons but in the interrupted test, at 20 tons load, it was observed that the extrusion had started and the length of the extruded product was 25 cm. The density of this extruded product was found to be 99.80 %, while the density of the extruded product at maximum load was found to be 100 %. For comparison of analytical extrusion pressures with experimental pressures the load under steady state condition was considered.

It was also noticed that at 500°C the difference between peak load and the steady state load is less than that at 400°C. It may be due to the fact that beyond 400°C the state of the material has changed.

The difference in peak load and steady state load, at any given reduction ratio, increases with decreasing temperature. Similarly, at constant temperature, this difference inoreases with increasing reduction ratio. Such a behaviour may be due to strain hardening tendency of porous products at different temperatures and reduction ratios. A linear relationship was obtained when a graph between the difference of peak load and steady state load (ΔL) was plotted against log R, as shown in Fig. 6.19. This is further discussed in Chapter VII.

6.3.2 Extrusion Pressure

The relationship between extrusion pressure, p, and log R shown in Fig. 6.20 was found to be linear for low

reduction ratios (R < 10:1) and can be expressed as

$$p = A + B \log R \quad N/mm^2$$

where A and B are constants and whose values were derived from Fig. 6.20 and are given in Table 6.11.

TABLE - 6.11

VALUES OF CONSTANTS A AND B AT DIFFERENT TEMPERATURE(R< 10:1)

S.No.	Temperature ^oC	A	B
1	300	43.4	270.6
2	400	40.9	179.9
3	500	25.8	130.1

At higher reduction ratios (R> 10:1) the relationship between p and log R was also linear but values of A and B were different as shown in Table 6.12. The extrusion pressure increases with increase in reduction ratios, at a constant temperature (Fig. 6.20). The inerease in extrusion pressure at 300°C is more steep than that at 500°C. It may be mentioned that extrusion experiments could not be conducted for high reduction ratios at 300°C due to limitation of capacity of the press.

The relationship are same as that in the case of square dies (section 6.2), but the values of constants A and B are different. As the temperature increases the value of A and B decreases.

TABLE - 6.12

VALUES OF CONSTANT A AND B AT DIFFERENT TEMPERATURES (R > 10:1)

S.No.	Temperature ^{o}C	A	B
1	400	28.7	349.8
2	500	12.4	219.2

When extrusion pressure, p was plotted against log T for different reduction ratios linear behaviour as shown in Fig. 6.21 was observed and can be expressed as:

$$p = a - b \log T \quad N/mm^2$$

A change in slope of the curve was observed at 400°C for all the reduction ratios except 1.6:1 and 2.0:1 as observed in case of square dies.

6.3.3 Density Measurements

The density of the different sections (Fig. 6.22) of extruded products, after getting the steady state load, are shown in Table 6.13. Also the densities of the material inside the container and that of conical portion are included in the Table 6.13.

For a given reduction ratio the density increases with increase in temperature of extrusion. At the lowest reduction ratio (R=1.6:1), the density of the extruded product varies from 98.24 to 98.50 % as the temperature increases from 400 to 500°C while the density of the

TABLE - 6.13

DENSITIES OF THE EXTRUDED PRODUCT AND BILLET BEING EXTRUDED THROUGH WEDGE SHAPED DIES

R / T °C	1.6:1				2.0:1				3.5:1			
	A	B	C	D	A	B	C	D	A	B	C	D
300	Incoherent mass was achieved								94.35	98.16	98.16	98.03
400	94.58	98.74	98.24	97.80	94.60	98.48	98.46	98.20	95.00	98.75	98.74	98.33
500	94.76	98.54	98.54	98.23	95.21	98.92	98.91	98.60	96.11	99.34	99.32	98.83

TABLE - 6.13 (Contd.)

T °C \ R	7.0:1				12.0:1			
	A	B	C	D	A	B	C	D
300	98.12	99.01	99.00	98.89	98.30	99.33	99.32	99.24
400	98.25	99.51	99.50	99.43	98.88	99.71	99.71	99.65
500	98.54	99.84	99.83	98.69	98.72	100.00	100.00	99.91

NOTE:- At high reduction ratios (30:1, 45:1,and 80:1) the densities in regions B, C and D were measured and found to be 100% theoretical densities at 400°C and 500°C. The density in portion A varies between 99.2 to 99.8% at 400°C and 99.6 to 100% of theoretical density, as R varies from 30:1 to 80:1.

unextruded product in the container varies from 97.80 to 98.20 %. The density of the product which comes out first designated by 'A' (Fig. 6.22)during the experiment is 94.5% at 400°C and 94.7 % at 500°C. These results show that in wedge shaped dies extrusion starts before complete densification which is continued in the extrusion process.

The density of the extruded product at 500°C for R, 12:1, is 100 % except the starting portion designated as 'A'. The density at higher reduction ratios 30:1, 45:1 and 80:1 is practically 100 % at all temperatures except the starting portion, 'A'.

6.3.4 Tensile Properties

The tensile properties of the extruded product upto reduction ratio 15:1 at room temperature are shown in Table 6.14. At the two lowest reduction ratios 1.6:1 and 2.0:1, the product extruded at 300°C was found to be incoherent (section 6.5). However, coherent mass was obtained for these reduction ratios at higher extrusion temperatures, 400 and 500°C. At a given extrusion temperature the strength improves with increasing reduction ratio. As the extrusion temperature increases from 300 to 500°C for a constant reduction ratio, a substantial drop in tensile strength but large increase in ductility was observed. It was also noticed that the tensile strength of the product extruded through wedge die are 10-20 % higher than that of the product extruded through square die (Table 6.5) where as elongation at low reduction ratios, 1.6:1 and 2.0:1 is

20-30 % less but at high reduction ratios the values are comparable.

Tensile properties for higher reduction ratios could not be obtained as it was not possible to make tensile samples due to the fact that the diameter of extruded product was small.

6.3.5 Comparison Between Analytical and Experimental Extrusion Pressures

Analytical extrusion pressures were obtained at 400 and 500°C for all the reduction ratios by taking the actual length of the billet being extruded (H = 21 mm) which remain in the container after achieving the steady state condition of extrusion. A fine mesh (53 elements) was used with friction coefficient, 0.05 for low reduction ratios (1.6:1 to 7.0:1) and 0.10 for high reduction ratios (12:1 to 80:1) as used in case of square dies. In calculating extrusion pressures the effect of density variation in the product and the billet being extruded under steady state condition of extrusion was considered by using yield criterion modified for porous material (section 5.3)for reduction ratio, 1.6:1 and reduction ratio,3.5:1 at extrusion temperature 500°C. The analytical extrusion pressures were also calculated by taking the density as theoretical density in all the sections (Fig. 6.22) for reduction ratio 1.6:1 and 3.5:1 at 500°C and were compared with experimental extrusion pressure. Results are given in Table 6.15.

TABLE - 6.14

TENSILE PROPERTIES OF EXTRUDED PRODUCT AT ROOM TEMPERATURE

(WEDGE DIE)

S. No.	T / R	300°C			400°C			500°C		
		UTS N/mm^2	YS N/mm^2	Elongation %	UTS N/mm^2	YS N/mm^2	Elongation %	UTS N/mm^2	YS N/mm^2	Elongation %
1	1.6:1	Incoherent Product			71.0	65.0	1.4	56.0	47.0	1.95
2	2.0:1	Incoherent Product			109.0	98.0	3.8	82.0	76.0	6.0
3	3.6:1	139.0	128.0	8.6	123.0	103.0	11.2	112.5	94.5	22.8
4	7.0:1	153.0	135.0	24.9	130.0	118.0	28.8	117.0	106.5	36.6
5	15:1	154.3	136.0	30.5	134.8	120.0	35.7	119.0	107.0	38.7

TABLE - 6.15

EFFECT OF DENSITY FOR ANALYTICAL EXTRUSION PRESSURE

S.No.	R	T ^{o}C	Experimental Pressure N/mm^2	Analytical Extrusion Pressure N/mm^2	
				ρ_o = 100 %	Varying density
1	1.6:1	500	52.65	59.6	56.3
2	3.5:1	500	94.30	93.9	91.8

The results given in Table 6.15 show that the density has an effect on the value of analytical extrusion pressure, The use of yield criterion modified for porous material in the present investigation is justified because it takes into account the observed experimental condition i.e. variation of density in the material during steady state extrusion.

Therefore, the analytical extrusion pressures, so obtained using yield criteria modified for porous material, were compared with the experimental extrusion pressures at 400 and 500 ^{o}C for all reduction ratios investigated and are given in Table 6.16.

The above table shows that for low reduction ratios the difference between analytical and experimental values is about 6 to 10 % . It may be due to the fact that at these reduction ratios the value of α may be less than 0.05 which has been taken for our analytical studies. In case of high reduction ratios the difference is only 1 to 3 % which shows a very good agreement between analytical and experimental

TABLE - 6.16

COMPARISON OF EXPERIMENTAL WITH ANALYTICAL EXTRUSION PRESSURE (WEDGE DIE)

S. No.	R	Extrusion Temperature ^{o}C	Friction Co-efficient	Extrusion Pressure	
				Exp. N/mm^2	Analytical N/mm^2
		300	-	101.3	-
1	1.6:1	400	0.05	75.1	86.2
		500	0.05	52.4	56.3
		300	-	120.5	-
2	2.0:1	400	0.05	92.6	87.8
		500	0.05	66.4	62.1
		300	-	192.1	-
3	3.5:1	400	0.05	134.5	129.7
		500	0.05	94.3	91.8
		300	-	270.7	-
4	7.0:1	400	0.05	194.5	200.1
		500	0.05	136.3	131.1
		300	-	-	-
5	12:1	400	0.10	349.3	336.1
		500	0.10	230.5	218.2
		400	0.10	480.0	460.2
6	30:1	500	0.10	312.0	295.7
		400	0.10	558.2	547.3
7	45:1	500	0.10	349.3	348.6
		400	0.10	637.5	630.3
8	80:1	500	0.10	410.5	421.95

extrusion pressures. The analytical extrusion pressure was found to be lower in wedge shaped dies as compared to that of square edge dies for the same length of the billet.

6.3.6 Velocity Vectors

Figures 6.23(b), 6.24(b), 6.25(b), 6.26(b) and 6.27(b) show the velocity vectors for reduction ratios, 1.6:1, 3.5:1,7.0:1, 30:1 and 80:1 respectively at 500°C assuming friction coefficient as 0.05 for low reduction ratios($R < 10:1$) and 0.10 for high reduction ratios ($R > 10:1$). Results show that the continuity requirement is satisfied at 400 and 500°C for all reduction ratios. Experimentally also, coherent mass was achieved at these temperatures for all reduction ratios. The magnitudes of the velocity vectors near the conical surface, are more than the velocity at the die axis, which is in contrast to those of square dies where the material movement across the die surface is less.

The magnitude of resultant velocities plotted against the distance in y-direction from die axis along the different planes marked in Figs. 6.23(a) to 6.27(a) for reduction ratios 1.6:1, 3.5:1, 7.0:1, 30:1 and 80:1 at 500°C are shown in Figs. 6.28 to 6.32. The velocity distribution shows that the region of homogeneous deformation is less in low reduction ratios compared to high reduction ratios as the resultant velocities curves meet in a smaller region in case of low reduction ratios. At the exit plane, the velocity is maximum along the die axis and reduces to zero at the point of second discontinuity while the velocities along other planes from

the die axis remain constant for fairly long distances. However, it increases as the conical surface of die is approached and then it becomes zero at the conical surface. Magnitudewise this increase is not more than 20% of the velocity along the die axis. This clearly shows that near the conical surface there is extensive movement of material takes place, while in case of square dies the velocities remain constant for a small distance from die axis and then approach to zero value (Figs. 6.28, 6.31 and 6.32) which shows that extensive movement of material takes place only in a small region of die near the die axis. Due to this difference in the flow pattern of the material, better coherent mass in case of wedge die extrusion is possible.

In the case of R, 1.6:1, for wedge die the increase in velocity as described above is not observed and there is continuous decrease of velocity from die axis to conical surface of die (Fig. 6.28) where it attains zero value. This indicates that corresponding to low reduction ratios, there might exist,so called DMZ but however, in high reduction ratios the high flow condition near the conical surface of die completely rules out the possibility of the existence of DMZ. Thus, the DMZ is not formed at 45° as suggested earlier but it depends upon reduction ratio and extrusion temperature.

6.3.7 Average Pressure Contours

Figures 6.23(c), 6.24(c), 6.25(c), 6.26(c) and 6.27(c) show the average pressure contours for wedge shaped

dies for reduction ratios, 1.6:1, 3.5:1, 7.0:1, 30:1 and 80:1 at 500°C respectively. The nature of pressure contours for wedge die are, in general, transverse to the material movement and most of them extends upto the die axis. The shape of the contour is symmetrical with respect to the die axis showing extensive movement of the material i.e. extensive plastic flow inside the die and results in coherent and sound product. Whereas in the case of square dies many of the pressure contours are parallel to die axis and terminate at the ram surface. This situation is not good for coherency and soundness of the product. Thus,wedge dies appear to be better for the coherency and soundness of the product.

In lowest R, 1.6:1 at 500°C the pressure is built up, at the conical surface to the extent that it is even more than the extrusion pressure which was obtained analytically. This indicates the existence of a zone of relatively slower motion of material. This is similar to the one called hydrostatic zone, observed in square die. However, this zone is absent in high R's. This observation suggests that the DMZ does not exist at an angle of 45° from the die axis but the angle depends upon the R under question. On the basis of this observation it may be concluded that for lowest R the DMZ extends towards the opposite direction of the metal flow and along the conical surface of the die. The same was observed in square dies as well. It was reported in section 6.2 that in case of square dies in low R's the DMZ extends in the opposite direction of metal flow and in lowest R (1.3:1) becomes almost parallel to

the die axis. As the R increases the DMZ shrinks towards the square edge of the die i.e. DMZ is formed at an angle more than 45° from the die axis. This observation is verified by wedge dies where, for higher R's, the DMZ is eliminated completely.

The shaded region between the actual extrusion pressure contour (EPC) and the contour which represents the yield stress is the region of plastic flow (PZ) where there is an extensive movement of material. This region, from the die surface to the die axis, is large enough in these dies and consequently indicates a better flow of material and better coherent product. The other shaded regions are same as explained in section 6.2. With increasing reduction ratios the pressure contours get confined to a narrow region towards the point of second discontinuity. These contours are transverse to the material flow and, therefore, we can expect increasing strength and coherency with respect to reduction ratios. This is clearly observed in Tables 6.5 and 6.14. It is also noticed that extruded product through wedge die, are stronger than that of square die. It may, therefore, be concluded that it is homogeneous deformation prevailing in the case of wedge die which is responsible for stronger product and not redundant work which prevails in square dies as proposed earlier [3,5].

Qualitatively, it is necessary that the pressure contours remain transverse in the large region of the die for extensive and homogeneous movement of material and this is possible only in wedge dies. In this context, therefore,

wedge dies are better for extrusion of powder preforms. These pressure contours also show that the pressure persists even after the point of second discontinuity (Figs.6.23(c)to 6.27(c)) suggesting the presence of internal compressive stresses in the extruded products.

6.3.8 Average Effective Strain Rate Contours

Figures 6.23(d), 6.24(d), 6.25(d), 6.26(d) and 6.27(d) show the average effective strain rate contours for reduction ratios, 1.6:1, 3.5:1, 7.0:1, 30:1 and 80:1 respectively at 500°C. The effective strain rate contours have parallelism with pressure contours as both of them are transverse contours so the former can be interpreted in the same way as pressure contours as far as the soundness and coherency of the product are concerned. It was seen experimentally, that in case of lowest R, 1.6:1, coherent mass was obtained at 400 and 500°C, while in case of square dies coherent mass was not obtained at 400°C for the same reduction ratio. This has been explained in section 6.2 on the basis of the shape of contours. As the reduction ratio increases, like the pressure contours, the effective strain rate contours get confined to a narrow region towards the point of second discontinuity and these contours extend upto the die axis from the container surface as shown in Figs. 6.26(d) and 6.27(d) for reduction ratios 30:1 and 80:1 at 500°C.

In comparison to square dies for the same R, the rate of deformation is high in wedge die and the rate of

increase of deformation is also very high as the R increases. The maximum effective strain rate contours is of unit 1.5 for R, 1.6:1 at 500°C and it increases to the unit 260 corresponding to R, 80:1. In case of square dies the rate of increase of deformation is not so high as the maximum effective strain rate contour for R, 80:1 is only unit 90 at the same temperature. Hence, there are better chances of coherency in wedge shaped dies which was confirmed experimentally also. The maximum effective strain rate contours exist near the second point of discontinuity in a very narrow region. It was also noticed that the deformation, after point of second discontinuity, persists for longer length of extruded product than in square dies suggesting the presence of internal compressive stresses in the product.

6.4 METALLOGRAPHIC INVESTIGATIONS

6.4.1 Microstructural Studies : Square Edge Dies

These were undertaken to investigate the microstructural changes that occur in the material during its entry into the die and its subsequent emergence as an extruded product. This way a correlation was sought to be established between the microstructural changes and the pressure contours, effective strain rate contours and flow of material during the extrusion process as influenced by temperature and reduction ratios.

Microstructural investigations have been carried out at four different locations as indicated in block diagram

(Fig. 6.33) for different reduction ratios, 1.3:1, 3.2:1, 10:1, 40:1, 80:1 at 500°C (Figs. 6.34 to 6.38). The corresponding features in terms of pressure, effective strain rate distribution and velocity vectors have also been indicated.

On the basis of these features certain rationalizations could be made regarding the fundamental parameter(s) whose effect on the microstructure needs consideration. These are as follows :

(i) Location 1 - Pressure and Effective Strain Rate Contours
(ii) Location 2 - Pressure and Effective Strain Rate Contours
(iii) Location 3 - Effective Strain Rate Contours
(iv) Location 4 - Velocity Vectors.

Establishment of a correlation of the type envisaged would help in a quantitative appreciation and understanding of the extrusion process.

6.4.1.1 Effect of Reduction Ratios

(a) Location - 1

At a low reduction ratio (1.3:1) and extrusion temperature, 500°C, microstructure reveals the presence of coarse sub-structure within a particulate mass (Fig.6.34(a)). The existence of particle identity in fractured surface of tensile specimen made from the extruded product (Fig.6.34(f)) indicate that 'coherent mass' may have just about formed. Thus, for all practical purposes the majority of the overall deformation imparted has been localized to a particle proper. Existence of a high temperature has, therefore, led

to the formation of a coarse sub-structure. A similar sub-structure was formed all along the billet edge adjacement to container wall. This observation is consistent with the pressure contours indicating the hydrostatic zone to be parallel to the die axis and the effective strain rates are low (Figs. 6.4(e, and f)).

With an increase in R to a value 3.2:1, a well defined grain structure has appeared (Fig. 6.35(a)) whose average size is smaller than the particulate size observed at 1.3:1 (Fig. 6.34(a)). An increase in R has resulted in particle deformation and in bringing about cohesion. A fair proportion of the sub-structure is aligned in the direction of deformation (Fig. 6.35(a)). Thus, at this reduction ratio, the deformation imparted in combination with the temperature has primarily contributed to the formation of a coherent product which was not the case at R value 1.3:1.

As the R value is further raised to 10:1 the overall effect is that equiaxed grain structure is well defined, grain growth occurs and also that sub-structure tends to be coarse and not aligned in any direction. Further, practically no porosity is visible (Figs. 6.36(a) and (b)).

At R value of 40:1, partial directionality is observed within the sub-structure (Fig. 6.37(a)). However, at a reduction ratio of 80:1, the sub-structure is coarse and directionality if any is at a minimum. Existence of grain is clearly manifested (Figs. 6.38(a) and (b)).

Taking an overall view, at low reduction ratio the net effect is that with initial transmission of pressure the

particulate mass undergoes thermally activated softening. This state of the material is conducive to the formation of fully coherent mass showing directionality at higher reduction ratios i.e. at 3.2:1 and 10:1. At reduction ratios higher than this, no directionality is observed but only sub-structure formation is accomplished which is coarsest at an R value of 80:1. Thus, it may be inferred that at this reduction ratio both the deformation and temperature are effectively combining to produce grain coarsening and sub-structure coarsening. This analysis reflects the importance of high pressures developed in the corner of the container near the ram and the low effective strain rates in contributing to the state of microstructure described earlier and is in conformity with the pressure variation as shown by the pressure contours corresponding to these reduction ratios (Figs.6.4(e), 6.8(c), 6.13(c), 6.14(c) and 6.15(c)).

(b) Location - 2

Considering the structural changes at location-2 i.e. just outside the DMZ boundary, there is very little difference between the microstructure at the earlier location-1 and just outside the DMZ at the lowest reduction ratio. This is because the hydrostatic zone is parallel to the die axis, an observation in conformity with the pressure contours (Fig. 6.4(e)). At R value 3.2:1 directionality is observed (Fig. 6.35(b)). On raising the R value to 10:1, heavy uneven fibering is observed (Fig. 6.36(c)) which evens out at R values 40:1 and 80:1 (Figs. 6.37(b) and 6.38(c)). Distinct

sub-structure formation with directionality is visible from R value 10:1 onwards (Fig. 6.37(b)). In this region the pressure is not maximum, as in the case at the location-1. This is so because it is being transmitted from the ram into the interior and as such its magnitude would gradually reduce as the extrusion location is approached. Transmittance of pressure would cause the material to flow. In the region just outside DMZ, both these factors namely pressure transmission leading to its gradual reduction and the consequent material flow are contributing to the structural changes.

(c) Location - 3

At a region just where the extrusion proper is going to occur i.e. near the exit plane, the value of the pressure drops to the level of yield stress as a consequence to a gradual tapering off in pressure transmission. This would result in the creation of material flow leading to a condition of high effective strain rates as shown by the Figs. 6.9(f), 6.9(d), 6.13(d), 6.14(d), 6.15(d)). At low R value 3.2:1, the microstructure is showing grain coarsening and coarse sub-structure (Fig. 6.35(c)). Pressure being small, and the effective strain rate being 'low' (not enough to counteract the effect) the temperature effect predominates resulting in the formation of coarse grains and sub-structure. For all practical purposes, the existence of the sub-structure was just about perceptible. Directionality is observed. Same is the case at the next higher R value (10:1), although

directionality is now more pronounced (Fig. 6.36(d)). Thus, the effect of increasing the effective strain rate is being clearly manifested. At R value of 40:1, besides directionality formation of sub-structure is clearly seen (Fig. 6.37(c)). Remembering the temperature to be 500°C, the high density of sub-structure clearly demonstrates that the effective strain rate component is the predominant factor in controlling the microstructure. The existence of high values of effective strain rate (30 units as shown in Fig. 6.14(d)) are in conformity with this reasoning.

It is worth mentioning here that the microstructures immediately after the point at which extrusion has occurred and the one at which it has just begun, are similar. This is an interesting observation.

(d) Location - 4

Finally, microstructural investigations were also carried out within the extruded product, close to the die axis and near the periphery of the specimen. This was done to ascertain the changes between the microstructure just at the point of extrusion and that within the extruded product. At an R value of 1.3:1 the microstructure along the die axis was equiaxed in nature (Figs. 6.34(d) and (e)), although near the periphery it showed slight directionality and the presence of sub-structure (Figs. 6.34(b) and (c). The tensile properties and the low elongation value (Table 6.5(a)) were consistent with fracture appearance as shown in Fig. 6.34(f). At this R value, although the product is macroscopically coherent,

but it is not so at the microscopic level. The tensile properties are thus consistent with the microstructure. As the R value is increased, the important change in the microstructure is that the extent of directionality is getting more pronounced and the fibering is becoming heavier (Figs. 6.36(e) and 6.37(d)). This led to an improvement in the tensile properties as indicated by fracture surface appearance as shown in Figs. 6.35(h) and 6.36(i). Thus the overall improvement in properties upto the R value of 30:1 is explained. However, with an increase in reduction ratio, the steady state pressure value is continuously increasing in comparison to the value at R, 1.3:1, as the reference base. Thus, for each R, although a steady state pressure is being attained, the increase in its value with reduction ratio vis-a-vis the conditions at R value 1.3:1, as the reference base, should be regarded as an indicative of a continuous increase in the extent of 'work hardening'. Therefore, with an increase in R value there should be an enhancement of tensile properties upto a limiting R value and thereafter become almost constant. The tensile properties data (Table 6.5) are in accordance with above reasoning.

Microstructural observations were also made on transverse sections. Typical micrographs thus obtained for reduction ratios 3.2:1 to 80:1 at 500°C are shown in Figs. 6.35(f and g), 6.36(f, g and h), 6.37(e) and 6.38(e). At an 'R value of 3.2:1 a very small amount of porosity is seen and the overall structure is by and large equiaxed (Figs. 6.35(f and g)). At R value 10:1, there is a definite trend towards fibering

(Figs. 6.36(f)), which eventually leads to the attainment of fragmented grain structure (Figs. 6.37(e) and 6.38(e)) at R value 40:1 and 80:1, an indication that a large deformation has been imparted.

6.4.1.2 Effect of Temperature

The effect of temperature on microstructure and hence, the tensile properties were examined to a limited extent at R value 10:1. It was observed that at 500°C, the presence of sub-structure is seen to a limited extent.

At 300°C the sub-structure in the form of pits is visible only in certain regions (Figs. 6.39(a to h)). A nearly similar structure exists in the transverse section microstructure (Fig. 6.39(i)). Corresponding to 400°C, there is an increase in the sub-structure formation (Figs.6.40(a to d)). The extruded section shows presence of nonhomogeneous microstructure(Figs.6.40(e and f)). The transverse microstructure at 400°C, shows that the structure is somewhat coarse along the periphery(Fig.6.40(g)),compared with that at the centre (Fig.6.40(h)). However, this trend is completely reversed at 500°C(Figs.6.36(g and h)),where there appears to be extensive grain growth as a result of which grain size near the die axis(Fig.6.36(g)) is very large compared to the grain size near the periphery(Fig. 6.36(h)). Such a structural change is due to initiation of grain growth within the material mass which is effectively counteracted at the die walls leading to a relatively fine grain size at the periphery. Basing the recrystallization on the usual concept of

0.5 Tm and considering that the starting material is green and has attained ~ 85% of the theoretical density, an extrusion temperature ~ 300°C at best signifies a stage where recrystallisation has just begun (Fig.6.39(i)). Thus, the dense sub-structure is not annealed, thereby requiring a larger extrusion pressure. On raising the temperature to 400°C, the thermally activated softening processes are occuring very rapidly leading to grain coarsening and sub-structure coarsening. This softer state of the material would require relatively low pressure for affecting extrusion pressure as compared to that required at 300°C. This reversal mode of deformation has also been noticed while plotting extrusion pressure Vs. log T (Fig. 6.3) and thus this phenomenon is evidently clear by microstructure investigation. On raising the temperature to 500°C, although the grain size and the sub-structure has become very coarse, the changes are not significant enough in altering the state of the material in comparison to the state of affairs at 400°C.

6.4.2 Microstructure Studies: Wedge Shaped Dies

The discussion, so far, has been confined to the mode of deformation occurring in a square die. Besides it, extrusion studies have also been carried out in wedge dies primarily because it offers the possibility of elimination of DMZ as envisaged by the different theories propounded till now. Further, in view of the shape of the die (semi-cone angle of 45°) a more homogeneous deformation pattern would emerge during the extrusion process as has already been shown with the help

of the analytical studies. The following discussion shall be devoted to establish a correlation between the microstructural changes and the (i) velocity vectors, (ii) pressure and (iii) effective strain rate contours as influenced by temperature and reduction ratios during the extrusion through wedge shaped dies. An attempt shall also be made to ascertain, whether the basic differences between the behaviour of material, while being extruded through a square and a wedge shaped dies, as revealed by analytical studies could be correlated with the microstructural observations. Microstructural studies have been carried out at reduction ratios, 1.6:1, 7:1, 15:1 and 80:1 at 500°C. To examine the effects of extrusion temperatures on microstructural, studies were also carried out at different temperatures, 300, 400 and 500°C for reduction ratio, 7.0:1. These were carried out at four locations mentioned in the Fig. 6.33.

The main difference between the extrusion process through a wedge and square shaped die, is that in the former material movement is more marked along the conical surface in comparison to the die axis. As a consequence of this, a uniform material movement occurs from the adjoining areas into the regions corresponding to the conical surface. As a result of this difference, the nature of the microstructure at different locations while extruding through a wedge shaped die, would be different from what has been observed during extrusion through a square edge die.

6.4.2.1 Effect of Reduction Ratios

(a) Location - 1

The microstructure at location-1, resembled the corresponding microstructure in the square dies except that the extent of deformation appears to be more and consequently the sub-structure formation is more pronounced (Figs. 6.41 to 6.46). With an increase in the reduction ratio from 1.6:1 to 80:1, this features is retained as such (Figs. 6.41(a) to 6.44(a)). Additionally, it is observed that the overall grain size is smaller, the product more coherent and the sub-structure much finer than what is obsserved in the case of square dies (Figs. 6.34(a) to 6.38(a)). These features are observed all along the rear end of the billet. This observation is consistent with the pressure and effective strain rate contours which are uniformly distributed in the billet, originating from the container surface and terminating at the die axis. Reasoning in support of this contention has already been given in the foregoing para.

(b) Location - 2

Representative microstructures at this location are shown in Figs. 6.41(a and b), 6.42(a and b), 6.43(a) and 6.44(a). This location is characterized by the start of the conical portion. At reduction ratio of 1.6:1, the microstructure revealed a non-homogeneous wavy pattern, indicative of the existence of high pressure zones. This is consistant with the observation, that hydrostatic zone is present near the

location 2 (Fig. 6.23(c)). As reduction ratio is increased to 7:1, although the non-homogeneity in the deformation pattern is absent, directionality has been introduced (Figs. 6.42(c and d)). This is consistent with the observation that at this reduction ratio, there is no hydrostatic high pressure zone (Fig. 6.25(c)). A further increase in the reduction ratio to 15:1 and 80:1 respectively, did not appreciably alter the microstructure, except that the presence of coarse sub-structure could be seen. The sub-structure was aligned in the direction of deformation (Figs. 6.43(b) and 6.44(b)). This is in conformity with the observation that no hydrostatic zone is present at reduction ratios higher than 3.5:1. The magnitude of effective strain rate is low (0.1 - 0.2 unit) thereby clearly signifying that the temperature effect is predominant leading to the formation of coarse sub-structure.

On traversing from location 2 to location 3, occurrence of directionality can be easily detected (Figs.6.41 to 6.46) There is an increase in the density of sub-structure and a reduction in grain size on raising the reduction ratio from 1.6 to 15:1 (Figs. 6.41(b), 6.42(e), 6.43(c)). On raising the reduction ratio to 80:1, the grain size and sub-structure size were coarser than that observed at 15:1 (Fig. 6.44(c)). These observations are consistent with the effective strain rate value and can be explained as before.

(c) Location - 3

At location 3, i.e., towards the end of the conical surface where the material is just on the verge of being

extruded, the reduction ratio had a pronounced effect on the microstructure (Figs. 6.41(c), 6.42(f), 6.43(d) and 6.44(d and e)). It may be noted that effective strain rate is maximum at this location and increases markedly with reduction ratio. At R value of 1.6:1, there is no change in the structure with respect to location 2. However, from R, 7:1 and above, pronounced directionality is observed giving way to heavy fibring at reduction ratio of 15:1 and 80:1. At the reduction ratio, 80:1, fragmentation is also observed (Figs. 6.44(d and e)) indicative of very large deformation that is being imparted. This is possible due to merging of sub-grain boundary along the direction of flow leading to their poor identification. This is expected in view of the fact that the magnitude of the effective strain rate increases from 10 units at reduction ratio, 7:1, to 260 units at reduction ratio of 80:1. This has not been observed in the case of extrusion through square die where for the same temperature and reduction ratio, the maximum value of strain rate encountered is ~ 90 units.

(d) Location - 4

At location 4, i.e. in the extruded product, the general trend of the microstructures observed is similar to that observed at (i) Location-3 and (ii) in the extruded sections in square dies. Certain pertinent observations regarding extrusion through wedge dies need to be recorded here. Firstly, because of a better overall homogeneous deformation the extrusion pressure values are consistently lower than the corresponding values observed in square dies

extrusion. For similar reasons and also because of appreciably larger strain rates, the strength of the extruded product in the present instance is at least 10 - 20 % higher than what is observed in the case of square dies. Except at low reduction ratio, 1.6:1, the elongation values for extrusion through wedge and square dies are comparable. The consistency of experimentally measured tensile strength has been found to be better in the case of wedge die as compared to square die. This is again, due to the fact that deformation in wedge die is more homogeneous than through square die.

Microstructural obsservations on the transverse section (Figs. 6.41(f), 6.42(i), 6.43(g) and h)) can be explained as before for square dies.

6.4.2.2 Effect of Extrusion Temperature

The microstructure for reduction ratio 7.0:1 at 300, 400 and 500°C are shown in Figs. 6.42, 6.45 and 6.46. Comparing the temperature effect on extrusion through wedge die keeping constant reduction ratio, 7:1, it was noticed that the size of sub-structure increased with increasing temperature. It was also noticed that the structure of extruded product along the periphery and die axis showed reversal while increasing the temperature from 400 to 500°C, a phenomenon similar to that observed in case of square die. However, corresponding to lowest reduction ratio, 1.6:1, this reversal is not noticed (Figs. 6.41(f) and g)) and correspondingly it was noticed that the straight line nature

of the plots does not change the slope in p Vs. log T curve.

6.4.3 Macrostructural Studies

In order to identify the shape of DMZ in square dies microexamination of partially extruded billet was also performed.

The shape of DMZ boundary for reduction ratios, 2.1:1, 10:1 and 20:1 at 300°C are shown inFigs. 6.47, 4.48(a and b)and 6.49(a and b). It was noticed that at these reduction ratios and temperature the DMZ boundary is clearly identifiable due to incoherent flow of metal along the boundary. The grains are highly deformed along both sides of boundary as shown in Fig. 6.50 for reduction ratio, 10:1 at 300°C. However, at higher reduction ratios (R> 20:1), the boundary no more remains incoherent. Whether or not this boundary is identifiable by way of incoherency, the grains are observed to be heavily deformed, elongated and thereby giving rise to fibrous orientation along the boundary. Grains appear to change their direction of flow as they approach the boundary, thus in all the cases, the boundary should be identifiable through microstructural investigations. The boundary, as predicted by average pressure contours, appears to be well in conformity with the macrostructural observations. Shape of DMZ changes with reduction ratio. As the reduction ratio increases, the DMZ boundary shifts towards the corner of the die (Figs. 6.47 to 6.49) while at low reduction ratios, the DMZ boundary becomes parallel to the die axis. However, this observation differs very widely in comparison to 45°

orientation of the boundary, as predicted by slip line field theory.

6.5 DEFECTS IN EXTRUDED PRODUCTS

It was observed during powder extrusion at lower reduction ratios and temperature, mainly 300°C, coherent product was not obtained both in square and wedge shaped dies. However, on raising extrusion temperature the coherent mass was obtained both in square and wedge shaped dies at these reduction ratios. In the present section the reason for the lack of coherency in extruded product whenever obtained has been discussed on the basis of average pressure and average effective strain rate contours obtained by FEM. A model has been proposed for the criterion of coherency of the product which had been discussed in section 6.2.

6.5.1 Square Edge Die

Figures 6.5(a and b)and 6.52(a and b) show the surface and longitudinal section of the product extruded through reduction ratios 1.3:1 and 1.6:1 at 300 and 400°C respectively. In these products, coherency was lacking. At 300°C corresponding to R, 1.3:1 the product fractured longitudinally as well as laterally (Fig. 6.51(a)) where as at 400°C for the same reduction ratio only lateral cracks were observed both on the surface in longitudinal section of the product (Fig. 6.51(b). These cracks are pretty long in width but most of these do not extend upto the periphery of

the extruded product. For reduction ratio 1.6:1 at 300°C the lateral cracks (Fig. 6.52(a)) are still present, most of these extend upto the periphery of the product. However, at 400°C for this reduction ratio the width of these cracks reduces considerably (Fig. 6.52(b)). The product, at 300° for reduction ratio 2.1:1 and at 500°C for the lowest reduction ratio 1.3:1, are fully coherent as shown in Figs. 6.53(a) and (b). Their sections also show complete coherency thus, the product appears to achieve a limiting condition of coherency above reduction ratio 1.6:1 which may be designated as lowest limit of coherency.

The cracks in the extruded product can be explained by velocity vectors, average pressure contours and average effective strain rate contours drawn by FEM. In most of the cases, lateral cracks were observed and the width of the cracks is maximum at the centre of the product. This was due to fact that at the centre the material has maximum flow while at the surface of the die the material flow is negligible. Average pressure and average effective strain rate contours for reduction ratios, 1.6:1 and 2.0:1, show that the homogeneous metal flow and deformation was confined to a very small region near the point of discontinuity and also the EPC line (corresponding to analytical extrusion pressure contour) is below the horizontal line, passing through the point of discontinuity. Due to smaller region of extensive movement of material, homogeneous deformation takes place only in limited space which results in cracks in the extruded product. The continuity requirement was also not satisfied

at 400°C for reduction ratios 1.3:1 and 1.6:1, which clearly predict that coherent mass should not be obtained which was confirmed experimentally. In the cases where coherent product was obtained experimentally e.g. at 500°C for R, 1.3:1 and at 300°C for R, 2.1:1 and above (Figs. 6.53(a and b)) the continuity requirement was satisfied and EPC line remains almost horizontal, suggesting a limiting reduction ratio where the product was fully coherent. The pressure contours and strain rate contours could not be drawn at 300°C due to lack of yield stress data.

6.5.2 Wedge Shaped Die

Figure 6.54(a) shows the incoherent product extruded through reduction ratio 1.6:1 and 2.0:1 at 300°C. In these reduction ratios only lateral cracks at the periphery of the product are visible which extend through cross-section. This has been termed as snakeskin [37]. At 400°C coherent mass was obtained at these reduction ratios as shown in Fig.6.54(b) but the cracks were visible at the starting portion only (Fig.6.55(a)). At 500°C fully coherent mass was obtained and the cracks even at starting portions are not visible as shown in Fig. 6.55(b).

Like square dies, in wedge dies, at low reduction ratios, the maximum flow of material occurs at centre of die which results into the formation of cracks in the extruded product. Although velocity, pressure and effective strain rate contours could not be plotted at 300°C due to lack of yield stress data, but it is expected that the trend would

be similar as observed at other temperatures. The average pressure and average effective strain rate contours for reduction ratios 1.6:1 and 2.0:1 at 500°C show that the EPC line is horizontal and extends upto the centre of the die, i.e. homogeneous deformation occures in a very wide region from die surface to the centre of the dies as explained earlier (Section 6.3). The same thing was seen by effective strain rate contours at 500°C corresponding to reduction ratio 1.6:1 and 2.0:1,i.e. extensive movement of material takes place from die surface to the centre of die which result in coherent mass at 400°C and 500°C for all the reduction ratios.

Therefore, the model proposed on the basis of FEM fully explains and predicts the coherency of the extruded product, for all reduction ratios and temperatures investigated, and is fully borneout by experimental observations.

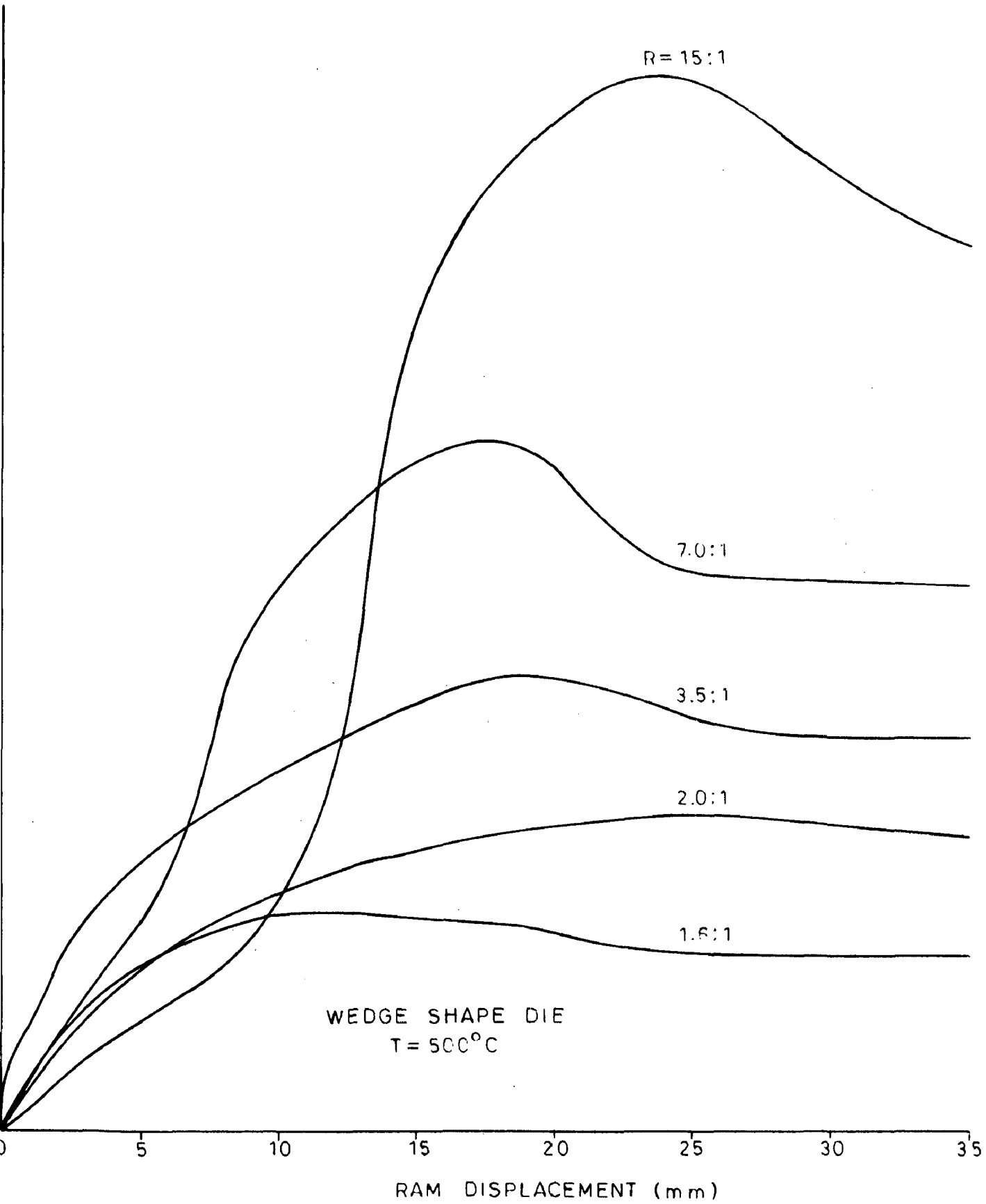

FIG.6.18(a)– LOAD RAM DISPLACEMENT DIAGRAMS

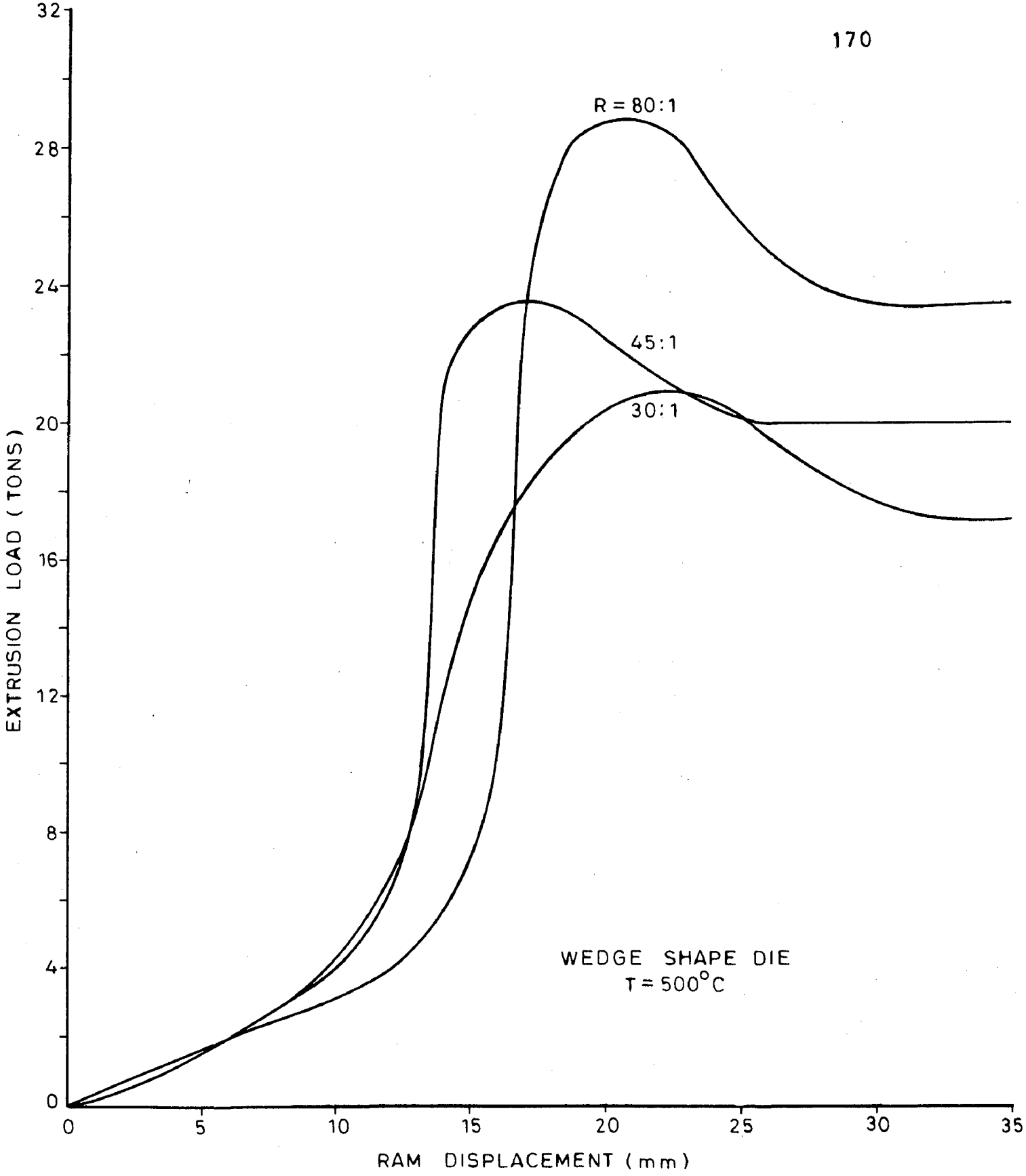

FIG.18 (b). LOAD – RAM DISPLACEMENT DIAGRAMS

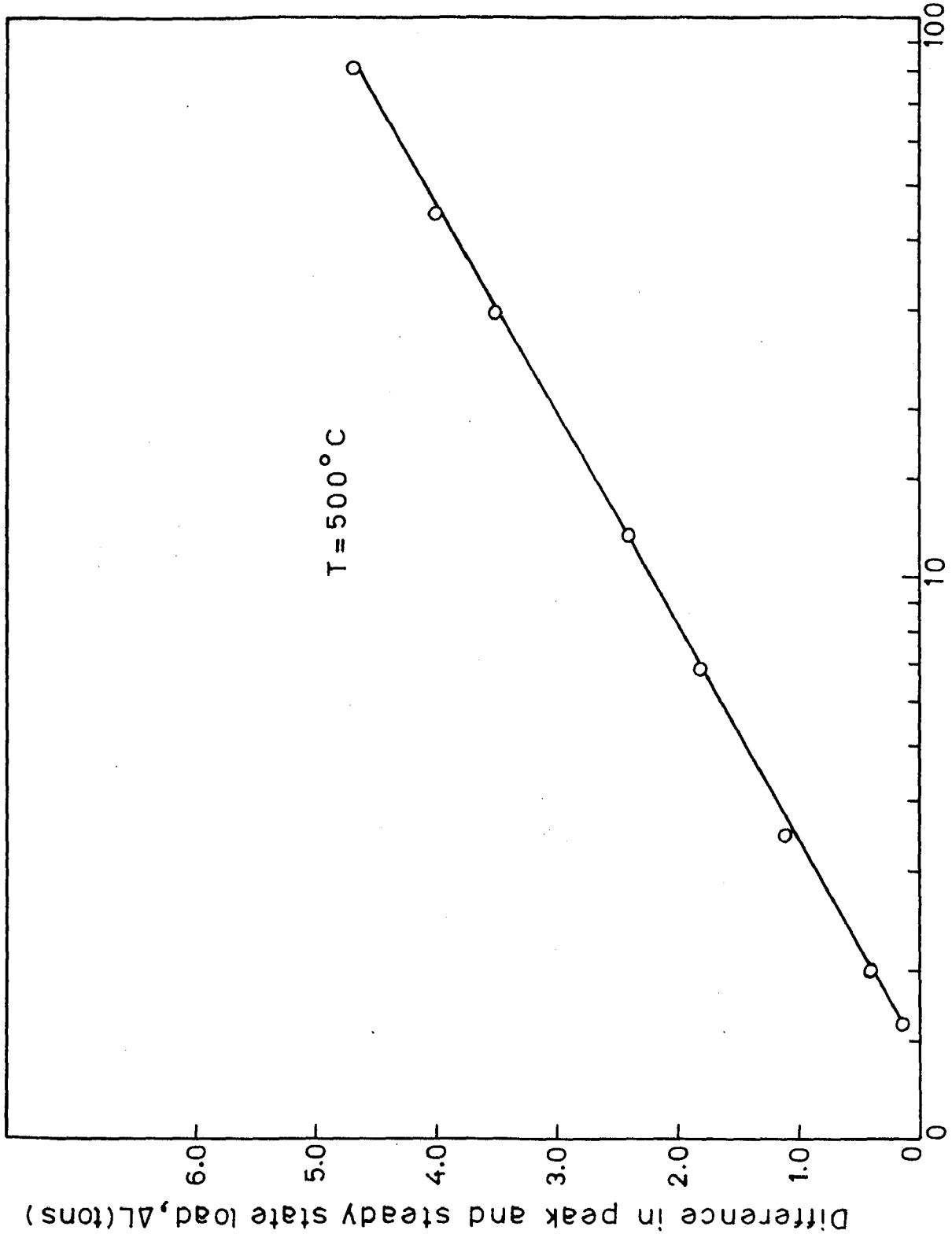

FIG. 6.19 EFFECT OF REDUCTION RATIO ON ΔL.

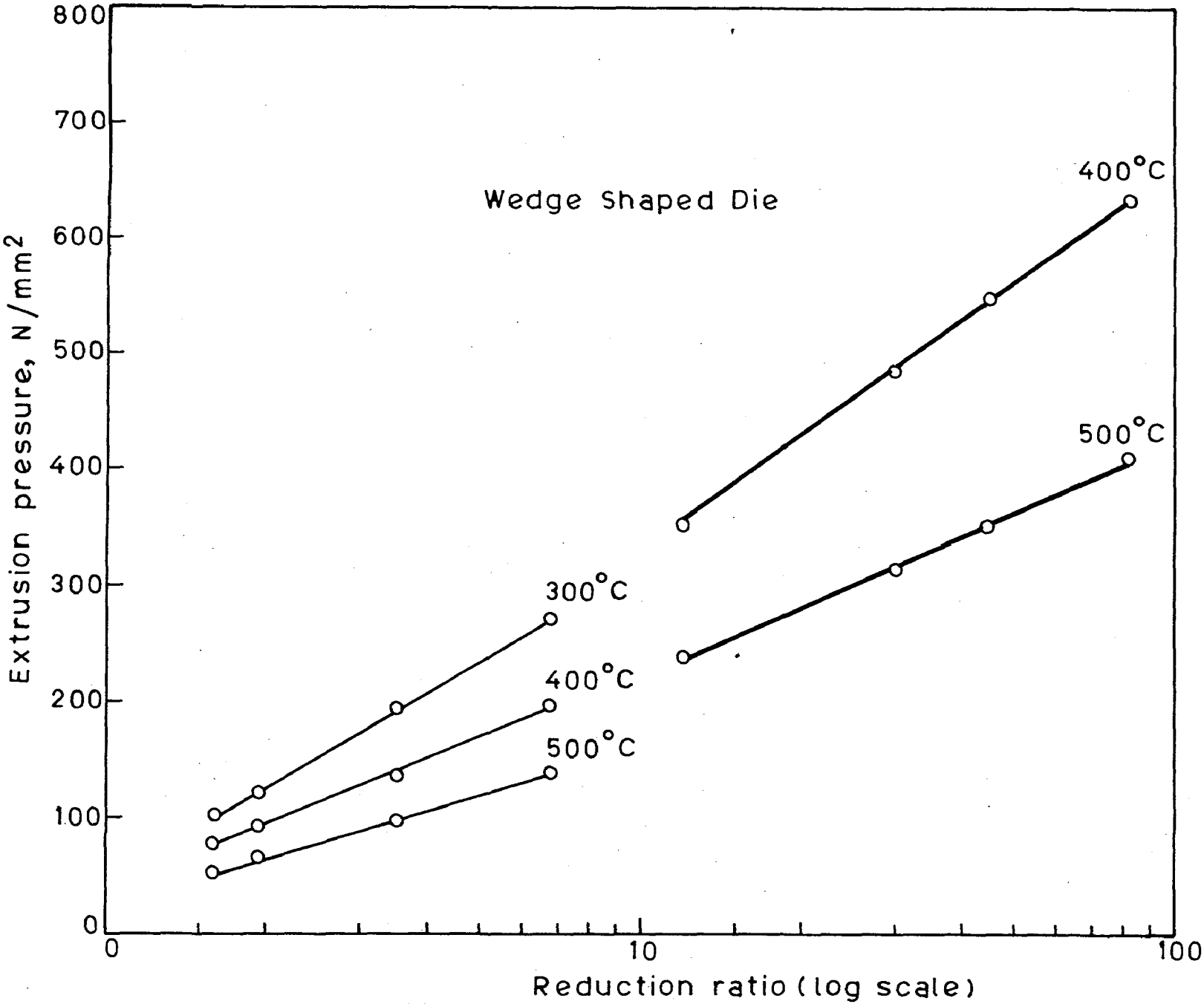

FIG.6.20 EFFECT OF REDUCTION RATIO ON EXTRUSION PRESSURE.

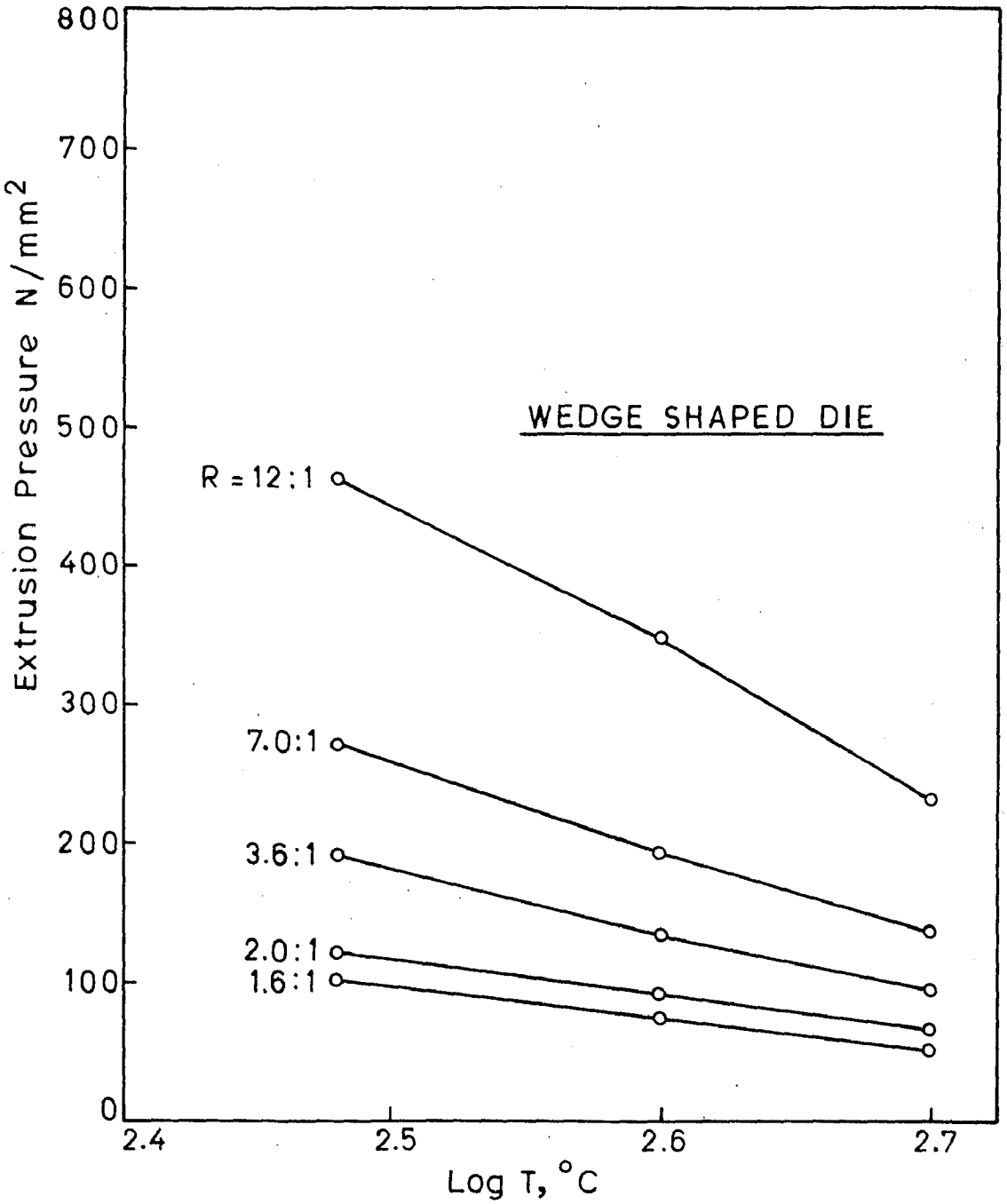

FIG.6.21 EFFECT OF TEMPERATURE ON EXTRUSION PRESSURE.

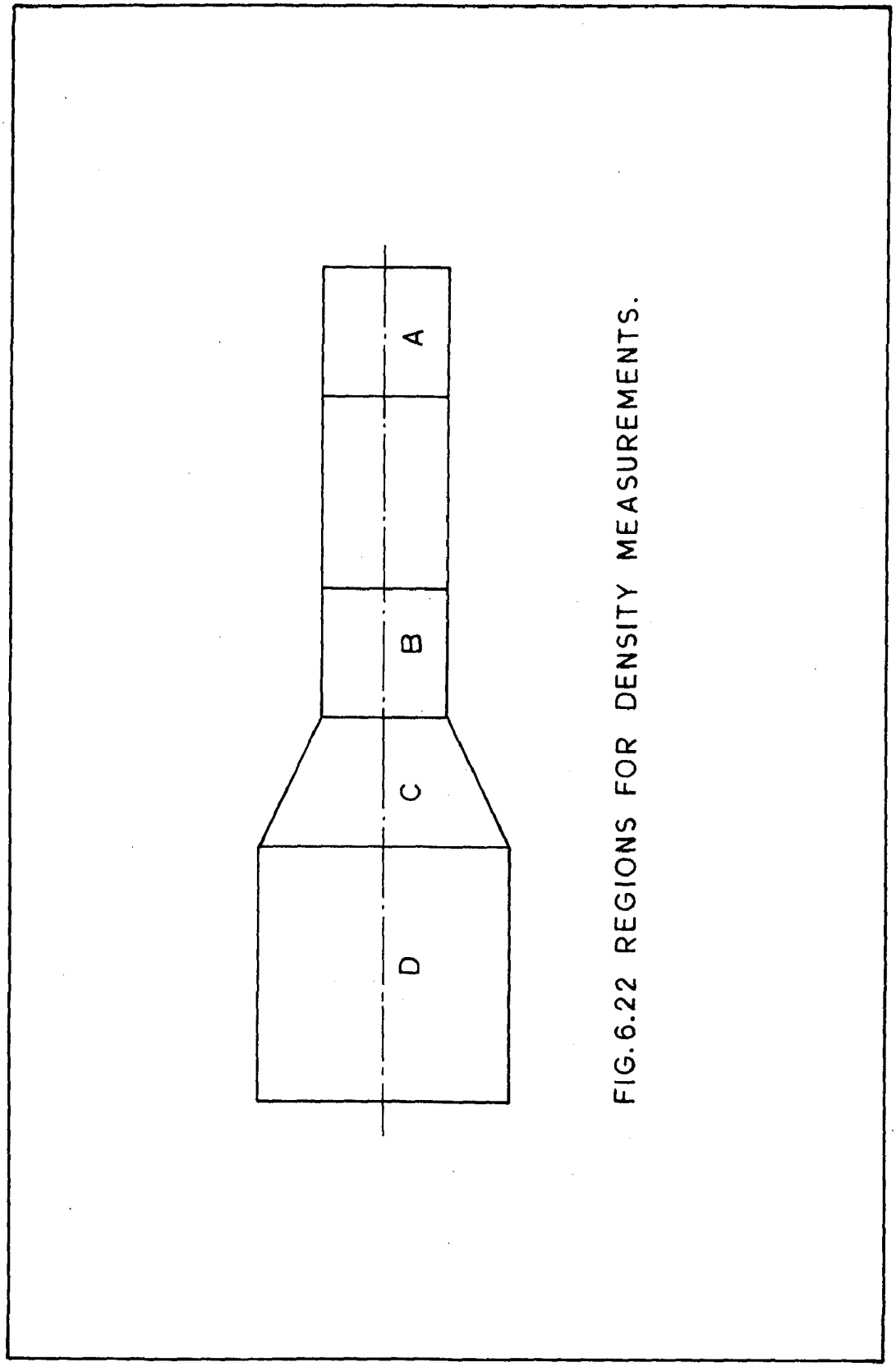

FIG. 6.22 REGIONS FOR DENSITY MEASUREMENTS.

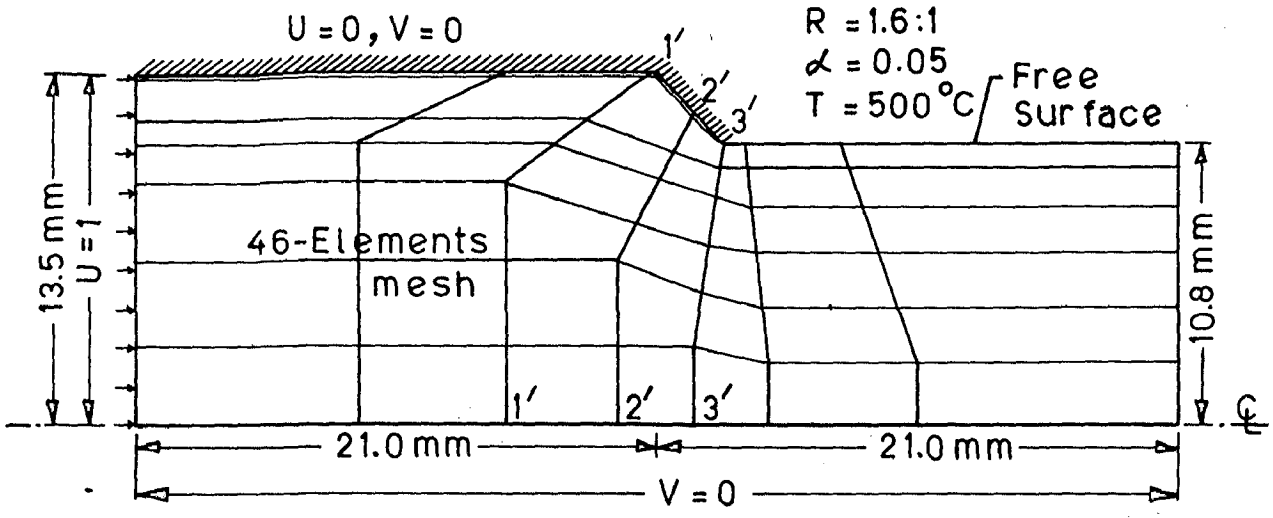

FIG. 6.23 (a) MESH AND BOUNDARY CONDITIONS.

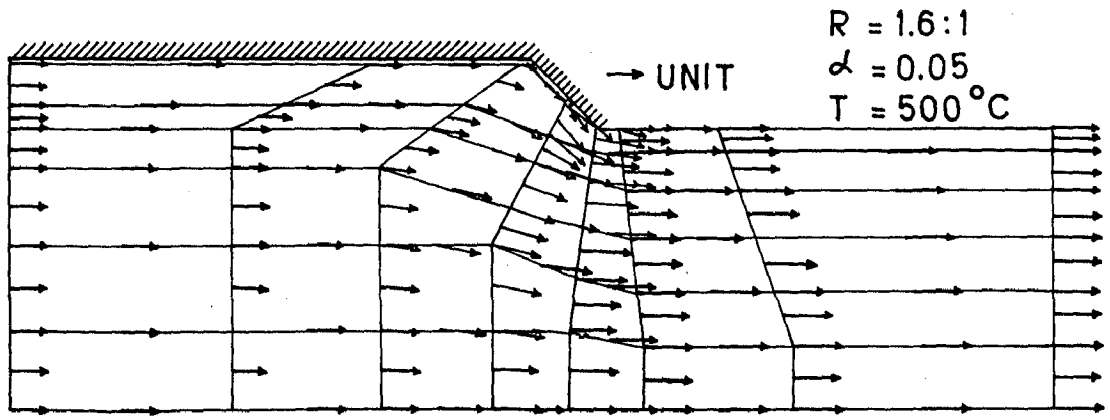

FIG. 6.23 (b) VELOCITY VECTORS. (46 elements mesh)

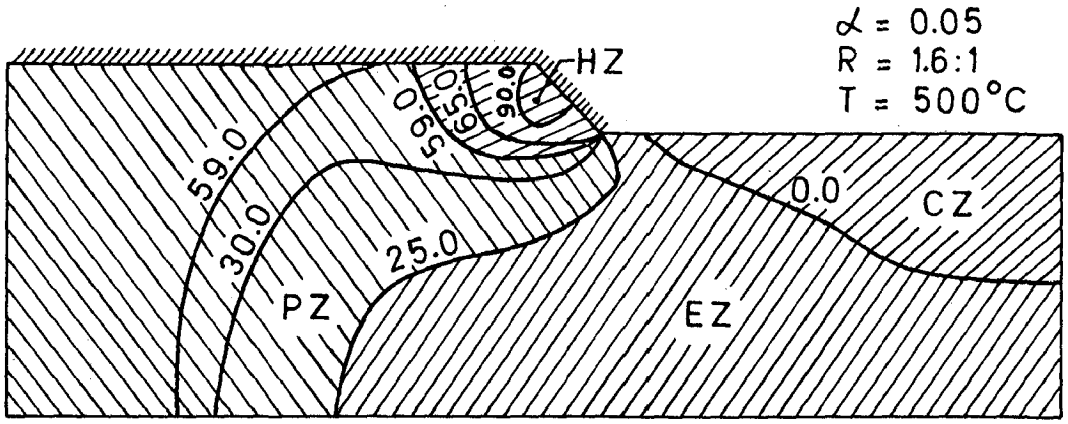

FIG.6.23 (c) AVERAGE PRESSURE CONTOURS (46 elements mesh)

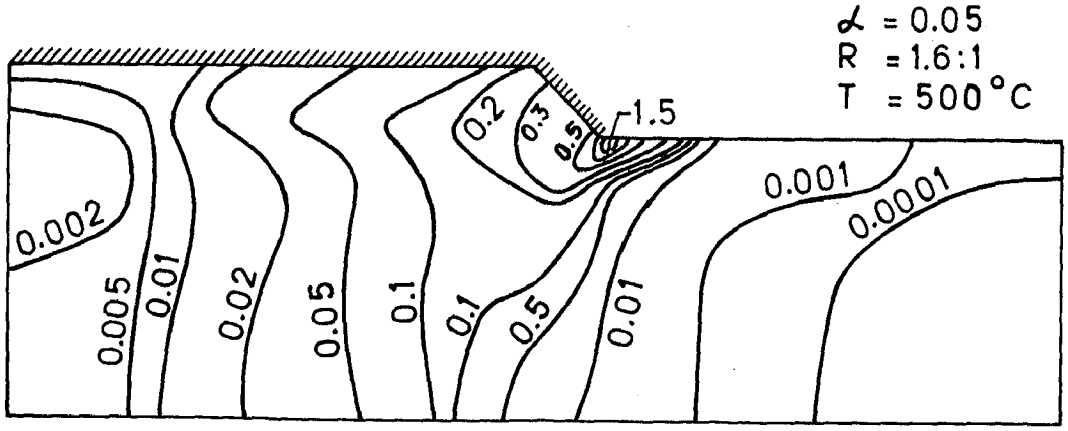

FIG.6.23 (d) EFFECTIVE STRAIN RATE CONTOURS.(46 elements mesh)

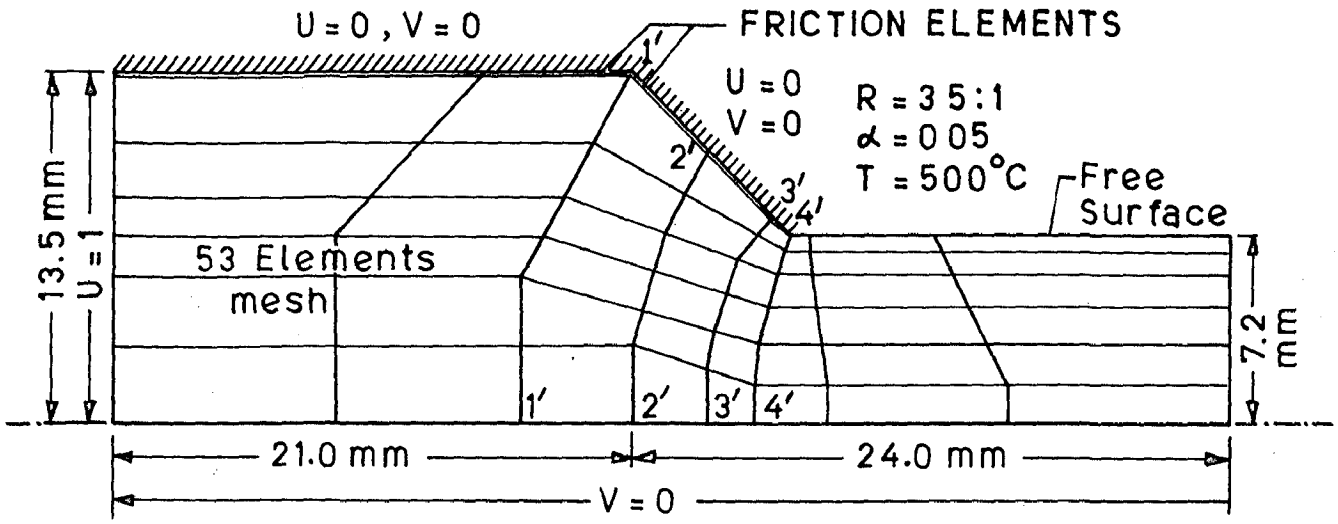

FIG. 6.24 (a) MESH AND BOUNDARY CONDITIONS.

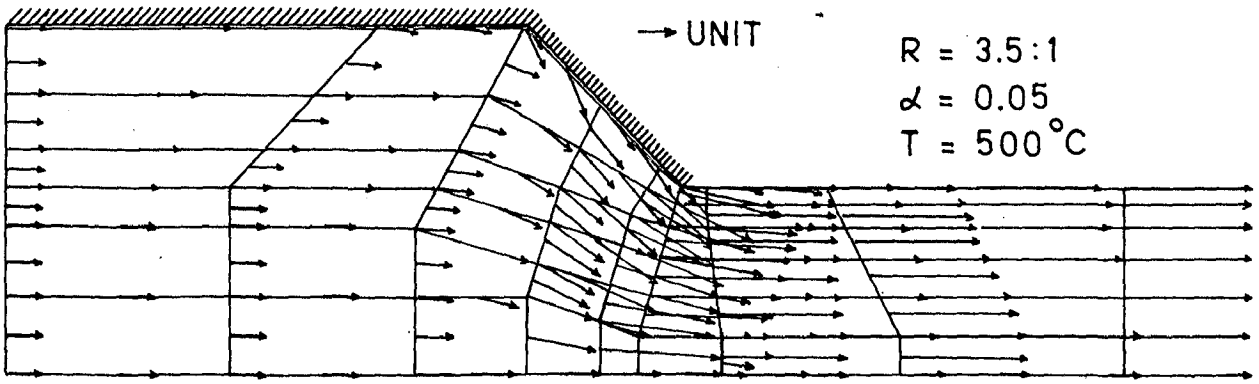

FIG. 6.24 (b) VELOCITY VECTORS. (53 elements mesh)

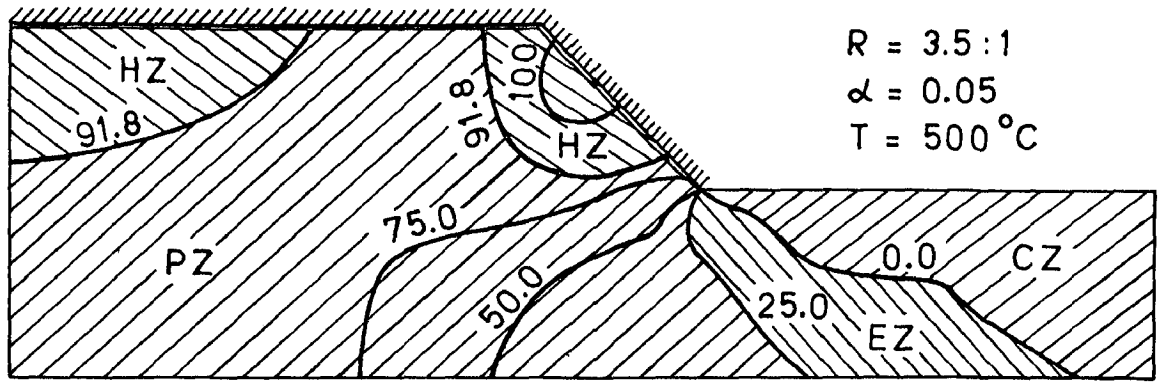

FIG. 6.24 (c) AVERAGE PRESSURE CONTOURS. (53 elements mesh)

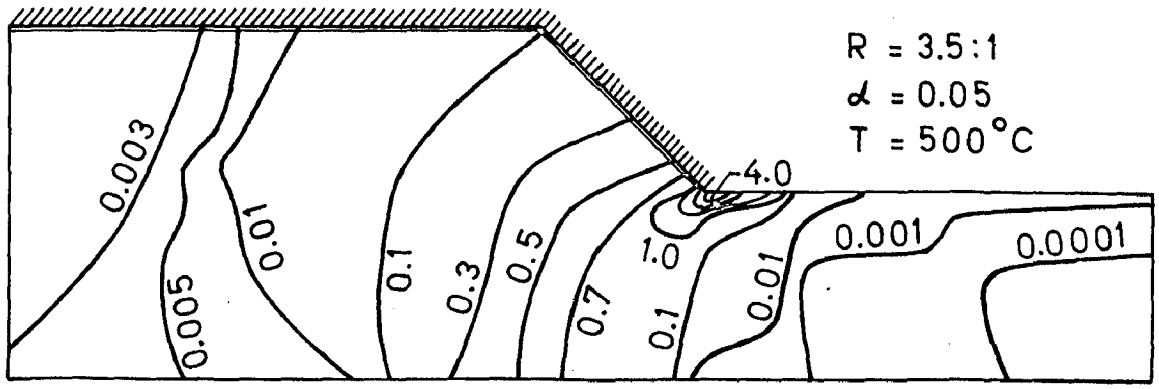

FIG. 6.24 (d) AVERAGE EFFECTIVE STRAIN RATE CONTOURS. (53 elements mesh)

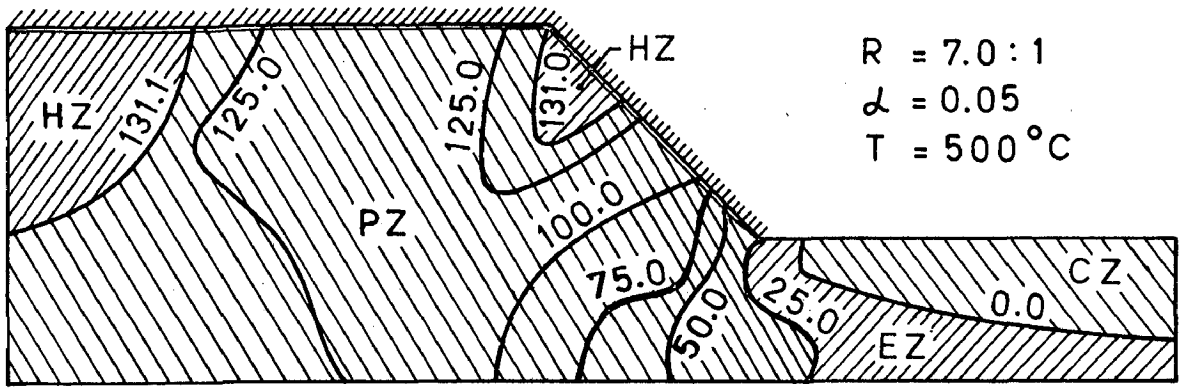

FIG.6.25 (c) AVERAGE PRESSURE CONTOURS (53 elements mesh)

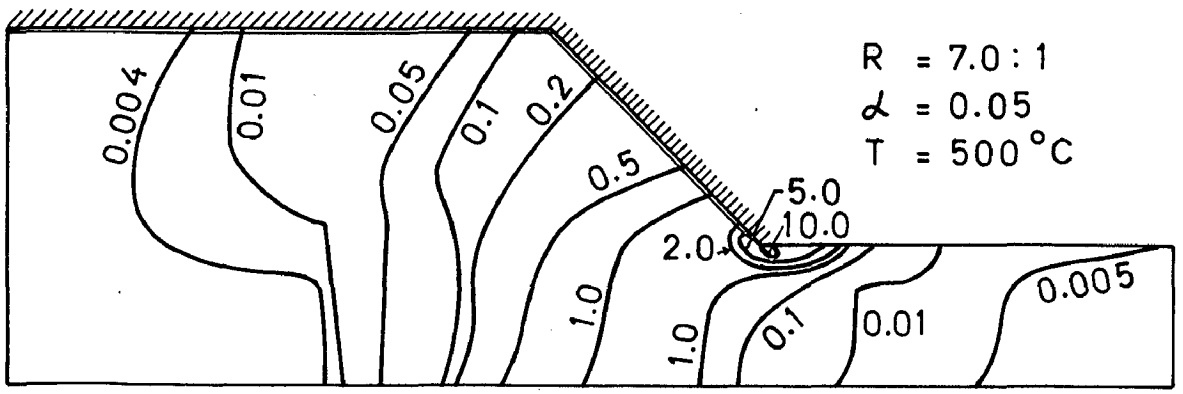

FIG.6.25 (d) AVERAGE EFFECTIVE STRAIN RATE CONTOURS. (53 elements mesh)

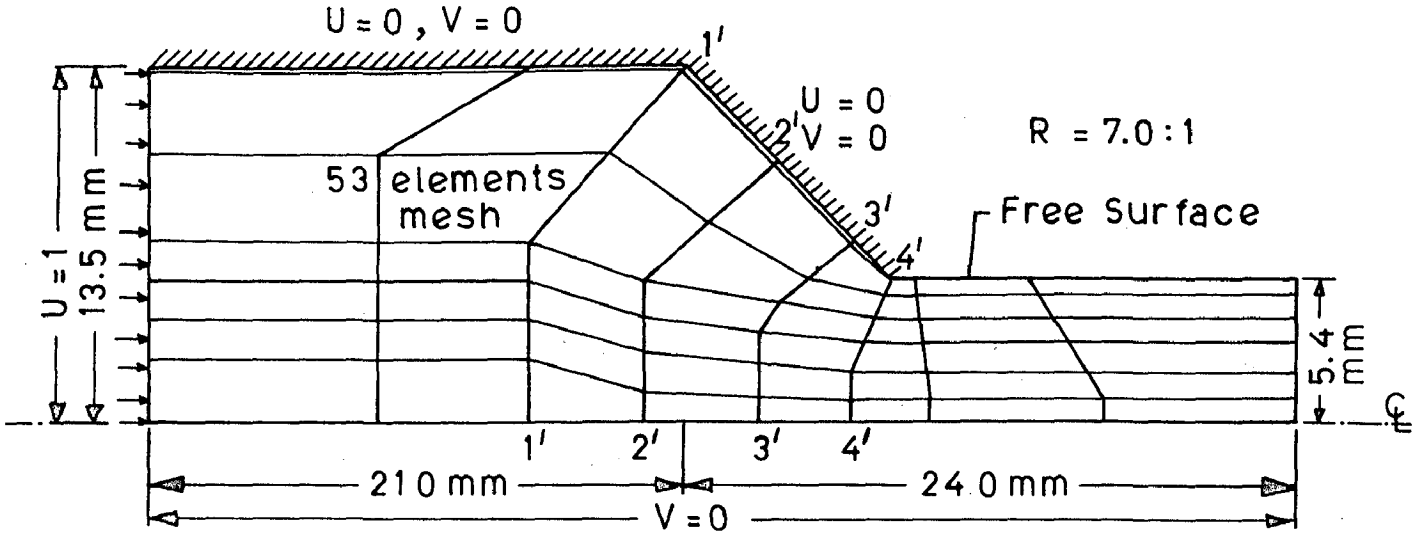

FIG.6.25(a) MESH AND BOUNDARY CONDITIONS.

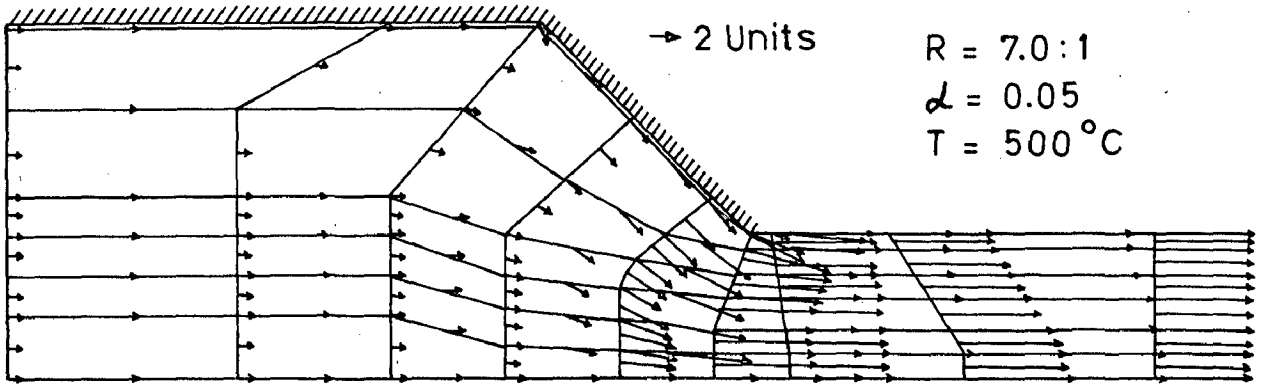

FIG.6.25(b) VELOCITY VECTORS (53 elements mesh)

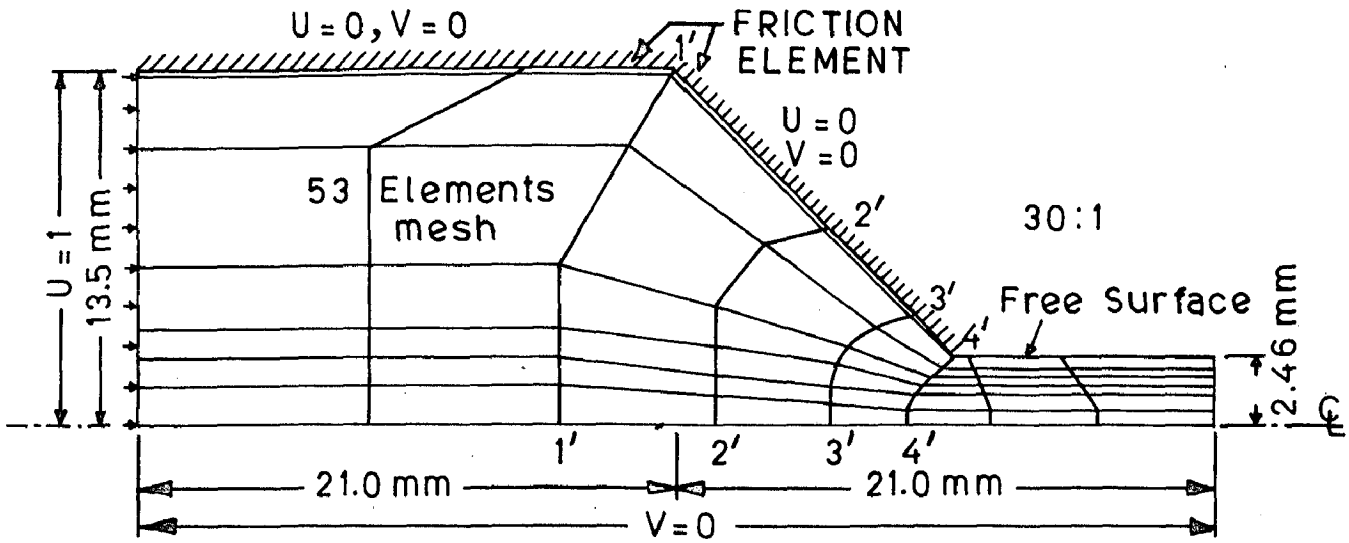

FIG.6.26(a) MESH AND BOUNDARY CONDITIONS.

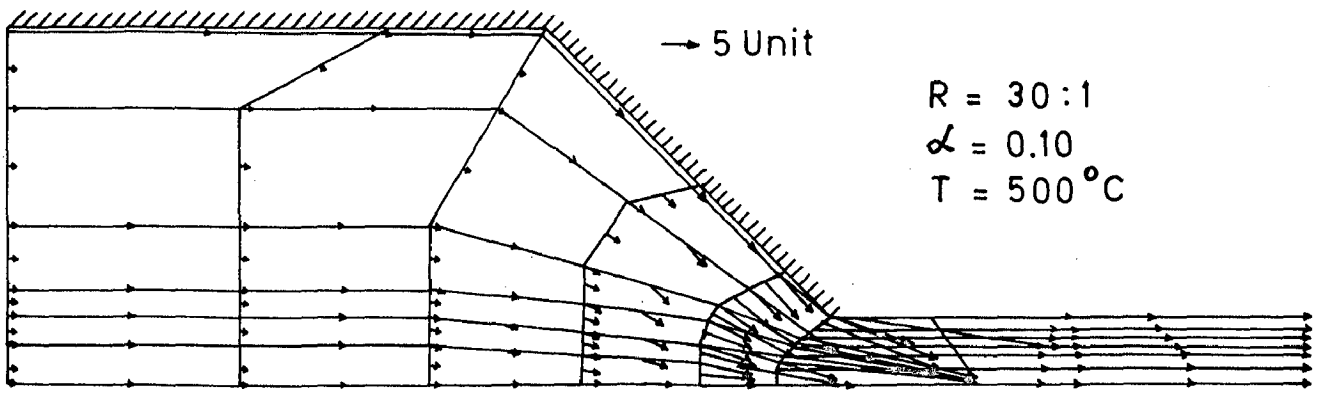

FIG.6.26(b) VELOCITY VECTORS.(53 elements mesh)

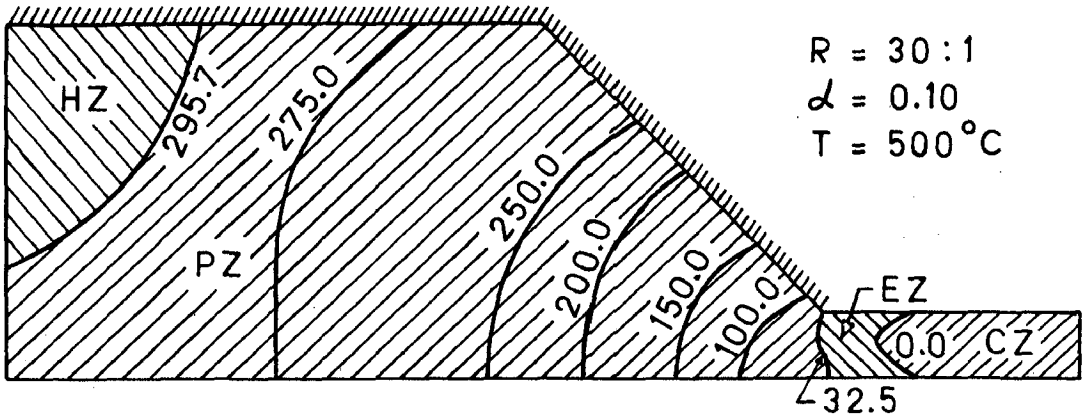

FIG.6.26 (c) AVERAGE PRESSURE CONTOURS.(53 elements mesh)

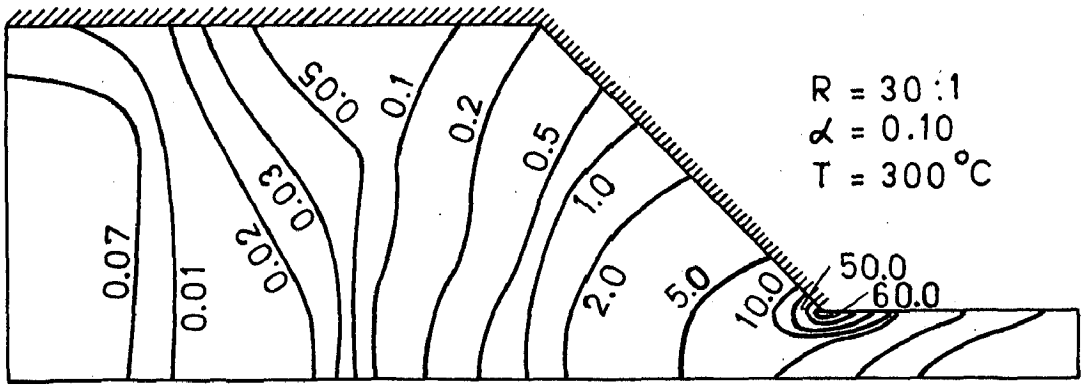

FIG.6.26 (d) AVERAGE EFFECTIVE STRAIN RATE CONTOURS. (53 elements mesh)

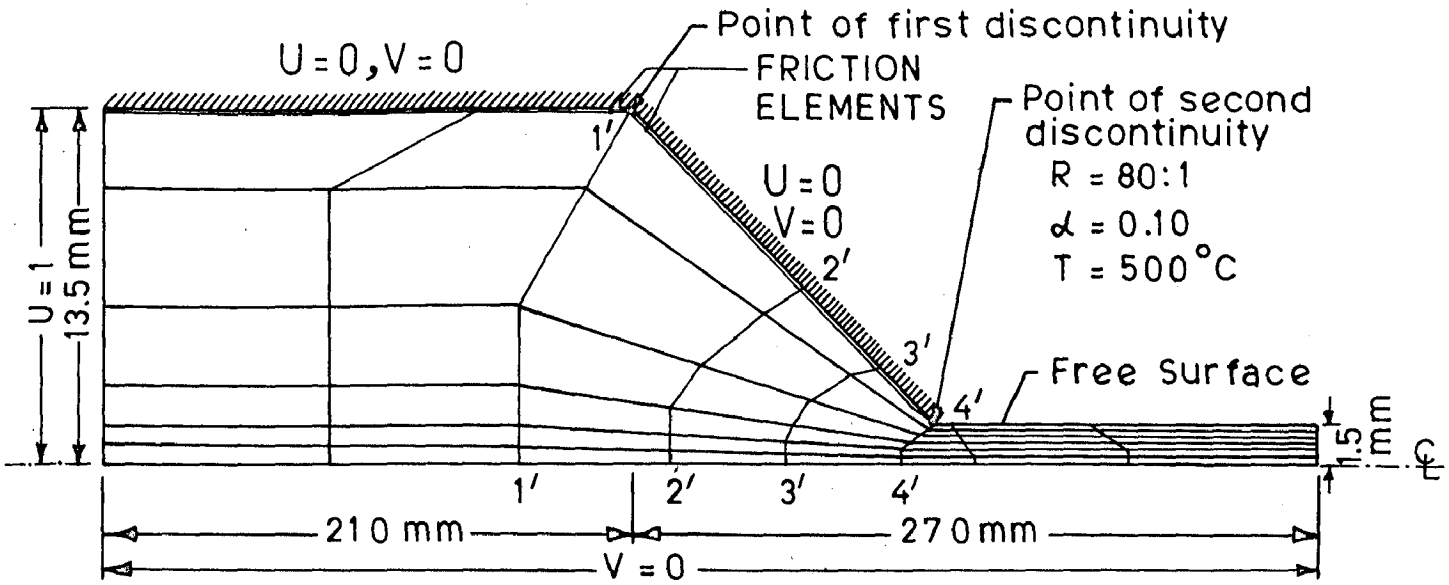

FIG.6.27(a) MESH AND BOUNDARY CONDITIONS.

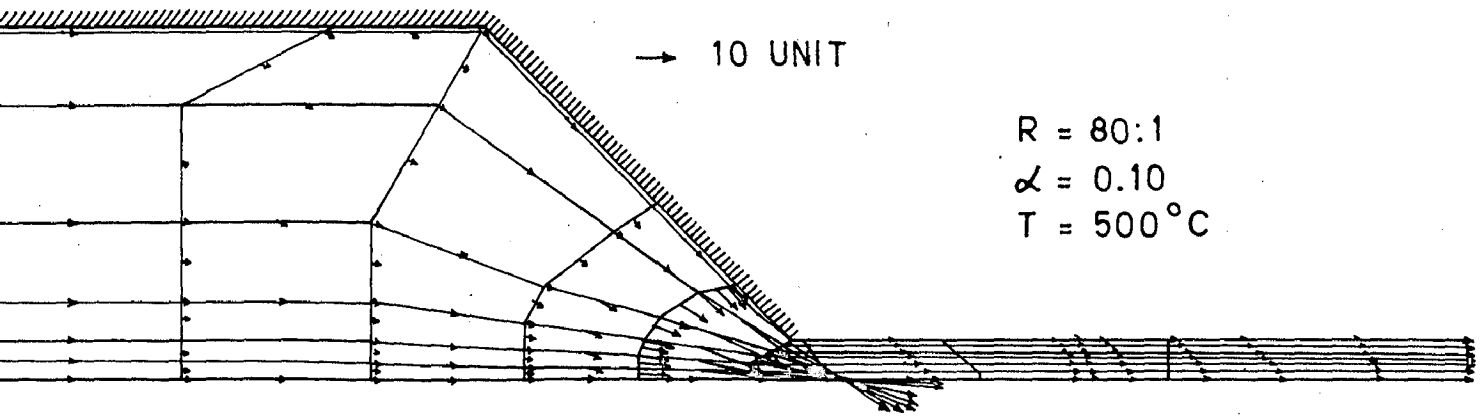

G.6.27(b) VELOCITY VECTORS.(53 elements mesh)

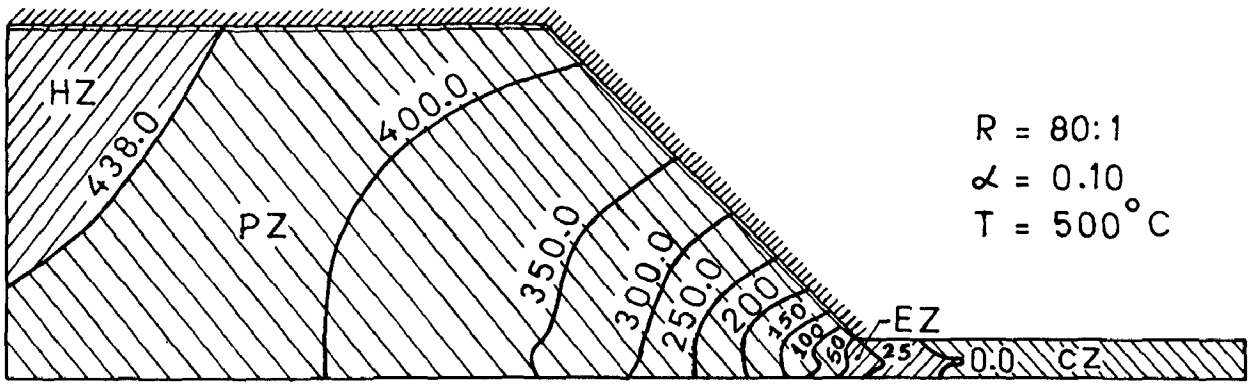

FIG.6.27(c) AVERAGE PRESSURE CONTOURS.(53 elements mesh)

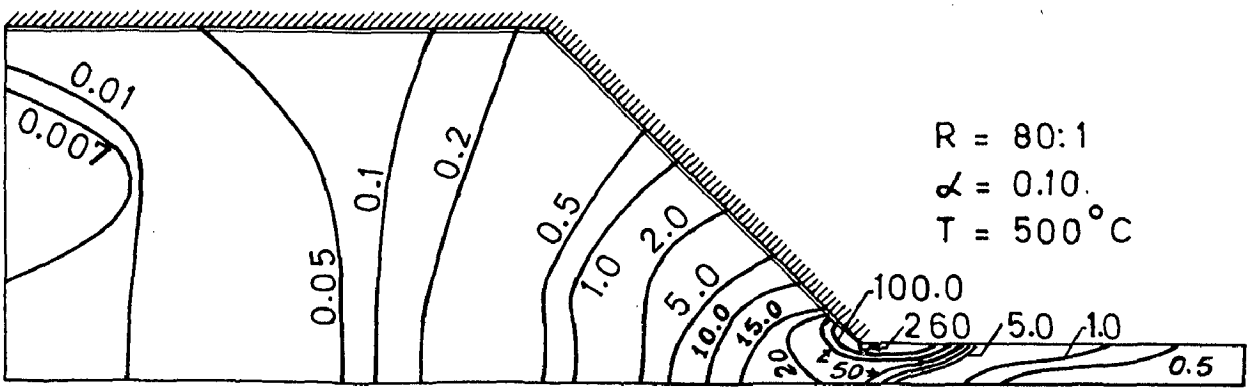

FIG.6.27(d) AVERAGE EFFECTIVE STRAIN RATE CONTOURS.
(53 elements mesh)

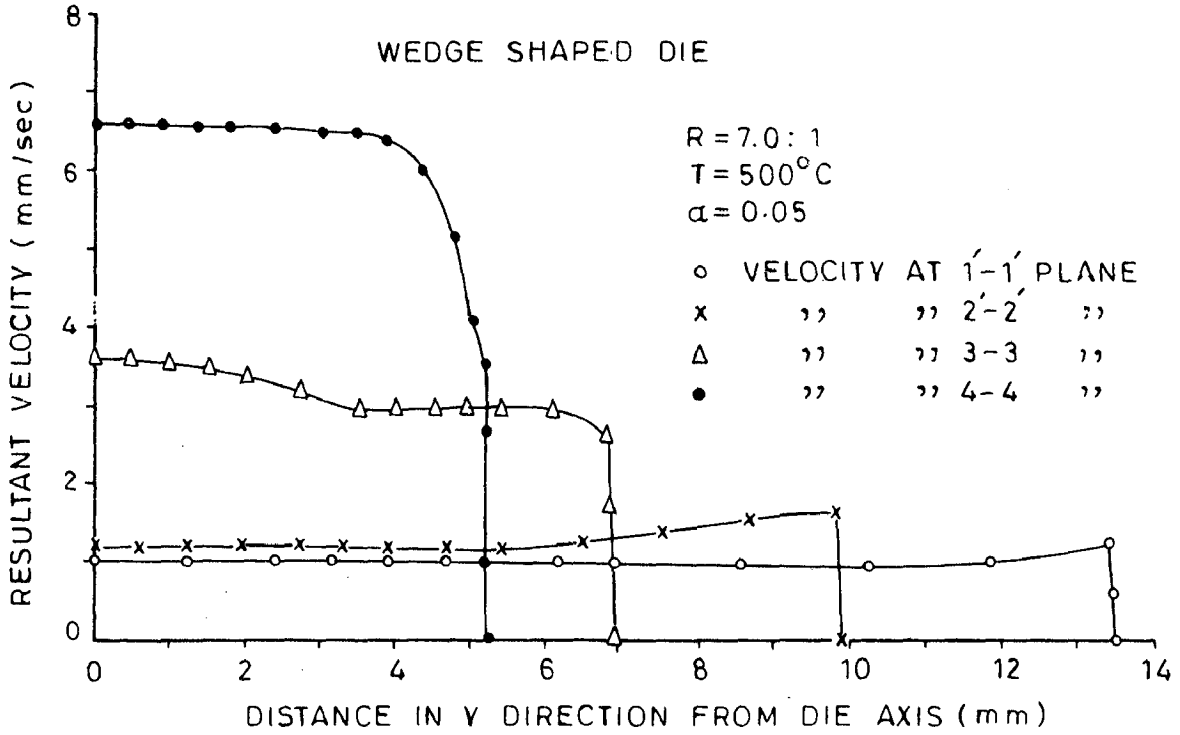

FIG.6.30–VELOCITY PROFILES PERPENDICULAR TO DIE AXIS

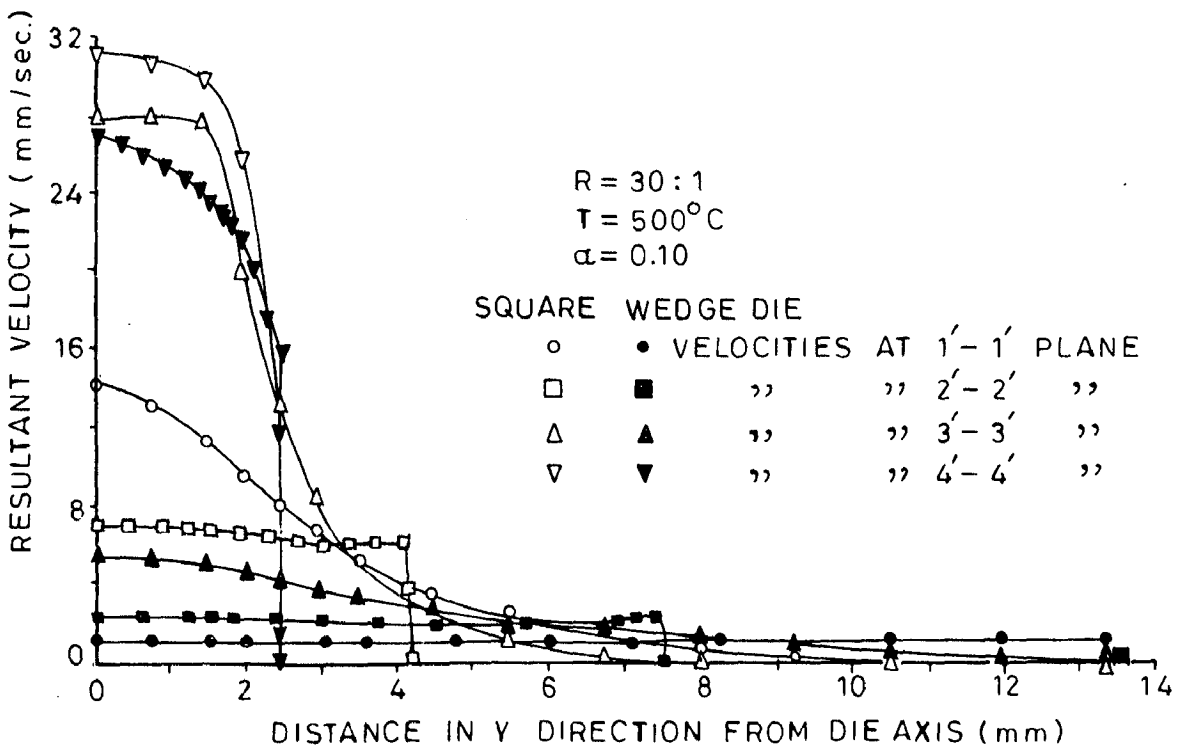

FIG.6.31–VELOCITY PROFILE PERPENDICULAR TO DIE AXIS

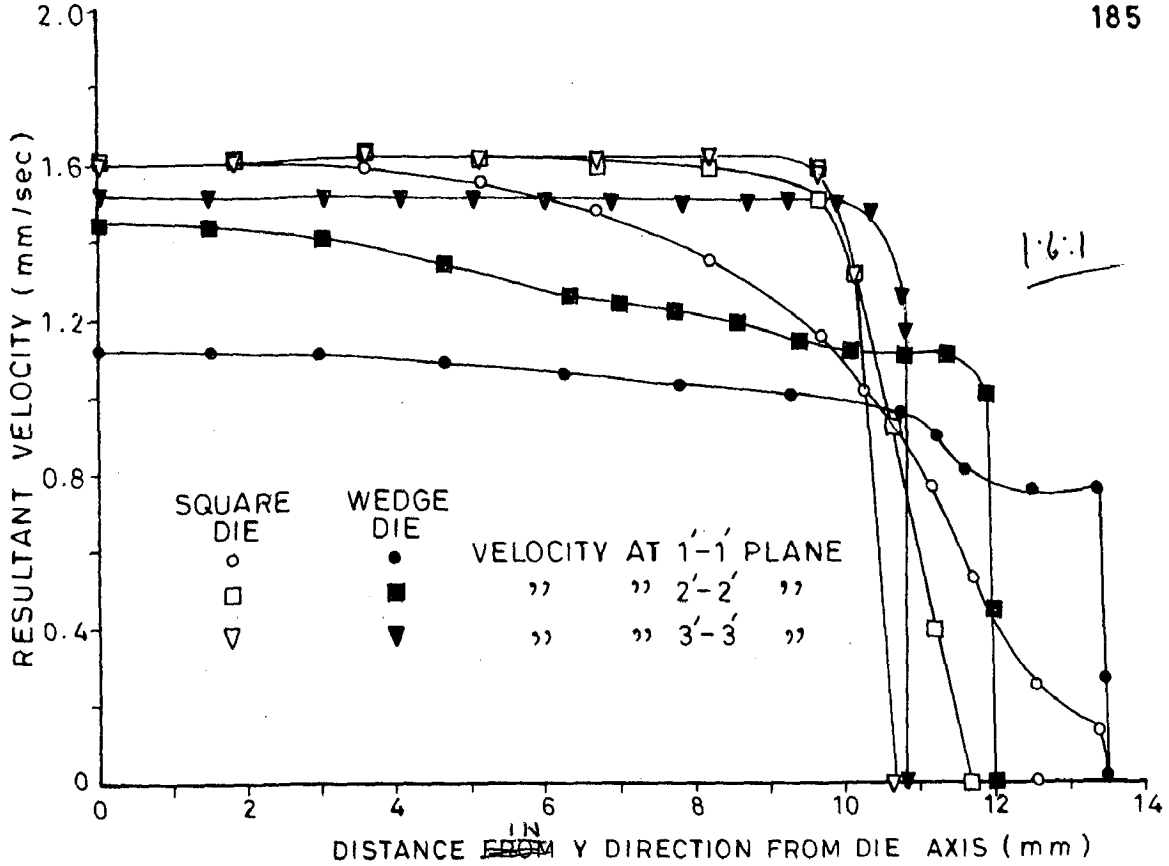

FIG.6.28-VELOCITY PROFILES PERPENDICULAR TO METAL FLOW

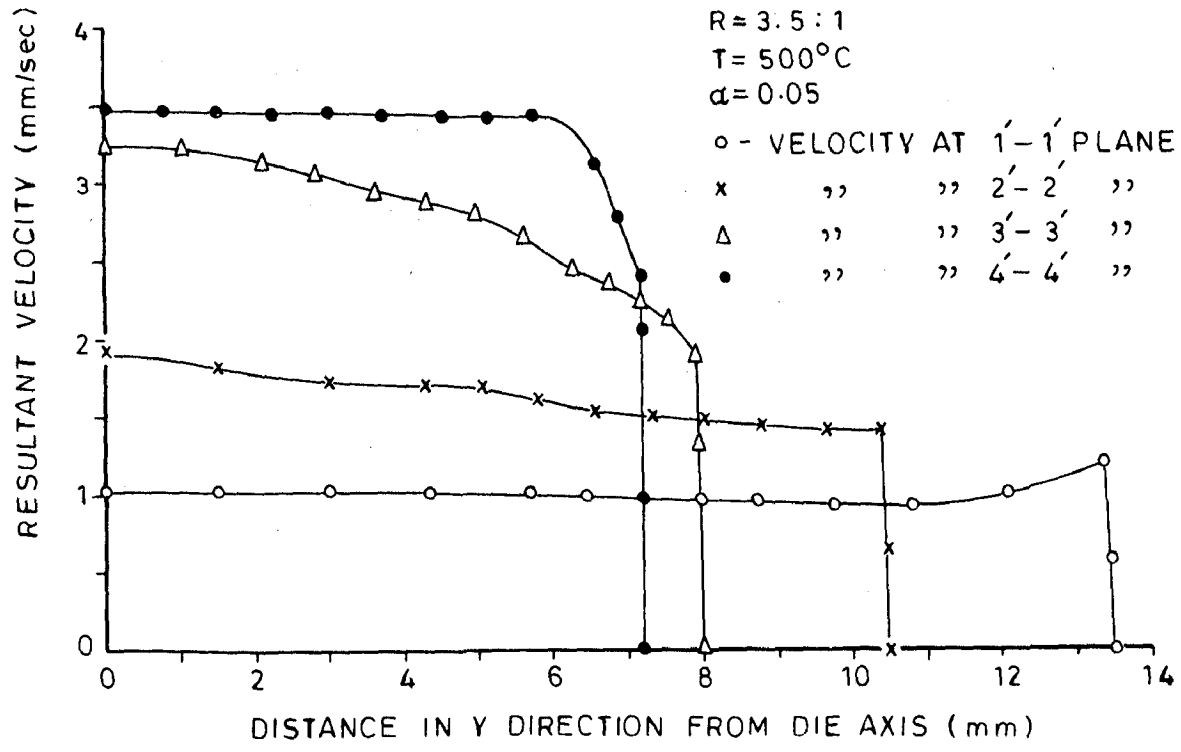

FIG.6.29- VELOCITY PROFILES PERPENDICULAR TO DIE AXIS

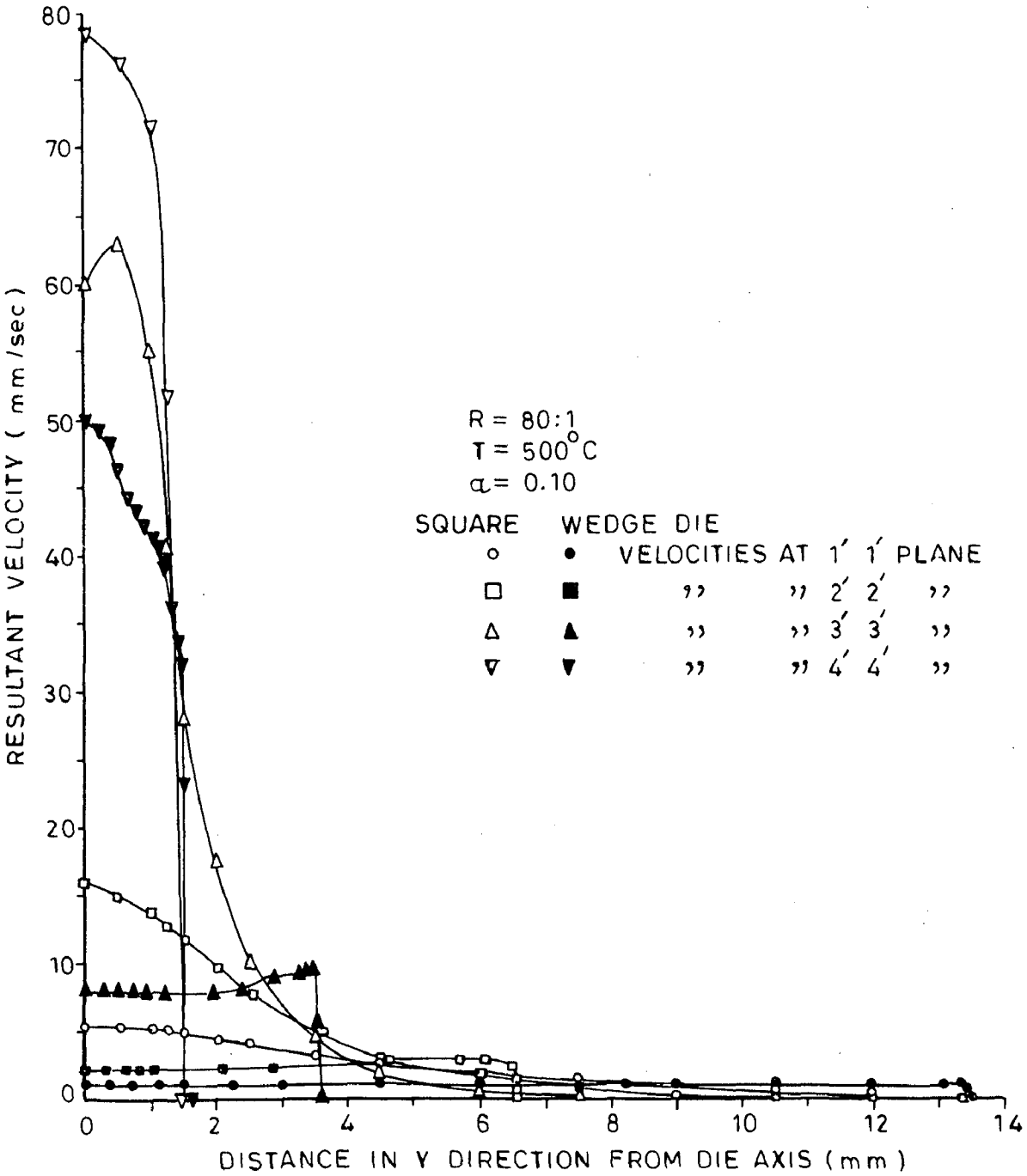

FIG.6.32- VELOCITY PROFILE PERPENDICULAR TO DIE AXIS

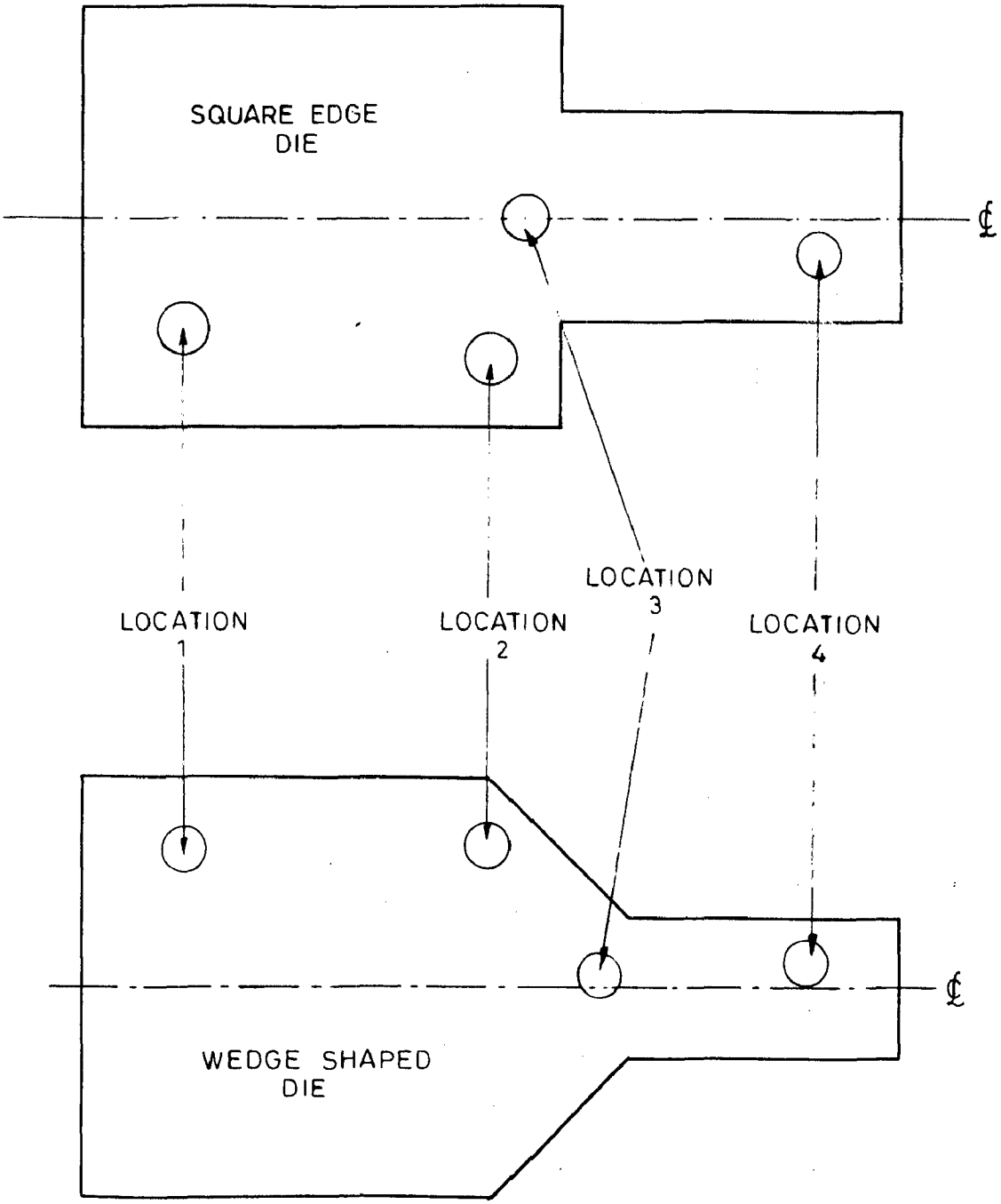

FIG.6.33-BLOCK DIAGRAM SHOWING LOCATION OF MICROSTRUCTURES

Fig. 6.34

Longitudinal section of partially extruded billet (Square die), R = 1.3:1 and T = 500°C (Circular spots indicate the electropolished regions and arrows - approximate locations of the microstructures)

(a) Coarse sub-structure
Polarised light, 1000 X

(b) Very coarse sub-structure in deformed grains
Bright field, 200 X

(c) Coarse sub-structure, oriented in the direction of metal flow
Polarised light, 500 X

(d) Undeformed grains
Bright field, 200 X

(e) Sub-structure in the form of pits
Polarised light, 500 X

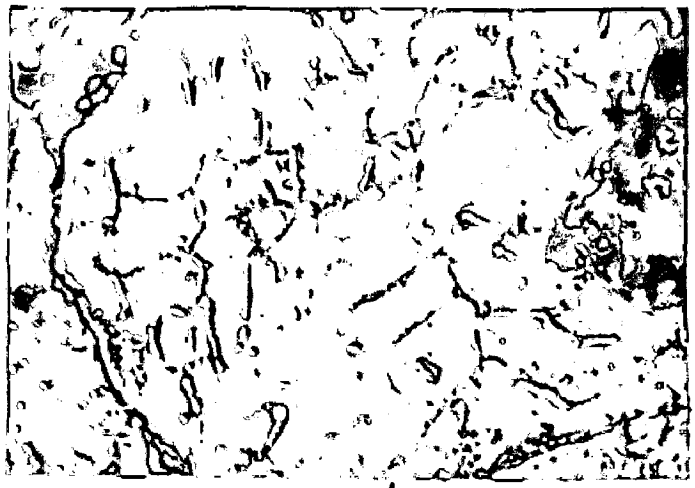

(a)

(b)

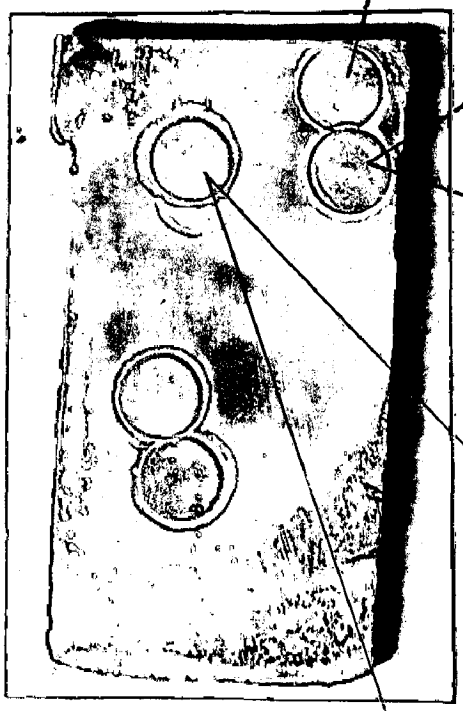

(c)

FIG. 6.34

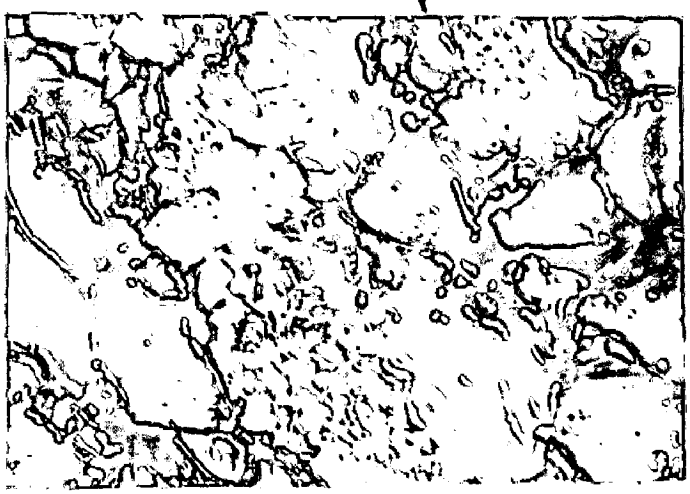

(e)

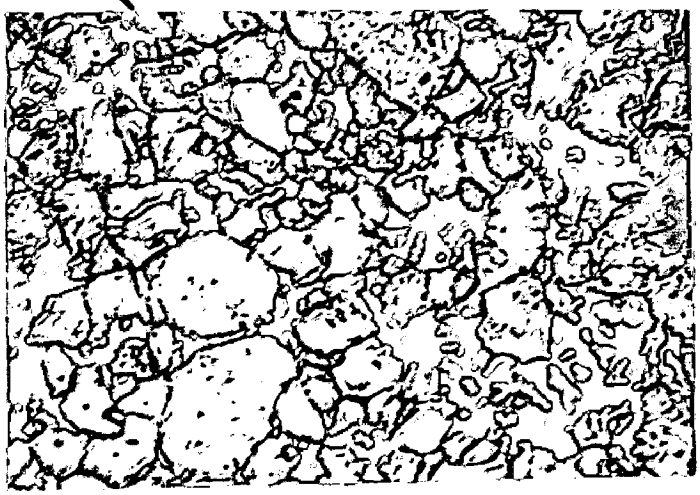

(d)

Fig. 6.34(f)

Fracture appearance of extruded product, R=1.3:1 and T=500°C

Individual particles identity observed

2650 X

FIG.6.34(f)

Fig. 6.35

Longitudinal section of partially extruded billet (Square die), R=3.2:1 and T=500°C
(Circular spots indicate the electropolished regions and arrows - approximate locations of the microstructures)

(a) Pits delineate sub-structure.
Polarised light, 1000 X

(b) Sub-structure in the form of pits inside heavily deformed grains.
Polarised light, 1000 X

(c) Pits are delineating sub-structure oriented along the grains.
Polarised light, 1000 X

(d) Directionality visible. Sub-structure is in the form of few pits only.
Bright field, 200 X

(e) As in (c).
Polarised light, 1000 X

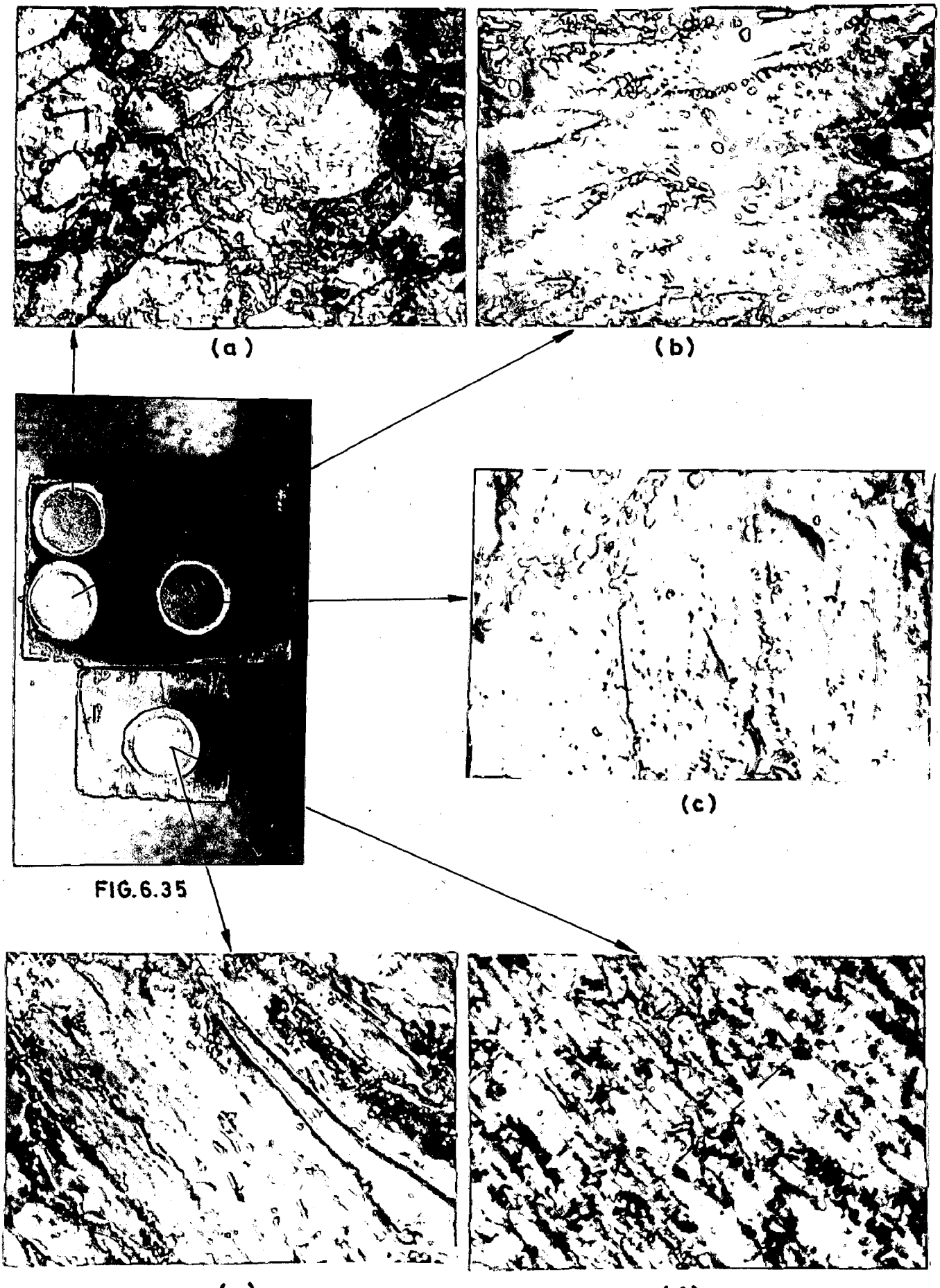

FIG. 6.35

Fig. 6.35(f)

Transverse section of the extruded product, R = 3.2:1 and T = 500°C. Fine grained structure.

Bright field, 200 X

Fig. 6.35(g)

Same as 6.35(f)

Pits delineate sub-structure.

Polarised light, 1000 X

Fig. 6.35(h)

Fracture appearance of extruded product, R = 3.2:1 and T = 500°C.

Grains heavily deformed,

2650 X

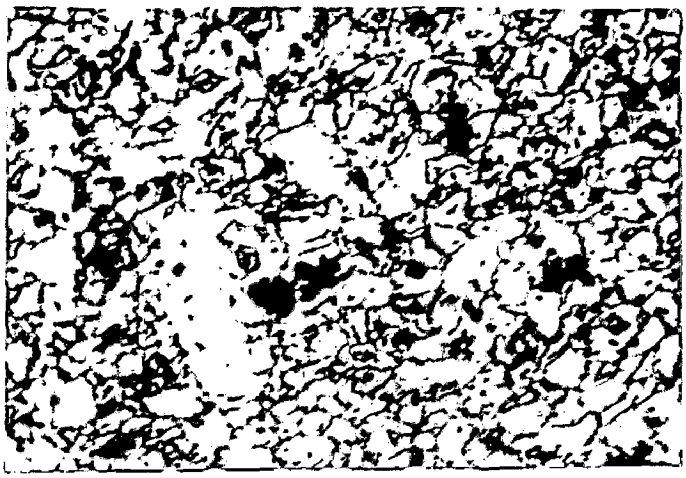

FIG.6.35 (f)

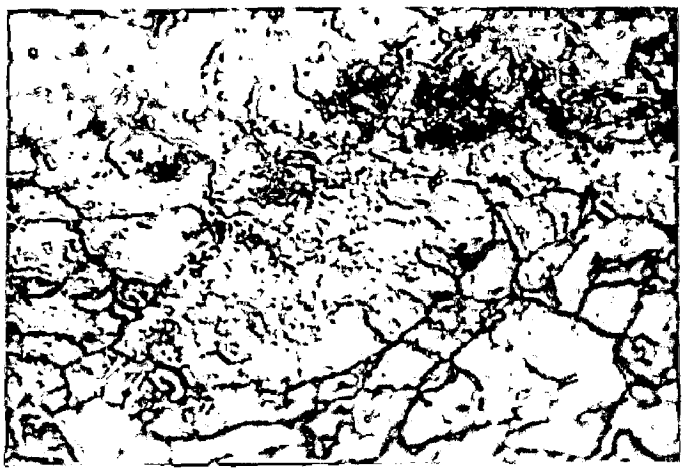

FIG.6.35 (g)

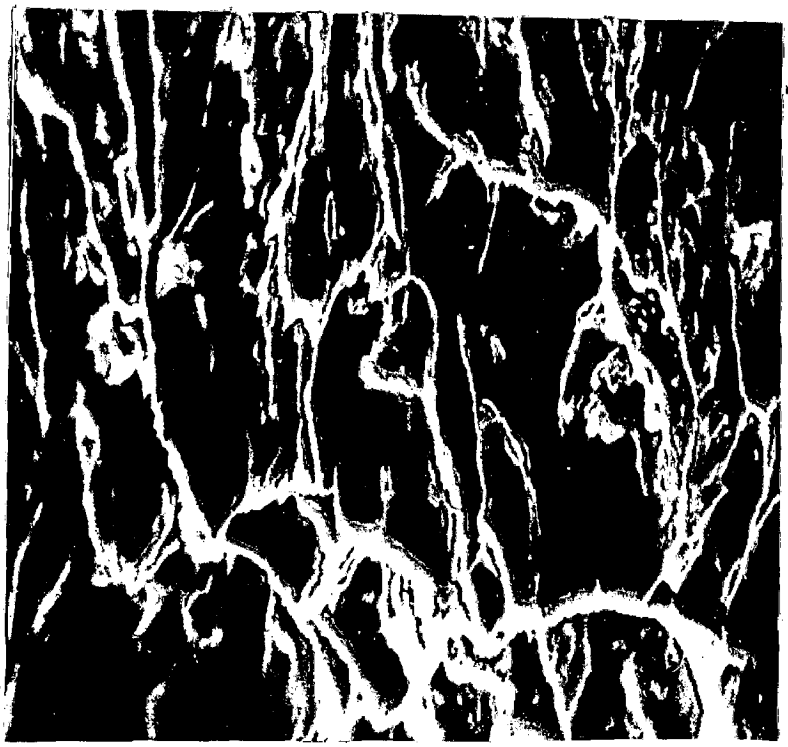

FIG.6.35 (h)

Fig. 6.36

Longitudinal section of partially extruded billet (Square die), R = 1.3:1 and T = 500°C (Circular spots indicate the electropolished regions and arrows - approximate locations of the microstructures).

(a) Equiaxed grains, showing evidence of recrystallisation.

Bright field, 200 X

(b) Sub-structure in the form of pits.

Polarised light, 1000 X

(c) Heavy uneven fibering.

Bright field, 200 X

(d) Pits visible in deformed grains.

Polarised light, 500 X

(e) Directionality observed.

Polarised light, 500 X

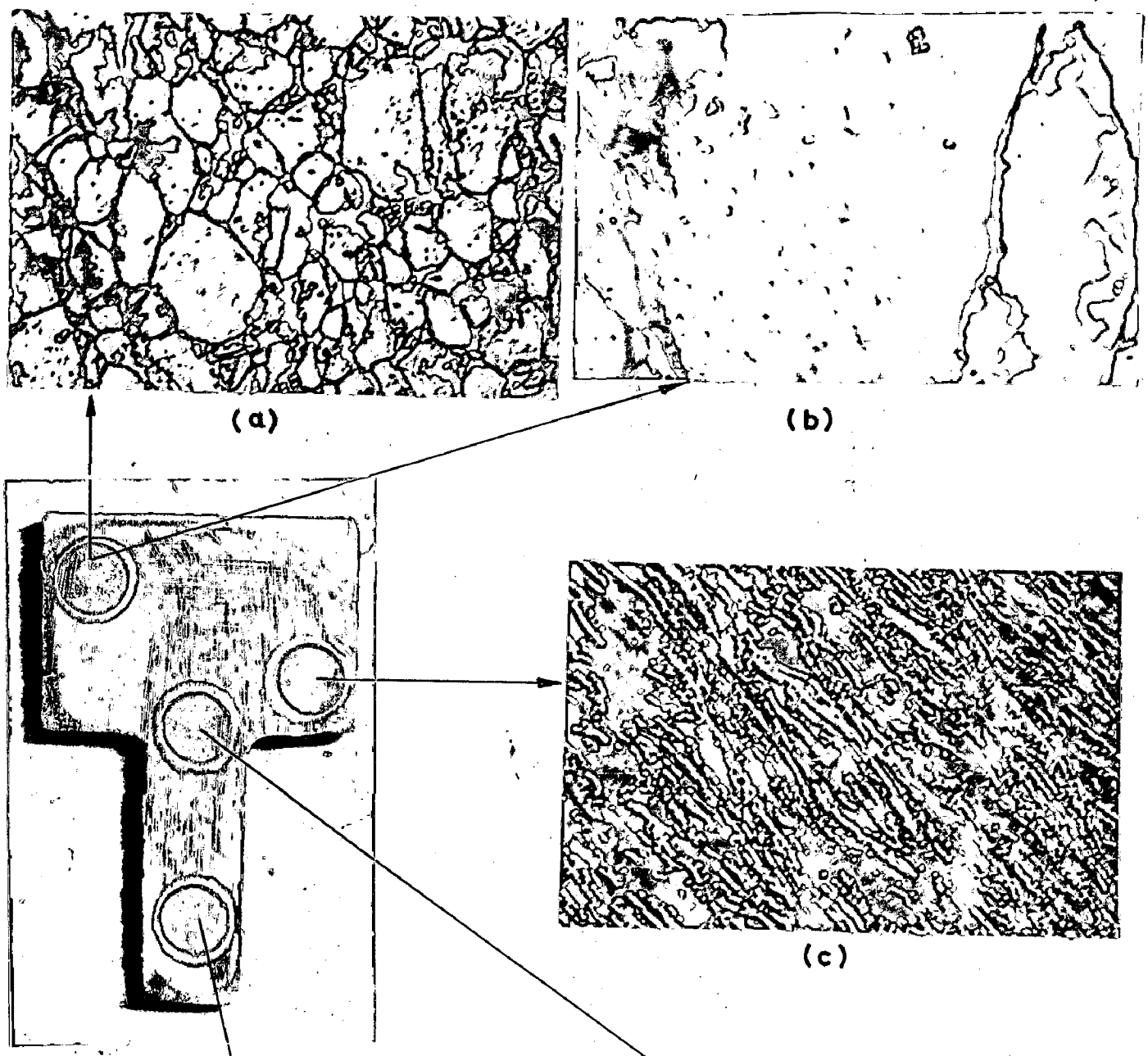

FIG.6.36

Fig. 6.36(f)

Transverse section of extruded product, R = 10:1 and T = 500°C.

Microstructure near the die axis shows deformed grains having partial directionality.

Bright field, 200 X

Fig. 6.36(g)

Same as 6.36(f)

Sub-structure in the form of pits only.

Polarised light, 1000 X

Fig. 6.36(h)

Transverse section of Extruded product, R = 10:1 and T = 500°C.

Microstructure near the periphery shows coarse grain structure with only few pits.

Polarised light, 1000 X

Fig. 6.36(i)

Fracture appearence showing extensive deformation.

3400 X

FIG.6.36 (f)

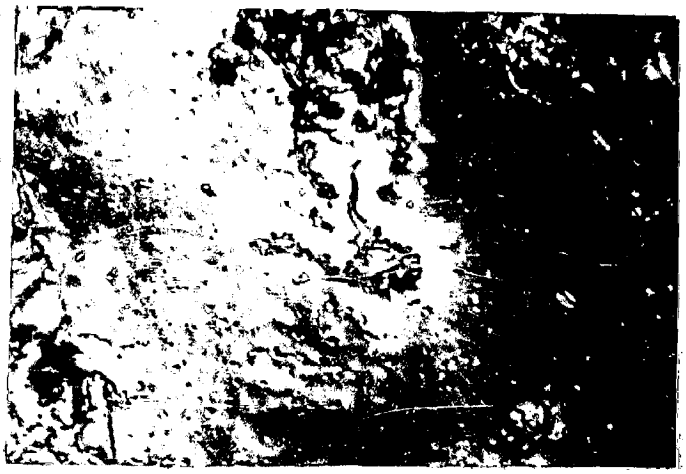

FIG.6.36 (g)

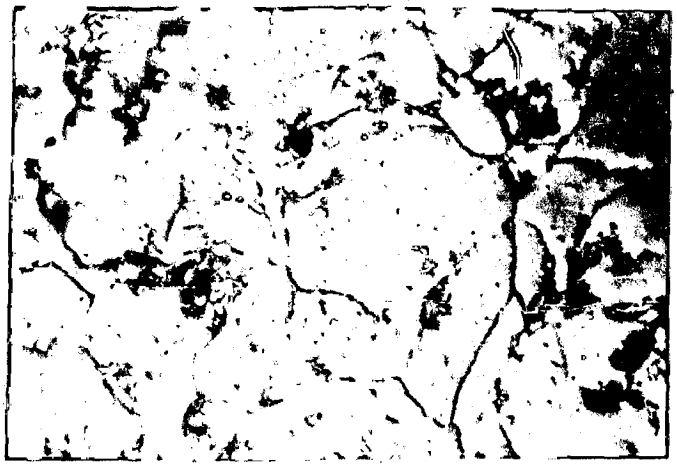

FIG.6.36 (h)

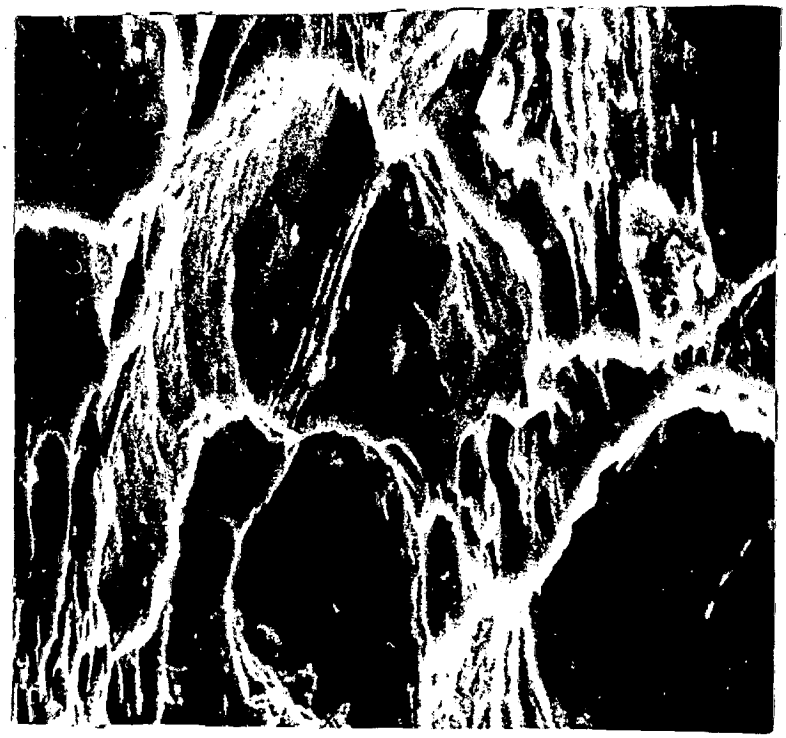

FIG.6.36 (i)

Fig. 6.37

Longitudinal section of partially extruded billet (Square die), R = 40:1 and T = 500°C (Circular spots indicate the electropolished regions and arrows - approximate locations of the microstructures).

(a) Heavy sub-structure.

Polarised light, 1000 X

(b) Heavy sub-structure in deformed grains.

Polarised light, 500 X

(c) Heavy pitting within the grains.

Polarised light, 1000 X

(d) Anodised structure of extruded product, fibrous structure.

Bright field, 200 X

(e) Transverse section Fragmented grains due to heavy deformation.

Polarised light, 1000 X

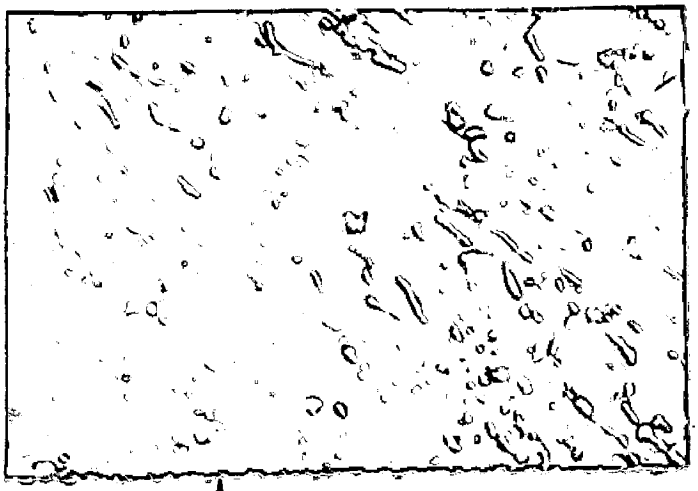

(a)

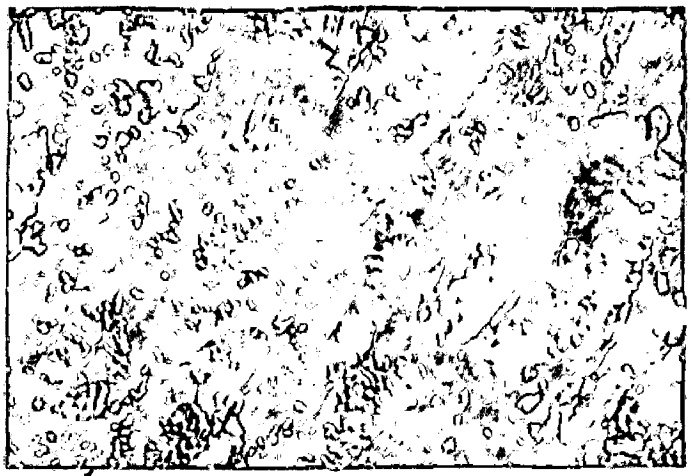

(b)

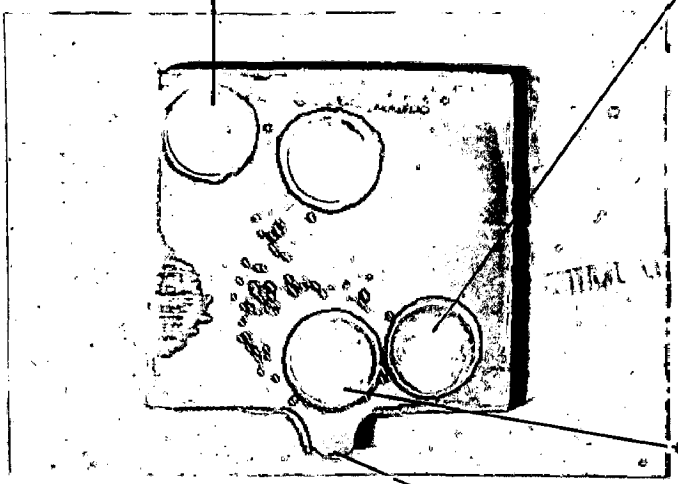

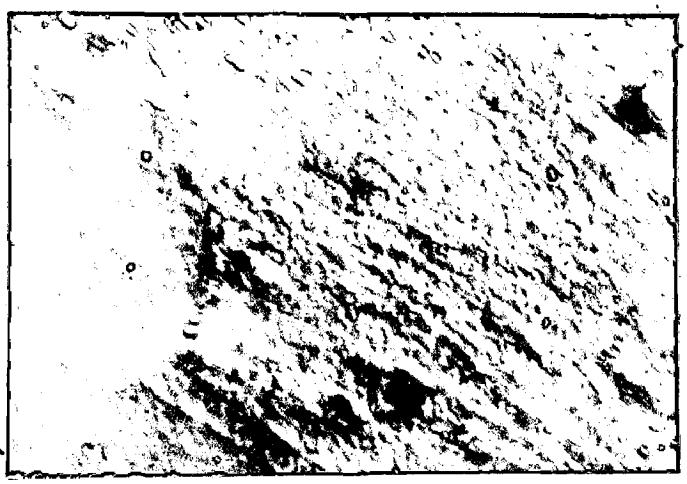

(c)

FIG.6.37

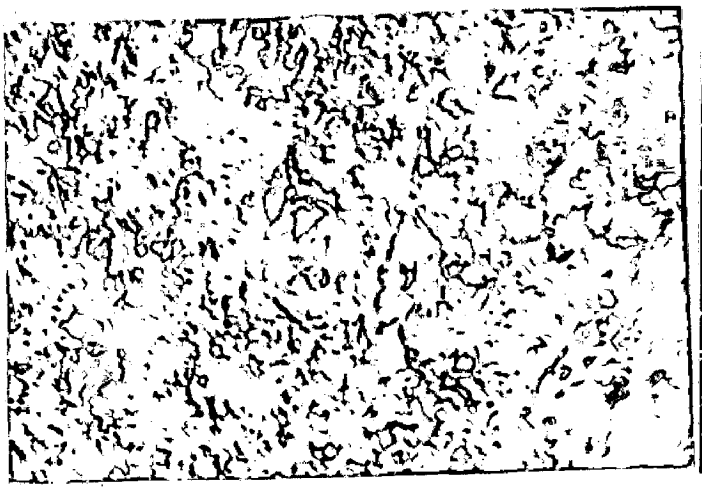

(e)

(d)

Fig. 6.38

Longitudinal section of partially extruded billet (Square dia), R = 80:1 and T = 500°C.
(Circular spots indicate the electropolished regions and arrows - approximate locations of the microstructures).

(a) Undeformed grains showing their identity.

Bright field, 200 X

(b) Coarse sub-structure.

Polarised light, 1000 X

(c) Heavy uneven flow and deformation of grains.

Bright field, 200 X

(d) Deformed grains showing little directionality.

Bright field, 200 X

(e) Transverse section Fragmented grains, sub-structure in the form of pits.

Polarised light, 1000 X

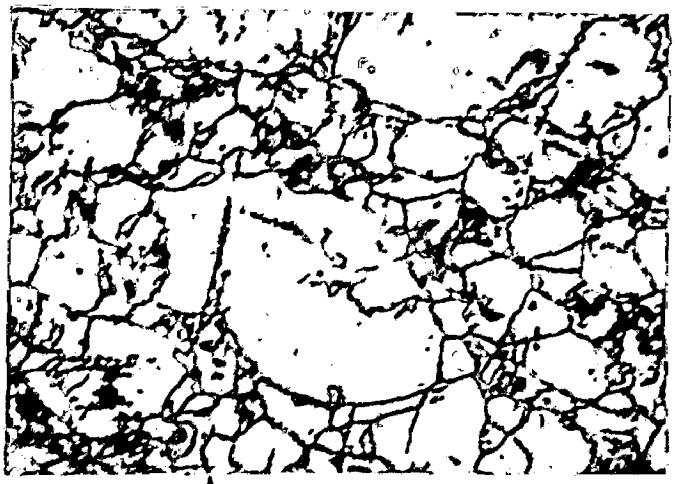

(a)

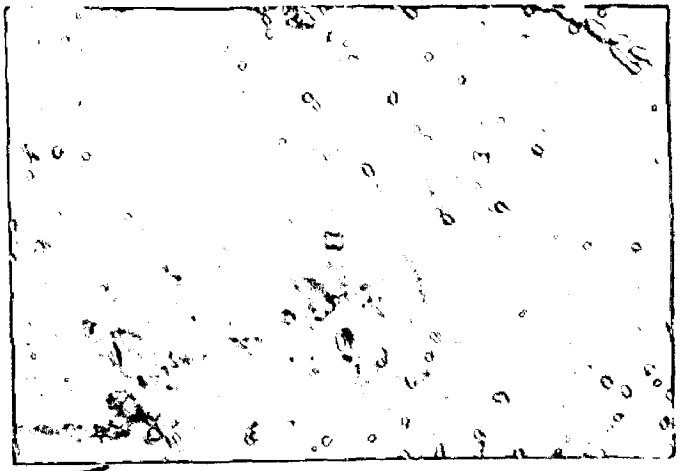

(b)

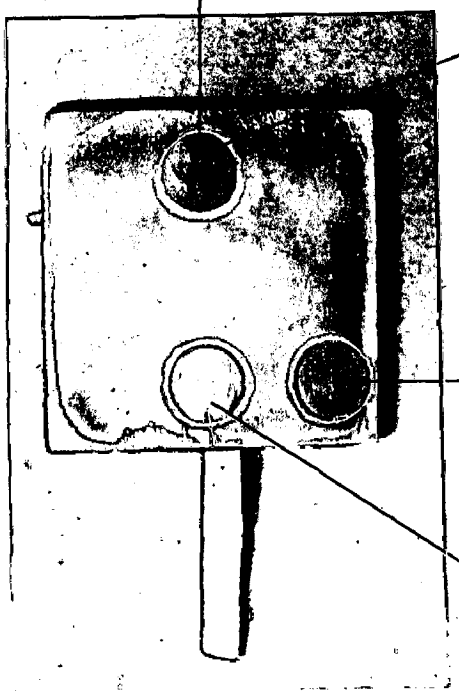

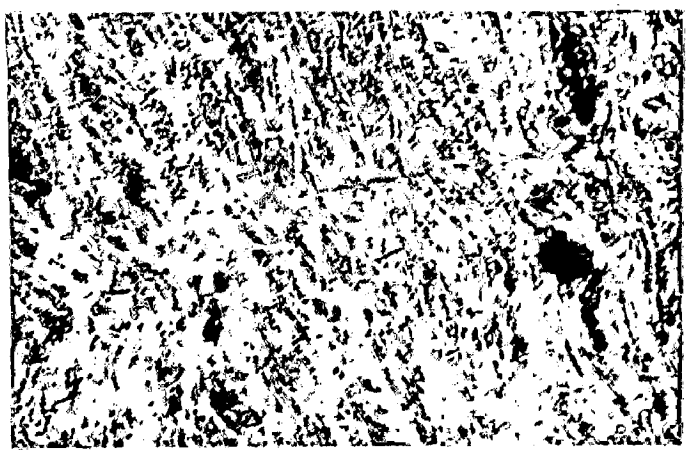

(c)

FIG.6.38

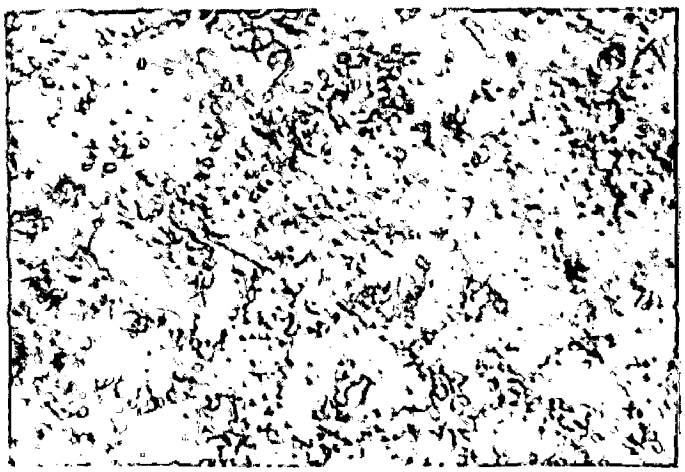

(e)

(d)

Fig. 6.39

Longitudinal section of partially extruded billet (Square die), R = 10:1 and T = 300 C.
(Circular spots indicate the electropolished regions and arrows - approximate locations of the micro-structure).

(a) Coarse and dense sub-structure in all the grains.

Polarised light, 1000 X

(b) Coarse sub-structure which is deformed along the grains.

Polarised light, 1000 X

(c) Grains are less deformed in comparison to (b).

Polarised light, 1000 X

(d) Very few pits inside heavily deformed grains.

Polarised light, 1000 X

(e) Deformed sub-structure aligned along grains.

Polarised light, 1000 X

(f) Pronounced directionality

Polarised light, 1000 X

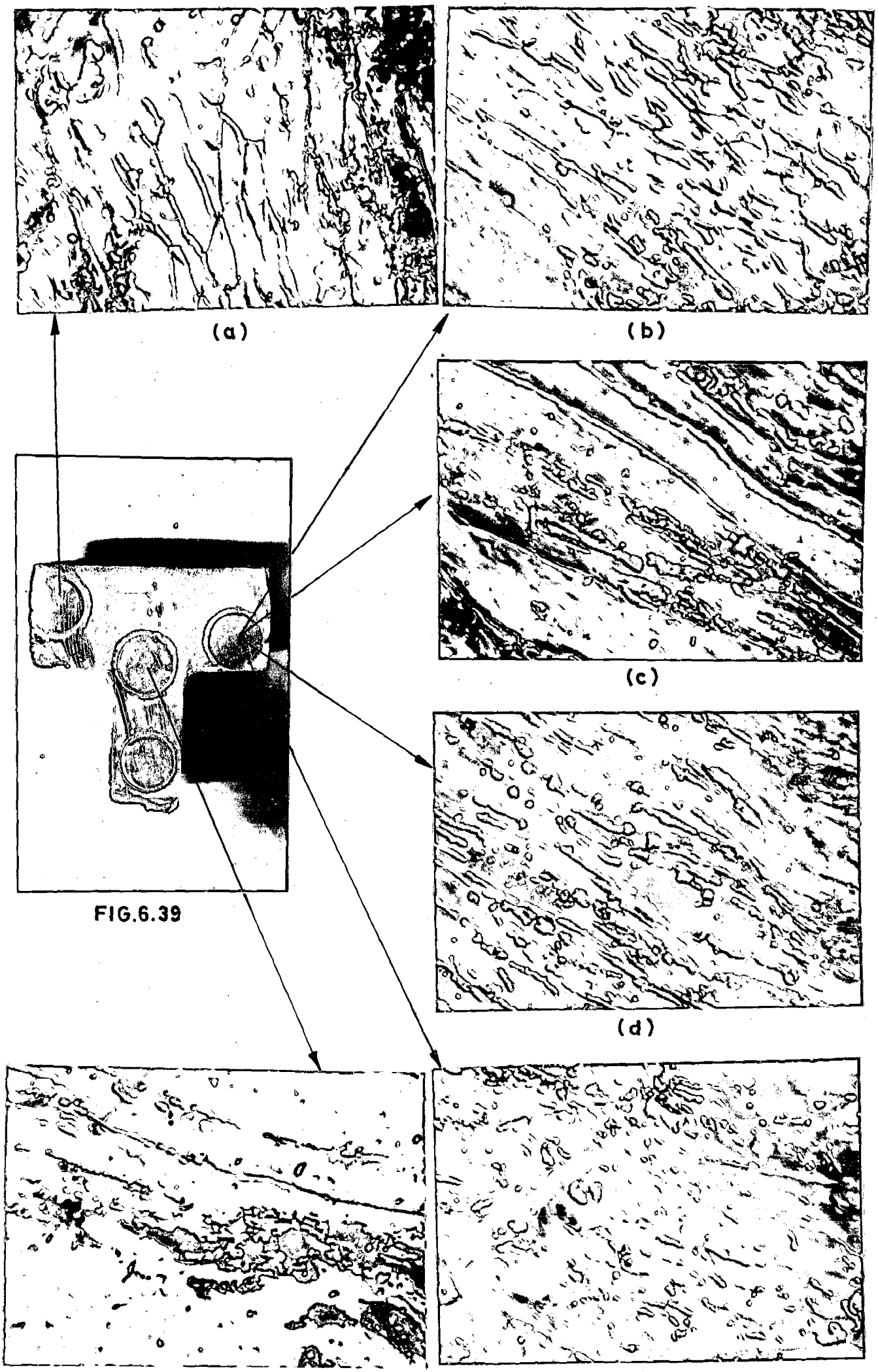

FIG.6.39

Fig. 6.39(g)

Extruded product, R=10:1 and T=500°C.

Fibrous structure.

Bright field, 200 X

Fig. 6.39(h)

Deformed grain showing directionality.

Polarised light, 1000 X

Fig. 6.39(i)

Transverse section of extruded product, R=10:1 and T=300°C.

Fine deformed grains with pits.

Polarised light, 1000 X

FIG.6.39 (g)

FIG.6.39 (h)

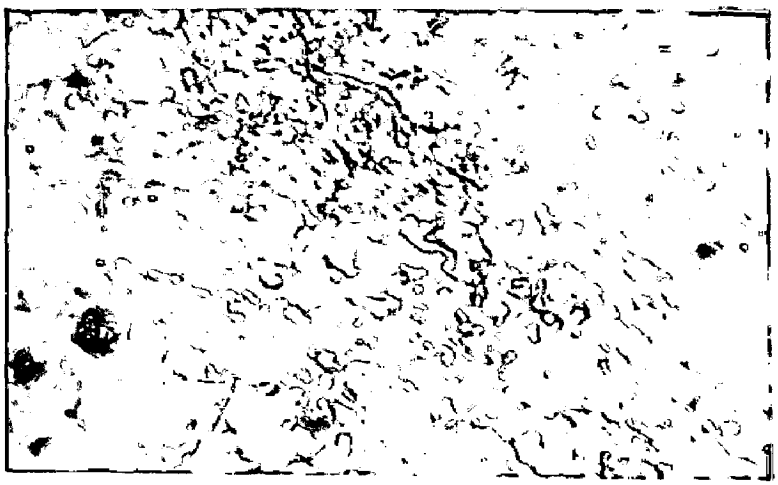

FIG.6.39 (i)

Fig. 6.40

Longitudinal section of partially extruded billet (Square die), R=10:1 and T=400°C
(Circular spots indicate the electropolished regions and arrows - approximate locations of the micro-structure.

(a) Particles identity and porosity is visible.

Bright field, 200 X

(b) Coarse sub-structure.

Polarised light, 1000 X

(c) Fine sub-structure.

Polarised light, 1000 X

(d) Pits inside deformed grains.

Polarised light, 1000 X

(e) Few pit inside deformed grains.

Polarised light, 1000 X

(f) A fine network of sub-structure.

Polarised light, 1000 X

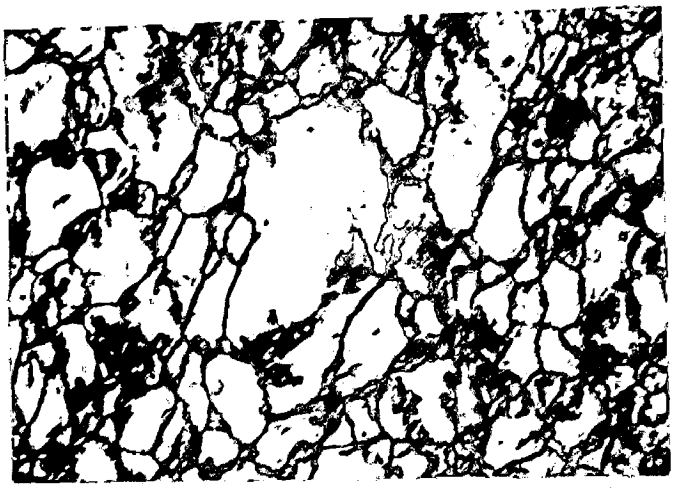

(a)

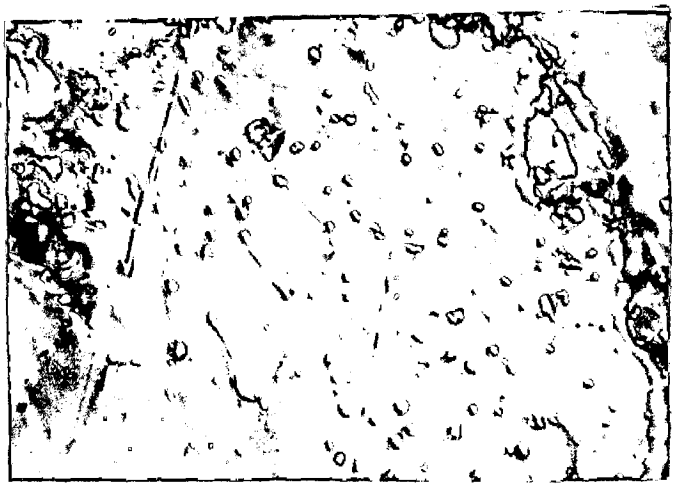

(b)

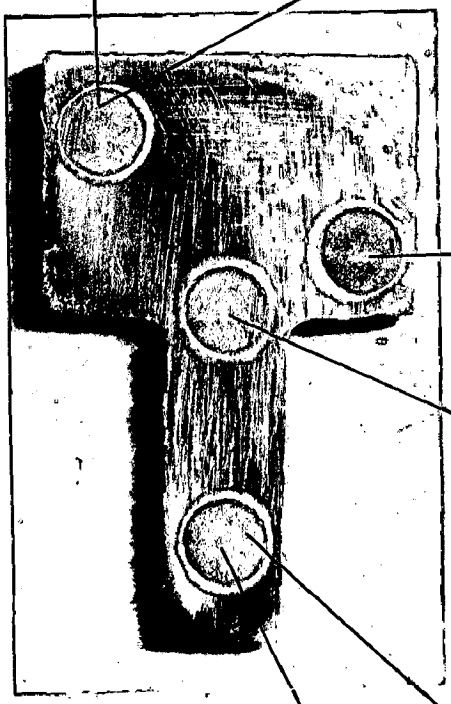

FIG.6.40

(c)

(d)

(f)

(e)

Fig. 6.40(g)

Transverse section of the extruded product R=10:1 and T = 400°C (near the die axis).
Only sub-structure visible.

Polarised light, 1000 X

Fig. 6.40(h)

Transverse section of the extruded product R=10:1 and T=400°C (near the periphery).
Heavy sub-structure.

Polarised light, 1000 X

FIG.6.40 (g)

FIG.6.40 (h)

Fig. 6.41

Longitudinal section of partially extruded billet (Wedge die), R=1.6:1 and T=500°C
(Circular spots indicate the electropolished regions and arrows - approximate locations of the micro-structures).

(a) Sub-structure.

Polarised light, 500 X

(b) Sub-structure oriented along grains.

Polarised light, 500 X

(c) Heavy flow, no sub-structure.

Polarised light, 1000 X

(d) Deformed grains having sub-grains.

Bright field, 200 X

(e) Deformed sub-structure.

Polarised light, 500 X

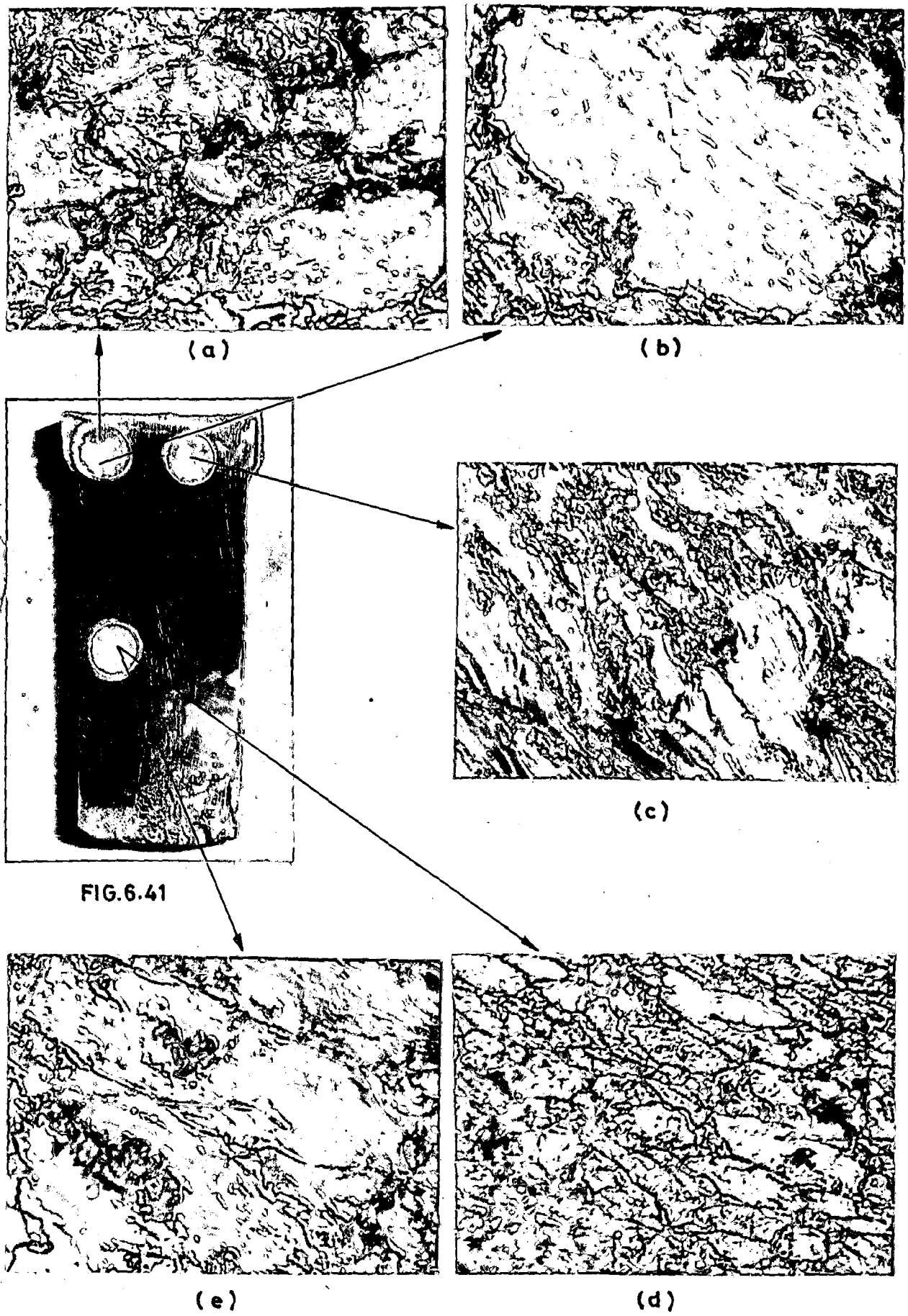

FIG.6.41

Fig. 6.41(f)

Transverse section of extruded product, R=1.6:1 and T=500°C.

Sub-structure.

Bright field, 200 X

Fig. 6.41(g)

Transverse section of extruded product, R=1.6:1 and T=400°C.

Same as 6.41(f).

Bright field, 200 X

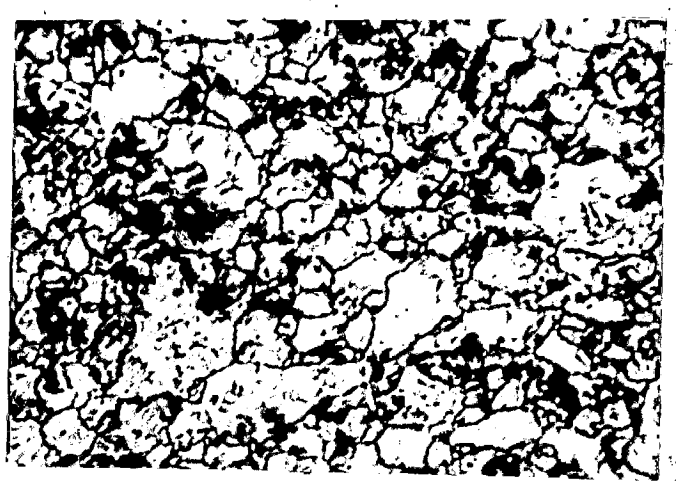

FIG. 6.41 (f)

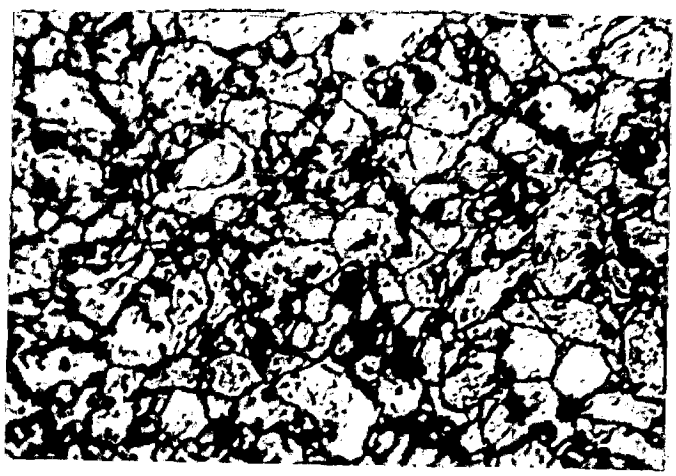

FIG. 6.41 (g)

Fig. 6.42

Longitudinal section of partially extruded billet (Wedge die), R=7.0:1 and T=500°C
(Circular spots indicate the electropolished regions and arrows ~ approximate locations of the microstructures.

(a) Heavy sub-structure.
Bright field, 200 X

(b) Heavy and coarse sub-structure; Grain grouth seen.
Polarised light, 1000 X

(c) Deformed grains containing oriented sub-structure.
Bright field, 200 X

(d) Pronounced directionality of sub-structure.
Polarised light, 1000 X

(e) Sub-structure in the form of pits.
Polarised light, 1000 X

(f) Deformed grains showing directionality.
Bright field, 200 X

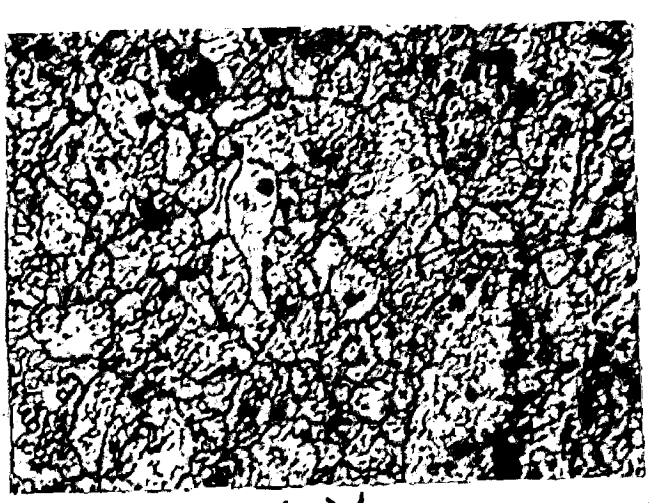

(a)

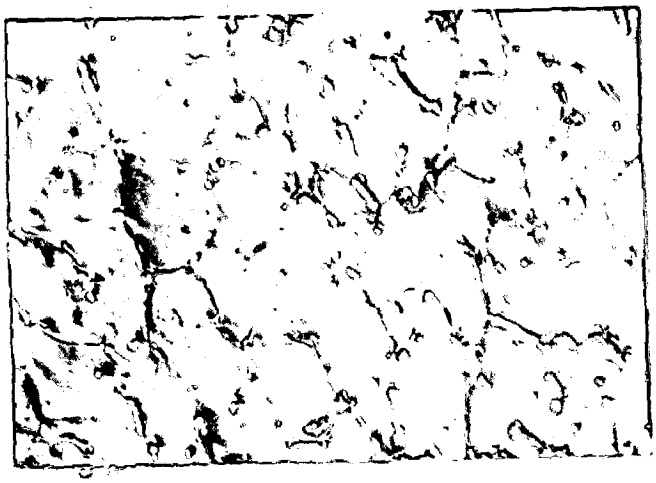

(b)

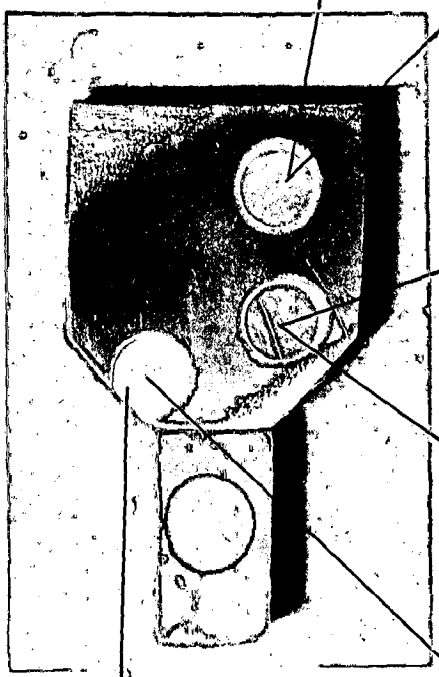

FIG.6.42

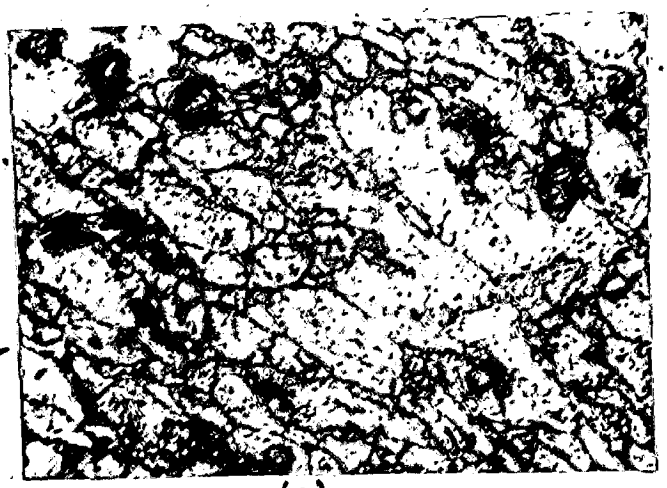

(c)

(d)

(f)

(e)

Fig. 6.42(g)

Extruded product (near periphery),R=7.0:1, T=500°C.
Fibrous structure, sub-structure in the form of pits.

Bright field, 200 X

Fig. 6.42(h)

Extruded product (near die axis),R=7.0:1, T=500°C.
Heavily deformed grains.

Bright field, 200 X

Fig. 6.42(i)

Transverse section of extruded product R=7.0:1, T=500°C (near periphery).
Only pits visible.

Polarised light, 500 X

Fig. 6.42(j)

Transverse section of extruded product R=7.0:1, T=500°C (Near die axis).
Coarse grain structure and sub-structure.

Polarised light, 500 X

FIG.6.42 (g)

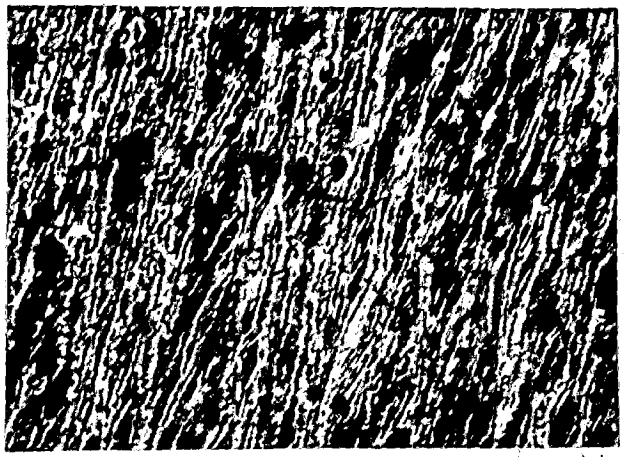

FIG.6.42 (h)

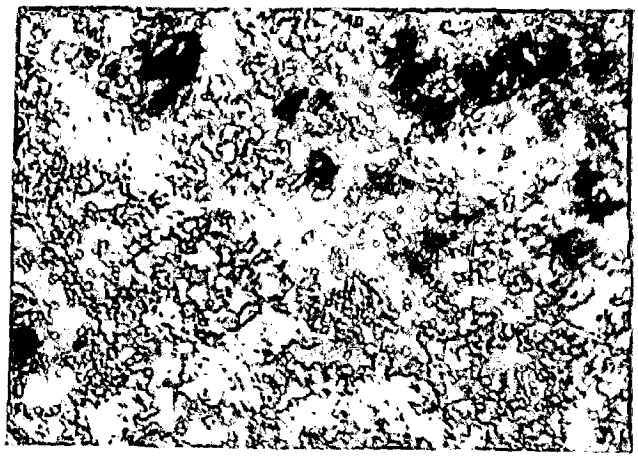

FIG.6.42 (i)

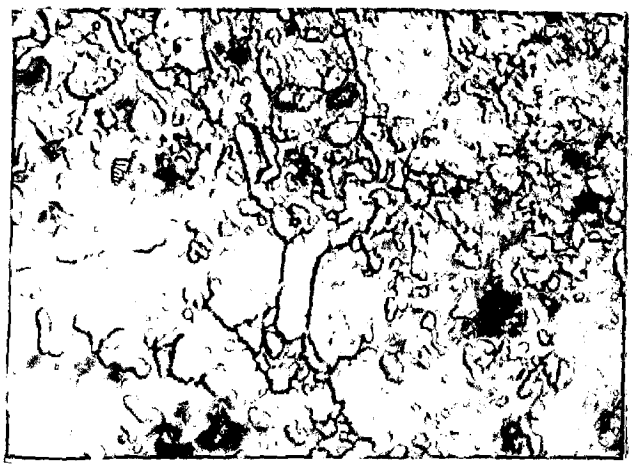

FIG.6.42 (j)

Fig. 6.43

Longitudinal section of partially extruded billet, (Wedge die), R=15:1, T=500°C
(Circular spots indicate the electropolished regions and arrows - approximate locations of the micro-structures).

(a) Heavy sub-structure, in undeformed grains.

Polarised light, 500 X

(b) Deformed sub-structure.

Polarised light, 1000 X

(c) Deformed grains with less sub-structure, than (a).

Polarised light, 500 X

(d) Fibrous structure.

Bright field, 200 X

(e) Showing directionality.

Bright field, 200 X

(f) Only directionality observed.

Polarised light, 1000 X

(a)

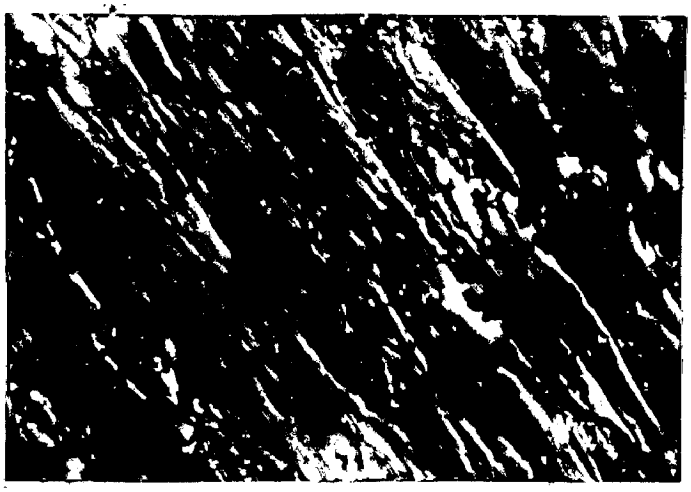

(b)

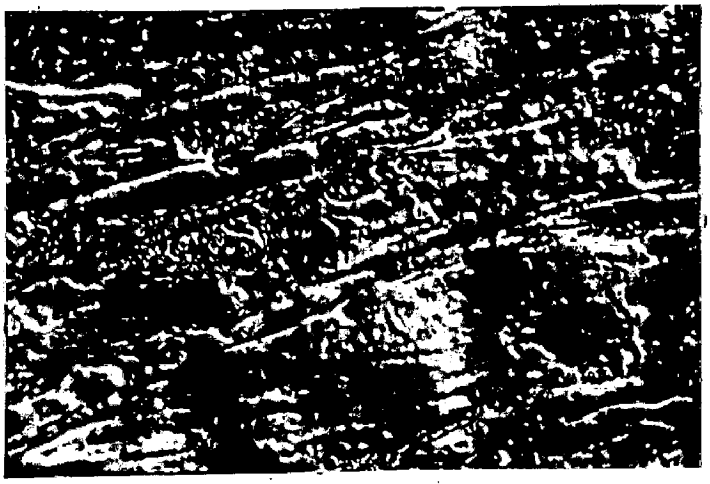

(c)

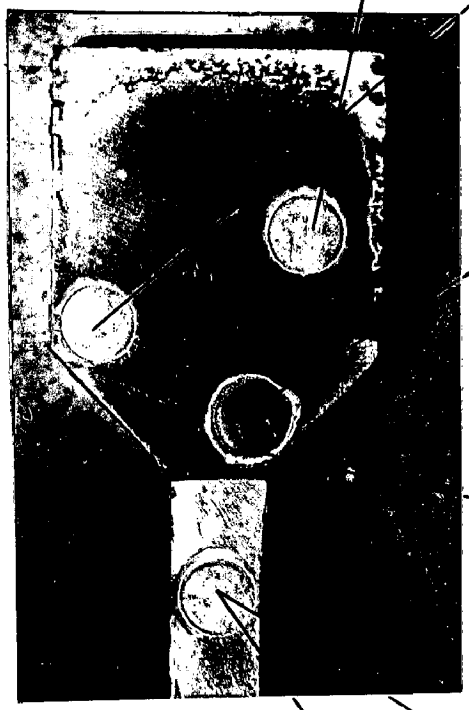

FIG.6.43

(d)

(f)

(e)

Fig. 6.43(g)

Transverse section of extruded product,
R=15:1, T=500^{o}C.
Fine grained structure.
Bright field, 200 X

Fig. 6.43(h)

Same as (g).
Sub-structure.
Polarised light, 1000 X

FIG.6.43 (g)

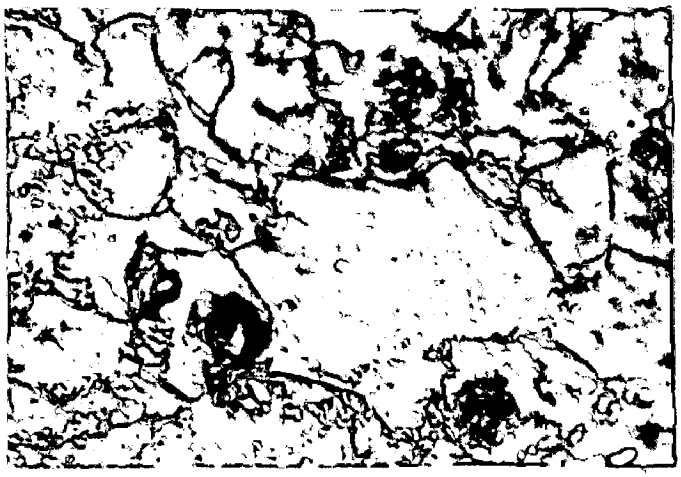

FIG.6.43 (h)

Fig. 6.44

Longitudinal section of partially extruded billet (Wedge die), R=80:1, T=500°C.
(Circular spots indicate the electropolished regions and arrows - approximate locations of the microstructures).

(a) Sub-structure.

Polarised light, 1000 X

(b) Deformed sub-structure in the form of pits.

Polarised light, 1000 X

(c) Pits are oriented along the deformation.

Polarised light, 1000 X

(d) Fragmented grains (no flow and no directionality).

Bright field, 200 X

(e) Fine sub-structure in the form of pits.

Polarised light, 1000 X

(f) Anodised structure showing directionality and sub-structure.

Polarised light, 1000 X

(a)

(b)

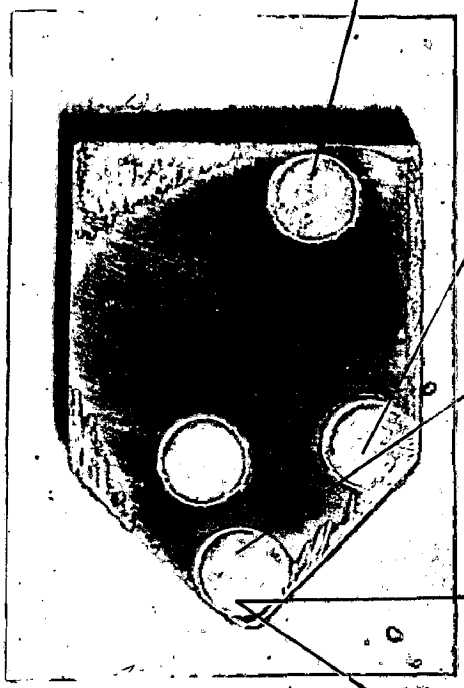

FIG. 6.44

(c)

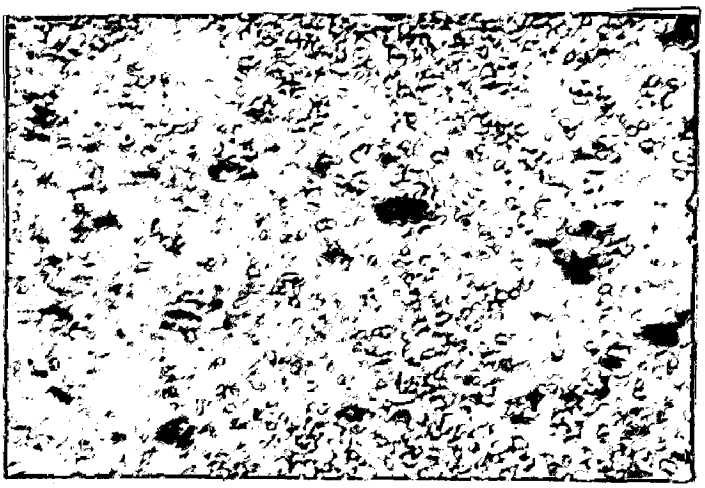

(d)

Extruded Product

(f)

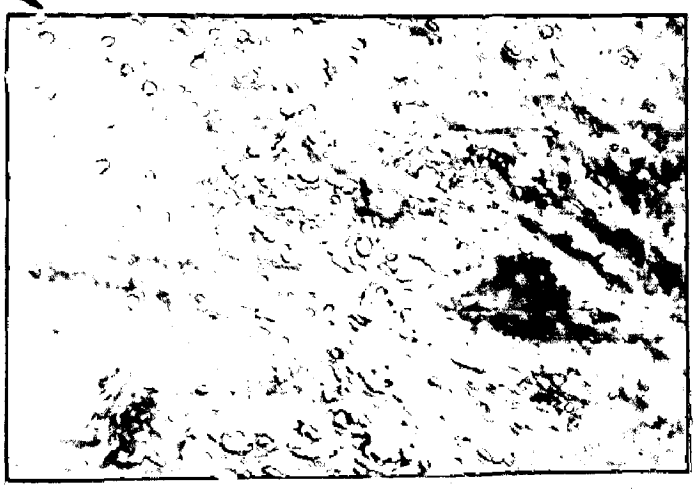

(e)

Fig. 6.45

Longitudinal section of partially extruded billet (Wedge die), R=7.0:1, T = 300°C
(Circular spots indicate the electropolished regions and arrows - approximate locations of the microsctructure).

(a) Heavy sub-structure in all the grains.

Bright field, 200 X

(b) Heavy sub-strcuture.

Polarised light, 1000 X

(c) Deformed sub-structure in the form of pits.

Polarised light, 500 X

(d) Directionality and sub-structure in the form of pits.

Bright field, 200 X

(e) Pits are aligned in the direction of flow.

Polarised light, 1000 X

(a) (b)

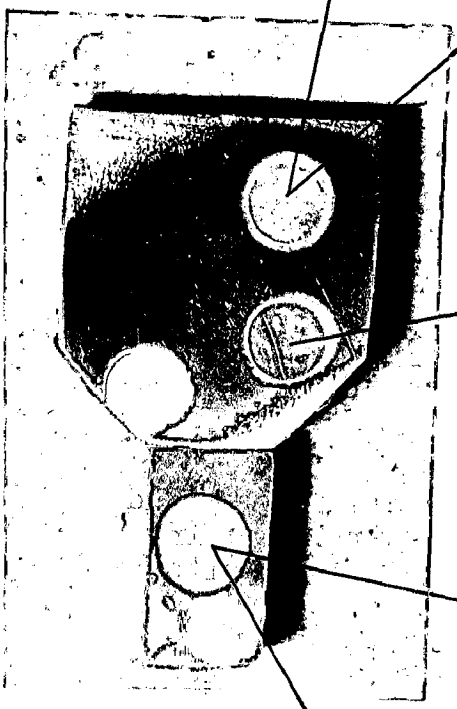

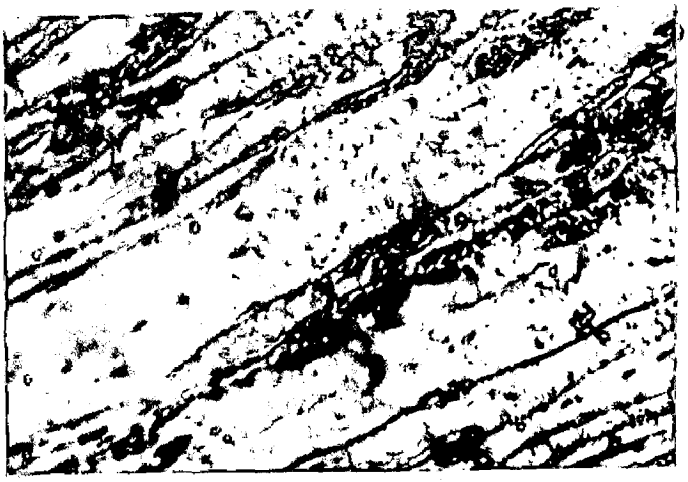

(c)

FIG.6.45

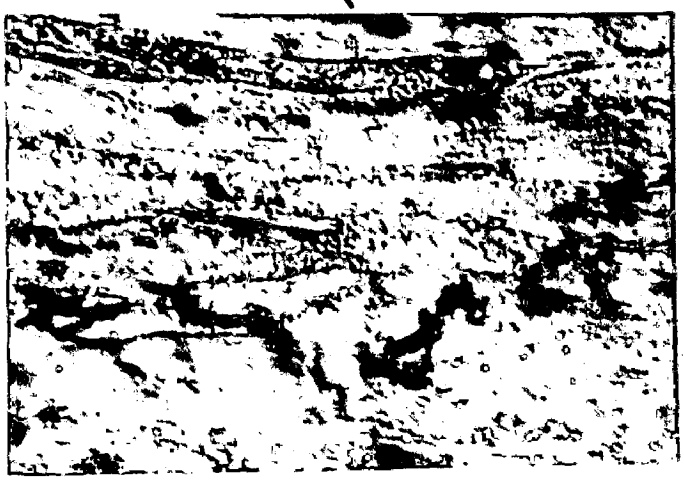

(e)

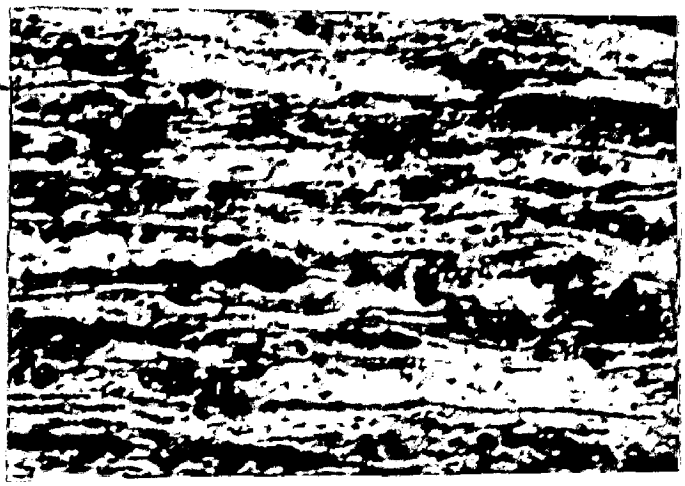

(d)

Fig. 6.45(f)

Transverse section of extruded product (Wedge die), R=7.0:1, T=300°C.
Fine grain structure.

Bright field, 200 X

Fig. 6.45(g)

Same as (f)

Sub-structure in the form of few pits.

Polarised light, 1000 X

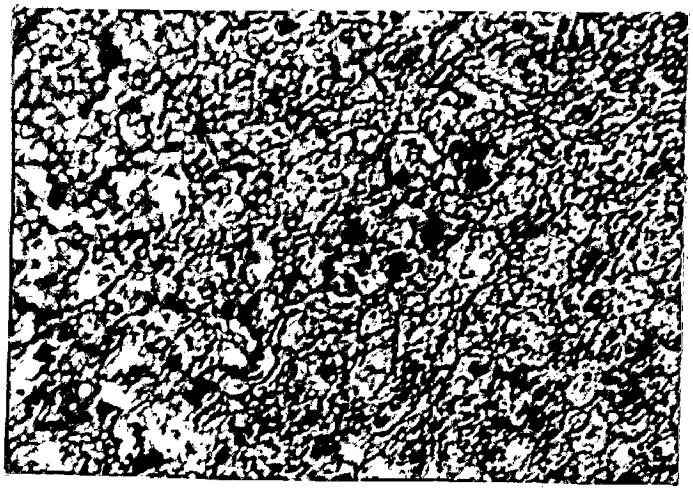

FIG.6.45 (f)

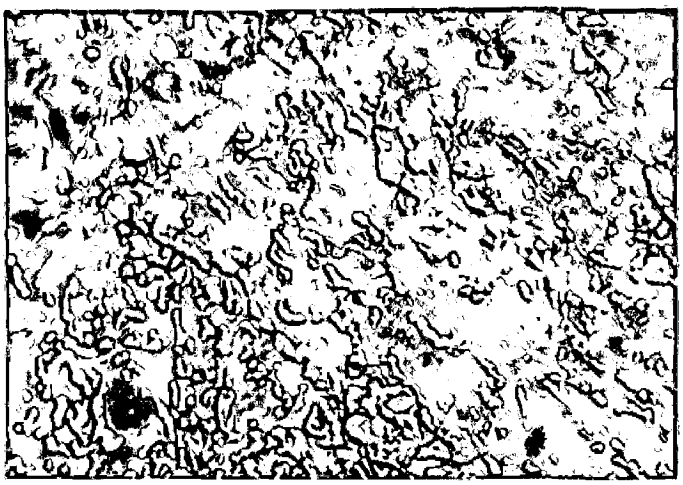

FIG.6.45 (g)

Fig. 6.46

Logitudinal section of partially extruded billet (Wedge die), R=7.0:1, T=400°C (Circular spots indicate the electropolished regions and arrows - approximate positions of the structures).

(a) Grain growth observed.

Bright field, 200 X

(b) Coarse sub-structure.

Polarised light, 1000 X

(c) Extensive flattening of grains(deformed sub-structure).

Polarised light, 500 X

(d) Heavily deformed grains, sub-structure in the form of pits.

Polarised light, 500 X

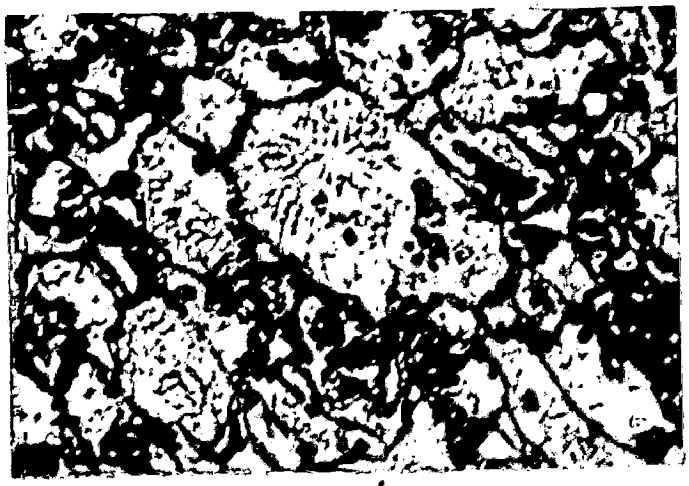

(a)

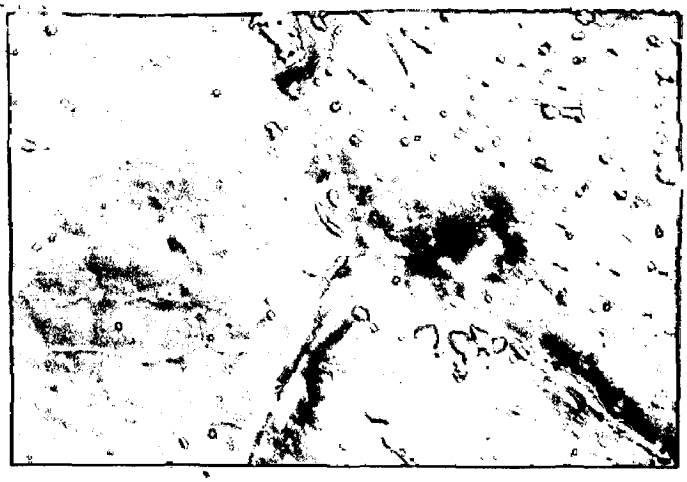

(b)

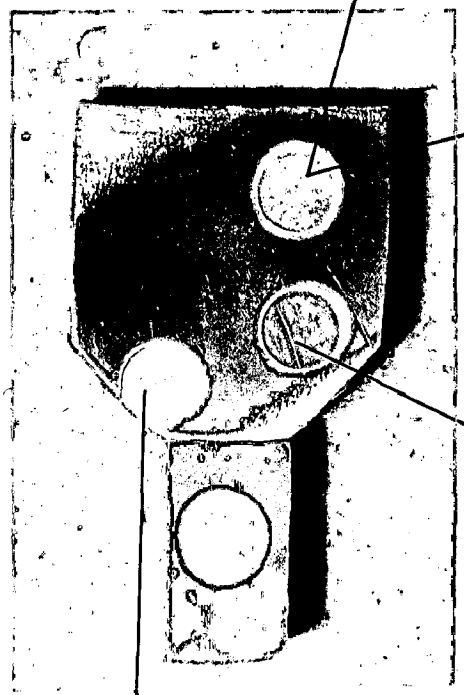

FIG.6.46

(c)

(d)

Fig. 6.46(e)

Extruded product (Wedge die), R=7.0:1,
T=400°C.
Directionality observed.
Bright field, 200 X

Fig. 6.46(f)

Same as (e)
Directionality and fine sub-structure.
Polarised light, 1000 X

Fig. 6.46(g)

Transverse section of extruded product
(Wedge die), R=7.0:1, T=400°C.
Heavy concentration of pits.
Polarised light, 500 X

FIG.6.46(e)

FIG.6.46(f)

FIG.6.46(g)

Fig. 6.47

Macrograph showing incoherent DMZ boundary, R=2.1:1, T=300°C.

Fig. 6.48(a)

Macrograph showing incoherent DMZ boundary. Macrograph of partially extruded billet showing incoherent DMZ boundary.

Fig. 6.48(b)

Scanning Electron Macrograph showing only DMZ boundary, R=10:1 and T=300°C

20 X

Macrograph showing incoherent DMZ boundary, R =2.1:1, T=300°C.

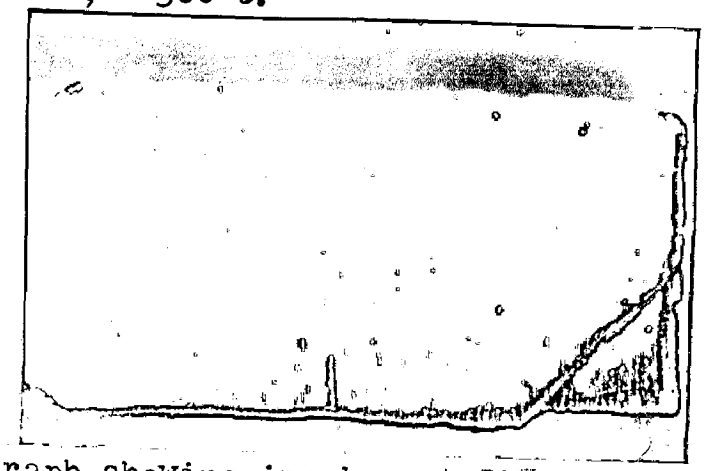

Macrograph showing incoherent DMZ boundary.
Macrograph of partially extruded billet showing incoherent DMZ boundary.

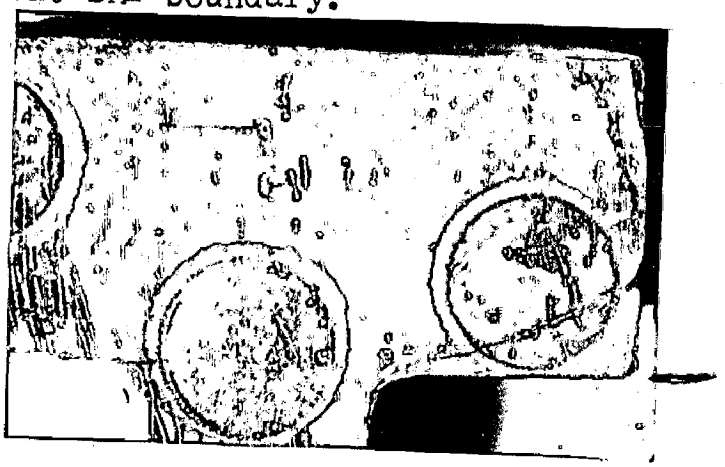

Scanning Electron Macrograph showing only DMZ boundary, R=10:1 and T=300°C 20X

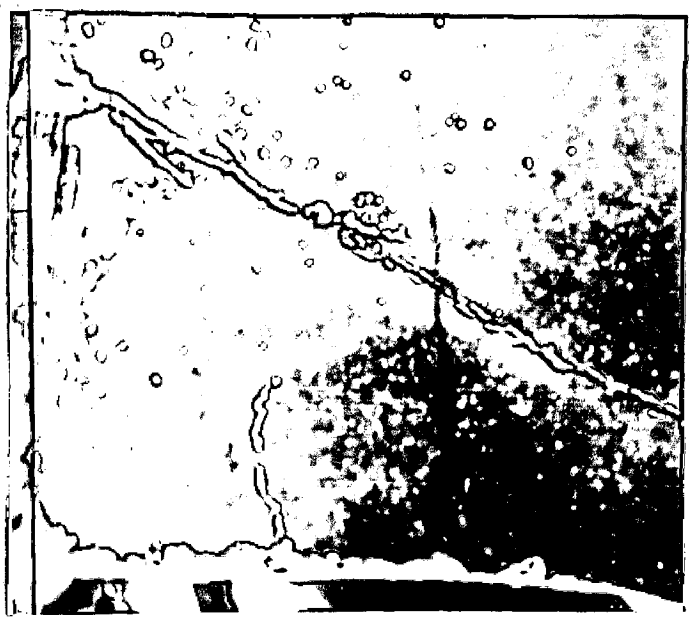

FIG.6.48(b)

Fig. 6.49(a)

Macrograph of partially extruded billet showing incoherent DMZ boundary, R=20:1 and T=300°C.

Fig. 6.49(b)

Scanning Electron micrograph showing only DMZ boundary, R=20:1 and T=500°C.

20 X

Fig. 6.50

Flow of material on both sides of incoherent DMZ boundary, R = 10:1 and T = 300°C.

Polarised light, 200 X

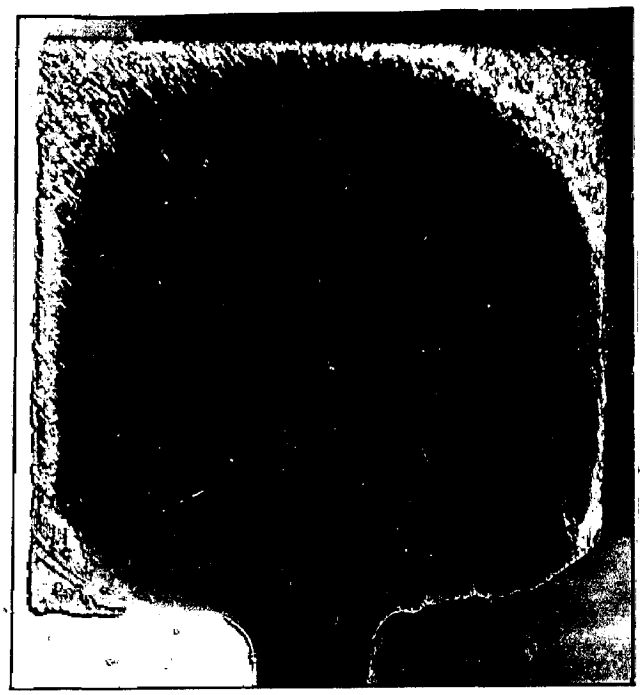

Macrograph of partially extruded billet showing incoherent DMZ boundary, R=20:1 and T=300°C.

Scanning Electron micrograph showing only DMZ boundary. R=20:1

20µ

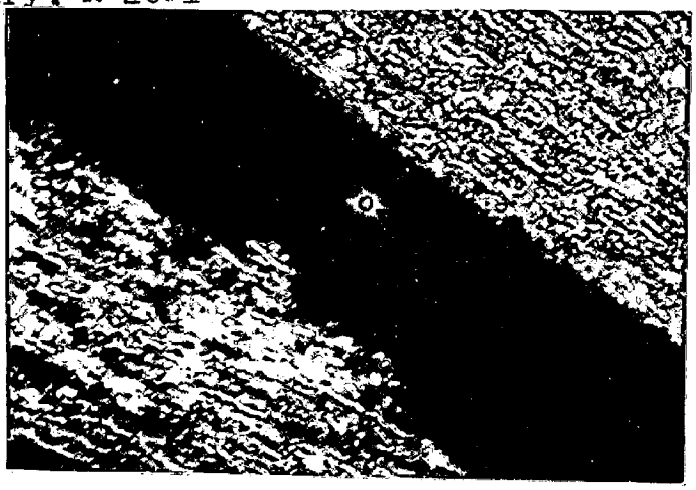

Flow of material on both sides of incoherent DMZ boundary, R =10:1 and T= 300°C.

Polarised light

Fig. 6.51

Defect in products extruded through square die at reduction ratio, 1.3:1.

(a) Incoherent extruded product at 300°C showing longitudinal as well as lateral cracks.

(b) Incoherent extruded product at 400°C showing lateral cracks on the longitudinal section.

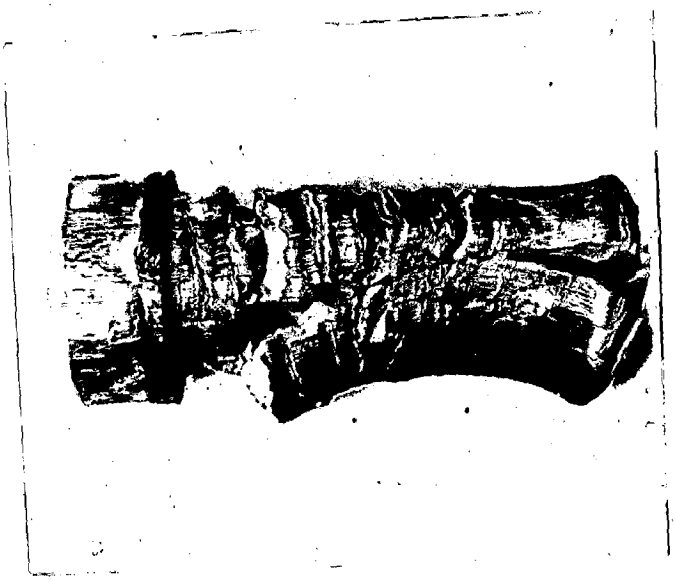

FIG.6.51(a)

FIG.6.51(b)

Fig. 6.52

Defect in products extruded through square die at reduction ratio, 1.6:1.

(a) Incoherent product at 300°C showing cracks on the surface and longitudinal section.

(b) Incoherent product at 400°C showing cracks on the longitudinal section only.

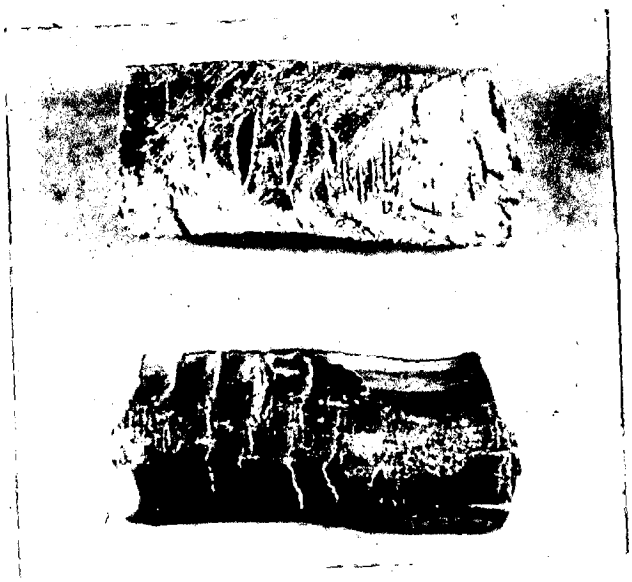

FIG. 6.52 (a)

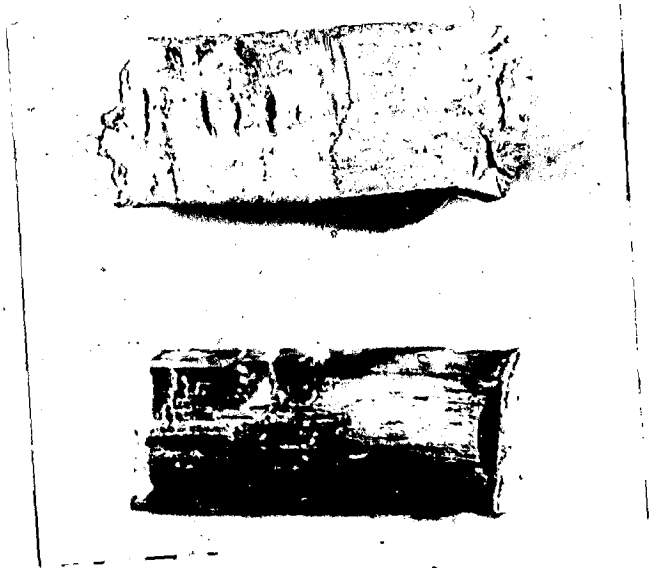

FIG. 6.52 (b)

Fig. 6.53

Coherent products extruded through square die at low reduction ratios.

(a) Coherent product R=2.1:1 and T=300°C.

(b) Coherent product R=1.3:1 and T=500°C.

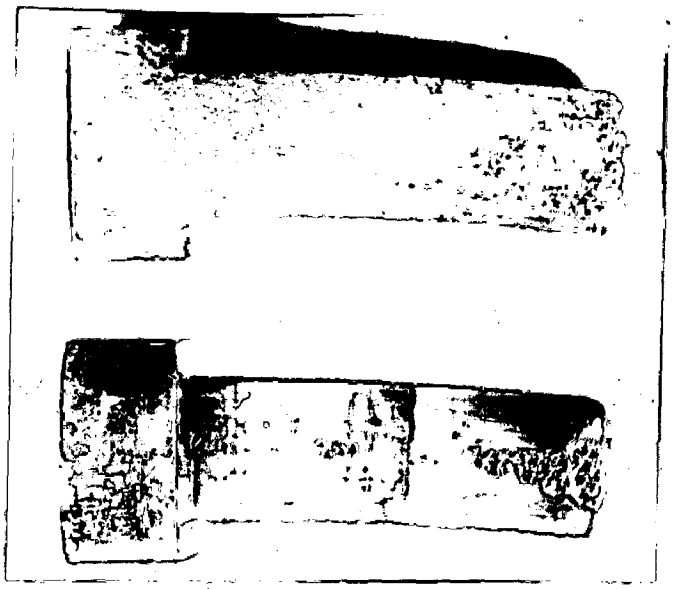

FIG.6.53 (a)

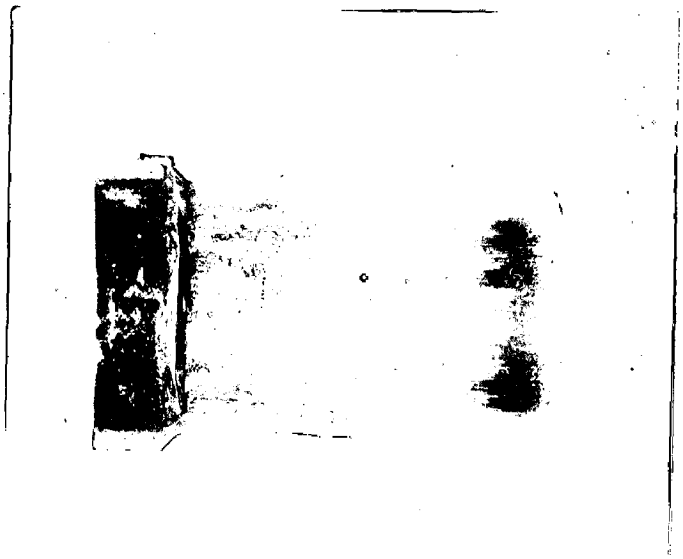

FIG.6.53 (b)

Fig. 6.54

Products extruded through wedge shaped dies at low reduction ratios.

(a) Incoherent extruded product at 300°C for R=1.6:1 and R=2.0:1 showing lateral cracks called snakeskin.

(b) Coherent extruded product at 400°C for R = 1.6:1.

Products extruded through wedge shaped dies at low reduction ratios.

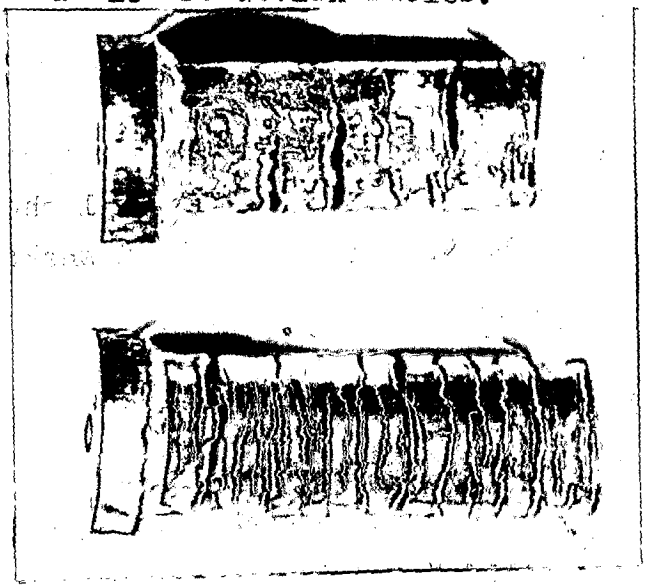

(a) Incoherent extruded product at 300°C for R=1.6:1 and R=2.0:1 showing lateral cracks called snakeskin.

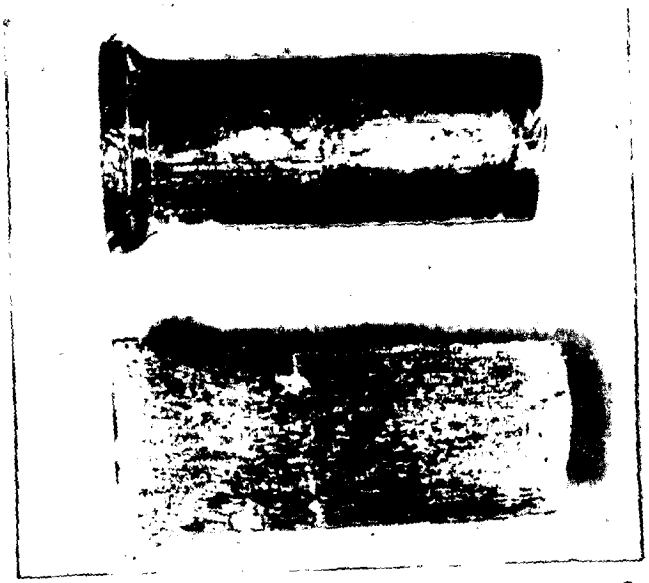

(b) Coherent extruded product at 400°C for R = 1.6:1.

Fig. 6.55

Defects in the starting portion of the products extruded through wedge shaped dies at low reduction ratios.

(a) Cracks at the starting portion of the product extruded at 400°C for R=1.6:1 and 2.0:1.

(b) Starting portions of the product show no crack extruded at 500°C for R=1.6:1 and 2.0:1.

Defects in the starting portion of the products extruded through wedge shaped dies at low reduction ratios.

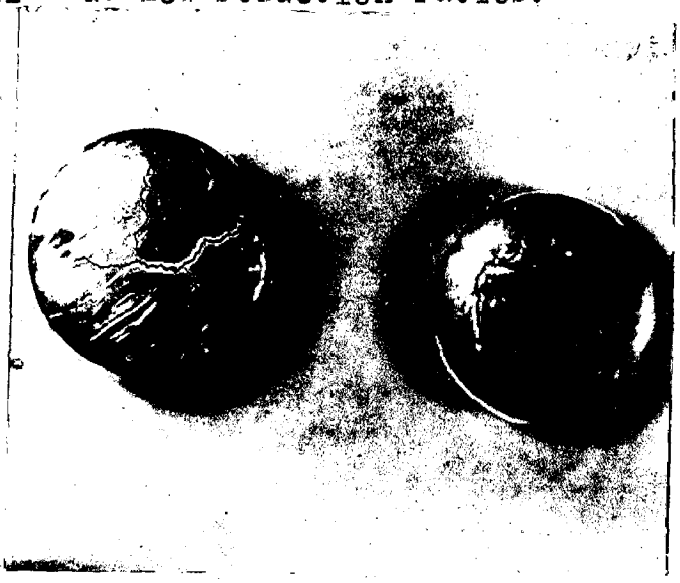

(a) Cracks at the starting potion of the product extruded at 400°C for R=1.6:1 and 2.0:1.

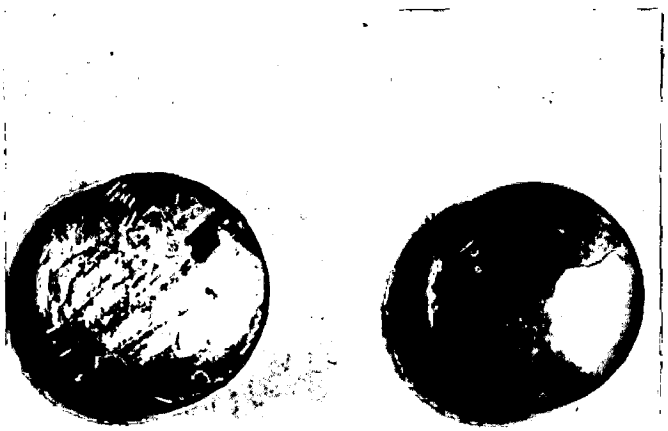

(b) Starting portions of the product show no crack extruded at 500°C for R=1.6:1 and 2.0:1.

C H A P T E R - VII

GENERAL DISCUSSION

7.1 INTRODUCTION

In the preceeding chapter an attempt has been made to systematically analyse the experimental observations and highlight the important experimental features. However, it was felt that the process of extrusion involves number of parameters and while explaining certain experimental results, many a times correlation of one result with the other got lost. In order to establish such correlation and to emphasise the important observations which have so far not been discussed in depth, the need of this chapter arose. Some of the important areas, where elaborate discussion is needed, are:

i) Concept of DMZ.

ii) Concept of flow and deformation during extrusion.

iii) Densification in wedge shaped dies.

7.2 CONCEPT OF DMZ

It is agreed that there exists DMZ as it could be delineated experimentally in certain cases. However, as putforward in slip line field theory that it is inclined to an angle of 45° to die axis for all reduction ratios is not true. In fact, the orientation of DMZ boundary varies with reduction ratios, as shown in Figs.6.47 to 6.49. For low reduction ratios it is somewhat parallel to the die axis and it becomes nearly perpendicular to die axis when reduction

ratio is increased. At intermediate reduction ratio there is likely to be near vicinity of 45° orientation. As the material movement is evident in DMZ it may be more appropriate to call it hydrostatic zone (HZ). It was also seen that the pressure more than extrusion pressure appears to develop in certain regions near the container surface. This way it would be better to identify these regions as regions of hydrostatic pressure where overall material movement is very low. The orientation of this region with respect to metal flow has a great bearing on the overall performance of the process. In fact when EPC line is parallel to the die axis, the forces are so oriented that it is practically shear which is predominent before extrusion (Fig. 7.1(a)). Such a situation prevailing in low reduction ratio would lead to incoherent product. However, at high reduction ratios its orientation being nearly perpendicular to the die axis, the forces now are predominently compressive in nature (Fig. 7.1 (b) and as a result of this the coherent product was obtained.

On the basis of the concept outlined above it could be concluded that coherency of the product is unlikely to be related with the parameters like so-called redundant work as proposed earlier. This is further discussed in the following section. On the contrary, it is expected that material would be coherent whenever the relative deformation between the particles (representing mass in quantised fashion*) is gradual

---

* So far the material is treated as continuum in all analytical theoreis. However, this is far from the fact that the powder material represented by individual particles does not easily lose its identity in the extrusion process therefore the existance of particles and its influence on the overall deformation is very important in the process.

and of high magnitude. Such a situation exist in wedge shaped dies, where the contoure in the container ensures gradual deformation all along the section of the billet. In this case also,there are only compressive forces which are developing. Hence, it is expected and has been rightly obtained a better extruded mass through wedge shaped dies.

7.3 CONCEPT OF FLOW AND DEFORMATION DURING EXTRUSION

It has been reported that in the relation

$$p = A + B \log R \qquad ..(7.1)$$

Corresponding to extrusion process, the constant 'A' represents redundant work and 'B' represents homogeneous work of deformation. It has also been reported that the redundant work is proportional to the area where massive shear zones develop inside the mass being extruded and it is different from the work causing homogeneous deformation. It has been argued that the quantity of redundant work is primarily dependent upon the reduction ratio. It is not clear how this concept of redundant work which varies with reduction ratio has arbitrarily been linked with the constant 'A', as it is a constant for all reduction ratios falling along the line depicted by the Equation (7.1).

It has been reported in the past as well in the present investigation that the relationship modifies to

$$p = A_1 + B \log R \qquad ..(7.2)$$

For lower reduction ratios where A_1 is a very small quantity compared to 'A' of Equation (7.1). This fact can be

interpreted that for lower reduction ratios, curves have tendency to pass through the origin. However, on account of frictional condition prevailing in the process these deviate from the origin. In this context no attempt has been made to explain as to why the linear relationship changes its slope in the region of reduction ratios being 7:1 to 10:1. In fact, the value of 'A' is precisely dependent upon this change of slope, so in order to interpret this value it is necessary to reasonout why at all the slope has changed.

The change of slope can be very precisely understood from the mode of deformation and flow conditions inside the mass being extruded. Both these factors are very heterogeneous in nature. Flow conditions are depicted in pressure contours where as deformation condition can be depicted in strain rate contours. In the context of low reduction ratios it is evident that high flow condition exists to a fairly large section of extruded product. In this region grains flow without exhibiting noticeable deformation. This region, therefore, may be treated as a region of frictionless flow and no part of extrusion pressure is used up in initiating such a flow. As the die constraint are approache the flow conditions get reduced and deformation conditions get improved. As a result contours of high strain rate start developing in this region showing extensive deformation. The grains in this region undergo massive shearing and hence, high order of shape change leading to fibrous structure. Such a situation prevails when flow and pressure conditions are

-m. However, in the close vicinity of die constrain

interpreted that for lower reduction ratios, curves have tendency to pass through the origin. However, on account of frictional condition prevailing in the process these deviate from the origin. In this context no attempt has been made to explain as to why the linear relationship changes its slope in the region of reduction ratios being 7:1 to 10:1. In fact, the value of 'A' is precisely dependent upon this change of slope, so in order to interpret this value it is necessary to reasonout why at all the slope has changed.

The change of slope can be very precisely understood from the mode of deformation and flow conditions inside the mass being extruded. Both these factors are very heterogeneous in nature. Flow conditions are depicted in pressure contours where as deformation condition can be depicted in strain rate contours. In the context of low reduction ratios it is evident that high flow condition exists to a fairly large section of extruded product. In this region grains flow without exhibiting noticeable deformation. This region, therefore, may be treated as a region of frictionless flow and no part of extrusion pressure is used up in initiating such a flow. As the die constraint are approached the flow conditions get reduced and deformation conditions get improved. As a result contours of high strain rate start developing in this region showing extensive deformation. The grains in this region undergo massive shearing and hence, high order of shape change leading to fibrous structure. Such a situation prevails when flow and pressure conditions are both optimum. However, in the close vicinity of die constrain

(namely a region so far recognised as DMZ) the flow conditions become highly unfavourable. Therefore, chances of massive deformation are also minimised. This is reflected in strain rate contours being small in magnitude in this region.

This massive deformation as described above is localised near the die boundary and as the reduction ratio increases the extensive deformation proceeds towards the die axis. Corresponding to reduction ratios 7:1 to 10:1 this extensive deformation (in other words the effect of die constraint) happens to reach the die axis. As a result resistance is experienced throughout the extrusion cross-section when such a reduction ratio is approached which was earlier confined to localised section. Due to this restriction imposed by the reduction ratio the material requires minimum pressure for initiation of flow. This maximum pressure gets consumed in overcoming this restriction. Due to this the initial curve happens to change its slope. So the change of slope is precisely due to the effect of die constraint extended upto the die axis. Depending upon the quality of the material being extruded and hence the inter-particle friction, the quantity of slope change is likely to occur. As such, therefore, value of 'B' is a material dependent quantity and this inturn influences the value of 'A' obtained by this curve.

This change in slope appears to be independent of geometry of die (and hence die design) as similar trend was

obtained in the case of wedge shaped dies also. However, the change of slope in case of wedge shaped dies is of greater extent because the constraint is spread over the large area of inclined surface of the die in comparison to the point in case of square edge dies.

The author has come to the conclusion on the basis of above discussion that constants 'B' and 'A' are with material as well as die design variables and precisely depend upon the particle characteristics and subsequent deformation of the powder being extruded. The difference in the slopes obtained in the present investigation and that corresponding to Sheppard [1] experiments for aluminium powder extruded at 300 ^{o}C, shown in Fig. 6.2, can be accounted on the basis of difference in powder characteristics employed. To attribute 'A' towards redundant work and 'B' towards the homogeneous work of deformation has, therefore, no sound basis and hence the interpretation proposed in the present investigation is well supported by the analytical and microstructural investigations.

7.4 DENSIFICATION IN WEDGE SHAPED DIES

It is established that densification in square edge dies completes before the extrusion starts, exception being in the case of very low reduction ratios. However, in case of wedge shaped dies corresponding to all reduction ratios the densification is incomplete till certain length of the extruded product has come out. It was also noticed that load-ram displacement diagrams in wedge shaped dies (Figs.6.18(a and b))is different

from that of square edge die in the sense that extrusion begins before the attainment of peak load. Such a difference in densification behaviour may be explained on the basis of frictional conditions during steady state and non-steady state extrusion. It has been already concluded that inter-particle friction in presence of different pressure zones inside the mass being extruded influences greatly the extrusion pressure Vs. log R relationship. This peak load may also be related to frictional conditions inside the mass being extruded.

The peak load may be regarded as a sort of barrier for initiating extrusion process; unless it is crossed, extrusion can not sustain. This way the peak load is a dividing zone between non-steady state and steady state extrusion in the case of wedge shaped dies. This peak load is more pronounced in the case of wedge shaped dies than that of square edge dies. As discussed in section 6.3, the difference in peak load and steady state load shows a linear relationship to log R. Therefore, this difference may be related to the total static friction prevelent in the process. As the process gets initiated, the dynamic friction being lower in comparison to static friction, the load required to sustain the process also reduces . Therefore, in the case of wedge shaped dies the material situated near the die entrance does not suffer from the frictional constraint as stated above including the boundary friction. This part of the material, therefore, starts moving with decreased frictional conditions resulting in incomplete densification. The

material immediately following this portion, however, has to undergo higher frictional constraints leading to formation of peak load and hence complete densification before coming out of the die. Explanation of existence of peak load due to temperature quenching [60] at the die/billet interface, does not seem to be valid, because in the present investigation the temperature of die and billet are same before extrusion. Also argument given earlier [7] about the source of peak load being high concentration of dislocation and their consequent dynamic recovery lacks in concept.

It was observed that complete densification was not achieved during the entire extrusion process for low reduction ratios. This can be explained from the fact that in these cases good flow conditions with lowest possible interparticle friction exists in the large portion of the extruded section. It was observed in these cases by microstructural studies that particles situated near the die axis (when viewed longitudimal sections) do not at all deform.

Inter-relationship between peak load and interparticle friction is further confirmed by the fact that the difference between peak and steady state loads decreases with increase in extrusion temperature. Higher temperature may reduce interparticle friction and hence, difference in these loads. It may be concluded, therefore, that densification phenomenon during extrusion process is purely related with static and dynamic interparticle frictions. Not only this, the dynamic interparticle friction contributes towards

'work hardening' of the extruded product, because with increasing reduction ratio, the strength of the extruded product goes on increasing. Dynamic interparticle friction in wedge shaped dies may be related with homogeneous work of deformation and on the basis of experimental results it may be concluded that this homogeneous work is responsible for overall strength and coherency of the product.

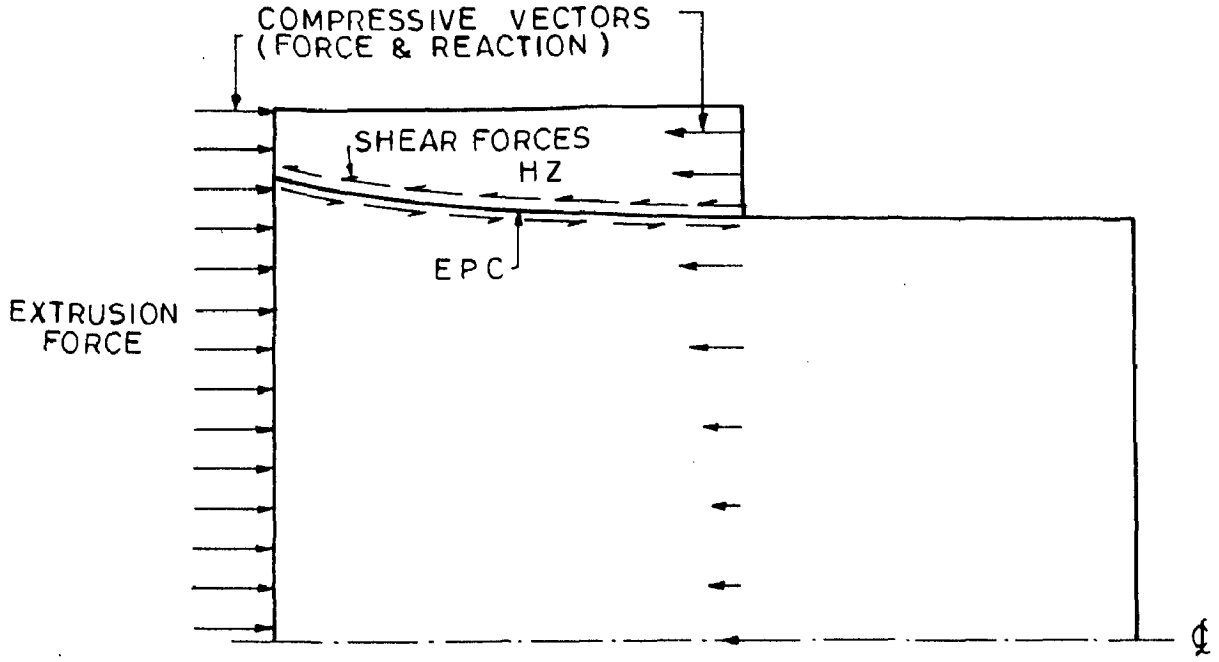

(a) PREDOMINENT SHEAR FORCES IN LOW REDUCTION RATIO

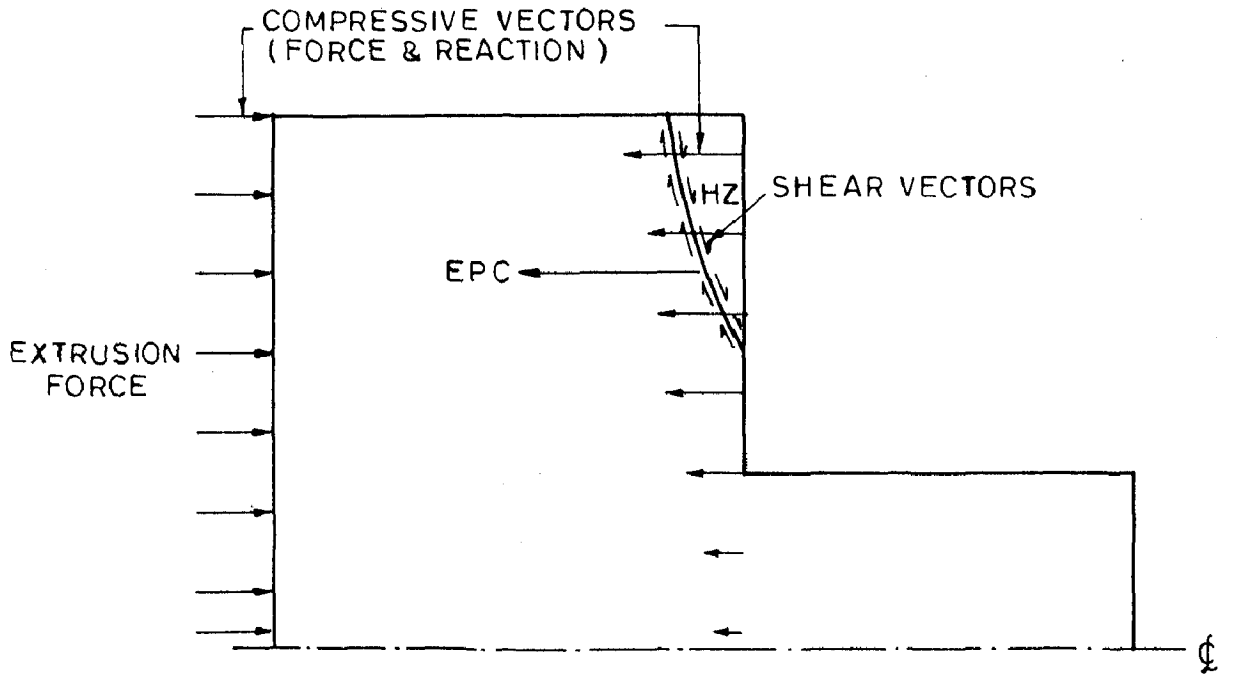

(b) PREDOMINENT COMPRESSIVE FORCES IN HIGH REDUCTION RATIO

FIG.7.1—ORIENTATION OF FORCES DURING EXTRUSION THROUGH SQUARE EDGE DIES.

C H A P T E R - VIII

CONCLUSIONS

The main conclusions which emerge from the present analytical and experimental studies, are given below :-

1 Finite element method, using velocity-pressure formulation, is a better technique to calculate extrusion pressure than the slip-line field theory and upper bound technique. Pressures thus obtained are in close agreement with the experimental extrusion pressures for both the type of dies.

2 Using Finite Element Method velocity vectors, average pressure and average effective strain rate contours are computed. These bulk parameters help to understand the exact state of material flow and deformation during extrusion process.

3 On the basis of position of the extrusion pressure contour (EPC) line on average pressure contour diagram, a model is proposed which explains the extent of coherency in the extruded product.

4 Experimental studies reveal that, the extrusion pressure varies linearly with the extrusion parameters (reduction ratio and extrusion temperature) for both the dies and for all the reduction ratios. This behaviour may be explained on the basis of metal flow and deformation during extrusion.

5 It is possible to obtain coherent product during extrusion by both the type of dies for reduction ratios as low as 2.1:1 at all temperatures. However, coherent product has also been obtained for both the dies even at lower reduction ratio, 1.3:1 at 500°C.

6 The hundred percent density of the extruded product can not be achieved at low reduction ratios for both the type of dies. While at high reduction ratios, fully dense product has been obtained.

7 The peak load, observed in the case of wedge shaped dies, is possibly the limiting load for sustaining the extrusion process. This load peak may be due to the static friction including boundary friction.

8 The steady state extrusion pressure in the case of wedge shaped dies is less than that required for square edge dies (same billet length) at the same temperature and reduction ratio. At the same time product, obtained by wedge shaped dies, is having atleast 10-20 % more strength then the product obtained with the square dies.

9 The orientation of the dead metal zone boundary changes with the variation in the reduction ratios. At low reduction ratios, it remains nearly parallel to the die axis while at high reduction ratios, it reduces in size and gets confined to the corner

of the die by assuming nearly perpendicular position with respect to the die axis.

10 There is a sudden change in the slope of the p vs log T curve at 400°C. It may be due to the change in the mode of deformation at this temperature.

11 Effect of extrusion parameters on the microstructural features of the extruded product and billet have also been linked with the bulk parameters.

Lastly, it can be concluded that the work for homogeneous deformation contributes more than the redundant work for obtaining a coherent extruded product. This is in partial contradiction with the theories and propositions in vogue.

REFERENCES

1 T. SHEPPARD and P.J.M. CHARE;
Powder Metallurgy, 15 , No. 29, 17-41 (1972).

2 A.S. EL-SABBAGH;
Powder Metallurgy International, 7 , No. 2,97-100(197?).

3 P.J.M. CHARE and T. SHEPPARD;
Powder Metallurgy, 16, No. 32, 437-458 (1973).

4 P.J.M. CHARE and T. SHEPPARD;
Int. J. of Powder Met. and Powder Tech., 10, No.3, 203-205 (1974).

5 T. SHEPPARD and P.J.M. CHARE;
Powder Metallurgy, 18, No. 35, 1-14 (1975).

6 T. SHEPPARD;
Proc. of the 15th Int. MTDR Conference, Macmillan Press Ltd., London, 559-667 (1975).

7 T. SHEPPARD and H. McSHANE;
Powder Metallurgy, 19, No.3, 126-133 (1976).

8 N. HANSEN;
Trans. Met. Soc. AIME, 242, 954-955 (1968).

9 N. HANSEN;
Powder Metallurgy, 12 , No.23, 23 (1969).

10 T. SHEPPARD and A. GREASLEY;
Powder Metallurgy, 20, No. 11, 26-35 (1977).

11 E. GREGORY and C.G. GOETZEL;
Trans. AIME, 212, 868-874 (1958)

12 C.R. SHAKESPEARE and D.A. OLIVER;
Powder Metallurgy, 7, No. 7, 203 (1964).

13 T. SHEPPARD;
Powder Technology, 10, 257-271 (1974).

14 J. BHATTACHARYA;
Metall. Met. Form., 2, No. 42, 36-38 (1975).

15 R.V. WATKINS, R.G. REED and W.L. SCHOLLOID;
' New Methods for the Consolidation of Metal Powders', 1, Edited by H.H. Hausner, Plenum Press, New York, 181-193 (1967).

16 J.J. DUNKLEY and R.J. CAUSTON;
Powder Metallurgy International, 8, No.3, 97-100(1976).

17 J.J. DUNKLEY and R.J. CAUSTON;
Int. J. of Powder Met. and Powder Tech., 13, No. 1, 13-20 (1977).

18 T.T. VOILLIER and M.G. JONES;
Powder Metallurgy, 2, No.22, 78-83 (1977).

19 W. THOMPSON, J.K. RUSSELL and R.H. BROWN;
Annals of CIRP, 25, 107-112 (1977).

20 ERIC GREGORY;
Metal Progress, 75, 113 (1959).

21 A. SINGH and R. DAVIES;
Proc. of 13th Int. MTDR Conf., Macmillan Press Ltd., London, 449-453 (1972).

22 M. NEGM and R. DAVIES;
Proc. of 15th Int. MTDR Conf., Macmillan Press Ltd., London (1975).

23 P. LOEWENSTEEN
' Powder Metallurgy', Edited by Werner Leszynspi, Inter Science Publishers, New York(1967).

24 T. CHANDRA and J.J. JONAS;
Met. Trans., 1, 2079 (1970).

25 T. CHANDRA and J.J. JONAS;
Met. Trans., 2, 877 (1971).

26 P. FELTHAN;
Metal Treatment and Metal Forging, 23, 440-444 (1956).

27 G.W. ROWE;
' Introduction to the Principle of Metal Working ', Edward Arnold (Publishers) Ltd., London (1977).

28 H. McSHANE, M.G. TUTCHER and T. SHEPPARD;
Powder Metallurgy, 21, No. 2, 47-51 (1978).

29 T. SHEPPARD and A. GREASLEY;
Powder Metallurgy, 21, No. 3, 155-162 (1978).

30 W. JOHNSON and H. KUDO;
' The Mechanics of Metal Extrusion ', Manchester University Press (1962).

31 J.M. ALEXANDER;
Proc. Int. Mech. Engg., 35, 173 (1959).

32 S. KOBAYASHI and E.G. THOMSEN;
Int. J. Mech. Science, 7, 127-143 (1965).

33 T. SHEPPARD and D. RAYBOULD;
J. Int. Metals, 33, 101 (1973).

34 J.F. ADIE and J.M. ALEXANDER;
Int. J. Mech. Science, 9, 349-357 (1967).

35 E.G.THOMSON and T. JORDAN;
J. Mech. and Physics of Solids, 4, 184 (1956).

36 T. SHEPPARD and H. McSHANE;
Powder Metallurgy, 19, No.3, 121-125 (1976).

37 B. AVITZUR;
' Metal Forming Processes and Analysis ',
McGraw - Hill Book Company (1968).

38 W. JOHNSON and P.B. MELLOR;
' Plasticity For Mechanical Engineers ',
Oxford University Press, London (1971).

39 E.G. THOMSON, C.T. YANG and S. KOBAYASHI;
'Plastic Deformation in Metal Processing ',
The Macmillan Press, New York (1965).

40 R. HILL;
' The Mathematical Theory of Plasticity ',
The Clarendon Press, Oxford (1971).

41 C.R. CALLADINE;
' Engineering Plasticity ', Pergaman Press (1969).

42 O.C. ZIENKIEWICZ and G.C. NAYAK;
Proc. 3rd Conf., Matrix Method in Structural
Mechanics, Wright Patterson Air Force, Ohio (1971).

43 G.C. NAYAK and O.C. ZIENKIEWICZ;
Int. J. Numerical Method Engg. 5, 113-135 (1972).

44 O.C. ZIENKIEWICZ and P.N. GODBOLE;
J. of Strain Analysis, 10, No.3, 180-183 (1975).

45 O.C. ZIENKIEWICZ and P.N. GODBOLE;
Int. J. Num. Meth. Engg., 8, 3-16 (1974).

46 J.W.H. PRICE and J.M. ALEXANDER;
Second Int. Symposium, S. Margherita, Italy (197

47 G.Y. GOON, P.I. POLUCHIN, W.P. POLUCHIN and B.A. PRUDCOWSKY;
Metallurgica (Russian),(1968).

48 P.N. GODBOLE;
Ph.D. Thesis, University of Wales, Swansea (1974).

49 O.C. ZIENKIEWICZ, P.C. JAIN and E. ONATE;
Int. J. Solids Structure, 14, 15-38 (1978).

50 P.C. JAIN;
Ph.D. Thesis, University of Wales, Swansea (1976).

51 O.C. ZIENKIEWICZ;
' The Finite Element Method in Engineering Science',
McGraw-Hill Book Company, New York (1971).

52 KONNETH H. HUEBNER;
' The Finite Element Method for Engineers ',
John Wiley and Sons, New York (1975).

53 P. PERZYNA;
'Fundamental Problem in Viscoplasticity ',
Recent Advances in Applied Mechanics, Acadamic Press, New York, 243-377 (1966).

54 O.C. ZIEKIEWICZ and I.C. CORMEAU;
Int. J. Num. Meth. Engg., 8, 821-845 (1974).

55 ' ASTM Standards On Metal Powders and Products ',
American Soc. for testing and Materials (1968).

56 K.H. MOYER;
The Int. J. of Powder Metallurgy and Powder Technology 15, No. 1, 33-42 (1979).

57 P. HOOD;
Ph.D. Thesis, University of Wales, Swansea (1974).

58 P. HOOD;
Computer Report - CR 65, The NASS SYSTEM REPORT, University of Wales, Swansea (1974).

59 H.A. KHUN and C.L. DOWNEY;
Int. J. of Powder Metallurgy, 7, No. 1, 15-25 (1971

60 W.R.D. WILSON;
Int. J. Mech. Science, 13, 17 (1971).